

<https://doi.org/10.15388/vu.thesis.141>

<https://orcid.org/0000-0003-1424-9109>

VILNIUS UNIVERSITY

CENTER FOR PHYSICAL SCIENCES AND TECHNOLOGY

Martynas

VELIČKA

SERS Spectroscopy of Biological Fluids and Cells

DOCTORAL DISSERTATION

Natural Sciences,
Physics (N 002)

VILNIUS 2021

This dissertation was written between 2016 to 2020 at the Institute of Chemical Physics, Vilnius University.

Academic supervisor:

Prof. Habil. Dr. Valdas Šablinskas (Vilnius University, natural sciences, physics – N 002).

Dissertation Defence Panel:

Chairman – Prof. Habil. Dr. Vidmantas Gulbinas (Center for Physical Sciences and Technology, natural sciences, physics – N 002).

Members:

Prof. Dr. Saulius Bagdonas (Vilnius University, natural sciences, physics – N 002).

Prof. Dr. Liutauras Marcinauskas (Kaunas University of Technology, natural sciences, physics – N 002).

Dr. Lina Mikoliūnaitė (Center for Physical Sciences and Technology, natural sciences, physics – N 002).

Assoc. Prof. Dr. Tomas Šalkus (Vilnius University, natural sciences, physics – N 002).

The dissertation shall be defended at a public meeting of the Dissertation Defence Panel at 13:00 on 9th of March 2021 in Room A101 of the National Center for Physical Sciences and Technology.

Address: Saulėtekio av. 3, NFTMC, Room A101, Vilnius, Lithuania

Tel. +370 5 264 8884; e-mail: office@ftmc.lt

The text of this dissertation can be accessed at the Vilnius University Library, as well as on the website of Vilnius University:

www.vu.lt/naujienos/ivykiu-kalendorius.

<https://doi.org/10.15388/vu.thesis.141>

<https://orcid.org/0000-0003-1424-9109>

VILNIAUS UNIVERSITETAS
FIZINIŲ IR TECHNOLOGIJOS MOKSLŲ CENTRAS

Martynas
VELIČKA

Biologinių skysčių ir ląstelių paviršiaus sustiprintos Ramano sklaidos spektroskopija

DAKTARO DISERTACIJA

Gamtos mokslai,
Fizika (N 002)

VILNIUS 2021

Disertacija rengta 2016-2020 metais Vilniaus universiteto Cheminės fizikos institute.

Mokslinis vadovas:

prof. habil. dr. Valdas Šablinskas (Vilniaus universitetas, gamtos mokslai, fizika – N 002).

Gynimo taryba:

Pirmininkas – prof. habil. dr. Vidmantas Gulbinas (Fizinių ir technologijos mokslų centras, gamtos mokslai, fizika – N 002).

Nariai:

prof. dr. Saulius Bagdonas (Vilniaus universitetas, gamtos mokslai, fizika – N 002).

prof. dr. Liutauras Marcinauskas (Kauno technologijos universitetas, gamtos mokslai, fizika – N 002).

dr. Lina Mikoliūnaitė (Fizinių ir technologijos mokslų centras, gamtos mokslai, fizika – N 002).

doc. dr. Tomas Šalkus (Vilniaus universitetas, gamtos mokslai, fizika – N 002).

Disertacija ginama viešame Gynimo tarybos posėdyje 2021 m. kovo mėn. 9 d. 13:00 val. Nacionalinio fizinių ir technologijos mokslų centro A101 auditorijoje.

Adresas: Saulėtekio al. 3, NFTMC, A101 audit., Vilnius, Lietuva

Tel. +370 5 264 8884; el. paštas: office@ftmc.lt

Disertaciją galima peržiūrėti Vilniaus universiteto bibliotekoje ir VU interneto svetainėje adresu:

www.vu.lt/naujienos/ivykiu-kalendorius.

ACKNOWLEDGEMENTS

The years of the PhD studies like the real life itself were full of moments of joy and sorrow, which manifested in sleepless nights and tears of joy. Therefore, the experience I have gained during these years is far beyond the content of the few hundred pages written below. For that experience I would like to express my gratitude to everyone who made it all possible.

First, I would like to thank my supervisor Prof. Habil. Dr. Valdas Šablinskas who has guided and supported me since I came to the department just after finishing my second-year of bachelor studies. The knowledge passed down and the challenges brought up to me have resulted in the confidence and expertise in the field of spectroscopy that I have now. I would also like to give thanks to Milda - a great co-worker and friend who helped me to get a foothold in this field.

Second, I would like to thank the colleagues of the Institute of Chemical Physics Justinas, Vidita, and Kęstutis for sharing their knowledge and always giving a hand or a thoughtful hint when I was lost or unsure.

Third, I thank my two former students Sonata and Edvinas for helping me with some of the experiments and agreeing to join me in the “let’s do science on ourselves” club. Together with them I deeply thank the rest of the *Molecule* gang – Dovilė, Rasa, Rimantė, and Gerda for the joyful atmosphere, moral support, and fruitful discussions in the office.

Further, I thank the staff of the Vilnius University Hospital Santaros clinics and the Antibacterial Phototechnology group of the Faculty of Physics for collaborating in the conducted research and helping me to combine my love for biology with the knowledge in physics and spectroscopy.

Additionally, I thank all of my friends but especially Šarūnė and Tadas for sharing a somewhat completely different and refreshing view of the world.

Finally, I am grateful to my parents Eglutė, and Stanislovas and my grandmother Marija for raising me, for their continuous support and wisdom. Thank you, dear sister Giedre and my brother-in-law Mantas for your company and passion for nature related activities. I would like to thank my wife Milda for seeing in me more than I could and showing me that even in moments when you think that this is it, you can always find a little bit of strength to gather yourself and move on.

I give thanks to all the animals and plants for providing me calmness, and awe.

CONTENTS

ACKNOWLEDGEMENTS	5
LIST OF ABBREVIATIONS	8
INTRODUCTION.....	10
GOALS AND TASKS OF THE THESIS	12
STATEMENTS OF THE THESIS.....	13
CHAPTER 1. BIOMEDICAL APPLICATION OF VIBRATIONAL SPECTROSCOPY	19
1.1. A BRIEF OVERVIEW OF THE VIBRATIONAL SPECTROSCOPY TECHNIQUES AND IMPLEMENTATION.....	19
1.2. NONCONVENTIONAL VIBRATIONAL SPECTROSCOPY TECHNIQUES.....	22
1.3. DATA ANALYSIS	33
CHAPTER 2. SERS SPECTROSCOPY OF KIDNEY AND BLADDER CANCERS	37
2.1. CANCER AS A DISEASE	37
2.2. VIBRATIONAL SPECTROSCOPY OF CANCERS.....	43
2.3. EXPERIMENTAL DETAILS OF VIBRATIONAL SPECTROSCOPY OF CANCERS	45
2.4. SPECTROSCOPIC ANALYSIS OF THE EXTRACELLULAR FLUID: RESULTS AND DISCUSSION	50
CHAPTER 3. SERS STUDY OF INACTIVATION OF PATHOGENIC BACTERIA.....	78
3.1. PATHOGENIC BACTERIA	78
3.2. EXPERIMENTAL DETAILS OF THE SERS ANALYSIS OF BACTERIA.....	80
3.3. SERS STUDY OF BACTERIA: RESULTS AND DISCUSSION.....	81
CHAPTER 4. SERS STUDY OF PHARMACEUTICALS AND DRUGS IN BLOOD AND SALIVA.....	90
4.1. BLOOD AND SALIVA.....	90

4.2. EXPERIMENTAL DETAILS OF THE SERS SPECTROSCOPY OF BLOOD	97
4.3. SERS STUDY OF BLOOD: RESULTS AND DISCUSSION.....	101
4.4. EXPERIMENTAL DETAILS OF THE EC-SERS SPECTROSCOPY OF SALIVA	118
4.5. EC-SERS STUDY OF SALIVA: RESULTS AND DISCUSSION ...	121
CONCLUSIONS	134
FUTURE PROSPECTS	135
SANTRAUKA LIETUVIŲ KALBA	137
ĮVADAS.....	137
TIKSLAS IR UŽDAVINIAI.....	139
GINAMIEJI TEIGINIAI.....	140
DISERTACIJOS SANDARA	145
TYRIMŲ METODIKA	146
PAGRINDINIAI REZULTATAI.....	149
IŠVADOS.....	168
BIBLIOGRAPHY	169
APPENDIX I.....	184
APPENDIX II	188

LIST OF ABBREVIATIONS

AgNPs – silver nanoparticles

APAP – N-acetyl-para-aminophenol (acetaminophen)

ATP – adenosine triphosphate

ATR – attenuated total reflection

CCD – charged-coupled device

ccRCC – clear cell renal cell carcinoma

CE – counter electrode

Chl – chlorophyllin

DFT – density functional theory

EC-SERS – electrochemical surface enhanced Raman scattering

ECF – extracellular fluid

GC/MS – gas chromatography tandem mass spectroscopy

HCA – hierarchical clustering analysis

IR – infrared

LC/MS – liquid chromatography tandem mass spectroscopy

LOD – limit of detection

LSPR – localised surface plasmon resonance

MIR – middle infrared

Nd:YAG – neodymium doped yttrium aluminium garnet

NIR – near infrared

OTC – over-the-counter

PCA – principal component analysis

PMT – photomultiplier tube

RE – reference electrode

ROS – reactive oxygen species

SERS – surface enhanced Raman scattering

FT – Fourier transform

FTIR – Fourier transform infrared

TEM – transmission electron microscopy

TNM – tumor, nodes, metastases

TURBT – transurethral resection of bladder tumour

UV – ultraviolet

Vis – visible

WE – working electrode

WLC – white light cystoscopy

INTRODUCTION

Progress in all fields of science is primarily driven by the ability to gather more specific information about the object under study. Thus, the constant desire for progress leads to the demand for development of new advanced research methods or finding novel applications for the conventional ones. In biology and especially in modern medicine the benefit of improvement of the collected experimental data specificity is self-evident. Such improvement leads to a better understanding of the complex mechanisms of diseases, increased sensitivity of disease detection, and the overall higher quality treatment of the patients.

In order to gather specific information about biological samples, efficient methods of the chemical composition analysis are needed. A few practical methods, which give information about the chemical composition on the level ranging from the atomic to the molecular, are available. One of the methods widely used for structural analysis is vibrational spectroscopy. It provides information about the vibrational modes of the molecules and is extremely sensitive to the chemical changes of the analyte. This is why vibrational spectroscopy methods – IR absorption and Raman scattering – are increasingly applied for the determination of the chemical composition of the analyte. These methods allow the analysis of molecular structure of biological samples or molecular interactions in such substances [1-5]. Vibrational spectroscopy methods are very useful in practical applications since in comparison to the other methods of structural analysis, in the most cases sample preparation does not involve laborious and time-consuming steps. Also, the need of relatively small amount of the sample and the possibility to implement microscopy methods allows the spectroscopic analysis of very small submicrometer or even micrometer size samples. As a result, methods of vibrational spectroscopy have already been successfully applied for the analysis of various biological structural components – proteins, membranes, cells, biological fluids or tissues [6-10].

Vibrational spectroscopy as a tool for the analysis of biological samples is attractive not only due to easy implementation, but also due to the usefulness of the provided chemical information. For example, it is known that every disease is resulted and can be linked to chemical changes in the cell structure, genome, metabolism, etc. In fact, the identification of these changes is the primary goal of clinical diagnosis. Therefore, sensitivity of vibrational spectroscopy methods to the subtle chemical changes opens up a possibility of the early detection of various illnesses. By analysing and comparing the

chemical composition of certain tissues, cells, bodily fluids one can detect the minute changes that lead to the development of the disease even before the first symptoms appear. Such advance in the early detection would be extremely useful. This is why such application of vibrational spectroscopy is currently on high demand and extensive research in this field is being done to implement these methods in clinical practice [11-13]. Besides the early detection of diseases, the short collection time of the spectra is also a property of vibrational spectroscopy methods which in combination with applications of portable devices and fiber optics could be used during the live surgery for the collection of independent information *in vivo*. Such approach could aid the surgeons to make the correct decisions in split time [14, 15].

However, vibrational spectroscopy approach is not that easy and the high potential of such method is not fully employed in the clinical applications yet. The use of vibrational spectroscopy methods in clinical analysis is yet to become a common practice because of several apparent reasons. One of the reasons is that the spectra of complex samples which are composed of various molecular species are difficult to interpret correctly. The spectra consist of numerous vibrational bands, many of which overlap each other. For this reason, in the most studies the easier approach is taken and only tentative assignments of the spectral bands are typically made. The tentative assignment could often be misleading and even lead to false conclusions. In order to specify the assignment of the vibrational bands, additional analysis of the chemical constituents and high-level theoretical *ab initio* calculations should be applied [16-18]. Such approach is not only time consuming, but also requires large-scale computational resources and therefore is often avoided. Another problem, which is not solved yet, is determining the most efficient strategy of sample preparation for the spectroscopic analysis. The straight-forward way is to measure transmission spectra of the whole tissue sample. However, due to the technical sample preparation problems this is not always the most reasonable approach. For example, when small tissue sections (around 5 μm) are prepared the cells are damaged and their cytosol content can deteriorate. As already mentioned, the spectral differences resulting from the chemical changes related to the disease are extremely small and they can be overlooked or be overburdened by the spectral information of the common structural molecules of the tissue. Analysis of the sample can be made easier if one can limit the amount of the unnecessary molecules in the sample. In case of biological tissues, this can be accomplished by analysing the extracellular fluid instead of the whole tissue [19-21]. What's more, in such

cases the possible use of the data pre-processing and chemometric multivariate methods can be helpful [22-24].

Every so often the concentration of molecules of interest in the studied samples is too low for the analysis via conventional vibrational spectroscopy methods. This is particularly true for Raman scattering spectroscopy. Nonetheless, analysis of the samples containing minute amounts of analyte can be performed using non-conventional spectroscopic techniques like surface enhanced Raman scattering. Using metal nanoparticles, the Raman scattering signal can be greatly enhanced, and thus even trace amounts of molecules can be detected. This is very effective for identification of certain types of molecules, for example drugs or their metabolites, in the bodily fluids [25-27]. Furthermore, the surface enhanced Raman scattering can be combined with electrochemistry what allows the control of analyte adsorption and can facilitate selective enhancement of Raman signal of the analyte molecules [28, 29]. However, the most of SERS studies are performed only on model samples, cell cultures, etc. since the analysis of real-life samples is disturbed by the presence of additional constituents in the sample. Hence, even though the results of such studies are satisfactory they do not reflect the true biomedical problem. In the end, if one wishes to implement the SERS method in the clinical practice, the analysis of real-life samples must be carried out.

GOALS AND TASKS OF THE THESIS

Regarding the existing problems of the practical applications of vibrational spectroscopy stated above, the main goal of the thesis is the development of novel vibrational spectroscopy application methods for the analysis of biological samples – tissues of the urinary tract cancers, bacteria cells, and biological fluids, such as blood, saliva and interstitial fluid. The prime focus of the work is to adapt the vibrational spectroscopy methods together with the data processing methods for analysis of biological and medical samples. To achieve this goal, several specific tasks were formulated:

1. To apply SERS spectroscopy method for the analysis of cancer tissues from various human organs and to estimate their potential in clinical use.
2. To implement SERS spectroscopy method for the study of pathogenic bacteria.
3. To adapt colloidal SERS and EC-SERS spectroscopies for the detection of pharmaceutical and psychoactive drugs or their metabolites in biological fluids, and to estimate the sensitivity of the methods and their potential in clinical use.

STATEMENTS OF THE THESIS

1. SERS spectroscopy of extracellular fluid can be efficiently used for detection of cancerous tissue areas with specificity and sensitivity of 93%. However, depending on the tissue, spectral bands of different molecular compounds such as glycogen or cysteine/lactic acid should be used as spectral markers.
2. SERS spectroscopy is sensitive enough to track the damages of the *E. coli* bacteria cell membrane induced by chlorophyllin-based photosensitization.
3. SERS spectroscopy allows the detection of traces of pharmaceuticals and their metabolites in human blood down to millimoles per liter – clinically meaningful concentrations.
4. EC-SERS spectroscopy of human saliva can be applied for the identification of consumption of psychoactive drugs. In case of caffeine the detection limit is as low as 15 micromoles per liter.

PUBLICATIONS INCLUDED IN THE THESIS

Peer-review publications

1. M. Velička, M. Pučetaitė, V. Urbonienė, J. Čeponkus, F. Jankevičius, V. Šablinskas, Detection of cancerous kidney tissue by means of SERS spectroscopy of extracellular fluid, *Journal of Raman spectroscopy*, 2017, **48**, 1744.
2. M. Pučetaitė, M. Velička, V. Urbonienė, J. Čeponkus, R. Bandzevičiūtė, F. Jankevičius, A. Želvys, V. Šablinskas, G. Steiner, Rapid intra-operative diagnosis of kidney cancer by attenuated total reflection infrared spectroscopy of tissue smears, *Journal of Biophotonics*, 2018, **11**, 1.
3. S. Adomavičiūtė, M. Velička, V. Šablinskas, Detection of aspirin traces in blood by means of surface-enhanced Raman scattering spectroscopy, *Journal of Raman Spectroscopy*, 2020, **51**, 919.
4. B. Žudytė, M. Velička, V. Šablinskas, Ž. Lukšienė, Understanding *Escherichia coli* damages after chlorophyllin-based photosensitization, *Journal of Biophotonics*, 2020, **13**, 1.
5. M. Velička, E. Zacharovas, S. Adomavičiūtė, V. Šablinskas, Detection of caffeine intake by means of EC-SERS spectroscopy of human saliva, *Spectrochimica Acta Part A: Molecular and Biomolecular Spectroscopy*, 2021, **246**, 118956.

6. E. Zacharovas, M. Velička, G. Platkevičius, A. Čekauskas, A. Želvys, G. Niaura, V. Šablinskas, Discrimination between cancerous and normal bladder cancer tissues via SERS Spectroscopy, Submitted.

Conference proceedings

1. M. Velička, M. Radžvilaitė, J. Čeponkus, V. Urbonienė, M. Pučetaitė, F. Jankevičius, G. Steiner, V. Šablinskas, Assignment of vibrational spectral bands of kidney tissue by means of low temperature SERS spectroscopy, *Proc. of SPIE* 10068, 2017.
2. V. Šablinskas, M. Velička, M. Pučetaitė, V. Urbonienė, J. Čeponkus, R. Bandzevičiūtė, F. Jankevičius, T. Sakharova, O. Bibikova, G. Steiner, *In situ* detection of cancerous kidney tissue by means of fiber ATR-FTIR spectroscopy, *Proc. of SPIE* 10497, 2018.
3. S. Adomavičiūtė, M. Velička, V. Šablinskas, Screening of usage of OTC drugs by means of SERS spectroscopy, *Proc. of SPIE* 10894, 2019.
4. M. Velička, S. Adomavičiūtė, E. Zacharovas, V. Šablinskas, Application of label-free SERS and EC-SERS for detection of traces of drugs in biological fluids, *Proc of SPIE*, 11257, 2020.

PAPERS NOT INCLUDED IN THE THESIS

1. M. Pučetaitė, M. Velička, J. Pilipavičius, A. Beganskienė, J. Čeponkus, V. Šablinskas, Uric acid detection by means of SERS spectroscopy on dried Ag colloidal drops, *Journal of Raman Spectroscopy*, 2016, **47**, 681.
2. J. Pilipavičius, R. Kaleinikaitė, M. Pučetaitė, M. Velička, A. Kareiva, A. Beganskienė, Controllable formation of high-density SERS-active silver nanoprisms layers on hybrid silica-APTES coatings, *Applied Surface Science*, 2016, **377**, 134.
3. E. Gaubas, T. Čeponis, L. Deveikis, D. Meškauskaitė, S. Miasojedovas, J. Mickevičius, J. Pavlov, K. Pūkas, J. Vaitkus, M. Velička, M. Zajac, R. Kucharski, Study of neutron irradiated structures of ammonothermal GaN, *Journal of Physics D: Applied Physics*, 2017, **50**, 1.
4. E. Gaubas, T. Čeponis, J. Mickevičius, J. Pavlov, V. Rumbauskas, M. Velička, E. Simoen, M. Zhao, Pulsed photo-ionization spectroscopy in carbon doped MOCVD GaN epi-layers on Si, *Semiconductor Science and Technology*, 2018, **33**, 1.
5. M. Valldeperas, M. Talaikis, S. K. Dhayal, M. Velička, J. Barauskas, G. Niaura, T. Nylander, Encapsulation of aspartic protease in nonlamellar lipid liquid crystalline phases, *Biophysical Journal*, 2019, **117**, 829.

6. V. Šablinskas, R. Bandzevičiūtė, M. Velička, J. Čeponkus, V. Urbonienė, F. Jankevičius, A. Laurinavičius, D. Dasevičius, G. Steiner, Fiber attenuated total reflection infrared spectroscopy of kidney tissue during live surgery, *Journal of Biophotonics*, 2020, **13**, 1.
7. S. Adomavičiūtė, M. Velička, V. Šablinskas, Fiber based SERS studies of cancerous tissues: toward clinical trials, *Proc. of SPIE* 11257, 2020.
8. R. Bandzevičiūtė, J. Čeponkus, M. Velička, V. Urbonienė, F. Jankevičius, A. Želvys, G. Steiner, V. Šablinskas, Fiber based infrared spectroscopy of cancer tissues, *Journal of Molecular Structure*, 2020, **1220**, 1.
9. Š. Svirskas, S. Balčiūnas, M. Šimėnas, G. Usevičius, M. Kinka, M. Velička, D. Kubicki, M. E. Castillo, A. Karabanov, V. V. Shvartsman, M. de Rosário Soares, V. Šablinskas, A. N. Salak, D. C. Lupascu, J. Banys, Phase transitions, screening and dielectric response of CsPbBr₃, *Journal of Materials Chemistry A* 2020, **8**, 14015.

CONFERENCE ABSTRACTS

1. M. Velička, J. Čeponkus, V. Šablinskas, Low Temperature Vibrational spectroscopy of cancerous biological tissue, Chemistry and Physics at Low Temperatures, Biarritz, France, 2016.
2. J. Pilipavičius, R. Kaleinikaitė, M. Pučetaitė, M. Velička, A. Kareiva, A. Beganskienė, Study of silver nanoprisms assembly on hybrid silica-APTES coatings prepared via sol-gel process, Hint Workshop: Nanostructured Materials: Protective and Functional Coatings, Surface Treatment, Bioceramics, Biocomposites and Membranes, Vilnius, Lithuania, 2016.
3. V. Urbonienė, M. Velička, J. Čeponkus, M. Pučetaitė, F. Jankevičius, V. Šablinskas, G. Steiner, Intra-operative on-line discrimination of kidney cancer from normal tissue by IR ATR spectroscopy of extracellular fluid, SPIE Photonics West, San Francisco, USA, 2016.
4. M. Velička, V. Urbonienė, F. Jankevičius, V. Šablinskas, Inkstų vėžio diagnostika paviršiaus sustiprintos Ramano sklaidos spektriniu metodu, Jaunųjų mokslininkų konferencija, Vilnius, Lithuania, 2017.
5. M. Velička, M. Radžvilaitė, J. Čeponkus, V. Urbonienė, M. Pučetaitė, F. Jankevičius, G. Steiner, V. Šablinskas, Assignment of vibrational spectral bands of kidney tissue by means of low temperature SERS spectroscopy, SPIE Photonics West, San Francisco, USA, 2017.
6. M. Radžvilaitė, M. Velička, V. Šablinskas, Low temperature study of extracellular fluid of kidney tissue by means of surface-enhanced Raman scattering spectroscopy, Open Readings, Vilnius, Lithuania, 2017.

7. M. Velička, M. Pučetaitė, J. Čeponkus, V. Urbonienė, F. Jankevičius, V. Šablinskas, Towards the detection of cancerous kidney tissue areas using surface enhanced Raman scattering spectroscopy, International Conference on Enhanced Spectroscopies, Munich, Germany, 2017.
8. M. Velička, M. Pučetaitė, J. Čeponkus, S. Adomavičiūtė, V. Urbonienė, F. Jankevičius, V. Šablinskas, Vėžinių inksto sričių nustatymas paviršiaus sustiprintos Ramano sklaidos metodu, Lietuvos nacionalinė fizikos konferencija, Vilnius, Lithuania, 2017.
9. M. Velička, S. Adomavičiūtė, V. Šablinskas, Formation of metal nanoparticle films for trace analysis of OTC drugs in biological fluids by means of SERS spectroscopy, European Congress on Molecular Spectroscopy, Coimbra, Portugal, 2018.
10. M. Velička, M. Pučetaitė, V. Urbonienė, R. Bandzevičiūtė, J. Čeponkus, F. Jankevičius, V. Šablinskas, G. Steiner, ATR-FTIR spectroscopy: towards *in vivo* detection of cancerous tissue areas, European Congress on Molecular Spectroscopy, Coimbra, Portugal, 2018.
11. S. Adomavičiūtė, M. Velička, V. Šablinskas, Detection of aspirin traces in blood by surface enhanced Raman scattering, Open Readings, Vilnius, Lithuania, 2018.
12. V. Šablinskas, M. Velička, M. Pučetaitė, V. Urbonienė, J. Čeponkus, R. Bandzevičiūtė, F. Jankevičius, T. Sakharova, O. Bibikova, G. Steiner, *In situ* detection of cancerous kidney tissue by means of fiber ATR-FTIR spectroscopy, SPIE Photonics West, San Francisco, USA, 2018.
13. R. Bandzevičiūtė, M. Velička, J. Čeponkus, V. Urbonienė, F. Jankevičius, V. Šablinskas, G. Steiner, Fiber based infrared spectroscopy of various cancer tissues, International Conference on Molecular Spectroscopy, Wroclaw, Poland, 2019.
14. E. Zacharovas, M. Velička, Elektrocheminio SERS metodo taikymas kofeino pėdsakų seilėse nustatymui, Lietuvos nacionalinė fizikos konferencija, Kaunas, Lithuania, 2019.
15. S. Adomavičiūtė, M. Velička, V. Šablinskas, Nereceptinių vaistų likučių kraujyje diagnostiniai tyrimai SERS spektriniu metodu, Lietuvos nacionalinė fizikos konferencija, Kaunas, Lithuania, 2019.
16. R. Bandzevičiūtė, J. Čeponkus, M. Velička, V. Urbonienė, G. Mickūnaitė, F. Jankevičius, V. Šablinskas, G. Steiner, Šviesolaidinė ATR infraraudonoji spektroskopija vėžinių audinių diagnostikai, Lietuvos nacionalinė fizikos konferencija, Kaunas, Lithuania, 2019.

17. E. Zacharovas, M. Velička, V. Šablinskas, Detection of caffeine traces in saliva using electrochemical SERS method, Open Readings, Vilnius, Lithuania, 2019.
18. S. Adomavičiūtė, M. Velička, V. Šablinskas, Traces of paracetamol in blood as studied by means of colloidal SERS, Open Readings, Vilnius, Lithuania, 2019.
19. B. Žudytė, M. Velička, Ž. Lukšienė, V. Šablinskas, Understanding *E. coli* damage after chlorophyllin-based photosensitization using SERS, Open Readings, Vilnius, Lithuania, 2019.
20. S. Adomavičiūtė, M. Velička, V. Šablinskas, Screening of usage of OTC drugs by means of SERS spectroscopy, SPIE Photonics West, San Francisco, USA, 2019.
21. M. Velička, S. Adomavičiūtė, E. Zacharovas, V. Šablinskas, Label-free SERS and EC-SERS spectroscopies for detection of medicine traces in biological fluids, Summer School Spectroelectrochemistry, Dresden, Germany, 2019.
22. M. Velička, S. Adomavičiūtė, E. Zacharovas, V. Šablinskas, Application of label-free SERS and EC-SERS for detection of traces of drugs in biological fluids, SPIE Photonics West, San Francisco, USA, 2020.
23. S. Adomavičiūtė, M. Velička, V. Šablinskas, Fiber based SERS studies of cancerous tissues: toward clinical trials, SPIE Photonics West, San Francisco, USA, 2020.
24. E. Zacharovas, M. Velička, G. Platkevičius, A. Želvys, V. Šablinskas, Study of urinary bladder cancer by means of surface enhanced Raman scattering spectroscopy, Open Readings, Vilnius, Lithuania, 2020.

SCIENTIFIC NOVELTY

The experiments presented in this work describe the novel application of surface enhanced Raman spectroscopy for identification of the cancerous tissues via spectroscopic analysis not of the whole tissues but of their extracellular fluid. Low temperature SERS spectroscopy was for the first time applied for the analysis of such samples. Furthermore, various spectral markers of cancerous tissues were identified. The results of this study prove that SERS spectroscopy could be applied for the accurate discrimination between the cancerous and normal tissues. If developed further this method has the potential to be applied in clinical practice.

Implementation of the SERS spectroscopy for studies of the inactivation of the pathogenic bacteria (*E. coli*) via chlorophyllin-based photosensitisation

has led to new insight in the mechanism of action of this procedure – the disruption of the bacteria cell membrane.

The SERS and EC-SERS spectroscopies were adapted for detection of drug and pharmaceutical molecules in biological fluids namely saliva and blood. For the first time spectroscopic analysis of the real-life samples of such type was performed. It was shown that detection of such molecules with clinically relevant concentrations in biological fluids can be achieved using the SERS and EC-SERS spectroscopies.

AUTHOR'S CONTRIBUTION

The experimental work, data analysis, and the writing of the publication of the SERS analysis of the kidney cancer were performed by the author of the thesis. The experimental work and analysis of the bladder tissue spectra were performed in collaboration with Edvinas Zacharovas. The spectroscopic experiments on the pathogenic bacteria, data analysis and publication writing were performed by the author of the thesis. The experimental work for the analysis of acetyl salicylic acid and acetaminophen in blood as well as data analysis and publication writing were performed in collaboration with Sonata Adomavičiūtė-Grabusovė. The experimental work, data analysis and publication writing on the EC-SERS analysis of the caffeine in saliva were performed by the author of the thesis.

Samples of kidney and bladder tissues, and samples of pathogenic bacteria were obtained in collaboration with Urology centre of Vilnius University Hospital Santaros clinics and Antibacterial phototechnology group of the Institute of photonics and nanotechnology of Vilnius University, respectively.

CHAPTER 1.

BIOMEDICAL APPLICATION OF VIBRATIONAL SPECTROSCOPY

1.1. A BRIEF OVERVIEW OF THE VIBRATIONAL SPECTROSCOPY TECHNIQUES AND IMPLEMENTATION

Vibrational spectroscopy is at present a well-established group of methods for chemical analysis of various substances and materials. It can be employed for surface or interface characterisation as well as for the determination of the crystal structure of the sample. Individual molecular species can also be the subject of the study. Precise characterization of the chemical structure of molecules and the changes of their properties in various environments and physical states of matter can be analysed. Therefore, high precision qualitative and quantitative analysis can be conducted using techniques of vibrational spectroscopy. The two most prominent techniques of vibrational spectroscopy are infrared (IR) absorption and Raman scattering spectroscopies.

It is known that electromagnetic radiation interacts with the matter through absorption, scattering and other types of mechanisms followed by exchange of energy between the radiation and the matter. The absorption of electromagnetic wave is manifested through the transition between the different energy states of an atom, a molecule or a molecular system. In the case of absorption of the infrared light, these transitions take place between the vibrational energy levels of the molecule or the molecular system. Naturally, as in the other physical phenomena the quantification principle holds and the energy of the absorbed quanta of the infrared light must be equal to the energy difference between the two vibrational energy levels. Hence, vibrational energy levels correspond to the energy of the molecule which it has due the different periodic motions of the bound atoms or atom groups.

Infrared radiation covers a wavelength range from around 800 nm to 1000 μm . If viewed from the standard wavenumber notation used in the field of vibrational spectroscopy, this range would span from 12500 cm^{-1} to 10 cm^{-1} . The spectrum of infrared light is further divided into three regions: the near infrared region (NIR) which covers the range of 12500-4000 cm^{-1} , the middle infrared region (MIR) spanning 4000-200 cm^{-1} , and the far infrared region – 200-10 cm^{-1} . The infrared light which falls in the NIR region can be absorbed by exciting combinational and overtone vibrations of the molecule. Therefore, the information gathered by NIR spectroscopy is mostly

nonspecific, difficult to interpret and requires mathematical analysis. Absorption of light in the FIR region is manifested by excitation of vibrations of heavy nuclei or some intermolecular vibrations. FIR spectroscopy is mostly implemented for structural analysis of crystals or doped materials. The spectra collected using light falling in the MIR region are by far the most specific. This is because frequency of the MIR light corresponds to the frequency of the fundamental molecular vibrations and therefore can be selectively absorbed or scattered. The chemical structure of the different molecular species (and the set of their fundamental vibrations) is never the same so are the MIR spectra of these molecules. This is why vibrational spectra collected using light in the MIR region are sometimes considered as the fingerprints of the molecules. These spectra are used for the precise determination of chemical composition of the samples.

At present, it is most convenient to use Fourier transform (FT) spectrometers to collect the infrared absorption or scattering spectra. Spectrometers of this type are advantageous because the whole spectrum is collected at once. Therefore, the time needed for the sample analysis is decreased. Since the technique is quite standard, it will not be described into detail here.

Raman scattering is another type of light interaction with molecules. It is a non-elastic type of scattering of monochromatic light during which the energy of the scattered light is changed (increased or decreased). Not delving into the specific details, the mechanism of Raman scattering can be explained by the light interaction with the electron cloud of the molecule. The polarizability of the molecule is modulated by the periodic changes of the length of the atomic bonds – vibrations of the molecule. Consequently, the difference in the energy of the incoming and scattered light is also carrying the information of the vibrations of the molecule.

Raman scattering and infrared absorption spectroscopies both provide information about the molecular vibrations and in this way are complementary spectroscopic techniques to one another. However, there are quite a few differences between them. For example, in certain cases some of the vibrational modes are Raman active and infrared inactive or vice versa. This can be observed in molecules which have an inversion centre. Symmetric vibrations of such molecules are Raman active and asymmetric vibrations are infrared active. This and other kinds of constrictions of the vibrational transitions are called selection rules and can be studied in more detail via investigation of the symmetry point group of the molecule. Moreover, in

Raman spectroscopy some of the molecular vibrations are sensitive to the polarization of the excitation light.

Raman scattering is a very inefficient scattering process (only one out of a million photons is Raman scattered while the rest of photons are Rayleigh scattered). Thus, a powerful monochromatic light source is needed to make Raman scattering spectroscopy into a viable technique, which could be used for chemical analysis. Nowadays, lasers are the excellent source capable of producing high intensity monochromatic light and are used extensively. However, the use of powerful visible range light sources can induce the electronic transitions in most of the samples that have some colour or impurities in their structure. In some cases, the excitation of the electronic transition can be used as a benefit since in the case of near electronic excitation the Raman scattering signal can be greatly enhanced. This method is also known as the resonant Raman scattering (RRS) spectroscopy and is used for the study of protein molecules. Even so, most of the time excitation of molecules with the visible light produces a fluorescence background in the Raman scattering spectra which overwhelms the characteristic vibrational bands of the molecule. When this happens, information about the chemical structure of the molecule is lost. Fluorescence can be minimized or completely avoided using laser light sources whose excitation wavelength falls into the near infrared region. However, in this case higher laser power should be used since the Raman scattering signal is inversely proportional to the excitation wavelength to the power of four. Another drawback of using lasers as an excitation source is the possibility of the thermal degradation of the sample. For the most part it is a concern in Raman microscopy when excitation light is focused onto a spot of small area. Besides the damaging of the sample thermal degradation can influence the collected spectrum due to changes in the chemical structure of the sample and complicate the analysis.

Both dispersive and Fourier transform spectrometers can be used for the collection of Raman scattering signal. Dispersive spectrometers are typically used together with the ultraviolet (UV) and visible (Vis) excitation light sources since efficient diffraction gratings can be fabricated. Detection of light is carried out with photomultiplier tubes (PMT) or charge couple device (CCD) arrays. In the case of NIR excitation sources, a faster way of collecting the spectrum is using Fourier transform spectrometers. The loss of signal intensity can be then compensated by increasing the number of spectrum accumulations and averaging.

Compared to the infrared absorption spectroscopy Raman scattering spectroscopy is more versatile and can be utilized easier. New advances in

Raman scattering techniques allow the spectra of the sample to be collected at long distances or even through the packaging what in the case of infrared absorption is not viable. What's more, the influence of water is a big issue in the infrared absorption spectroscopy. Even with small amounts of water, the IR spectrum of the molecules under study can be overwhelmed by the spectral absorption bands of the water molecules. Another shortcoming of infrared absorption spectroscopy is the possibility of the material to be a very strong absorber of IR radiation. In such case the IR absorption spectra will be saturated and distorted.

Since vibrational spectroscopy methods are precise and allow the chemical analysis of the molecular systems, they can be applied in various fields to study the chemical composition and to characterise the samples. The analysis of biological samples is not an exception. The qualitative and quantitative nature of the spectroscopic analysis opens up new possibilities for the application of vibrational spectroscopy. The early detection as well as the monitoring of the evolution of diseases, identification of various substances or detection of their use can be performed using vibrational spectroscopy methods. These methods can also be employed for the development of new medical products, investigation of the change of the functional properties of molecules in different media and how it affects the patients. Conventional spectroscopic techniques are not always the most convenient choice for such implementation. This is why many unconventional approaches and methods were developed. There are several such techniques like the coherent anti-Stokes Raman scattering (CARS) spectroscopy or the surface enhanced infrared absorption spectroscopy (SEIRAS) which compared to the standard techniques provide more information or enhance the sensitivity. Be that as it may, only the methods that were implemented in this work will be described here in more detail. The drawbacks and benefits of implementing these methods will be discussed, and their application for the studies of biological fluids will be overviewed.

1.2. NONCONVENTIONAL VIBRATIONAL SPECTROSCOPY TECHNIQUES

1.2.1. ATR-FTIR spectroscopy

Basic infrared absorption measurements are done in a light transmission mode where the incoming light enters through one side of the sample and is detected in the opposite. However, not all samples can be analysed in this

geometry and setup. As mentioned earlier, there are additional techniques that allow alternative measuring modes which make the measurements easier, faster or more flexible. One of these methods is the attenuated total internal reflection (ATR) spectroscopy. This method is built upon the optical phenomenon of the total internal reflection. In ATR spectroscopy this phenomenon is happening at the interface between the ATR element and the sample in direct contact with it. For this to take place the ATR elements should be made from materials having high optical density (refractive index) and in contrast the sample should have a small refractive index. Even though it is declared as a total internal reflection, some of the light reflecting from the ATR element penetrates into the other medium (the studied sample). This penetrating light is called the evanescent wave since it decays exponentially with increasing distance from the interface. The evanescent wave is partially absorbed in the sample, and the information of the absorption of the sample is gathered with the reflected wave.

If one knows the refractive indexes of the two media and the wavelength of the incoming light, the penetration depth (d) can be calculated by the following equation:

$$d = \frac{\lambda}{2\pi n_{\text{ATR}} \sqrt{\sin^2 \alpha - \frac{n_s^2}{n_{\text{ATR}}^2}}} \quad (1)$$

Here n_s and n_{ATR} correspond to the refractive indexes of the sample and the ATR element respectively, λ is the wavelength of the incoming light, and α represents the angle of incidence. On average, the penetration depth varies in the range of 1-3 micrometres, thus only a small thickness of the sample is being probed. This solves the problem of collecting the spectrum of the samples that strongly absorb IR radiation.

ATR elements can be manufactured to have a single or multiple internal reflection consequently increasing the number of interactions between the evanescent wave and the sample, and thus increasing the signal. Most common high optical density materials used for the manufacturing of the ATR elements are listed in the Table 1.

Table 1. Most common materials used for manufacturing of ATR elements and their refractive indexes.

Material	Refractive index
Diamond	2.38
Zinc Selenide	2.41
Silicon	3.42
Germanium	4

Switching from the conventional IR absorption spectroscopy setup to the ATR method is easily done via various commercially available accessories. ATR units can also be coupled with microscopes enabling ATR microscopy and imaging. Almost all types of samples (liquids, gasses, solids) can be analysed using ATR spectroscopy and there are no restrictions of sample thickness since the light penetrates only the thin surface layer of the sample. During measurements a good physical contact of the material under study and the ATR element must be ensured. This does not concern liquid samples. However, solid samples have to be pressed against the ATR element.

The spectrum collected using the ATR setup contains the same information about the vibrational spectral bands of the molecule as the IR absorption spectrum. Yet the two spectra are not equivalent. Since the penetration depth (recall equation (1)) is dependent on the wavelength of the incident light. The absorption bands which are at the higher wavenumber region tend to be less intense than the vibrational bands located at the lower wavenumber range. In order to compare the ATR spectrum to the IR absorption spectrum, this has to be taken in to account and the former spectrum has to be corrected. To the user's convenience, presently this is typically performed by the operating software.

ATR method is non-destructive and can be implemented without any major difficulties and as a result it has found uses in numerous fields. The uses of ATR spectroscopy in biomedical applications have been increasing throughout the years. ATR-FTIR spectroscopy has been shown to be useful for diagnosing and investigating the chemical changes of various cancers like melanoma [30, 31], brain cancer [32], lung cancer [33], ovarian cancer [34], and more. Biological fluid studies utilizing ATR spectroscopy showed that it

is possible to determine the blood glucose level [35], to identify the periodontal disease from saliva [36] or malaria from blood [37].

1.2.2. Surface enhanced Raman scattering (SERS) spectroscopy

Conventional Raman scattering spectroscopy is a powerful tool for chemical analysis, but there is one major drawback of employing it. The sensitivity of Raman scattering is not sufficient for the analysis of samples when the concentration of the analyte is below 1 mM. This is a considerable disadvantage since detection and investigation of molecules with low concentration is especially needed when considering in biomedical applications. In such cases another unconventional method – the surface enhanced Raman scattering (SERS), can be employed. Briefly, the SERS method is based on the enhancement of the electric field by the plasmonic effect arising in the local vicinity of the metal nanostructures and the possible charge transfer between the nanostructure and the analyte molecule. The total enhancement factor of the Raman scattering signal, depending on the method used for the enhancement, can be even up to 10^{10} .

When discovered the SERS method was not understood and thought to be a result of the changed experimental conditions. Yet, several decades later it can be to some extent explained profoundly. The enhancement arising in the SERS method is explained via two basic models: the electromagnetic model and the chemical model.

The electromagnetic model explains the more significant part of the SERS enhancement through the interaction of the electric field of the incident radiation with the metallic nanoparticles. The mechanism of action is described as follows. If the radius of the metal nanoparticle is smaller in comparison to the wavelength of the light ($r \ll \lambda$), then at any given moment the electric field of the incoming wave interacts with the whole nanoparticle at once. Upon interaction, the electric force displaces the electrons of the nanoparticle. Because the electric field is oscillating, it initiates the collective oscillations of the surface electrons (plasmons) in the nanoparticle. Furthermore, this displacement of charge can be described as an induced dipole in the nanoparticle, which in respect to the oscillations of charge changes direction. The oscillating dipole creates its own local electric field around the nanoparticle (see Fig. 1).

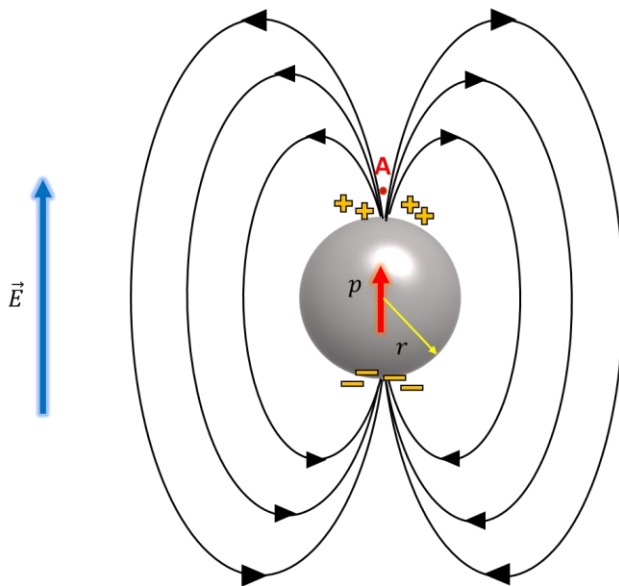


Fig. 1. Interaction of the electric field of the incoming light with the metal nanoparticle.

Since the direction of the induced dipole is parallel to the external electric field, there are two points along the axis of the induced dipole where the sum of both the external and the local electric fields is the highest. At these two points, for example point A (see Fig. 1.), the effect of the enhancement of the electric field is produced. Therefore, if the molecule under investigation is located at one of these points, it is affected by the increased electric field and as a consequence the Raman scattering is also enhanced. This is why, the surface enhanced Raman scattering is considered to be a fourfold process – Raman scattering enhancement is dependent on the electric field to the power of four. This is reasoned by the fact that the total enhancement is the product not only of the enhancement of the electric field of the incoming light but the enhancement of the electric field of the scattered light as well [38].

In order to produce the maximum enhancement one important criterion – localised surface plasmon resonance (LSPR) condition, must be satisfied. Briefly, LSPR is the resonance between the natural oscillation frequency of the plasmons and the frequency of the incoming light. Once the resonance condition is adequately met the strength of the local electric field greatly increases hence the overall enhancement is increased. The local

electric field created by the induced dipole of the nanoparticle can be expressed as:

$$E_{\text{loc}} = \frac{3\varepsilon_m}{\varepsilon(\omega) + 2\varepsilon_m} E_{\text{ext}}. \quad (2)$$

Here E_{ext} is the electric field of the incoming radiation, ε_m – the dielectric permeability of the surrounding medium, $\varepsilon(\omega)$ – dielectric permeability of the metal. The dielectric permeability of the metal is dependent on the frequency of the radiation as:

$$\varepsilon(\omega) = \varepsilon_\infty \left(1 - \frac{\omega_p^2}{\omega^2 + i\gamma_0\omega} \right). \quad (3)$$

Here the ω represents the frequency of the incoming radiation, γ_0 – is the damping constant related to the collisions of the free charge carriers with cations and the lattice defects, and ω_p – is the plasma frequency described in the Drude model as:

$$\omega_p = \sqrt{\frac{ne^2}{m_{\text{ef}}\varepsilon_0\varepsilon_\infty}}. \quad (4)$$

The ε_∞ in the equation (4) is the dielectric permeability related to the optical response of the cations, ε_0 – dielectric permeability of the vacuum, m_{ef} – effective mass of the electron, n – number of free electrons, and e – electric charge.

The forementioned localised surface plasmon resonance condition can be observed in the equation (2). In order for the local electric field to obtain the highest value, the value of dielectric permeability of the metal from which the nanoparticle is made has to be negative and twice as high as the value of dielectric permeability of the surrounding medium. However, in reality dielectric function is a complex number. Thus, the later resonance condition is applied to the real part of the dielectric permeability (related to the dispersion of radiation) function and the imaginary part (related to the absorption or radiation) is required to be as small as possible. Materials which satisfy these conditions are noble and coinage metals like silver, gold, platinum, copper, etc. The value of the real part of the dielectric function of

these metals is large and negative while the value of the imaginary part is reasonably small. Based on their chemical properties and dielectric functions in the range of visible light, the two most popular metals used for the SERS spectroscopy are gold and silver [39].

The frequency of the incoming light (or the wavelength for that matter), which satisfies the condition of the LSPR, is dependent on many variables. The most important of these are the shape and the size of the nanoparticles. For example, the LSPR wavelength increases when the size of the particle increases. The shape of the nanoparticles plays a big role since depending on the shape there can be one (spheroids), two (rods) or even multiple (prisms and other complex shapes) dipole resonances. These, of course, will have different wavelengths corresponding to their resonances what can be exploited if more than one excitation wavelength is used. Also, by varying the shape and size of the nanoparticles, the LSPR wavelength can be tuned to match the wavelength of the incoming light [40]. The LSPR wavelength can be determined from the UV-Vis absorption spectra of the nanoparticles.

One more effect associated with the electromagnetic model is the coupling of the resonances of the two or more nanoparticles. In such case where two nanoparticles are in a proximity the local electric field of both nanoparticles enhance the Raman scattering of the molecule if it is located in between the two nanoparticles. Such structure of two nanoparticles is called a “hot-spot”. The formation of “hots-spots” is essential for the high enhancement factor and is also considered to be the explanation for the so-called dark mode effect [41]. The term dark modes describe the dipole resonance modes which can be unseen in the UV-Vis absorption spectrum of the nanoparticles. These modes can explain the fact that the SERS effect can be achieved even having the excitation wavelength far from the plasmon resonance frequency of the single nanoparticle.

The electromagnetic model explains the enhancement factor whose value can be around 10^4 - 10^7 . However, the enhancement factor is strongly dependent on the distance between the molecule and the nanoparticle. The highest enhancement is observed only in the close vicinity of the surface of the nanoparticle and drops significantly when the distance increases. Nonetheless, effects described by the electromagnetic model are always present when nanoparticles made from metal (having free electrons) are used. That is why, it is considered to be the most important and is always included in the explanation of the SERS effect.

The chemical model, even though it explains a smaller part of the SERS enhancement, is still an important mechanism and has to be considered. There

are several effects that could be viewed as chemical enhancement. Therefore, for the sake of clarity, the chemical model is described as any modification of the Raman polarizability tensor, which is a result of the adsorption of the molecule onto the metal surface. Most notable of these effects is the photo-induced charge-transfer in the metal-adsorbate complex. The formation of this complex can lead to a non-direct excitation of the molecule. Because of the formation of the chemical bond, the orbitals of the adsorbate and the Fermi level of metal interact. The change of the electronic state of the adsorbate molecule may lead to the energy difference between the Fermi level and the highest occupied molecular orbital (HOMO) or lowest unoccupied molecular orbital (LUMO) to become equal or to be matched by the energy of the radiation used for excitation. In such case the absorbed photon could induce a charge transfer between the HOMO to the unoccupied energy level above the Fermi level or from the occupied energy levels lower than Fermi level to the LUMO. The schematic representation of the possible charge transfer pathways is presented in the Fig. 2. The SERS photon is then the direct result of the relaxation by emission of a photon.

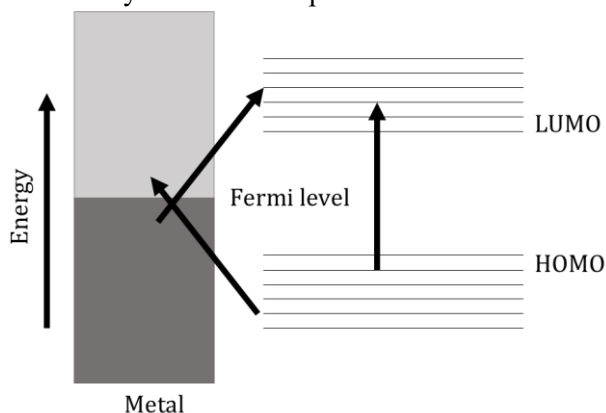


Fig. 2. The schematic representation of the charge-transfer mechanism in the SERS phenomenon.

The chemical enhancement model typically explains the enhancement factor whose value is only around 10^1 - 10^2 . Also, though not completely necessary the chemical model has its highest contribution only in the specific cases when the molecule is adsorbed chemically – a bond forms between the metal surface and the adsorbate. This is why the chemical model tends to be not considered in most cases.

The intensity of the SERS signal depends not only on the parameters of the active layer but also on the properties of the analyte itself. The intensity of the SERS signal depends on the coverage of the surface of the nanostructure. The more of the analyte molecules adsorb the more intense vibrational bands are observed. To evaluate the correct enhancement factor, this has to be taken into account and the coverage of the nanoparticles should be calculated. This can be performed using adsorption isotherms. However, the intensity increases only to a certain point at which the additional analyte molecule adsorption can even decrease the signal. This is supposed to be reasoned by the dampening of the resonance of the nanoparticles. Also, different adsorption properties of the molecules lead the different orientation of the analyte molecules relative to the surface and hence different selection rules for the enhanced vibrations [42]. It is well-known that the vibrational modes which are perpendicular to the surface are enhanced the most [43]. This is why the SERS spectra of many molecules differ from the conventional Raman scattering spectra.

The enhancement of the Raman scattering intensity that can be achieved employing the SERS method can be quantified by evaluating the enhancement factor [38, 42, 44]. It is normally calculated by the following equation:

$$EF = \frac{I_{\text{SERS}}}{I_{\text{Raman}}} \cdot \frac{N_{\text{Raman}}}{N_{\text{SERS}}}, \quad (5)$$

where I_{SERS} and I_{Raman} represent the intensity of the vibrational band associated with the same vibration in SERS and Raman scattering spectra, respectively. The N_{SERS} and N_{Raman} are the total number of molecules involved in the both scattering processes. The evaluation of the latter parameters is not trivial and more experiments are needed for that reason. Another method for quantification of the enhancement is possible. In analytical chemistry it is easier to calculate the so-called analytical enhancement factor. It can be calculated by the following equation:

$$AEF = \frac{I_{\text{SERS}}}{I_{\text{Raman}}} \cdot \frac{c_{\text{Raman}}}{c_{\text{SERS}}}, \quad (6)$$

here the c_{SERS} and c_{Raman} represent the concentrations of the analyte molecules used for collection of the SERS and the Raman scattering spectra, respectively. It must be noted that the analytical enhancement factor cannot be used for the precise characterization of the colloidal solutions or the SERS active substrates. However, analytical enhancement factor is quite useful

when different types of signal enhancement methods are employed for the same problem if the same set of experimental parameters are used.

Due to the high enhancement factor produced in the surface enhanced Raman spectroscopy this method is extremely sensitive and is a valuable tool for chemical analysis [45]. It was shown that even single molecule analysis can be performed by applying the SERS spectroscopy [46-48]. The SERS spectroscopy as a method is used in many fields. It was used in the food industry to detect the contaminants [49, 50] or pathogenic species [51, 52]. It was used for analysing and characterising of inorganic materials [53, 54]. In the field of biomedical sciences SERS spectroscopy is constantly being applied as a faster and more affordable way for the identification of various diseases markers in biofluids such as tears, urine, saliva, blood, etcetera [55, 56]. In addition, this method is implemented for identification and characterization of various cancerous tissues [57, 58].

The versatility of the colloidal SERS approach is that the shapes, sizes and composition of nanoparticles can be tailored to various applications and environments. The particles can be isolated [59, 60], or functionalised to be adsorb certain molecular species [61, 62]. However, the viability to employ the SERS spectroscopy as a common detection method is determined by the reproducibility of the used substrates. Uncertainty of the reproducibility of the SERS substrates is a well-known issue, which was and is addressed constantly [63, 64]. Of course, implementation of the SERS method does not necessarily require the use of colloidal solutions. Instead, other nanostructured metal surfaces can be used as SERS substrates. That is why a lot of effort is being put to create the non-colloidal SERS active surfaces [65, 66].

1.2.3. Electrochemical surface enhanced Raman scattering (EC-SERS) spectroscopy

Another method for implementing the SERS effect is using the roughened surface of an electrode in an electrochemical experimental setup. Such method is called electrochemical SERS (EC-SERS) spectroscopy and can provide supplementary information about the molecule under study or allow control of the adsorption processes. Both, electromagnetic and chemical effects described earlier are used to explain the mechanism of the EC-SERS. As with the colloidal solution approach, the enhancement factor depends on the preparation of the active layer (electrode surface), which has to be roughened. Several preparation methods can be used. The surface can be roughened

electrochemically, structures can be created via electrodeposition, or nanoparticles from the colloidal solution can be simply dried onto the surface.

One benefit of the EC-SERS spectroscopy is the possibility to apply and vary the electric potential of the SERS active surface. In such a way, the adsorption properties and orientation of the analyte molecules relative to the surface can be changed and analysed. The electrochemical information collected during the measurements can be used to evaluate the chemical changes and other properties of the adsorbate. Applied electric potential also shifts the energy of the Fermi level of the metal and consequently reduces or increases the difference of the Fermi level with the HOMO or LUMO energy levels of the molecule. This in turn leads to the differences in charge-transfer enhancement mechanism described above and the increase of Raman scattering enhancement (see Fig. 3.)

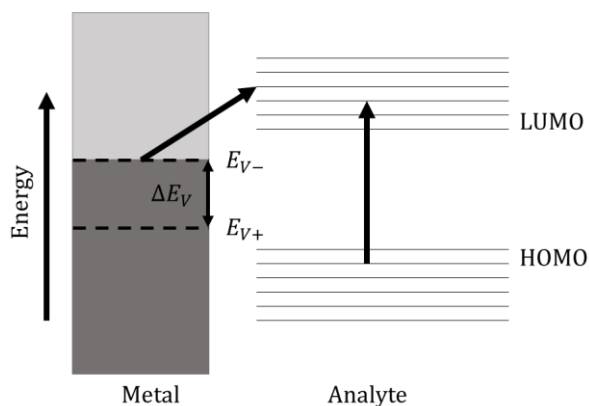


Fig. 3. Schematic representation of the change of the Fermi level in the metal by varying the applied potential.

Besides the Raman spectrometer, the standard EC-SERS setup requires a potentiostat-galvanostat. It is a device used in electrochemical research, which is able to apply and control the applied voltage with high precision. In most cases it has three main electrodes connected with it. One of these is the working electrode (WE), which in case of EC-SERS spectroscopic measurements has to be made from the SERS active metal. The second electrode is called the counter electrode (CE), which closes the electrical circuit and the third is the reference electrode (WE), which is used for a precise evaluation of the electric potential. All of these electrodes come in a variety of shapes, designs and materials that can be tailored to the specific experiment.

During measurements, these electrodes are placed in an electrochemical cell filled with the solution of the analyte molecules. Electrochemical cells are often custom-made in order to fit the design to the requirements of experimental setup. Moreover, there are various other variables and parameters that have to be chosen before and during the collection of the spectrum. These include the choosing of the electrolyte solution, electrochemical window (the range of applied potential), scanning speed at which the potential is going to be applied, etc. There are no standard parameters fit for every situation and one or all of them can change depending on the analyte, required information or setup. Hence, it will not be discussed in detail here.

Even though the electrochemical SERS method is not as widely used as the SERS spectroscopy, it has also been applied in various fields. It has been shown that EC-SERS can be used for sensitive detection of molecules in bodily fluids [67] or detection of disease markers [68]. Studies on bacteria have also been performed [69]. Since the EC-SERS method is sensitive to the change of the geometry of the surface species it can additionally be employed as a sensor for structural changes of biomolecules [70, 71].

1.3. DATA ANALYSIS

1.3.1. Pre-processing of the spectra

The analysis of the spectral data collected using vibrational spectroscopy methods is generally started with the pre-processing of the collected spectra. This is done in order to eliminate the discrepancies, which arise during signal acquisition and could influence further quantitative or qualitative analysis. The discrepancies, which cannot be avoided during the measurements, are associated with various effects like scattering, the influence of the gasses in the composition of the atmosphere, etcetera. Also, variation of the parameters of the sample itself, for example thickness, non-homogeneous composition, and other can influence the spectrum and need to be taken into account as well. The pre-processing steps are chosen in respect to the method used for collection of the spectrum and the type of the sample.

The standard steps of the pre-processing involve the compensation of the atmospheric effects, especially the influence of CO₂ and H₂O gasses (in case of infrared absorption spectroscopy), baseline correction and normalization. There are several baseline correction algorithms, which are used depending on the sample and the setup. For example, some algorithms simply eliminate

the offset of the spectrum or deal with the influence of scattering. There are more complex baseline correction algorithms like rubberband. This method is based on finding the convex hull of the set of data points – the smallest convex polygon, that encloses the data points. This method is used to correct more complex deviations of the baseline and can be found in most of the spectroscopic software programs. Concave rubber band-correction is another algorithm used for correcting the baseline. This method is iterable and can correct baselines which beside other effects are distorted by fluorescence. Spectra normalization is used to eliminate the differences in overall intensity of the vibrational bands caused by the variations of sample thickness or other parameters.

Other pre-processing methods like smoothing or post zero-filling (in case of FT devices) are sometimes also employed to obtain the better signal-to-noise ratio. However, they should be used with caution since the overuse can lead to the loss of spectral resolution and information. Finally, derivatives of the spectra are calculated when there is a need to distinguish the overlapped spectral bands.

1.3.2. Methods of chemometric analysis

When the spectra are pre-processed further qualitative or quantitative spectroscopic analysis is possible. Qualitative analysis (identification of the molecules in the sample) can be done simply by comparing the collected spectra with the library spectra of pure components. For this reason, various libraries of organic and inorganic compounds are available online [72, 73]. The spectra of isomers and derivatives of the most common molecular compounds, collected with different spectroscopic methods, can be found in these libraries. Various manufacturers of spectroscopic devices also include spectral libraries within their spectral software package. This is quite beneficial since it is most efficient if one can use the spectral library composed of the spectra collected using the same type of device and the same set of parameters as the test spectra. Therefore, often a creation of a library of pure components is the first step of the sample analysis.

In most spectra, the intensity of the spectral bands is proportional to the concentration of the molecules under study. This allows the quantitative analysis of the studied sample. If relationship between the concentration and intensity is linear, the concentration can be determined by calculating the integral intensities of the characteristic vibrational bands. Ratio of the integral intensities of the spectral bands in the spectrum of the pure compound and in

the spectrum of the sample will correspond to the concentration of the molecules present in the sample. If the relationship is not linear or unknown, a calibration curve (a graph of the integral intensity value versus the concentration of the molecule) must be made in order to determine the concentration of the molecules in the sample.

However, some samples have complex spectra, which cannot be so easily distinguishable, and simple quantitative or qualitative analysis cannot be carried out. Also, sometimes only the analysis of a large data set is only possible since a lot of spectral variation present in the individual spectrum does not represent the true nature of the problem. Both cases are true for the studies of biological samples since biological tissue or fluid is a complex sample containing many molecules. Therefore, bigger data set is needed to confirm the relationships between the spectral markers and the chemical changes of the sample. In these cases, chemometric analysis methods are also utilized.

Methods of chemometric analysis are mathematical multivariate analysis methods used for analysing the chemical information. These methods allow the user to correlate the data provided by the instrument (spectra) to the change of physical properties of the sample (concentration, structure, etc). Thus, using chemometric analysis it is possible to separate a vast number of data points into categories which are similar in respect to their spectral features, that correspond to the chemical changes within the sample.

One such method is the hierarchical cluster analysis (HCA). This method groups the data set into clusters ordered in a branching manner and presented as a dendrogram. The first branch contains the whole data set. It splits into smaller branches that contain the most similar data points and so forth. The similarity between the data points is evaluated by calculating the sum of the squared error (SSE) by the following equation:

$$SSE = \sum_{i=1}^K \sum_{x \in C_i} ED(c_i, x)^2. \quad (7)$$

Here, the K is the number of clusters, x – is the object belonging to the i^{th} cluster C_i , c_i is the centroid of the C_i , and ED corresponds to the Euclidean distance between the centroid and the object. During the clustering procedure the algorithm groups the data into clusters which minimize the SSE. This way the points closest to the centroid are categorised as a cluster. Two types of algorithms can be utilized for the HCA. The first group of algorithms start

from one individual cluster and splits it into smaller and smaller clusters (divisive clustering). The second group of algorithms considers all objects of the data set as individual clusters and then groups them until one all-inclusive cluster remains (agglomerative clustering). The most often used Ward's algorithm belongs to the agglomerative group.

Another widely used multivariate analysis method is the principal component analysis (PCA). The PCA is used to simplify the complexity of the data set with high dimensionality in the meantime keeping the trends and patterns of the data. This is performed via geometrically projecting the data onto lower dimensions, called principal components. The principal components are found by first calculating the covariation matrix. In case of two-dimensional (X, Y) data, the covariation matrix can be written as:

$$C = \begin{pmatrix} \text{cov}(X, X) & \text{cov}(X, Y) \\ \text{cov}(Y, X) & \text{cov}(Y, Y) \end{pmatrix}, \quad (8)$$

Where the covariance is calculated as follows:

$$\text{cov} = \frac{1}{n-1} \sum_{i=1} (X_i - \bar{X})(Y_i - \bar{Y}). \quad (9)$$

Upon solving the eigenvalues and eigenvectors of the covariance matrix (9) the eigenvalues are arranged from the largest to the smallest and this arrangement is then called a set of principal components. The larger the value of the principal component is, the more variation of the data set it represents ("explains"). In order to minimize the dimension, a number (m) of principal components with the highest values are chosen, and the rest are neglected. Then, the new data are calculated according to the following equation:

$$D_{new} = V_m D. \quad (10)$$

Here, the D_{new} – represents the new data set, D – the original data set, and V_m is the matrix of the chosen number of eigenvectors. This way the projection of the original data set in the space of the m eigenvectors is calculated.

CHAPTER 2.

SERS SPECTROSCOPY OF KIDNEY AND BLADDER CANCERS

2.1. CANCER AS A DISEASE

Cancer is by far one of the most prevalent diseases in the world. It is the leading cause of debilitation for humans and animals alike. The rate of cancer diagnosis in humans is increasing every year, and the future projections are grim. It is predicted that the annual worldwide cases of cancer are going to increase to 24 million new cases worldwide by 2035 [74].

The term “cancer” describes a collection of related diseases where the abnormal cells of the body begin to divide uncontrollably and through the body fluids spread into other parts of the body (metastasize). Almost all types of cells can become cancerous and therefore this disease can originate throughout the whole body. Regarding the cell type, six major categories of cancers are distinguished. These are carcinoma, sarcoma, leukaemia, lymphoma, myeloma, and mixed types (having two or more components of the cancer). Because of the fast and uncontrollable proliferation, most cancers form tumours that obstruct the normal functioning of the organs and cause severe damage or death.

There are several causes of human cancers. Around 5% of all cancers are caused by viruses, 5% by radiation and 90% by carcinogenic chemicals. It is also believed that some types of cancer can result from an increased number of bacteria [75-77]. All these causes lead to the mutations of the cell genome – the change in its DNA structure. However, this process is not so straight-forward, as it is estimated that around 80 gene mutations or alterations are needed for a cell to become cancerous. As follows, the development of cancer is often analysed by multistage models, that consist of initiation, promotion and progressions stages. Nevertheless, not wanting to delve too deep in to the explanation of the cellular mechanism, the thorough analysis of cancer formation will not be provided here. A more curious reader can look for more information in the literature [78].

Typically, the tumours formed by the cancerous cells are classified into two types: benign and malignant tumours. One of the main characteristics of benign tumours is their slow growth. They can even stop growing or regress. Most of the benign tumours are not lethal. They do not metastasize and only damage the surrounding normal tissue by pushing against it and obstructing

the normal functionality of the affected organs. Malignant tumours on the other hand behave differently. Their growth is fast and it never regresses. These tumours are prone to metastasize and invade or replace the surrounding tissue. As a consequence, malignant tumours severally disrupt the functionality of the body and are most of the time lethal if not treated.

2.1.1. Main aspects of cancer development

As there are over 100 types of cancers [79] it is virtually impossible to briefly overview the intrinsic details of the cancer development. Nonetheless, a few crucial aspects of it should be mentioned. It can be stated that all the changes happening in the cancerous cells are all linked to one specific goal - sustaining of the continuous uncontrolled proliferation. Cancerous cells become immortal-like because of the deactivation of the controlled cell death. This is achieved by reversing the telomere (specific part of chromosomes) shortening and disrupting other chemical processes [80]. Also, to further increase their survival, cancer cells trick the immune system [81] and evade normal signalling [82]. The metabolism of the cancerous cells is also affected. Initially, when the tumour is small, its environment is sufficient with nutrients and oxygen required for the normal cell metabolism. However, the fast proliferation ultimately leads to a point where certain parts of cancer experience hypoxic (lacking oxygen) conditions, the lack of required nutrients, and inability to dispose waste. This is why cancers are shown to activate angiogenesis – the growth of a vascular system in its vicinity [83]. Cancers send signals to the body, which initiate the growth of new blood vessels around the cancer. This way cancer ensures the availability of nutrients. Still, the increased growth rate of the cancers requires a lot of energy. Hence it has also been shown that cancers increase the transportation and uptake of glucose molecules even beyond the requirement for sustaining the functionality of the cell [84]. Furthermore, cells of certain cancers produce ATP molecules (the molecular “energy carriers”) not in a normal fashion - via glucose oxidation, but via anaerobic glycolysis even though the yield of the latter process is 18 times smaller. This behaviour was first described by Otto Warburg and is known as the Warburg effect [85]. A lot more changes are happening in the cancerous cells, but it is beyond the scope here. Though many cancer development pathways are known, the changes happening in the cancer while it develops are still being researched and their functions are being analysed. However, one can say that the overall common hallmarks of carcinogenesis are genetic changes of the cell DNA that lead to sustaining

proliferative signalling, evading growth suppressors, resisting apoptosis (cell death), enabling replicative immortality, inducing angiogenesis, activating invasion and metastasis, reprogramming energy metabolism and evading immune destruction [86].

2.1.2. Staging and classification of cancers

The aggressiveness, invasiveness and overall size of the tumor depend on its stage of development. Five stages to describe the development and the spread of the disease are distinguished and used in histological analysis. The Stage 0 is the earliest stage where the tumor has not yet formed in the body. Only abnormal cells with a potential of becoming cancer are present. This stage is sometimes synonymously referred as a carcinoma *in situ*. Stage I describes the already formed tumours, which are small and located only in one area. These cancers are also called early-stage cancers. Stage II and stage III describe larger cancers that have grown into adjacent tissues or lymph nodes, but have not spread further into the body. Finally, stage IV describes cancers that have proliferated beyond the place of origin and have spread to other parts of the body – metastasised. These are also called metastatic cancers.

Besides staging, a more detailed classification is used to describe cancers. This system of classification is called TNM (tumor, nodes, metastases) [87]. This system describes cancer in accordance to its size and its localisation in relation to its origin (T), whether it has invaded the nodes of the lymphatic system (N), and if it has metastasised (M). A numbering value follows each letter symbol. Values from zero to four are used next to the symbol T where the larger number corresponds to the bigger size and larger spread of the cancer. The number 0 indicates that the main tumour cannot be found. Sometimes letters “a” and “b” are also provided next to the numbers for more detail. Values from zero to three are used next to the symbol N and increasingly correspond to a higher invasiveness into the lymph nodes. The symbols denoting metastases are followed only by the numbers 0 or 1, which like in the programming language correspond to the true or false values (absent or present metastases, respectively).

One more classification of cancers is their grading. The grading describes how abnormal the cancer cells look compared to the normal ones when viewed under a microscope. Tumor grades are denoted by the letter symbol “G” and the following number, which can take a value from one to four. Cancers whose cells look and behave mostly like normal cells are low grade tumours. These types of cancers (G1) are less aggressive. Intermediate tumours (G2) are

composed of somewhat abnormal looking cells. High grade tumours (G3) have poorly differentiated cells and have no structure or pattern. The highest-grade cancers (G4) consist of cells that look most abnormal and can spread and grow the fastest, and thus are the most aggressive.

2.1.3. Kidney cancer

Kidneys carry out an important role in the homeostasis of humans. The key function of these bean-shaped organs is the filtration of the blood. By eliminating unrequired substances (producing urine) they dispose waste products produced by metabolism, control the fluid, acid-base balance, and the concentration of electrolytes. Besides that, kidneys produce hormones that help to regulate the blood pressure.

Kidney cancer is one of the top ten common malignancies and accounts to around 3% of the annual diagnosed cancer cases [88]. There are six types of kidney cancer: renal cell carcinoma (85%), transitional cell carcinoma (8%), nephroblastoma also called Wilms tumor (5-6%), collecting duct tumours (< 1%), renal sarcomas (< 1%), and renal medullary carcinomas (< 1%) [89]. The renal cell carcinoma (RCC) represents the majority of cases of all kidney cancers and can be further categorised with more detail into several subtypes in accordance to the morphology, growth pattern, cell of origin and other parameters. The most common subtypes of the RCCs are: clear cell (75%), papillary (10%), chromophobe (5%), cystic-solid (1-4%), collecting ducts (1%), and other [90]. In most cases the mutation of the tumor suppressor gene – Von Hippel-Lindau gene (VHL), is the root cause of the development of the clear cell renal cell carcinomas (ccRCCs). This drives a cascade of changes and results in an activation of genes that regulate angiogenesis, glycolysis, and apoptosis. This is why human ccRCC tumours are rich in lipids, glycogen and are highly vascular [91].

As with all tumours, kidney cancer can be most efficiently treated when it is in the earliest stages of development. Depending on the size of the tumor, partial or radical nephrectomy (surgical removal) procedures are performed in order to treat the patient. Radical nephrectomy – the surgical removal of the whole kidney, is performed when the tumor is in the stages II-IV. This means that the tumor is large (more than 7 cm in the largest dimension) or has spread beyond the vicinity of the kidney. Partial nephrectomy is feasible when the tumor is in the stage II, but most of the time is performed if the cancer is diagnosed early (in the stage I of its development). Then, only the cancer can be removed, leaving the functioning normal tissue. The effective partial

nephrectomy surgery (the removal of all cancerous tissue) is a must. Thus, during a surgery it is critical to determine the exact border between normal and cancerous tissues. The standard procedure for this is the histological examination of the biopsied tissue. This procedure is carried out by making a thin tissue sample (sectioning) and staining the cells. Analysis is performed via optical microscopy during which the subjective conclusions on the cell shape, structure and overall tissue are made. The whole analysis is time costly since the biopsied tissue has to be brought to the histology laboratory, the sample has to be prepared and then analysed. Furthermore, the conclusions of the analysis are based on the expertise of the staff. This is why a tool that would allow precise discrimination between the cancerous and normal tissues and would provide additional information is in demand. One way this could be achieved is by analysing the small chemical changes induced by the disease.

2.1.4. Bladder cancer

The bladder like kidneys is an organ of the renal system. It is a muscular sack that excretes urine formed from the waste products of the human metabolism. Besides the storage and excretion of the urine, the bladder also prevents the reabsorption of the waste products back into the blood system.

Bladder cancer though detected less often than kidney cancer is still one of the most prevalent malignancies throughout the world [92]. It is more common to men being the fourth most prevalent. For men this disease occurs at least four times more often than for women. Bladder cancer is classified into three categories. These are the urothelial carcinoma, squamous cell carcinoma and adenocarcinoma. The urothelial carcinoma is by far the most prevalent with incidence rate around 95% [93]. Another classification of bladder cancer by the behaviour of the cancer into non-muscle-invasive and muscle-invasive cancers is used. Of all diagnosed bladder cancers around 70-80% of them are noninvasive. Noninvasive cancers are further classified into the ones confined to the mucosa (carcinoma *in situ* and papillary carcinoma) or submucosa. The mutation of the telomerase reverse transcriptase (TERT) gene responsible for DNA protection and cellular aging processes is thought to be one of the leading mutations that starts the bladder cancer development. It was found to be involved in at least 70% of bladder cancers [94].

Only the removal of bladder cancer is feasible when it is in the first stage of development or its size and localisation allow it. The removal is done via transurethral resection of bladder tumour (TURBT). When the tumour is

spread, the radical cystectomy procedure – the surgical removal of the whole bladder and sometimes the neighbouring tissues is performed.

The standard procedure for diagnosis of bladder cancer is white light cystoscopy (WLC) during which a biopsy of the tissue is taken. Photodynamic diagnosis (PPD) with the use of 5-aminolaevulinic acid or hexaminolevulinate acid also known as blue light cystoscopy is also being employed. However, these detection methods have their limits. The WLC lacks sensitivity when detecting small malignant tumours confined to the mucosa, specifically the carcinoma *in situ* [95]. The PPD is more sensitive, but it is less specific [96]. Without the good specificity and sensitivity of detection, a wrongful diagnosis can be made and it may be required to repeat the procedure. This is unfortunate and should be avoided as much as possible since the method of detection is invasive and pain during urination, urinary frequency, haematuria and infection are frequently occurring post-procedural effects. Another method implemented for the detection of bladder cancers is the bladder cell cytology. This procedure consists first of the gathering of bladder washings and second the analysis of the cells that were washed out. Bladder washings are gathered during or prior the cystoscopy procedure. During such procedure a certain amount of saline solution is repeatedly instilled to and recovered from the bladder [97]. After that, the cells that were washed out are gathered, and their morphology is analysed under a microscope. This type of detection has higher specificity but is not sensitive enough for efficient detection especially for the low-grade tumours [98]. The overall efficiency of the bladder washing analysis is evaluated to be around 40%. This is why a sensitive detection method with high specificity is needed.

2.1.5. Extracellular fluid

The definition of extracellular fluid is simple – it pertains all body fluids that are outside of the cells. Accordingly, blood plasma, interstitial fluid, lymph, and transcellular fluid are all parts of the extracellular fluid. The extracellular fluid plays an essential role in the metabolism of humans. Because of its composition, which is full of amino acids, sugars, fatty acids, coenzymes, hormones, salts, and other molecular species, it serves as the delivery system for cells transporting nutrients to and waste products away from the cells. In addition, it provides a stable environment for the cells, ensuring their normal functioning. In fact, the role of the extracellular fluid is so important that it is currently suggested that the interstitium – the contiguous fluid filled space between the structural barriers of cells or organs, should be

regarded as an organ itself [99]. The direct relation of the extracellular fluid with the metabolism of the human body results that the changes in the extracellular fluid can indicate various diseases or organ failure [100, 101]. Thus, the analysis of the extracellular fluid with the purpose of identifying diseases or other illnesses is often the easier and faster way. This is proved by the fact that blood test is one of the most often performed procedures for disease diagnosis.

2.2. VIBRATIONAL SPECTROSCOPY OF CANCERS

One way of solving the problem of the distinction of cancerous and normal tissues is the analysis of the chemical changes between these tissues. These chemical changes, which result from the changed metabolism and behaviour of the cancerous cells, are delicate, thus precise chemical analysis is required. Vibrational spectroscopy methods are one of the first choices when subtle chemical analysis of the samples needs to be conducted. Therefore, there are already numerous scientific researches conducted on the analysis of cancers via the FTIR absorption or the SERS spectroscopies. Both of these methods have been applied for the analysis of the cancerous tissues and cells of the brain [102, 103], breast [104, 105], lung [106, 107], and other [108, 109]. Also, vibrational spectroscopy studies focused not on the direct analysis of the cancerous tissues but on the detection of cancer through various biological fluids (also known as “liquid biopsies”) were conducted [110]. Kidney cancer and bladder cancer are not an exception and were analysed previously. Vibrational spectroscopy studies regarding the tissue analysis of these cancers showed that the FTIR absorption can be useful in discriminating the types of tissues. It was shown that the SERS spectroscopy can be utilized for bladder tissue imaging [111]. Furthermore, studies regarding liquid biopsies for bladder cancer detection were conducted using the FTIR absorption spectroscopy [112]. Despite that, several problems regarding the analysis of tissues exist. The minute chemical changes between the cancerous and normal tissues can be difficult to analyse from the collected spectra of bulk tissues. This is because the most intense bands will be related to and the overall shape of the spectra will be determined by the molecules which comprise the bulk tissue – the structural components of cells. Hence, discrimination via simple comparison of the spectra of normal and cancerous tissues is impossible. Even when statistical analysis methods are employed the discrimination of tissues is difficult. What is more, analysis of the tissues is burdened by the presence of water. This is especially important in case of the FTIR absorption

spectroscopy. Water is a good absorber of the infrared radiation and has intense vibrational bands located at $1400\text{-}1800\text{ cm}^{-1}$ and $2600\text{-}3800\text{ cm}^{-1}$. This again causes a problem to observe the slight changes in the chemistry. The spectral information of the small chemical differences is overlapped with the spectral information from the composites with high concentration. Because of this problem, tissue cryosections – thin slices of tissue - are often measured using FTIR absorption spectroscopy. However, the procedure of creating these cryosections is time-consuming and laborious. Also, as already mentioned during sectioning cells are damaged. A faster and more convenient way is to use the ATR-FTIR spectroscopy. The information is gathered only from the small depth of the sample thus the influence of the bulk tissue and water is minimized and the spectra of the tissue have more distinct features. However, the surface of the ATR element must be cleaned after every measurement. In this respect, the SERS spectroscopy is better suited for tissue analysis because information is collected only at the nano-structured surface (enhancement factor is the highest near the surface). However, the spectra of the bulk tissue will always have the spectral bands of conventional Raman scattering which can overlap the SERS bands and make the analysis difficult. Therefore, the measurement of the extracellular fluid is a better choice for the analysis of the cancer. The extracellular fluid samples can be made thin, thus eliminating the impact on the spectra from the bulk composites and water. Meanwhile, the extracellular fluid is directly linked to the metabolism of the cells since all nutrients and waste products are transported via this medium. The composition of the extracellular fluid, therefore, is also altered when the cells become cancerous and change their metabolism. In this regard the analysis of the extracellular fluid not only is more beneficial for vibrational spectroscopy but also retains the same or related information which would be gathered during spectroscopic tissue analysis. The possibility to discriminate the cancerous kidney tissue by analysing the extracellular fluid of the said tissue via FTIR absorption spectroscopy was already shown to be viable by our group [113].

2.3. EXPERIMENTAL DETAILS OF VIBRATIONAL SPECTROSCOPY OF CANCERS

2.3.1. Preparation and characterisation of colloidal solutions of silver nanoparticles

Colloidal solutions of two types of silver nanoparticles (AgNPs) were prepared in this work. The citrate reduced and stabilised silver nanoparticles were made by the oxidation-reduction reaction in accordance to the protocol described by Lee and Meisel [114]. Briefly, a 9 mg of silver nitrate (AgNO_3) (Fluka) was dissolved in 50 ml of deionized water ($18.2 \text{ M}\Omega\text{cm}^{-1}$), which was preheated to 45-50 degrees Celsius. Then, the whole solution was heated until a boiling point was reached. After that, 1 ml of an aqueous solution of 1% (m/v) of trisodium citrate ($\text{Na}_3\text{C}_6\text{H}_5\text{O}_7$) (Sigma Aldrich) was added to reduce and electrostatically stabilize the nanoparticles. The whole mixture was kept at near boiling temperature for an additional hour and then quickly cooled to room temperature in an ice bath. During the whole preparation procedure, vigorous stirring of the solution was applied. The prism shaped silver nanoparticles were prepared in accordance to the procedure described by D. Aherne et al. [115]. This is a two-step procedure comprised of the preparation of the seed particles and the growth of the nanoparticles. The preparation of the seed solution is as follows. At first, 5 ml of aqueous 2.5 mM solution of trisodium citrate is mixed with a 0.25 ml of 500 mg/l poly sodium styrene sulfonate (PSSS) (Fluka) solution and a 0.3 ml of 10 mM sodium borohydride (Sigma Aldrich) solution (as a strong reducing agent). Then 5 ml of a 0.5 mM solution of silver nitrate is dropwise added in the mixture with the speed of 2 ml/min. Upon addition of the silver nitrate the colour of the solution turns to light yellow. During the seed preparation procedure vigorous stirring was applied. The nanoparticle growth procedure begins with adding 75 μl of a solution of 10 mM of ascorbic acid (Sigma Aldrich) (as a weak reducing agent) and 25 μl of the freshly prepared seed solution to 5 ml of distilled water. Then, with a rate of 1 ml/min, 3 ml of a solution of 0.5 mM silver nitrate is dropwise added to the whole mixture. When the silver nitrate is added the colour of the solution starts to change and the final colour (size of the particles) depends on the volume of the seed solution. Finally, to stabilize the prepared nanoparticles a 0.5 ml of 25 mM trisodium citrate solution is added. The prepared colloidal solutions were refrigerated when not in use and it was determined that the spherically shaped nanoparticle solution

was stable for at least three weeks while prism shaped nanoparticle solution could be used for one week.

The prepared colloidal solution was centrifuged for 10 minutes with a speed of 6500 rpm in order to increase the nanoparticle concentration in the solution. After centrifuging, half of the initial volume was taken as a supernatant and discarded. The choice of the centrifuging speed will be discussed below.

The prepared colloidal solutions were characterized by measuring their UV-Vis spectra to determine the plasmon resonance wavelength of the nanoparticles. The spectra were collected in the wavelength region from 250 nm to 800 nm with a spectral resolution of 5 nm. Spectra were recorded using spectrophotometer Lambda 1050 (Perkin-Elmer) equipped with two sources: halogen and deuterium lamps. Three detector system (photomultiplier tube, InGaAs and PbS) was used for the signal detection. Since the Lee-Meisel synthesis procedure produces spherically shaped nanoparticles the average size of the nanoparticles was evaluated from the UV-Vis spectra of the solution in accordance to the Mie theory of scattering [116, 117]. The theoretical calibration curve, which can be used to calculate spherically shaped nanoparticle size, is as follows:

$$d = \sqrt{24.01 + 100 \cdot (\lambda_p - 385)^2} + 4.9, \quad (9)$$

here, the λ_p represents the peak absorption wavelength.

Transmission electron microscopy was applied in order to determine the shape of the nanoparticles in the solution and whether the solution is uniform. The micrographs of the dried colloidal solution were taken with Libra 200 (Carl Zeiss, Oberkochen, Germany) at the Institute for Polymer research in Dresden, Germany.

2.3.2. Sample preparation

The samples of both normal and cancerous kidney tissues were obtained from the Urology centre of Vilnius University Hospital Santaros clinics. The spectroscopic research of the kidney tissue was done with the approval from Vilnius region bioethics committee (doc. No. 158200-15-803-312). The tissue samples provided for the spectroscopic analysis were taken during partial or radical nephrectomy surgeries of patients from both sexes. Furthermore, other restrictions, for example age, weight, diet and other, were not applied for the

selection of patients whose kidney tissue samples were investigated. This was done in order to include all the possible aspects of the disease and to get a full picture of the problem from the point of spectroscopic analysis. When resected, the tissues were brought to the Physics Faculty of Vilnius University. The spectroscopic analysis of the extracellular fluid of the tissues was conducted in the vibrational spectroscopy laboratories of the Institute of Chemical physics within approximately a few hours of the surgery.

The extracellular fluid samples for the ATR-FTIR analysis were prepared directly on the ATR element in the following manner. First, a small piece of the tissue was resected from the bulk sample with a clean scalpel blade. Second, the cut off part of the tissue (with the cut side on) was gently pressed and slid over the ATR element, thus leaving a thin layer of extracellular fluid on top of it. Finally, the sample was let to dry and its spectrum was measured. Similarly, the samples for the SERS measurements of extracellular fluid were made. In this case, the freshly cut sample of kidney tissue was gently pressed and slid on the calcium fluoride (CaF_2) optical window instead of the ATR element. The ECF was left to dry and the drop of an already prepared colloidal solution was dried on top of it. More information about the colloidal solution which was chosen for this study and was used for Raman scattering enhancement will be described below in the results and discussion section. The preparation procedure was exactly the same for all samples and for both normal and cancerous tissues. Also, the same procedure of sample preparation was employed for the preparation of the sample for low temperature spectroscopy. A schematic representation of the ECF sample preparation is presented in the Appendix I, Fig. 1.

The samples of both normal and cancerous bladder tissues were also obtained from the Urology centre of Vilnius University Hospital Santaros clinics. The spectroscopic research of the bladder tissue was done with the approval from Vilnius region bioethics committee (document No. 2019/12-1178-665). The samples of the bladder tissue for the spectroscopic analysis were collected during cystoscopy, transurethral resection of the urinary bladder (TURB) or radical cystectomy (RC) procedures. No restrictions for choosing the participants of the study were applied. Participants were eligible for selection if there was a clinical or radiological suspicion of bladder cancer and cystoscopy, TURB or RC procedures were needed in accordance to the guidelines of bladder cancer of European Association of Urology. An informed consent was given by all selected patients. As during the spectroscopic kidney cancer analysis, the spectroscopic bladder cancer analysis was done within a few hours from the

surgery in the vibrational spectroscopy laboratories of the Institute of Chemical Physics of the Faculty of Physics.

The extracellular fluid samples of the bladder tissue for the SERS measurements were prepared in a similar fashion to the sample of ECF of the kidney tissue. However, in this case instead of the calcium fluoride optical window the aluminium surface was used as a substrate. This was done because during the analysis of the kidney tissue no differences of the spectroscopic data were found to be related to the substrate choice. Also, the aluminium substrate is disposable, and thus does not require cleaning after each sample what had to be done using calcium fluoride substrates. Avoiding the substrate cleaning procedure makes the spectroscopic analysis much faster. Beyond that, no other changes to the sample preparation procedure were made.

2.3.3. The ATR-FTIR absorption spectroscopy of the ECF films of kidney cancer

The IR absorption spectra of the extracellular fluid of kidney cancer were collected with the FTIR spectrometer Alpha (Bruker Optik GmbH, Ettlingen, Germany). A single reflection diamond ATR crystal, which was integrated in the ATR accessory, was used for the measurements. Globar light source and a KBr beam splitter were used. Signal detection was performed using deuterated triglycine sulphate (DTGS) detector. The spectra were recorded in the wavenumber region from 4000 cm^{-1} to 800 cm^{-1} with a spectral resolution of 4 cm^{-1} . A total of 64 interferograms were collected and averaged. A Fourier transform of the averaged interferograms was done in order to obtain a spectrum. Blackman-Harris 3 term apodization function together with a zero-filling factor of two were set as the main parameters of the Fourier transform procedure. The conversion from the collected ATR spectrum to the absorbance spectrum was done automatically with the use of the programming software “Opus” provided by Bruker.

2.3.4. The SERS spectroscopy of the ECF

The surface enhanced Raman scattering spectra were collected with the FT-Raman spectrometer MultiRAM (Bruker Optik GmbH, Ettlingen, Germany). The laser excitation source with the wavelength of $\lambda = 1064\text{ nm}$ and a power of $P = 300\text{ mW}$ was used since it was determined to give the highest intensity with least thermal degradation of the sample. Liquid nitrogen cooled germanium (Ge) diode detector was used to register the scattered light. The sample excitation and the collection of the scattered light were performed

with the 90-degree angle gold-plated hyperbolic mirror objective, which has a focal length of 33 millimetres. The objective has an integrated camera used for the visualization of the sample and precise choosing of the measuring position. The diameter of the laser beam at the focus point was 100 micrometres. The SERS spectra were collected in the wavenumber region from 4000 cm^{-1} to 150 cm^{-1} with a spectral resolution of 4 cm^{-1} . A total of 300 interferograms were normally collected and averaged. Fourier transform of the averaged interferograms was performed in order to obtain a spectrum. Blackman-Harris 3 term apodization function together with a zero-filling factor of two were set as the main parameters of the Fourier transform procedure.

Low temperature spectroscopy of the kidney tissue smears was performed by employing the cryostat Linkam LNP95 coupled with the temperature controlling stage FTIR600 (Linkam Scientific, Tadworth, United Kingdom). The temperature during the measurements was varied from 300 K to 100 K in the 20-degree intervals at which the temperature was kept constant while the SERS spectra were collected.

2.3.5. Spectral analysis of the ECF

Qualitative spectral analysis of the extracellular fluid of the kidney and bladder tissues was done by comparing of the averaged spectra of the ECF of the normal and cancerous tissues. The most prominent spectral differences (differences in intensity of the vibrational bands or their shift) were chosen for further investigation. Assignment of the bands was made in order to determine the chemical origin of the spectral differences and to check if they are in any way related to the biochemical changes of the cancerous cells. Spectra of the pure chemical components (bought from Sigma Aldrich) that were presumed to have the most influence to the overall spectra were collected using the same parameters. Theoretical calculations of the possible constituents of the extracellular fluid were calculated and their SERS spectra were simulated. Comparison between the calculated and experimental spectra was performed to ensure the validity of the vibrational band assignment.

Chemometric analysis namely hierarchical cluster analysis and principal component analysis were performed using Python (version 3.7) programming software in order to determine whether it is possible to employ the SERS method for determination of the class (cancerous or normal) of the analysed tissues. Before the statistical analysis was performed, spectra were pre-processed using Opus software (Bruker). Sensitivity and specificity of the proposed method were evaluated.

The spectroscopic data were also compared with the histological information of the cancers. The data regarding the types, stages and grades of the provided kidney and bladder cancers were obtained from the records of the histological examination of the resected tissues which was performed in Vilnius University Hospital Santaros clinics.

2.3.6. Theoretical calculations

Theoretical density functional theory (DFT) calculations were performed using Gaussian 09 software [118]. Molecule visualisation was done using Avogadro software [119]. Geometry optimization of the possible constituents of the ECF sample – adenine, cysteine, phenylalanine, tyrosine, glycogen (segment), was carried out at B3LYP/6-311G* level of theory. Silver nanoparticle was simulated by a 15-atom silver cluster and its geometry optimisation was carried out at B3LYP/LANL2DZ level of theory. Complexes between the silver atom cluster and different analyte molecules were optimised. During DFT calculations the silver cluster atoms were “frozen” since their position are not supposed to change during experiments. The Raman spectra were calculated for the simulated complexes and were used for assignment of the normal vibrations to the experimental spectrum. Computations were performed on resources at the High-Performance Computing Center “HPC Sauletekis” in Vilnius University Faculty of Physics.

2.4. SPECTROSCOPIC ANALYSIS OF THE EXTRACELLULAR FLUID: RESULTS AND DISCUSSION

With all the proper treatment and the thorough process of surgery, it is still observed that around the third of the kidney cancer patients’ relapse within a few years or a decade after treatment. The most common reason for this is the inability to identify and remove the whole area of where the cancer is spread. Therefore, the precise detection of the cancerous tissue is a vital part of the treatment. For this reason, novel diagnostic tools that could be used during surgery are on demand. Therefore, the SERS spectroscopy was applied for the detection of cancerous kidney and bladder tissues from the extracellular fluid. If developed to a clinically available application, this spectroscopy method could be used for the identification of cancerous tissues with high precision.

2.4.1. Characterisation of the colloidal solutions of silver nanoparticles.

First of all, the main characteristics of the synthesised nanoparticles – the wavelength resulting a plasmon resonance and particle size – were evaluated. The plasmon resonance wavelength was determined by measuring the UV-Vis absorption spectra of the colloidal solutions. The collected UV-Vis spectra are presented in the Fig. 4.

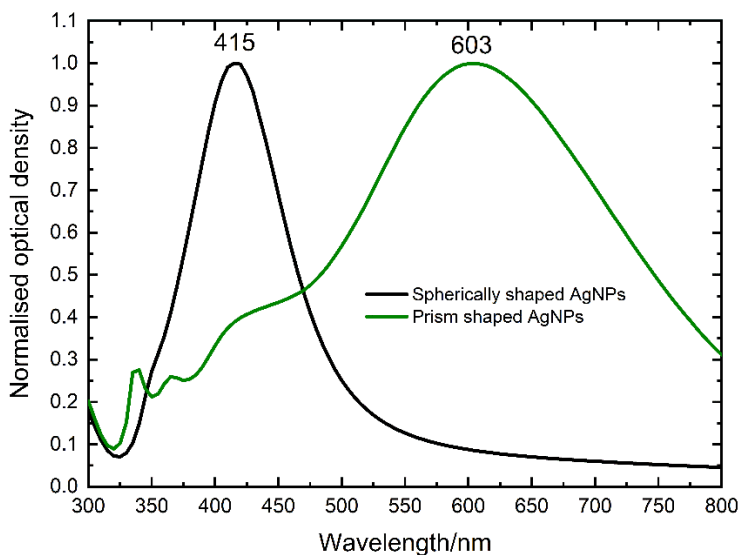


Fig. 4. The UV-Vis absorption spectra of the synthesised spherically shaped and prism shaped silver nanoparticles.

It can be observed that the UV-Vis absorption spectra presented in the Fig. 4 have a maximum value located at the 415 nm (spherically shaped AgNPs) and 610 nm (prism shaped AgNPs), which correspond to the value needed to satisfy the plasmon resonance condition. The average nanoparticle size was calculated for the spherically shaped nanoparticles by plugging the absorption maximum wavelength value into the equation derived from the Mie scattering theory – equation (9). The average particle size was calculated to be around 60 nm. Prism shaped nanoparticle size could not be calculated using this equation. However, it can be observed that the both UV-Vis absorption peaks are broadened. This suggests that the colloidal solutions are not uniform and contain nanoparticles of varying sizes. This was proved by taking TEM images of the same nanoparticles. The TEM images (see Fig. 5) showed that indeed various sizes of spherically or prism shaped nanoparticles were present in their respective solutions. The sizes of the spherical nanoparticles range

from 20 nm to 100 nm in diameter and from 30 nm to 90 nm of the prism shaped nanoparticles. Furthermore, it can be observed that nanoparticles with unexpected shapes like rods are present in the solution of the spherically shaped nanoparticles. However, the number of these particles is relatively small, and the whole solution can be viewed as mostly populated by the spherically shaped particles. It was also observed that leftover seed particles (spherical particles 10 nm in diameter) are present in the solution of prism shaped silver nanoparticles.

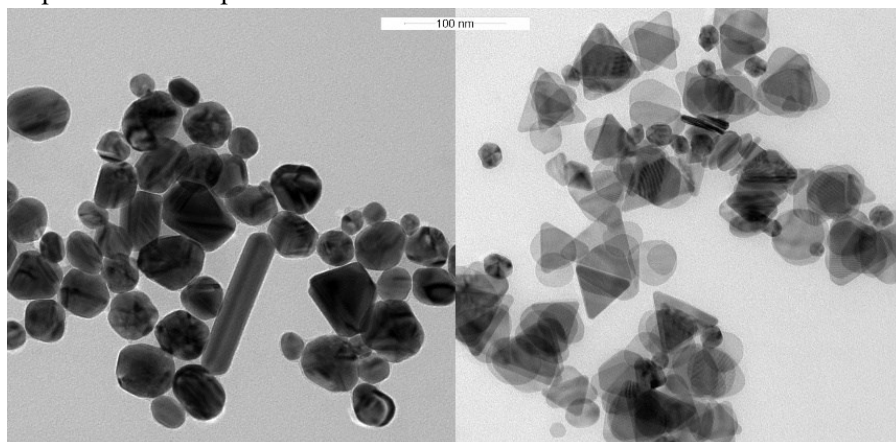


Fig. 5. The TEM images of the spherically (left) and prism (right) shaped silver nanoparticles.

The performance of the two colloidal solutions for enhancement of the Raman scattering signal was tested using an aqueous 1 mM solution of uric acid. Uric acid was chosen because of the efficient adsorption of the molecule. It was observed that a higher intensity of the SERS spectra was achieved using spherically shaped nanoparticles (see Appendix I, Fig. 2). Even considering that the nanoparticle concentration differs in the both solutions the same result is observed. This may be reasoned to the different adsorption behaviour of the molecules on the nanoparticles. Also, the prism shaped nanoparticles are less stable and tend to lose their shape over time or prolonged exposure to the oxygen rich environment. Therefore, in the further study the main focus was put only on the use of spherically shaped nanoparticles.

The UV-Vis absorption spectra of the colloidal solution of spherically shaped AgNPs were also collected after increasing the nanoparticle concentration via centrifuging. Several rotation speeds were tested and the one which led to the highest intensity of the absorption spectrum was chosen. This was determined to be the speed of 6500 rpm. At higher speeds, the intensity

of the UV-Vis absorption peak was observed to decrease, and its peak shifted to lower wavelengths. Furthermore, absorption was observed to increase in the longer wavelength region. This is mostly reasoned by the fact that when centrifuging with a higher centrifugal force the nanoparticles tend to form aggregates whose plasmon resonance condition is satisfied by the photons with longer wavelengths. The shift of the peak is reasoned by the increased number of smaller diameter nanoparticles which are concentrated because of the high centrifugal force. The UV-Vis spectra of the colloidal solution after centrifuging at different speeds are presented in the Appendix I, Fig 3. Additionally, the analytical enhancement factors of these colloidal solutions were calculated using equation (6). Analytical enhancement factors were calculated using the SERS spectra of an aqueous 1 mM solution of uric acid. The dependence of the analytical enhancement factor on the rotation speed applied during the centrifuging is presented in the Fig. 6.

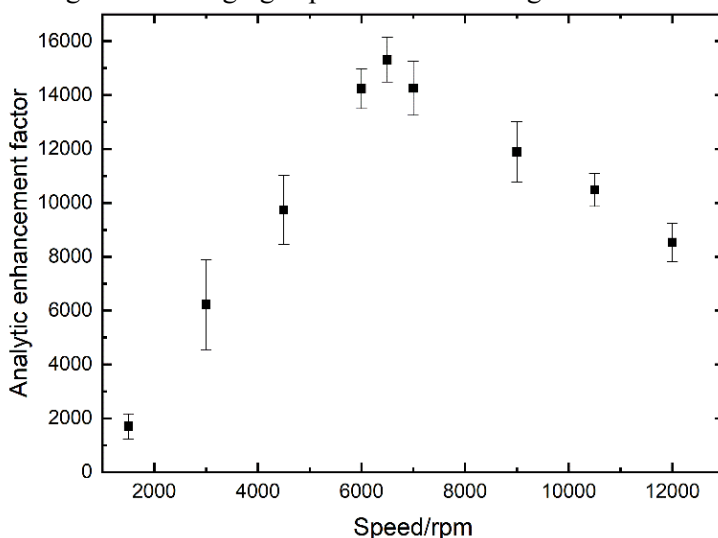


Fig. 6. The calculated analytical enhancement factors of the centrifuged colloidal solutions of spherical AgNPs.

It is noteworthy that the laser wavelength used in this study for the sample excitation (1064 nm) was quite far from the wavelength corresponding to the plasmon resonance (415 nm or 603 nm). This would suggest that plasmon resonance condition would not be satisfied and Raman scattering signal would not be enhanced. Typically, the excitation laser wavelength (and corresponding frequency) is desired to be close to the plasmon resonance frequency in order to achieve the highest possible SERS enhancement by the nanoparticles. However, in systems where the concentration of nanoparticles

is high, it is not crucial to satisfy this requirement. As mentioned earlier this is because in concentrated colloidal solutions metal nanoparticles strongly interact with each other. The interaction of electromagnetic fields produced by individual nanoparticles creates the so-called “dark modes” of the enhanced electromagnetic field. Because of the formation of such modes, Raman scattering signal of molecules can be enhanced even when the wavelength of the laser is far from the wavelength corresponding to the plasmon resonance [41]. Since the colloidal solution used in this research was centrifuged, the interactions between the metal nanoparticles allowed the use of the 1064 nm excitation wavelength. This resulted in the possibility to combine both the enhancement of the Raman scattering and the advantage of the infrared excitation source – low fluorescence signal of the sample. The latter aspect is quite important since biological samples tend to fluoresce when laser excitation wavelength in the visible range is used.

2.4.2. SERS analysis of the kidney tissue smears

In total 85 pairs of healthy and normal kidney cancer spectra were collected in this work. The histology examination results of the tissues used in this study are presented in the Table 2.

Table 2. The histology examination results of the 85 kidney cancer tissues.

Tissue type	Number of patients
Clear cell renal cell carcinoma	69
Chromophobe renal cell carcinoma	4
Renal oncocytoma	3
Multilocular cystic renal cell carcinoma	2
Papillary renal cell carcinoma	5
Unknown	2

Before the ECF sample analysis, conventional Raman spectra of the whole cancerous and normal tissues were collected. This was carried out in order to prove that the spectra of tissue do not provide clear information about the chemical differences between the two tissue types. The collected spectra of these tissues are presented in the Fig. 7. Both spectra are dominated by the vibrational bands of proteins – amide I (1660 cm^{-1}), $\delta(\text{CH}_2)$ (1448 cm^{-1}), phenylalanine (1003 cm^{-1}). As expected, no spectral differences which could

be used to easily distinguish the spectra of either normal or cancerous tissues were observed. This proved that the spectral discrimination between normal and cancerous tissues via conventional Raman scattering spectroscopy cannot be achieved efficiently.

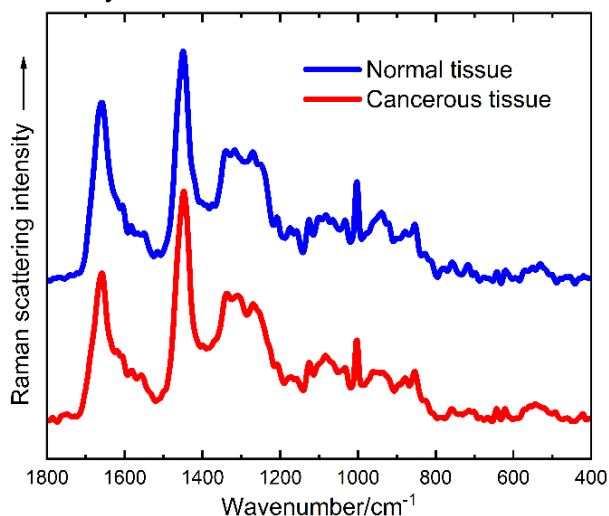


Fig. 7. Raman scattering spectra of normal and cancerous kidney tissues.

The ECF sample analysis was started by staining the ECF samples of kidney tissues and examining them under a microscope. This was performed on a randomly selected pair of the normal and cancerous kidney tissue samples in order to better comprehend the composition of samples under study. Samples for staining were prepared on a calcium fluoride glass substrate. Staining was performed using the cytological Papanicolaou's (PAP) stain (Shandon™ Rapid-Chrome Papanicolaou Staining Kit, *Thermo Fisher Scientific*, Waltham, Massachusetts, USA). The staining procedure was performed according to the protocol produced with the staining kit. The procedure is as follows. A sample is first immersed in 95% ethanol for 1 minute, then it is removed and immediately dipped 10 times in a solution of 95% ethanol. The following steps (performed continuously) written in short: 10 dips in distilled water, 1 minute immersed in haematoxylin, 10 dips in distilled water, 1 minute in bluing reagent, 10 dips in distilled water, 10 dips in 95% ethanol, 1 minute in Orange-G-6, 10 dips in 95% ethanol, 10 dips in 95% ethanol, 1 minute in EA-50, 10 dips in 95% ethanol, 10 dips in 95% ethanol, 10 dips in 100% ethanol, 10 dips in 100% ethanol, 10 dips in xylene, 1 minute in xylene. After this procedure, the sample was dried in an open environment. Optical microscopy images of the stained samples were

recorded with an optical microscope (*Motic*) using a 40×/0.65 objective. The images of the stained samples of cancerous and normal tissue smears are presented in Fig. 8.

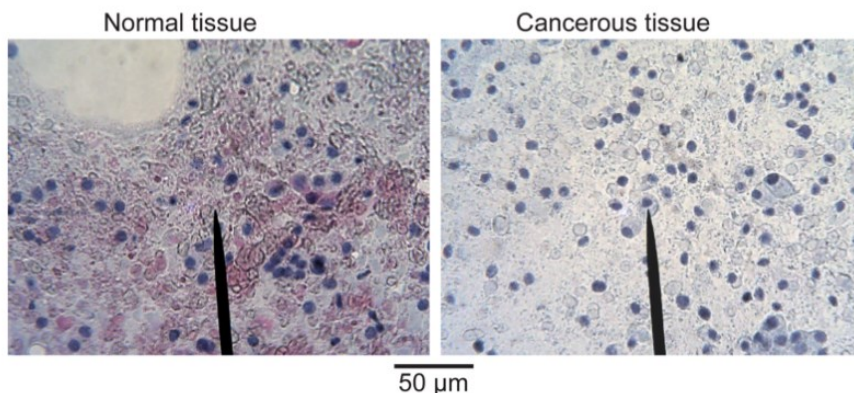


Fig. 8. Images of the stained ECF samples of normal (left) and cancerous (right) kidney tissues.

The images of the stained ECF samples have shown that besides the extracellular fluid, tissue smears contain a layer of single cells which were detached from the bulk tissue. This finding was quite beneficial since it provided an explanation for the appearance of the spectral bands related to the vibration of molecules whose presence is thought to be only in the cytoplasm of the cells. The bluish dots in the images correspond to the nuclei of the cells, which were coloured blue during the staining because of the low pH value of the nucleus.

It is known that spectra of complex samples like biological fluids which are composed of various molecules can sometimes change drastically in regard to the point of the measurement. Furthermore, the spectra can change with the changing thickness of the sample. Therefore, to test if this is the case for the samples used in this study, the SERS spectra of the ECF samples were collected in at least five randomly selected points for each sample. The collected spectra for one sample of normal kidney tissue are shown in the Appendix I, Fig. 4. The influence on the thickness of the sample was investigated as well. Samples with different thicknesses were prepared from randomly chosen cancerous kidney tissue by repeating the procedure of the ECF formation on the same substrate two or three times. This produced thicker layers of the ECF whose spectra were then collected. The spectral results of this analysis are presented in the Fig. 9. The presented SERS spectra were shifted along the y-axis for clarity.

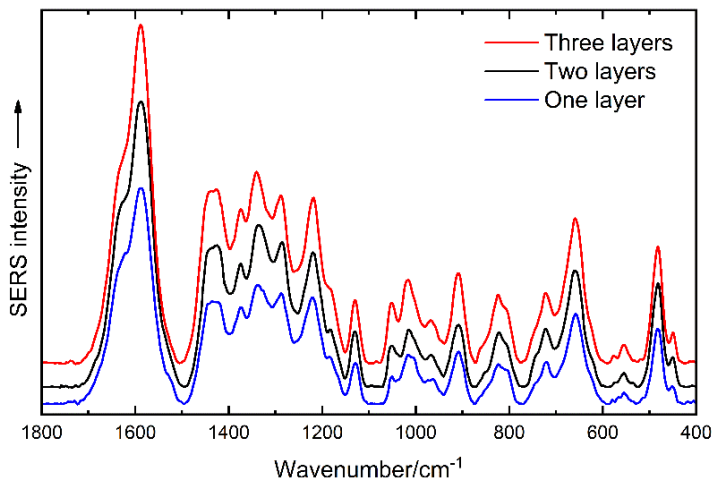


Fig. 9. The SERS spectra of different thickness samples of ECF of cancerous kidney tissue

The analysis of the reproducibility of the spectra has showed that the samples prepared in this research can be viewed as relatively homogeneous since the spectra collected at five random points of one sample did not show major differences. Small differences in the relative band intensities were noticed when analysing the spectra collected at different points of the sample. However, in comparison to the intensity of the spectral bands they were relatively small, and the main difference observed between the five SERS spectra is the change of the overall intensity. In fact, similar result was observed while testing the influence of the sample thickness. It was noticed that the increase in sample thickness does not result in the changes of the spectra. Only the overall intensity of the spectra increased. These observations can be reasoned by the fact that the active measurement area which is determined by the diameter of the focused laser beam (100 μm in diameter) is relatively high. This results in not one cell or organelle but rather several cells and an area of the ECF being measured at once. Such measurement condition can be interpreted as an averaging while taking a single scan. It must be however noted that increasing sample thickness should ultimately lead to the changes in the spectra. This should be observed when a sufficiently large number of cells is present in the sample. In such case the collected spectrum should start to resemble the spectrum of the whole tissue. In this research the prepared samples were a lot thinner, and this was never observed.

The experimental SERS spectra of the extracellular fluid of the normal and cancerous kidney tissues in the wavenumber region of $350\text{ cm}^{-1} - 3500\text{ cm}^{-1}$

are presented in Appendix I, Fig. 5. It is notable that besides the band of $\nu(\text{C-H})$ vibrations located at the 3000 cm^{-1} which in this case does not provide any meaningful information, no other vibrational bands are seen in the high wavenumber region. Therefore, the spectra were analysed only in the fingerprint region from 400 cm^{-1} to 1800 cm^{-1} where the characteristic bands are located. It should be noted that the spectra of the ECF of randomly chosen normal kidney tissue presented in the Appendix I, Fig. 4 and the spectra of ECF of normal kidney tissue in the Appendix I, Fig. 5 show different prominent spectral bands. Such result is observed in the several collected spectra. These changes are mainly reasoned by the different composition of the tissues collected from different patients. The intensity of spectral bands was observed to change and this most probably can be explained by the differences in overall health, lifestyle, etc. of each patient. Therefore, the spectral analysis of the averaged SERS spectra was carried out and will be discussed later on.

Spectral analysis of the ECF of cancerous and normal tissues was performed in the fingerprint region (from 1800 cm^{-1} to 400 cm^{-1}) since it was noticed that the differences in the SERS spectra were located in this region. Fig. 10 shows the SERS spectra of the ECF of kidney tissue in the fingerprint region. A difference spectrum produced by subtracting the SERS spectrum of the ECF of the normal tissue from the SERS spectrum of the ECF of the cancerous tissue is also presented. The shown spectra were shifted along the y-axis for clarity.

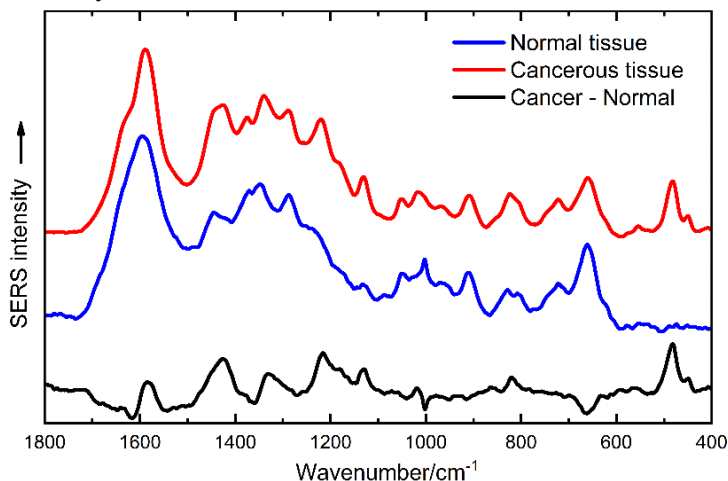


Fig. 10. The experimental SERS spectra of extracellular fluid taken from normal and cancerous kidney tissues and their difference spectrum in the wavenumber region from 1800 cm^{-1} to 400 cm^{-1} .

Several differences in the relative intensity of the vibrational bands were observed while analysing the fingerprint region of these two spectra presented in the Fig. 10. The most prominent of the differences between the two spectra are changes in the intensity of the three spectral bands located at 481 cm^{-1} , 1131 cm^{-1} , and 1220 cm^{-1} . These vibrational bands are well-pronounced and have high intensity in the SERS spectrum of extracellular fluid of cancerous tissue. In the SERS spectrum of ECF of normal kidney tissue these bands have a much lower intensity or do not appear at all. This suggested that the intensity of these spectral bands could be used as a potential spectral marker of kidney cancer.

2.4.3. Interpretation of the SERS spectra of ECF of kidney tissue

Interpreting of the vibrational spectra of biological samples is not trivial, since the complex composition of the cells or other composites makes it difficult to distinguish the exact nature of the observed vibrational bands. Therefore, most of the assignments of the experimental bands observed in the vibrational spectra of biological samples which can be found in the literature are only tentative.

In order to collect more information on the composition of the ECF of kidney tissue samples and to make a more precise assignment of the vibrational bands, low temperature SERS measurements were performed. This was performed since it was expected that at low temperatures the SERS spectra of the adsorbed molecules should be enhanced even more. This way the intensity only of the molecules closest to the surface of the nanoparticles should increase or increase the most. The selected ECF samples were stepwise cooled from room temperature (around 300 K) to 100 K. At each step the temperature was stabilised and then kept constant for the duration of the collection of the SERS spectrum. The SERS spectra of the ECF of cancerous kidney tissue of the patient A collected at three temperature values are presented in the Fig. 11.

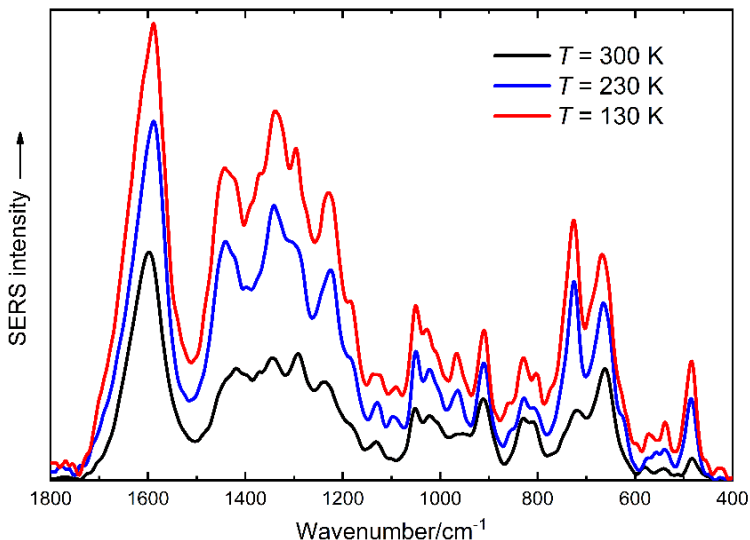


Fig. 11. The SERS spectra of the ECF of cancerous kidney tissue (patient A) collected at three different temperatures.

The low temperature SERS analysis of the ECF has provided information which proves the presence of certain molecules in the composition of the ECF samples. For example, it was observed that the intensity of the several bands in the SERS spectra of the ECF of cancerous tissue taken from patient A (see Fig. 11) increased when the temperature is decreased. Of these, some vibrational bands are in a good agreement with the spectra of adenine. The presence of vibrational bands of adenine could be resulted by several molecular species. For example, adenine is one of the four nucleic acids in the composition of DNA. Therefore, the spectral bands could be resulted by the adsorption of DNA on the nanoparticles. On the other hand, adenine is also a composite of adenosine triphosphate (ATP) what could indicate its adsorption. A few other spectral bands whose intensity was observed to change can be associated with the vibrations of cysteine molecule. Its worth noting that vibrations of guanine molecule are also observed in similar spectral regions. However, unlike the SERS spectrum of cysteine, the spectrum of guanine does not contain all of the observed spectral bands, and thus only the presence of cysteine was considered. Furthermore, the presence of cysteine is not an unexpected finding since it is established that the cancerous cells use cysteine as a source for energy. Thus, the uptake of cysteine and the concentration of this molecule in the cancerous tissue are increased [120, 121]. It is worth mentioning here that in some cases the spectral bands of cysteine can be

observed with a higher intensity in the ECF spectra of normal kidney tissue. This example can be seen in the spectra presented in the Fig. 10 (spectral band of located at 660 cm^{-1}). Such result could be reasoned by already mentioned differences of the composition of the patients' tissue and other factors like the tumor development. However, this result was not further investigated since it was not common. The vibrational bands of cysteine molecule can be observed more clearly in the low temperature SERS spectra of the ECF of cancerous tissue of patient B presented in the Fig. 12.

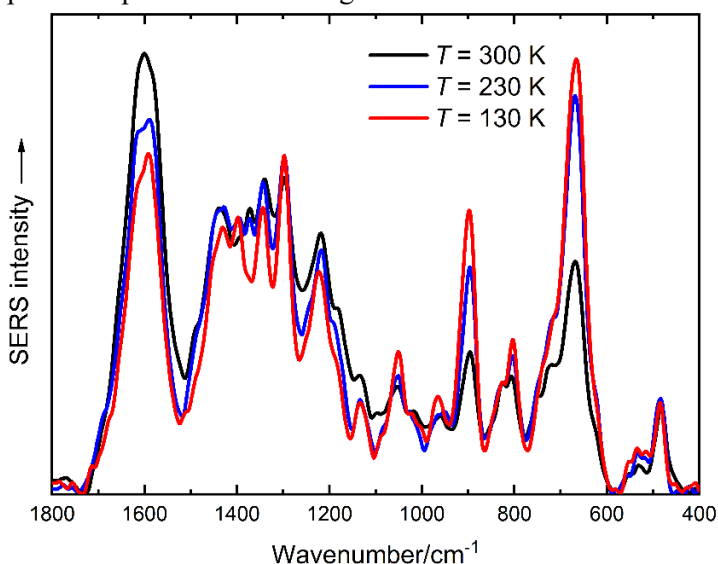


Fig. 12. The SERS spectra of the ECF of cancerous kidney tissue (patient B) collected at three different temperatures.

In this case only the increase in intensity of the vibrational bands of cysteine was observed. Besides the intense vibrational bands of cysteine other bands which were observed in the low temperature SERS spectra of the ECF of patient A in this case are not present. These differences of the two spectra indicated the presence of competitive adsorption. Molecules compete for adsorption on the surface on the nanoparticle and the ones that can adsorb better can inhibit the adsorption of other molecules. This can also explain the observed differences between the SERS spectra of ECF of kidney tissue taken from different patients.

Only several spectral bands observed in the SERS spectrum of the ECF of kidney tissue can be explained by the presence of adenine type molecules and cysteine. The assignment of other observed spectral bands was made in accordance to the literature and by comparison with the experimental SERS

spectra of the chemical components which are most likely to be present in the biological samples. The experimental SERS spectra of the possible constituents of the ECF are presented in the Appendix I, Fig. 6. To determine the normal vibrations of the molecules, DFT calculations of the complexes between these molecules and the nanoparticle surface, which was simulated by fifteen silver atom cluster, were performed. The calculated complexes are presented in Fig. 13. Since glycogen is a relatively large molecule (a branched polymer of glucose), only a segment of four glucose residues was considered and calculated. The Raman spectra of the optimised complexes were calculated and assignment of the vibrational bands observed in the SERS spectra of ECF of kidney tissue was made.

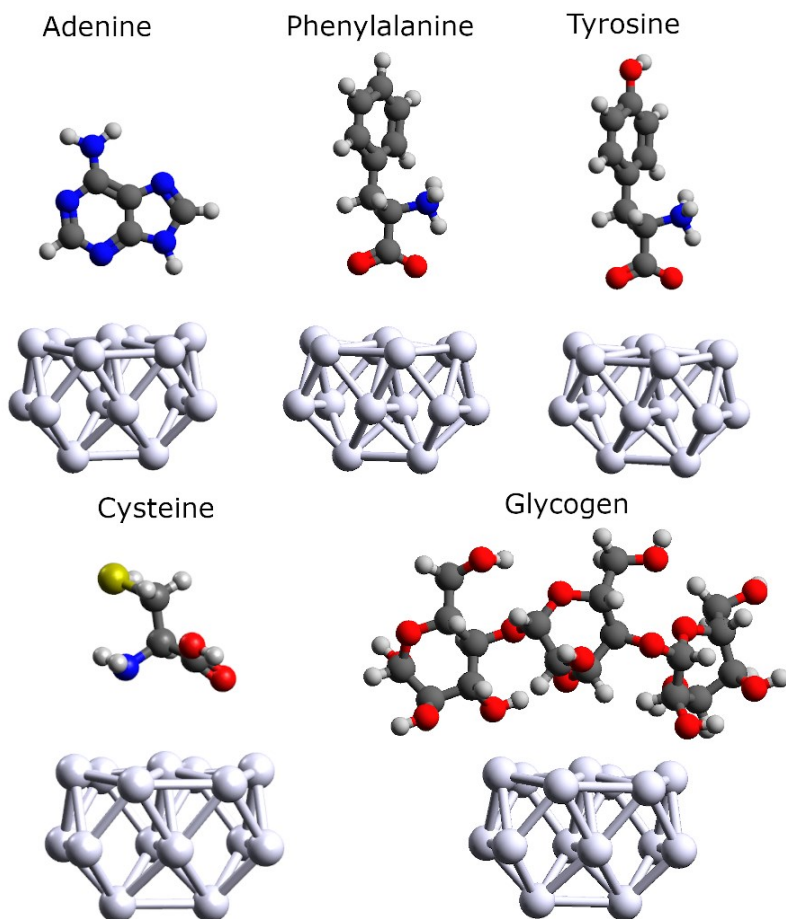


Fig. 13. The calculated complexes between biomolecules and a silver nanoparticle surface simulated by 15 silver atom cluster.

Results of the DFT calculations of the Raman spectra of the molecules adsorbed on a silver nanoparticle and the experimental SERS spectra of pure compounds have confirmed the finding that several vibrational bands observed in the SERS spectra of the ECF can indeed be explained by the vibrations of adenine, cysteine, phenylalanine, glycogen and several other molecules. Furthermore, assignment of the normal vibrations is in good agreement with the ones provided in literature. The calculated Raman spectra are not presented since the relative intensities of the vibrational bands differ substantially when compared to the experimental spectra. This results from the simplifications that are used in theoretical calculations. Because of that, without the complex calculations the SERS enhancement factor for a specific vibration cannot be evaluated, and thus it was not considered.

The spectral marker band located at 481 cm^{-1} was found to be related to the deformation vibrations of the glycogen molecule. Experimental spectrum was collected using the glycogen from bovine liver purchased from Sigma Aldrich. A solution of 1 mM of glycogen was prepared for the SERS measurements. The other spectral marker band, located at 1131 cm^{-1} was found to be most likely resulting from the vibrations of proteins or lipids - $\nu(\text{C-C})$, $\nu(\text{C-N})$. In addition, it was determined that the literature assignment of the spectral marker band which is located at 1220 cm^{-1} - the $\nu(\text{C-C}_6\text{-H}_5)$ vibration of phenylalanine and tyrosine, is not entirely correct, since in respect to this band the intensity of the other bands of these molecules is not high enough or the other vibrational bands are not observed at all. For example, the most intense spectral band of phenylalanine located at 1003 cm^{-1} . Therefore, it was determined that the increased intensity of the band at 1220 cm^{-1} in the SERS spectra of the ECF of cancerous kidney tissue is most likely resulted from the vibrations of proteins – amide III band. To summarize the interpretation of the SERS spectra of ECF of kidney tissues, a table of the assignments of the most prominent vibrational bands was made. The bands, their assignments, and literature references are listed in the Table 3.

Table 3. Tentative assignment of the SERS spectral bands.

Wavenumber/cm ⁻¹	Normal vibration	Molecule	Reference
481	Ring vibration	Glycogen	[122]
538	$\nu(\text{S-S})$	Adenine, Protein	[123, 124]
554	-	Adenine	[123]
625	$\delta(\text{C-C})$	Phenylalanine, Adenine	[125]
660	$\nu(\text{C-S}), \delta(\text{C-C})$	Cysteine	[126]
724	$\delta(\text{C-H})$	Adenine, ATP, Hypoxanthine	[122, 124, 127-129]
780	Ring vibration	Thymine	[127, 129]
797	-	Cytosine, Proteins,	[124]
829	Ring vibration, $\nu(\text{HCS})$	Tyrosine, Cysteine	[122, 126, 128]
853	$\nu(\text{C-C})$	Tyrosine, ATP	[122]
909	$\nu(\text{C-C})$	Cysteine	[126]
962	-	Phospholipids, Proteins, Cholesterol	[123, 124]
1003	$\nu(\text{C-C}),$ Ring breathing	Phenylalanine	[128, 129]
1052	$\nu(\text{C-O}), \nu(\text{C-N})$	Cysteine, lactic acid	[126]
1093	$\nu(\text{C-N})$	Hypoxanthine	[125]
1131	$\nu(\text{C-C}), \nu(\text{C-N})$	Lipids, Proteins	[123, 127]
1173	-	Cytosine	[124]
1220	$\delta(\text{C-N}), \delta(\text{CH}_2)$	Amide III	[130]
1289	$\delta(\text{C-C-H})$	Cysteine, Proteins	[124, 126]
1334	$\nu(\text{CH})$	Proteins, Adenine, DNA	[122-124, 127, 130]
1372	Ring breathing	Adenine, DNA	[124, 130]
1443	$\delta(\text{CH}_2), \delta(\text{CH}_3)$	Adenine, Proteins, Phospholipids	[122, 124, 127]
1585	$\nu(\text{C=C})$	Protein	[130]
1650	$\nu(\text{C=O})$	Amide I, α -helix (Proteins)	[122, 128, 129]

In accordance to the information provided in the Table 3 it can be stated that the proposed SERS spectral marker bands of cancer are associated with the vibrations of glycogen (deformation vibration at 481 cm⁻¹), vibrations of proteins or lipids ($\nu(\text{C-C}), \nu(\text{C-N})$ vibrations at 1131 cm⁻¹) and protein vibrations (amide III vibrations at 1220 cm⁻¹). This means that sample of the ECF of cancerous tissue contain more glycogen and the content or the structure of proteins in cancerous samples is changed. The increase in the concentration of these molecules can be explained by the changed metabolism

of the cancerous cells. As mentioned earlier because of the increased rate of the growth of the cancerous cells, certain parts of the tissue in later stages of cancer development are not sufficiently provided with oxygen. Oxygen molecules during the cellular respiration are used for the synthesis of the ATP molecules (energy units of the living organisms). In order to survive the hypoxic (lacking oxygen) environment, cancerous cells start to initiate fermentation reaction. It is known that fermentation is not an efficient process for the ATP synthesis – only two ATP molecules in case of fermentation compared to the 36 ATP molecules in cellular respiration are produced from one glucose molecule. Thereby, cancerous cells show the behaviour of increased glucose storage. In cells, glucose is stored in the form of glycogen. This behaviour of cancerous cells ensures that the increased demand for nutrients is met [131]. This characteristic behaviour of cancerous cells could be the reason of the appearance of the vibrational band associated with vibrations of glycogen in the SERS spectra of the ECF of cancerous kidney tissue. It is worth to note that glycogen molecules are typically stored in the cancerous cells themselves. This shows that that glycogen molecules detected via SERS method came from the inside of the kidney tissue cells present in the sample. There are two possible explanations for this result. First, glycogen molecules could have come into contact with the silver nanoparticles during the preparation of the sample. Some cells are damaged by the cutting of the tissue either during the resection procedure of sample preparation for spectroscopic analysis. The content of the ruptured kidney tissue cell which is held in the cytosol can then mix with the extracellular fluid. The glycogen molecules inside this mixture are then deposited on the substrate during the sample preparation. Second, it was already proven that that the single cells of the kidney tissue are present in the prepared layers of extracellular fluid. Taking this into account, the appearance of the spectral band of glycogen in the SERS spectrum can be reasoned by the direct interaction of the nanoparticles and the kidney tissue cells. It has been shown that when the colloidal suspension is introduced to the sample containing cells, silver nanoparticles, if they are small enough, tend to enter the cell [124]. In this way, the glycogen molecules could again directly interact with the nanoparticles. Both of the above-mentioned scenarios are valid, but it is hard to determine which of them is more likely to happen and reason the observed spectral characteristics.

Similarly, the intense spectral bands which are associated with the vibrations of proteins or lipids present in the SERS spectrum of the ECF of cancerous kidney tissue can also be explained by the change of biochemical

functions of the cancer. It is known that cells carry out numerous functions and metabolism processes in order to survive. Because of different environment conditions, the changed metabolism and fast proliferation leads to the differentially expressed and overexpressed proteins in cancerous cells or even expression and excretion of proteins in order to drive cell migration, invasion and adhesion [132-134]. Thus, the increased intensity of the bands related to protein structure cells is directly linked to the different metabolism of the cancerous cells. However, it is difficult to predict whether the proteins which are detected come from the cytosol (inside of the cell) or from the extracellular matrix.

2.4.4. Statistical analysis of the SERS spectra of ECF of kidney tissue.

The statistical importance of the spectral differences which were associated with vibrations of glycogen, proteins, and lipids was proven by collecting the SERS spectra of the ECF of 85 oncology patients. The averaged spectra of ECF of cancerous and healthy tissues are presented in the Fig. 14. All spectra were normalized using vector normalization. The presented spectra are shifted along the y-axis for clarity and the positions of the spectral marker bands are marked by dashed lines.

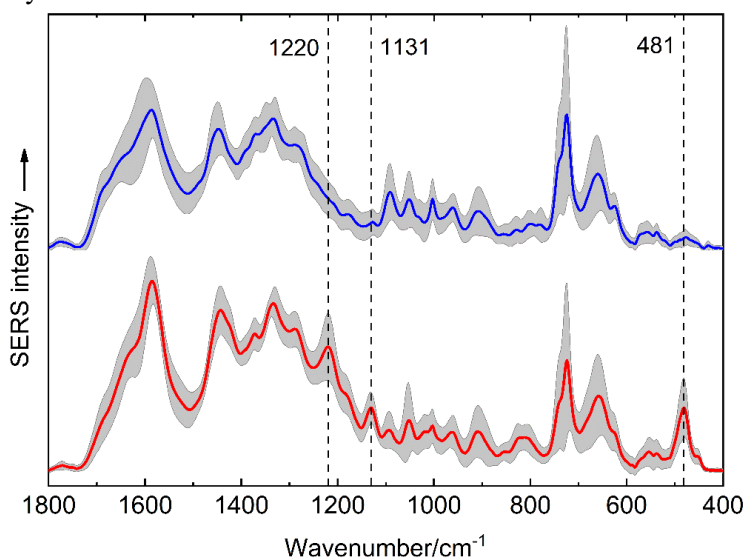


Fig. 14. The averaged SERS spectra of the ECF of normal (top) and cancerous (bottom) kidney tissues.

The grey areas in the SERS spectra presented in the Fig. 14 show the standard deviation of intensity of the vibrational bands. The changes in spectral band

intensity as already mentioned can be explained by the differences in the lifestyle and overall health of the patients. Since no patients have the same lifestyle, the concentrations of certain biomolecules can be higher or lower in the human body depending on the activity, diet, etcetera. On top of that, the intensity deviation observed in the SERS spectra of the ECF of cancerous tissue could be resulted by the differences in the chemical composition of the cancer itself. The different concentrations of biomolecules might be linked to the cell type of the cancer or even its stage. However, this research was not considered in this work and will be performed in the future when a larger data set will be gathered. As can be observed in the Fig. 14, the intensity of some vibrational bands can vary quite a lot. Nonetheless, it can be clearly observed that the increased intensity of the spectral marker bands (bands of glycogen and proteins and lipids) is the distinct characteristic of the SERS spectra of ECF of cancerous tissue. In fact, the vibrational bands associated with glycogen, proteins and lipids were observed to be more pronounced in the averaged spectra of extracellular fluid of cancerous kidney tissue. This shows that the appearance of these spectral marker bands in the experimental SERS spectrum of the ECF indicates the malignance of the tissue with high accuracy.

Having this in mind, statistical analysis of the experimental SERS spectra by means of hierarchical cluster analysis and principal component analysis was performed. Even though several methods can be employed for statistical analysis, hierarchical cluster analysis was chosen in this work, since the goal of analysis was the discrimination of only two groups (cancerous and normal). The experimental SERS spectra of the ECF of kidney tissues were compared in various regions. However, the best results were observed while comparing the spectra in the wavenumber region $530\text{--}430\text{ cm}^{-1}$. The PCA analysis was carried out in order to test the viability of the discrimination between the normal and cancerous tissue via statistical analysis. In addition, PCA analysis differs from the hierarchical clustering that it checks for the correlation of the spectral data. Both the hierarchical cluster analysis and principal component analysis were performed by adapting the prewritten sections of the python programming code. Ward algorithm was chosen to differentiate the clusters and to calculate the Euclidian distance between them during the hierarchical clustering. As mentioned before, hierarchical cluster analysis using Ward algorithm works by treating each spectrum as a separate cluster. At each step, two clusters that are most similar (the similarity is reflected by the shortest Euclidian distance between the clusters) are combined to form a new cluster. The treatment of each spectrum as an individual cluster is beneficial in this case, since the intensity changes of the vibrational bands between the spectra

of two patients makes them completely unique. While conducting the PCA, the first derivative of the SERS spectra was calculated, and a Savitzky-Golay filter (for smoothing the spectra) was applied. The results of the hierarchical cluster analysis are presented in the Fig. 15. The spectra of the extracellular fluid of normal and cancerous tissue are presented by letter notation and colour coding - blue letters “N” for normal and red letters “T” for tumor spectra. Out of the set of 85 pairs (cancer and normal) of SERS spectra of ECF, 80 spectra of cancerous kidney tissue were correctly identified as cancerous. Moreover, the SERS spectra of six samples prepared from normal kidney tissues were incorrectly indicated as cancerous. The reason of the assignment of the spectra of samples prepared for the healthy tissues to the incorrect cluster most probably lies in the tissue samples provided by the surgeons. To be specific, the error might have resulted from the area of the kidney that the sample tissue was cut from. The kidney tissue sample which was provided for spectral analysis could have been cut from the normal and cancerous tissue border. If that was the case, the SERS spectra of the extracellular fluid of normal tissue could have had the vibrational marker bands that are specific to the SERS spectra of the samples of the ECF of cancerous tissues. In contrast, if further analysis of such samples would be carried out it might show that the wrongly assigned spectra of the cancerous kidney tissue samples could for example be attributed to the benign tumor of the oncology patients.

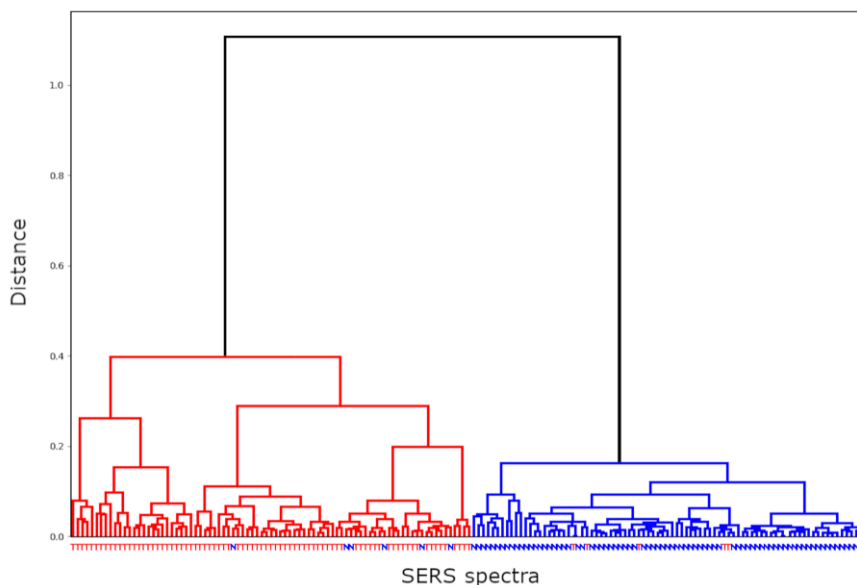


Fig. 15. The results of hierarchical cluster analysis of the SERS spectra of the ECF of kidney tissue.

The results of the hierarchical cluster analysis are promising, because even with a rather small set of samples accuracy of 93.5% for the overall correct categorization of the sample spectra and accuracy of 94% for accurate identification of the cancerous tissue was achieved. Similar results were observed in the PCA. The groups representing the SERS spectra of cancerous and normal tissues can be clearly distinguished. Out of the 85 spectra of the ECF of cancerous tissues, four spectra were wrongly grouped what results in the accuracy of identification of cancerous spectra of over 95%. In total, eight spectra of normal tissues were also put into the wrong category. Thus, the accuracy of the overall identification results in a 93%. The results of statistical analysis from the clinical point of view are also relevant since the sensitivity and specificity of such analysis were both evaluated to be at least 93%. The PCA score plot is presented in the Fig. 16. It should be mentioned that the use of the first components is valid in this case since vector normalization was applied to all spectra before the PCA.

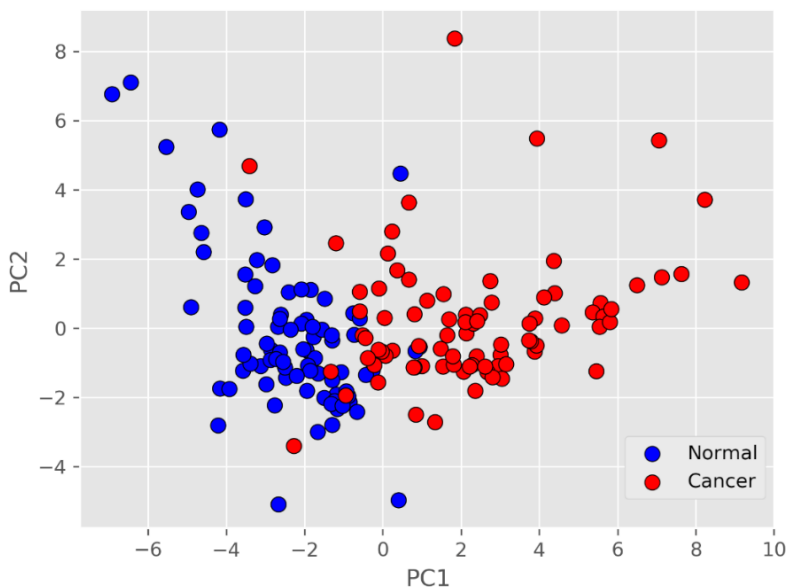


Fig. 16. The PCA score plot representing the results of the principal component analysis of the SERS spectra of the ECF of kidney tissue.

The SERS spectroscopy analysis of kidney tumor performed in this work has shown that this type of spectroscopic method could be used for accurate identification of cancerous and normal kidney tissues. By standardising the sample collection and ensuring the proper sampling procedures in the further research even more accurate results should be expected. Furthermore, the

sample preparation can be easily modified (optical fiber accessories or disposable substrates can be used), therefore this method has the potential to be developed for the use directly in the operating room.

2.4.5. The ATR-FTIR spectroscopy of the ECF of kidney tissue.

Since surface enhanced spectroscopy is not a conventional spectroscopic technique and has not been applied to the analysis of the ECF of the kidney tissue, results of the SERS analysis were double-checked by comparison with the ATR-FTIR spectroscopy. The ATR-FTIR spectra were collected for the total of 105 patients. As during the SERS analysis, a set of two tissue types normal and cancer were used for sample preparation and spectra were collected. In this manner, the spectral data for each patient consisted of two spectra. The results of the histological examination are presented in the Table 4.

Table 4. The results of the histological examination of the 105 kidney cancer tissues.

Tissue type	Number of patients
Clear cell renal cell carcinoma	90
Chromophobe renal cell carcinoma	2
Renal angiomyolipoma	1
Renal oncocytoma	6
Pyelonephritis	1
Multilocular cystic renal cell carcinoma	2
Papillary renal cell carcinoma	2
Tubulocystic renal cell carcinoma	1

The Fig. 17 shows a typical IR absorption spectrum of the ECF of the normal and cancerous kidney tissues. Spectra were shifted along the y-axis for clarity. The dominating bands seen in the spectra correspond to vibrations of alkane/alkene asymmetric/symmetric $\nu(\text{CH}_3)$ located at 2960 cm^{-1} and 2872 cm^{-1} , asymmetric/symmetric $\nu(\text{CH}_2)$ at 2925 cm^{-1} and 2854 cm^{-1} , alkene $\nu(\text{C-H})$ at 3077 cm^{-1} , $\delta(\text{CH}_x)$ ($x = 1, 2, 3$) located at 1460 cm^{-1} , 1398 cm^{-1} and 1311 cm^{-1} and amide $\nu(\text{NH})$ at 3286 cm^{-1} , $\nu(\text{C=O})$ (amide I) at 1650 cm^{-1} , $\delta(\text{N-H})$ (amide II) at 1540 cm^{-1} functional groups which are

characteristic to biological samples containing proteins, lipids and carbohydrates [135].

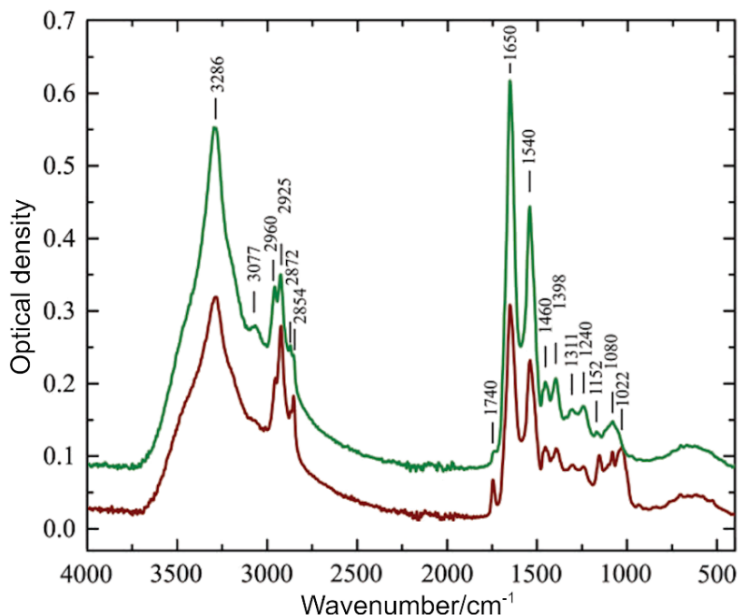


Fig. 17. The ATR-FTIR absorption spectra of the ECF of normal (green) and cancerous (burgundy) kidney tissues.

It can be observed that the ATR-FTIR absorption spectra presented in the Fig. 17 are similar. However, clear and distinct spectral differences between the spectra of ECF of cancerous and normal tissues can be observed. One of the prominent differences is the change of the intensity of the group of overlapped vibrational bands located in the wavenumber region from 900 cm⁻¹ to 1200 cm⁻¹. Three spectral bands observed in this region are located at 1022 cm⁻¹, 1080 cm⁻¹ and 1152 cm⁻¹ in the spectra of the smears taken from the cancerous kidney tissue. These bands are assigned to $\delta(\text{CHO})$ and $\nu(\text{C}-\text{O})$ vibrations of glycogen and glucose [136]. The increase in intensity of these bands indicates the increase in concentration of the said carbohydrates in the cancerous tissue. To ensure that the bands are arising because of increased concentration of the glycogen the ATR-FTIR spectrum of pure glycogen was collected and is presented in the Appendix I, Fig. 7. Analysis of the glycogen spectra has showed that as with the SERS spectroscopy the main difference between the spectra of the ECF of normal and cancerous tissues is in fact the abundance of glycogen in the cancerous tissue.

The averaged ATR-FTIR absorption spectra of the ECF of cancerous and normal kidney tissues are presented in the Fig. 18. The green and burgundy coloured areas in the spectra show the standard deviation of the intensity of the bands in the spectra of the ECF of normal and cancerous tissues, respectively. The grey area represents the overlap of the two areas.

Once again, the same spectral characteristics that were observed in the averaged SERS spectra were noticed here. The spectral marker bands (vibrational bands associated with glycogen located between 1000 cm^{-1} and 1200 cm^{-1} spectral region) can be clearly distinguished in the averaged spectra of the ECF of cancerous kidney tissue. In comparison, these marker bands are much lower in intensity in the ATR-FTIR absorption spectra of normal tissue.

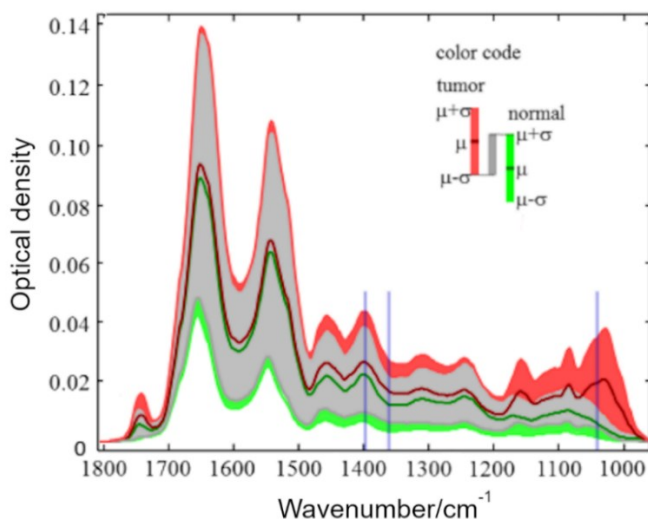


Fig. 18. The averaged ATR-FTIR absorption spectra of the ECF of normal (green) and cancerous (burgundy) kidney tissues.

The ATR-FTIR analysis of the dried kidney tissue smears proves the viability of SERS analysis. The information collected during analysis with both these methods support each other and it can be stated that the cancerous and normal kidney tissues can be efficiently discriminated by the increased intensity of spectral bands associated with glycogen vibrations. Increased glycogen concentration indicated that cancer cells predominantly produce energy by fast-rate glycolysis which allows faster proliferation and allows the cells to adapt to anaerobic conditions when the tumor grows far away from the blood vessels [137]. Particularly in the case of the ccRCCs, mutations in von Hippel-Lindau gene lead to accumulation of hypoxia-inducible factors

even when the tissue microenvironment is sufficiently oxygenated which, in turn, leads to uncontrollable accumulation of glycogen [91]. Low-rate glycolysis in normal cells serves as an efficient energy source, and thus low concentrations of glucose and glycogen in the smear samples of normal tissue cause the absence of their characteristic spectral bands.

2.4.6. The SERS analysis of the bladder tissue smears

In total tissue samples of 30 different patients were collected and analysed via SERS spectroscopy. The results of the histological examination for all of the collected samples are presented in the Table 5. All cancerous tissues were classified by TNM (tumor nodes, metastases), a clinically used standard for classification of spread of cancer.

Table 5. The results of histological analysis of the 30 bladder tissues used in the study.

Tissue type		Number of patients
Urothelial carcinoma	Low-grade pTa	9
	High-grade pTa	8
	High-grade pT1	3
	High-grade pT2a	2
	High-grade pT2b	1
	High-grade pT3a	2
Non-specific cystitis	–	5

As during the analysis of the kidney tissue smears, the SERS spectra were collected at five different points for each sample of extracellular fluid. This was performed in order to take into account the possible differences of the SERS spectra at different measuring points. The averaged SERS spectra of all extracellular fluid of normal, cancerous and cystitis-affected bladder tissues are presented in the Fig. 19. The spectra were vector normalized and are presented shifted along y-axis for clarity. Gray areas in the Fig. 19 indicate the standard deviation of the intensity of the SERS spectral bands. The intensity variation, like in the case with SERS spectra of the ECF of kidney tissue, may be reasoned by the differences in the total amount and distribution of structural molecules. This is reasoned by the patients' physiology, lifestyle, physical activity, and other factors. In addition, in the case of spectra of the ECF of cancerous tissues, the concentration of molecules in the sample may

be dependent on the stage or grade of the tumor. Furthermore, it is noteworthy that during the surgery the exact border line between normal and cancerous tissues is invisible. Therefore, the provided samples of cancerous tissue could include a small amount of healthy tissue and vice versa. In the presence of such sampling errors, the prepared samples of ECF might contain molecules from the foreign tissue and this then might be observed in the SERS spectra. As mentioned, to correct this, five spectra were collected at randomly chosen points for each sample.

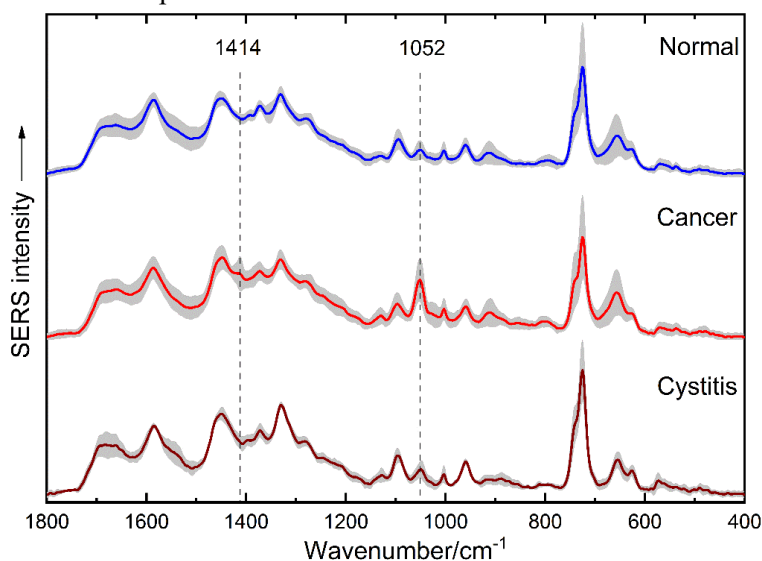


Fig. 19. The averaged SERS spectra of the extracellular fluid of normal, cancerous, and cystitis-affected bladder tissue samples.

As can be observed in the SERS spectra presented in the Fig. 19 all three types of samples have spectra with similar features. However, it was determined that prominent spectral differences are present in the SERS spectra of the ECF of the cancerous bladder tissue. These differences are the more intense vibrational spectral bands located at 1052 cm^{-1} and 1414 cm^{-1} , respectively. Though the spectral band located at 1052 cm^{-1} can be observed in the SERS spectra of the ECF of normal and cystitis-affected tissues, its intensity is at least twice lower. Meanwhile, the vibrational band at 1414 cm^{-1} is only observed in the spectra of the ECF of cancerous bladder tissue. To observe the possible spectral markers more clearly, the difference spectrum was made (see Appendix I, Fig. 8.). The averaged SERS spectrum of the ECF of normal tissue was subtracted from the averaged SERS spectrum of the ECF of cancerous bladder tissue. Observing the difference spectrum, the same

spectral markers can be distinguished more clearly. Furthermore, it can be observed that other spectral markers which were previously indistinguishable can be discriminated. These are the spectral bands at 1448 cm^{-1} and 660 cm^{-1} .

The assignment of the SERS spectral bands observed in the Fig. 19 can be made using the assignment of the spectral bands listed in the Table 3. This is because vibrational bands of similar molecules are expected to be observed for both kidney and bladder tissues. Therefore, it can be stated that the band located at 660 cm^{-1} is associated with the $\nu(\text{C-S})$ vibrations of cysteine. The band at 1052 cm^{-1} is associated with $\nu(\text{C-O})$ and $\nu(\text{C-N})$ vibrations of cysteine, lactic acid. As mentioned before, cysteine plays a major role in the development of cancer. In fact, the dependence of cancerous growth on the availability of cysteine was first observed in bladder cancer [120]. The increase in the amount of cysteine in the spectra is also indicated by the increased intensity of other vibrational bands associated with this molecule. However, the band at 1052 cm^{-1} is observed to increase more dramatically. This means that not only the increase in amount of cysteine but other molecules as well is influencing the observed differences. This is why this band was also assigned to vibrations of lactic acid molecules whose concentration is found to be increased due to the changed metabolism of glucose. Of course, cysteine is also found in proteins. The synthesis of proteins called growth factors is altered in cancer cells. For example, in bladder cancer cases, higher concentration of proteins which inhibit apoptosis or promote angiogenesis, lipid transport, and metabolism have been detected in both tissue and urine samples [138]. Therefore, the higher intensity of the spectral band at 1052 cm^{-1} could be partly explained by the higher concentration of the respective proteins in the cancerous tissue. This is also indicated by the other vibrational band which is observed only in the SERS spectra of the ECF of cancerous tissue. The spectral band doublet located at 1414 cm^{-1} and 1448 cm^{-1} is associated with CH_3 deformation vibration of proteins and amino acids [139]. Hence the changes in the intensity of this band can be reasoned by the changes in the genetic material present in the cancerous cells. One interesting feature of the SERS spectra of the ECF of bladder tissue is the absence of the spectral band associated with glycogen vibrations which was showed to be a good spectral marker for discrimination of cancerous kidney tissue. This result shows that finding a universal spectral marker for cancer is not a possible outcome and all cancer cases should be treated as individual and analysed separately.

Statistical importance of the spectral features was investigated by performing principal component analysis. The SERS spectra of the

extracellular fluid of bladder tissues were analysed in the spectral regions of the identified spectral marker bands. However, only the PCA in the region of the vibrational band located at the 1052 cm^{-1} revealed that the projection of the spectral data of the ECF of healthy, cancerous, and cystitis-affected tissues provides promising results. Thus, only the PCA of this region is further described. The spectral data of the samples prepared from the cancerous tissue clearly falls in a separate group while the spectral data of the samples prepared from normal and cystitis-affected tissues are grouped together. However, 4 of 21 points representing cancerous tissue samples fall into the group of points corresponding the healthy tissue data. Such result may be reasoned by the sampling of the cancerous tissue. A small amount of healthy tissue is often removed with the tumor during the surgery. Hence, as already mentioned, during extracellular fluid sample preparation the presence of such tissue might influence the spectral results since it would also contribute to the observed spectra. Furthermore, one data point representing the healthy set of points is grouped with the data representing the cancerous set of data. Nonetheless, the results are promising and suggest that it is indeed possible to discriminate between the normal and cancerous tissues via SERS spectroscopy of the ECF. Since the data set is not big enough a calculation of the accuracy of prediction is meaningless and was not performed. The results of the PCA clustering are presented in the Fig. 20.

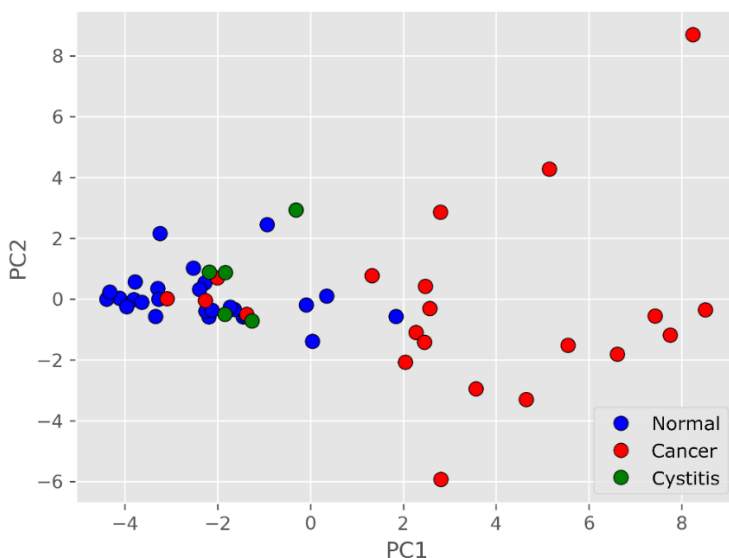


Fig. 20. The PCA score plot representing the results of the principal component analysis of the SERS spectra of the ECF of bladder tissue.

It is noteworthy that the points in the PCA score plot that correspond to the cystitis-affected tissues overlap with the group of points representing the healthy data set. This means that cystitis-affected tissue could be distinguished from the cancerous tissue but not from the healthy tissue by the intensity of the band located at 1052 cm^{-1} .

The spectral analysis of the cancerous tissues of the two renal system organs has shown promising results that the SERS spectroscopy can be employed for the precise discrimination of cancer. Furthermore, analysis of the extracellular fluid is easier and more informative than that of the whole tissue. In addition, low-temperature SERS spectroscopy as well as *ab initio* calculations were employed and provided more information about the nature of the observed spectral bands. The analysis of the SERS spectra has shown that the spectral markers for kidney and bladder tissue cancers are not the same. Kidney cancer can be distinguished most accurately via analysis of the intensity of the vibrational band of glycogen located at 481 cm^{-1} while cancerous bladder tissue via analysis of the intensity of the spectral band located at 1052 cm^{-1} . This vibrational band is associated with the vibrations of the cysteine and lactic acid molecules. Intensity of these bands in cancerous tissues increases thus indicating metabolic and chemical changes of the cancerous cells and their environment. Statistical analysis of the spectral data showed that identification of kidney cancer is viable with high accuracy. The sensitivity and specificity of the method reaches 93% which is sufficient and comparable to the methods of the clinical diagnosis. Statistical analysis of the spectral data of bladder tissue also provided promising results which showed that cancerous tissue can be well discriminated. However, a larger data set is required for the precise evaluation of the accuracy of the method.

CHAPTER 3.

SERS STUDY OF INACTIVATION OF PATHOGENIC BACTERIA

3.1. PATHOGENIC BACTERIA

Bacteria – an extremely diverse family of prokaryotic (having no nucleus) single-celled organisms, that inhabit almost all areas of the world. They are found in different environments from simple ones like soil to the very harsh ones like living in a pH of 0.06 or temperatures above 120 degrees Celsius [140]. This is why it is not strange that a lot of bacteria is found in the human environment and even the body. Most of the numerous species of bacteria are harmless to humans and can even be benefited from. For example, bacteria are used for chemical synthesis of various molecular species, pest control, food processing, etc. [141-146]. Also, bacteria in the digestion system of herbivores help them to break down cellulose and in humans to convert food to vitamins [147, 148]. However, a small percentage of all bacteria can be harmful to humans and cause diseases. These are called pathogenic and even though the number of such bacteria species are estimated to be fewer than a hundred they pose a considerable risk to human health. The pathogenic bacteria can cause such diseases as tuberculosis, pneumonia, diphtheria and other [149]. Food related pathogens are also causing a lot of illnesses. For example, it is estimated that nearly 1.7 billion cases of diarrheal disease are diagnosed every year in the world. This disease claims the lives of about 760000 children under the age of 5 years annually [150]. One of the culprits of food contamination is the *Escherichia coli* (*E. coli*) bacteria. In the decade from 2006 to 2016 more than 30 huge outbreaks of contaminated food were reported related with this type of bacteria. Out of these, an O104:H4 outbreak of 2011 caused damages to German farmers and industries which were worth around 1.1 billion euros and required emergency subsidies of around 200 million euros to 22 European Union member states. Furthermore, it is believed that microbiologically contaminated food can be potentially used for bioterrorism [151].

3.1.1. Inactivation of bacteria via photosensitisation

In order to produce healthy and safe food to the market the product has to be free of the pathogens. This can be done with various chemical and treatment procedures [152, 153]. However, because of the increasing demand, the food market is growing every year, and thus the ever-increasing amount of food

products has to be decontaminated [154]. This is why, a low cost and fast methods for microbial control are needed. One of the promising approaches to decontaminate food products is light dependent inactivation of pathogenic bacteria – photosensitization. This method is based on the photoactivation of photoactive compounds (photosensitizers) what in turn leads to the formation of reactive oxygen species (ROS). When activated the photosensitizer transfers from the ground state to an excited singlet state. Because of the short lifetime of this excited state the photosensitizer returns to the ground state via internal conversion thus releasing the excitation energy in a form of fluorescence or heat. The other pathway to the ground state is the conversion via intersystem crossing to the longer-living lower energy triplet state. From this state the photosensitizer returns to the ground state or it may interact with surrounding biomolecules and oxygen, producing various ROS [155]. These in turn should cause damage to the surrounding bacteria.

Molecules which contain a porphyrin ring in their chemical structure are the substances which are most often used as photosensitizers. Of these, chlorophyllin (Chl) is one of the most abundant, and thus cheapest to obtain [156]. It is a food additive (E 140) which is water soluble and has a negative charge. Furthermore, it was shown to exhibit good photosensitizing properties [157, 158]. Photosensitization using Chl was already successfully applied for decontamination of surfaces and fresh food products [159, 160]. It was shown that such treatment of the surface of fruit drastically reduced the naturally distributed mesophilic and pathogenic bacteria, yeasts and moulds. Furthermore, it was shown that the Chl-based photosensitization does not change the nutritional quality of the treated products [157, 161]. Moreover, the antimicrobial efficiency of this method is comparable with the high power pulsed light treatment approved by Food and Drug administration [162]. However, the inactivation of pathogens by photosensitization still needs to be improved and optimised. Thus, it is necessary to learn more about the mechanism of action of this method.

3.1.2. *Escherichia coli*

Escherichia coli is a vastly populated gram-negative rod-shaped bacterium found in the gut microflora of the warm-bodied animals but is also found in water, soil, and food. As like the other gram-negative bacteria the cell of *E. coli* has a thin peptidoglycan (containing lipopolysaccharides) layer sandwiched between the plasma membrane and the outer membrane of the bacterium what makes such type of bacteria resistant to many antibiotics and

other types of antibacterial treatment. *Escherichia coli* is an anaerobic bacterium (produces ATP without the need of oxygen). However, in the presence of oxygen it can also switch to the aerobic glycolysis. *E. coli* is one of the most diverse species of bacterium comprised of various strains of bacteria which differ in their genotypes and phenotypes. Most of the *E. coli* strains are harmless or even beneficial to humans. However, some types of *E. coli* namely the Shiga toxin-producing *E. coli* (STEC) and enterotoxigenic *E. coli* (ETEC) can cause severe illnesses arising from food poisoning.

3.2. EXPERIMENTAL DETAILS OF THE SERS ANALYSIS OF BACTERIA

3.2.1. Sample preparation

Bacteria samples both the treated via Chl-based photosensitization and the control (untreated), were provided by the Antibacterial Phototechnology group of the Institute of photonics and nanotechnology of Vilnius University. *Escherichia coli* bacteria were maintained on Luria-Bertani agar (LBA; Liofilchem, Roseto Degli Abruzzi, Italy; pH = 7.1) at a temperature of 37 °C. The stock suspension of the grown bacteria was diluted to $\sim 10^7$ CFU/ml (colony forming units per millilitre) and was used immediately. For the SERS analysis the bacterial suspension was first incubated in the dark with $5 \cdot 10^{-4}$ M Chl for one hour. Then, for one hour the sample was illuminated with 405 nm wavelength radiation. While preparing the control sample, bacteria were incubated in distilled water without illumination. Finally, *E. coli* samples were concentrated 5 times and used for the SERS measurements.

Samples for the SERS measurements of bacteria were prepared in the following manner. A Lee-Meisel colloidal solution which was concentrated by centrifuging at 6500 rpm and the bacteria suspension were mixed together with a ratio of 1:1. The specific colloidal solution and centrifuging parameters were chosen in accordance to the research done with the urinary tract cancers. The prepared mixture of colloidal solution and bacteria was deposited on the aluminium substrate as a 25 μ L drops and the SERS spectra were collected of both a solution and dried layer. Five spectra for all the samples were collected at random points of the sample in order to ensure that the spectral information which was collected from the sample was truly the spectral characteristic of said sample and not a random coincidence or interference.

3.2.2. The SERS spectroscopy of bacteria

Fourier transform (FT) Raman spectrometer MultiRAM (Bruker Optik GmbH, Germany) equipped with Nd:YAG laser (excitation wavelength 1064 nm) and liquid-nitrogen-cooled Ge diode detector was used to collect the SERS spectra of *E. coli* bacteria. All spectra were collected in the Raman shift region of from 4000 cm^{-1} to 200 cm^{-1} . Samples were irradiated, and the scattered light was collected in backscatter geometry using a gold plated 90° angle mirror objective with a focal length of 33 mm. This objective focused the laser light to a spot of 100 μm in diameter. The laser power was set to 100 mW during all measurements since it gave the highest signal intensity with the least thermal degradation of the sample. The resulting spectra were a Fourier transformed average of a 300 interferograms. Blackman-Harris 3-Term apodization function was applied and zero filling factor of 2 was used. Spectra were collected using the resolution of 4 cm^{-1} .

3.3. SERS STUDY OF BACTERIA: RESULTS AND DISCUSSION

Chlorophyllin-based photosensitization is an innovative and promising approach for the decontamination of fresh produce from microbial fouling [161]. Still, this method has limited susceptibility to gram-negative bacteria [163]. In order to optimize this technique and to find ways to combine it with other antimicrobials, it is necessary to understand the precise mechanism of the destruction of the bacteria cells. In order to evaluate the chemical alterations at the bacterium surface, induced by the Chl-based photosensitization, the SERS spectroscopy was employed. Therefore, the aim of this research was to apply SERS spectroscopy for the analysis of bacteria cell damage. Also, this research was intended for gathering more information about mechanism of inactivation of the main food pathogen *Escherichia coli* bacteria by Chl-based photosensitization.

First of all, pure chlorophyllin was analysed. This was done in order to check whether the chlorophyllin will contribute to the spectrum of bacteria after treatment. In the same regard the Raman spectrum of colloidal solution was also collected. The collected SERS spectra of a pure *E. coli* bacteria, 0.5 mM of aqueous solution of chlorophyllin, and a Raman spectrum of the colloidal solution of silver nanoparticles are presented in the Fig. 21. The presented spectra were shifted along the y-axis.

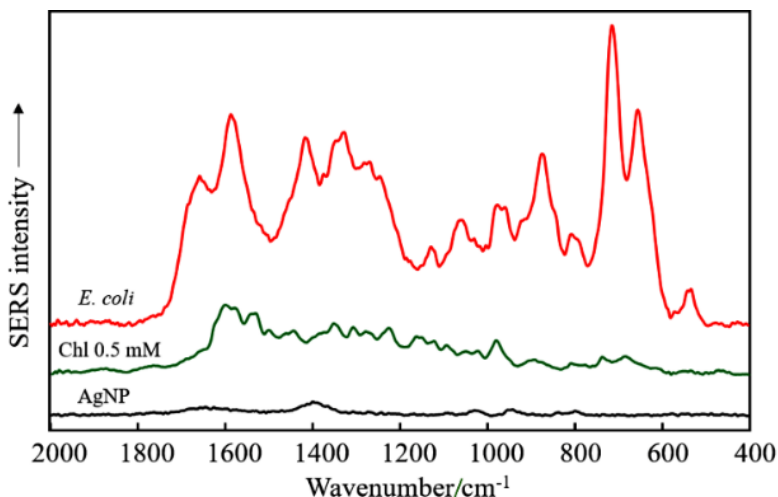


Fig. 21. The SERS spectra of *E. coli* bacteria, aqueous solution of chlorophyllin (0.5 mM), and a Raman spectrum of nanoparticles.

As can be seen in the comparison of the overall intensities of the collected SERS spectra presented in the Fig. 21 the SERS spectrum of pure bacteria has the most intense and prominent spectral features. Compared to it, the SERS spectrum of the colloidal solution of silver nanoparticles does not have any intense characteristic vibrational bands which could burden the analysis of the bacteria. Thus, the influence of the AgNPs was not considered as a possibility. The SERS spectrum of chlorophyllin is more intense and is comprised of several spectral bands. It is worth noting that the bands of chlorophyllin could be expected to be observed in the spectrum of damaged cells. However, the intensity of the SERS spectrum of chlorophyllin in comparison to the SERS spectrum of bacteria is relatively low – around three times less intense. Thus, the most intense spectral bands of the chlorophyllin molecule, located in the vicinity of 1600 cm^{-1} , should be overlapped by the amide vibrational bands in the spectrum of bacteria. Therefore, it is safe to assume Chl should not give any meaningful influence to the SERS spectrum of bacteria, since the same concentration of the solution (0.5 mM) was used to damage *E. coli* bacteria. The assignment of the normal molecular vibrations to the spectral bands of Chl was made in accordance to the literature [164] and is presented in the Table 5. The numbering of carbon atoms used for the assignment is related to the chemical structure of chlorophyllin and is presented in the Fig. 22.

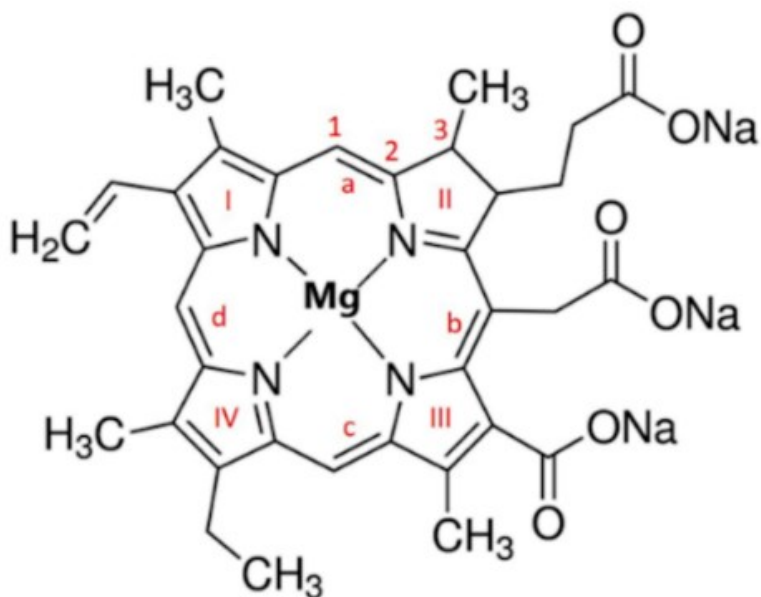


Fig. 22. The chemical structure of chlorophyllin and the numbering of its atoms.

Table 5. The most intense spectral bands of the SERS spectrum of chlorophyllin and their assignment. In accordance to the [164].

Wavenumber/cm ⁻¹	Assignment
1607	$\nu(\text{C2C1})$ a, b
1576	$\nu(\text{C2C3})$ III; $\nu(\text{C3C3})$ I
1532	$\nu(\text{C3C3})$ I; $\nu(\text{C2C3})$ III
1503	$\nu(\text{C2C3})$ I; $\nu(\text{C1C2})$ d
1448	$\nu(\text{C1C2})$ c, d; $\nu(\text{C2C3})$ I-III
1354	$\nu(\text{C2N})$ I, III; $\nu(\text{C2N})$ IV
1308	$\nu(\text{C2N})$ I; $\delta_{\text{in}}(\text{C1H})$ a
1283	$\nu(\text{C2N})$ II, IV; $\delta_{\text{in}}(\text{C1H})$ a, d
1269	$\nu(\text{C2N})$ II, IV; $\delta_{\text{in}}(\text{C1H})$ a, d
1225	$\delta_{\text{ip}}(\text{C1H})$ IV; $\delta_{\text{op}}(\text{C1H})$ d
1162	$\nu(\text{C3H})$ IV
1133	$\nu(\text{C2N})$ II; $\nu(\text{C2NC2})$ I
1052	$\nu(\text{C2C1})$ a; $\nu(\text{C2N})$ I, IV
1025	$\nu(\text{C2N})$ II; $\delta_{\text{ip}}(\text{C1C2N})$ II
981	$\delta_{\text{ip}}(\text{C1C2N})$ III

As already mentioned, the SERS analysis of the *E. coli* bacteria was performed both before the Chl-based photosensitization (control samples) and after in order to find the spectral differences resulting from the treatment of bacteria. It should be noted that it was determined that the performed chlorophyllin based photosensitisation procedure reduced the viable bacteria cell number by more than 98%. The SERS spectra of the *E. coli* bacteria before and after the treatment and the SERS spectrum of the aqueous solution of chlorophyllin (0.5 mM) are presented in the Fig. 23. For the sake of clarity, the presented spectra are shifted along the y-axis and the spectra of chlorophyllin was scaled (scaling factor of 3) so that intensities of the spectra would be comparable. The positions of the most prominent spectral bands are listed above each spectrum.

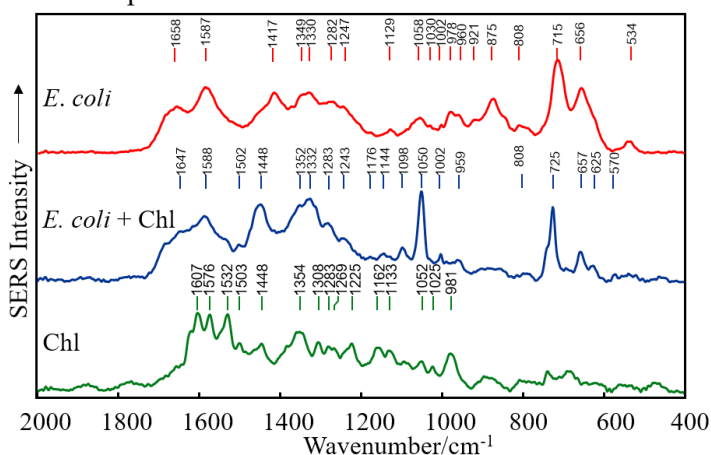


Fig. 23. The SERS spectra of: *E. coli* in the buffer solution (top), *E. coli* affected with $5 \cdot 10^{-4}$ M Chl for 1 h incubation with light dose: 36 J/cm^2 (middle), and aqueous solution of 0.5 mM of chlorophyllin (bottom).

It was noticed that in the spectra presented in the Fig. 23 clear spectral differences can be observed between the two spectra of *E. coli* bacteria. The most prominent spectral differences are the appearance of the two intense spectral bands located at 1448 cm^{-1} , 1098 cm^{-1} , and 1050 cm^{-1} in the SERS spectrum of the *E. coli* bacteria after the Chl-based photosensitization. In order to comprehend the changes happening in the samples after treatment assignment of the vibrational bands was made in accordance to the literature [165-167]. Assignment of the most prominent bands of the both *E. coli* spectra is presented in the Table 6.

Table 6. The positions of the SERS spectral bands of *E. coli* and *E. coli* after Chl-based photosensitization and their assignment. In accordance to the [165-167].

<i>E. coli</i>	<i>E. coli</i> + Chl	Molecular fragments	Assignment
Wavenumber/cm ⁻¹			
1658	1647	Proteins	Amide I, C=C, C=O
1587	1588	Proteins	Phe, Amide II
...	1448	Lipids	$\delta(\text{CH}_2)$
1417	...	Proteins	$\nu(\text{COO}^-)$, $\nu(\text{C=O})$
1349	1352	Proteins	$\delta(\text{CH})$
1330	1332	Proteins, carbohydrates	$\nu(\text{NH}_2)$, $\delta(\text{CH})$
1282	1283	Proteins, carbohydrates	$\nu(\text{COO}^-)$, $\nu(\text{C-O})$, $\delta(\text{CH}_2)$ Amide III
1247	1243	Proteins	Amide III
...	1176	Amino Acids	$\delta(\text{CH})$
...	1144	Lipids	$\nu(\text{C-C})$
1129	...	Nucleic acids	$\nu(\text{COC})$, ring breathing
...	1098	Carbohydrates, Lipids	$\nu(\text{C-C})$, $\nu(\text{C-O-C})$ or $\nu(\text{O-P-O})$
1058	...	Proteins, Carbohydrates	$\nu(\text{C-C})$, $\nu(\text{C-N})$
...	1050	Carbohydrates	$\nu(\text{C-C})$, $\nu(\text{C-N})$
1030	...	Proteins	$\nu(\text{C-C})$, ring breathing
1002	1002	Proteins	Phe ring breathing
978	...	Carbohydrates	
960	959	Proteins	$\nu(\text{C-N})$
921	...	Carbohydrates, Proteins	$\nu(\text{C-COO}^-)$
875	...	Proteins, Lipids	$\nu(\text{C-C})$, $\nu(\text{C-O-C})$, choline group
808	808	Amino acids	$\nu(\text{C-N})$ or $\nu(\text{O-P-O})$
...	725	Nucleic acids	Adenine, glycosidic ring mode
715	...	Nucleic acids, Lipids	Adenine, C-N membrane lipids
656	657	Amino acids	$\delta(\text{COO}^-)$
...	625		Aromatic ring skeletal
...	570	Carbohydrates	C-C skeletal
534	...	Carbohydrates	Glycosidic ring $\delta(\text{COC})$

The assignment of the spectral bands has shown that most of the observed spectral features in the SERS spectrum of the *E. coli* bacteria before treatment are related to the vibrations which are also common in the SERS spectra of biological tissues and cells [168]. These are mainly vibrations of proteins, carbohydrates, lipids, and amino acids. For example, vibrational bands in the SERS spectrum observed at 1658 cm⁻¹, 1587 cm⁻¹, 1282 cm⁻¹, 1247 cm⁻¹ are attributed to amide vibrations – vibrations of protein molecules. Other spectral bands related to the vibrations of the structural elements of proteins also

observed at 1417 cm^{-1} , 1349 cm^{-1} , 1030 cm^{-1} , 1002 cm^{-1} , and 960 cm^{-1} . Spectral bands related to the vibrations of carbohydrates or lipids which are common building structures of the cell wall are observed at 1330 cm^{-1} , 1282 cm^{-1} , 978 cm^{-1} , 921 cm^{-1} , 875 cm^{-1} , and 534 cm^{-1} . Only several bands in the SERS spectrum were found to be reasoned by the nucleic and amino acids. Vibrational bands of the same or similar origin are observed in the spectrum of the bacteria treated with chlorophyllin based photosensitisation. However, as already mentioned there are clear differences between the two SERS spectra. The major differences are the appearance of intense spectral bands located at 1050 cm^{-1} , 1448 cm^{-1} and 1098 cm^{-1} . Besides that, the intensity of the bands related to the normal vibrations of proteins or their structural elements drops in the SERS spectra of the treated bacteria. These bands are located at 875 cm^{-1} , and 657 cm^{-1} . It was also noticed that the spectral band related to the amide vibrations was red shifted from 1658 cm^{-1} to 1647 cm^{-1} what could indicate the structural changes of proteins.

In order to ensure the importance of the observed spectral changes the SERS spectra were collected at different randomly selected points of the sample. It was noticed that the above-mentioned spectral differences are observed throughout the whole sample and are not resulted from a random deviation in the composition of the samples or other type of interference. Only the overall intensity of the SERS spectra, between the spectra measured at different points of the sample, was observed to be changing. This is most likely reasoned by the uneven thickness of the sample. The average of the collected SERS spectra of *E. coli* bacteria before and after the Chl-based photosensitization are presented in the Fig. 24. The grey areas in the figure represent the deviation in the intensity of the bands. The recurrence of the spectral information shows that differences observed in the SERS spectra are in fact linked to the effect of the *E. coli* bacteria damage induced by the treatment with chlorophyllin. This is why these spectral differences could be regarded as potential spectral markers of the damaged bacteria.

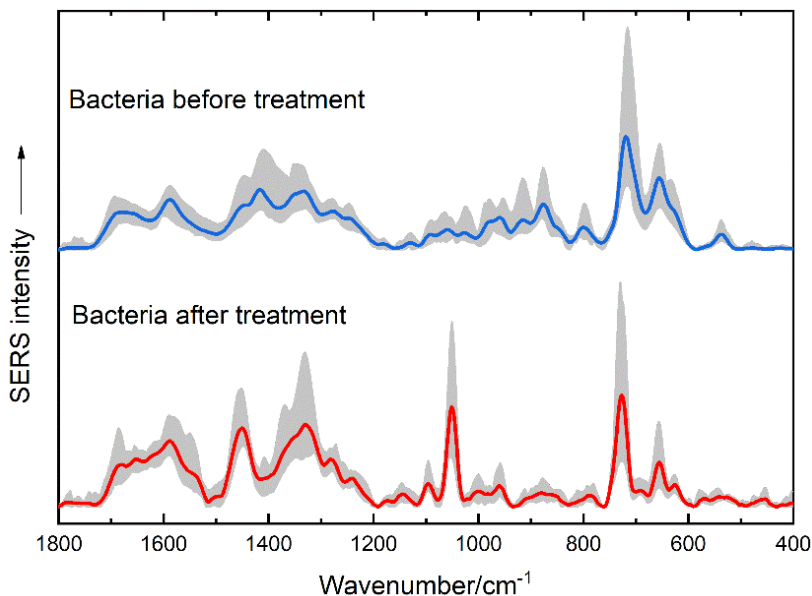


Fig. 24. The intensity changes of the spectral bands in the SERS spectral of the *E. coli* bacteria before and after the Chl-based photosensitization.

It has been shown that close contact between the bacteria and the photosensitizer is necessary for the disruption of bacterial membrane [169]. Usually, the interaction between anionic photosensitizers and bacteria is manifested by electrostatic interactions, which form between the photosensitizer and divalent cations (Mg^{2+} , Ca^{2+}) in the cell wall of bacteria [170]. It is accepted that the photosensitization treatment triggers the production of reactive oxygen species or singlet oxygen [155]. This depends on the chemical structure of the photosensitizer and the surrounding microenvironment [162]. It was proven that inactivation of *Salmonella* (another gram-negative bacterium) by Chl-based photosensitization was based on type II mechanism [165].

This inactivation pathway was confirmed by the results of this study which were carried out at the Antibacterial Phototechnology group. They have shown that main mechanism of Chl-based photosensitization inactivation of bacteria is indeed ROS-mediated – creation of singlet oxygen (1O_2) and hydroxyl radical ($\cdot OH$). This was proven by the fact that L-histidine a scavenger of these species was shown to preserve the destruction of bacteria by photosensitization [171]. Furthermore, it was shown that type I mechanism also occurs in Chl-based photosensitization induced *E. coli* inactivation and

that creation of ROS is not the only mechanism responsible for bacterial death, since L-histidine did not preserve all bacteria.

Having in mind the mechanism of action of the Chl-based photosensitization it is not at all surprising that the spectral band located at 1050 cm^{-1} , which is attributed to the vibrations of some sugars or amino sugars located in the membrane, is observed in the SERS spectrum of the treated bacteria [172]. It is known that the membranes of the cells contain various carbohydrates and the gram-negative bacteria cells have peptidoglycan layer (comprised of a crosslinked mesh of sugars and amino acids) between the two membranes. The low intensity of the spectral bands of these molecules in the SERS spectrum of unaffected bacteria can be explained by the close packing of molecules in the membrane of undamaged cells. In such case carbohydrate molecules cannot appear in the close vicinity of the metal nanoparticles and adsorb on their surface, what results in low Raman scattering enhancement factor. When the membrane is damaged, fragments of carbohydrates from the membrane structure, the peptidoglycan layer or even from the inside of the cell can get close to the nanoparticles. This in turn leads to the strong spectral bands of the fragments of the carbohydrates observed in the SERS spectra. This effect is expected when chlorophyllin is added to the media containing bacteria [165]. Furthermore, this hypothesis is backed up by the increased intensity of the spectral bands, located at 1448 cm^{-1} and at 1098 cm^{-1} . The first band is related to the $\delta(\text{CH}_2)$ and the second one to the $\nu(\text{C-C})$ normal vibrational modes of the lipids. Lipids are the base substance of all membranes, and thus the increase of intensity of the spectral bands related to lipid vibrations could indicate the disruption of the membrane. Also, it may indicate the oxidative stress response of the bacteria - lipid peroxidation of the *E. coli* cell membrane, which was described in the literature [173]. The other changes observed after Chl-based photosensitization treatment – the reduced intensity of the bands, located at 875 cm^{-1} , 657 cm^{-1} and spectral band, which got red shifted from 1658 cm^{-1} to 1647 cm^{-1} indicate that some changes related to the proteins and their structure are taking place as a result of the treatment of bacteria with chlorophyllin. Such chemical changes can be considered as an outcome of the ROS effect on bacteria [174]. To sum up these findings, the spectroscopic analysis of the treated bacteria leads us to believe that the disruption of the integrity of the cell membrane is the key effect of the Chl-based photosensitization. This idea can be confirmed by other studies which have shown that *E. coli* mutant NR698, which has no outer membrane is as susceptible for Chl-based photosensitization as well as gram-positive *Bacillus subtilis* [156].

The results of this study confirmed that chlorophyllin is able to attach to the cell wall of *E. coli* bacteria and that the mechanism of inducing lethal destruction of bacteria is the creation of reactive oxygen species (ROS). SERS analysis of the treated bacteria revealed that the main spectral markers of the chemical changes of bacteria are the increased intensity of the bands located at 1050 cm^{-1} , 1098 cm^{-1} , and 1448 cm^{-1} in the spectra of the treated bacteria. These bands correspond to the vibrations of carbohydrates and lipids respectively what indicates that there is a higher abundance of free carbohydrates and lipids in the sample of the treated bacteria. This change is most likely reasoned by the disruption of the cell membrane of bacteria by the ROS which are created during photosensitization. The damage to the integrity of the cell wall results in the availability of the structural molecules which are normally integrated in the bacteria membrane. The adsorption of these molecules onto the surface of spherically shaped silver nanoparticles employed in this work for the enhancement of the Raman signal led to the increased intensity of the observed spectral bands.

CHAPTER 4.

SERS STUDY OF PHARMACEUTICALS AND DRUGS IN BLOOD AND SALIVA

4.1. BLOOD AND SALIVA

As other biological fluids like cerebrospinal, synovial, pericardial fluids etcetera, blood and saliva are produced and secreted in the human body. Both of these fluids are complex substances which contain various molecular species like mineral ions, proteins, hormones and many more [175, 176]. Cells of different types are one more common component found in these fluids and are found in high concentrations. For example, the red and white blood cells and platelets produced in the bone marrow make around 45% of the blood of vertebrates while the rest is blood plasma. The primary function of blood is delivery of the necessary substances for metabolism throughout the whole body. Various nutrients, as well as oxygen, are transported via blood to the cells. On top of that, metabolic waste produced in the cells is transferred by blood to the organs for disposal. In contrast, saliva is mostly composed of water but also contains white blood cells, epithelial cells, various dissolved electrolytes, proteins and other biomolecules. At least four essential functions, namely lubrication, digestion, oral hygiene, solubilization are attributed to the uses of saliva. Moreover, the composition of saliva is interconnected with the composition of blood, thus molecules dissolved in blood are frequently detected in the composition of saliva [177].

4.1.1. Detection of molecules in blood and saliva

The fact that biological fluids are composed of molecules whose concentration is directly linked to the human metabolism results in the potential use of these biological fluids for the detection of diseases or their phenotypes, the use of certain drugs or pharmaceuticals, and the monitoring of the organ function. Metabolomics encompasses the fields of research dedicated to this goal. In most cases, detection of diseases via analysis of biological fluids is accomplished via specific biomolecular markers which are linked to the changed metabolism induced by the disease. Hence, the detected abnormalities (drastically increased or decreased concentration of biomarkers) indicate the altered function of organs and the presence of a certain disease. Various biomarker molecules are already employed for detection in clinical practice. These, for example, are certain proteins like prostate-specific antigen

(PSA) in the case of prostate cancer [178] or single molecular species like glucose in the case of diabetes [179]. Also, research is constantly done to discover new or more specific biomarkers [180-183]. However, it is not easily done because of the complex composition of the biological fluids and the constantly varying composition of the constituents.

Various analytical methods are employed for the detection of the biomarkers in biological fluids. The most common chemical analysis methods used for metabolomics are nuclear magnetic resonance (NMR), gas chromatography tandem mass spectroscopy (GC/MS) and liquid chromatography tandem mass spectroscopy (LC/MS) [184, 185]. These methods are known to be sensitive and allow precise analysis of the chemical composition and structure of the samples. These methods have been used for the analysis of blood in order to detect of various diseases like ovarian cancer [186], oral cancer [187], tropical diseases [188], and other. Saliva analysis employing these methods has shown that high precision identification of oral cancer [189] or breast cancer [190] can be achieved. As well as the detection of viruses and bacteria is possible [191, 192].

Other methods like immunoassays are also being employed to improve the analysis [193, 194]. Vibrational spectroscopy methods are also employed as a standalone technique for the analysis of all sorts of biological fluids [195]. However, conventional vibrational spectroscopy methods in most cases lack the sensitivity required to detect the low concentration of metabolites. Furthermore, the water absorption of the IR light and the fluorescence background seen in the Raman scattering spectra makes the application of these methods even harder. This is why the SERS spectroscopy as a method of choice for the detection of various biomolecules in biological fluids has been increasingly proposed. The advantages of the SERS spectroscopy – high signal enhancement and fluorescence quenching [38, 43], resolve the issues of application of vibrational spectroscopy mentioned above. Thus, it has been shown that the SERS spectroscopy could be potentially applied in clinical situations for the early detection and as a result prevention of severe outcomes of diseases [42, 44]. However, most of the time in such researches the analysis of the simplified samples is made. Only model solutions of biological fluids including saliva and blood are prepared and analysed. In such cases, the many pathways of the analyte interaction with the other components of the biological fluids are not taken into account. Therefore, this approach is not sufficient if the SERS method is supposed to be used for clinical practice. For this application, real-life samples have to be analysed in order for the analyte molecule to be transferred throughout the whole metabolic pathway. This type

of analysis is more difficult to perform, nevertheless it is necessary in order to be approved for clinical practice.

4.1.2. Acetyl salicylic acid (aspirin)

Acetylsalicylic acid (conventional name aspirin) is an orally admissible drug of the family of salicylates. It is an over the counter (OTC) analgesic (used against minor pains), antipyretic (anti-fever) and anti-inflammatory drug widely used throughout the entire world. Overdosing on aspirin is not very simple since a large amount of the drug must be taken. However, many patients have to take this drug daily both pure or as a constituent of other medications. The chronic ingestion results in the build-up of salicylic acid what leads to the salicylate poisoning. This is especially common for elders. The effect on health is observed if the concentration of salicylic acid in blood is 40-80 mg/dL or 3-6 mM and with higher concentrations it can cause dysfunction in renal and hepatic activity [196-198]. Naturally, acetylsalicylic acid is not discovered in the human body. When ingested aspirin is absorbed directly in the blood where it is primarily seen unhydrolyzed. However, in blood it is rapidly metabolised by the carboxyl esterase with the average half-life of around 20 minutes [199]. For example, this leads to almost all molecules of acetylsalicylic acid (27-30% is still present in blood) to be hydrolysed to salicylic acid at therapeutic intake dose, which normally equals to 1 g [199-201]. It should be noted that some amount of acetylsalicylic acid is hydrolysed in the gastrointestinal mucosa and liver. However, this leads to the same outcome since after that it is absorbed in the blood in its metabolised form – salicylic acid. As follows, in blood the hydrolysed form of this drug can be detected only for a short period of time. The direct detection of acetylsalicylic acid is also burdened by the fact that aspirin is known to bind to platelets and cyclooxygenases COX-1 (and depending on the dose to COX-2). Therefore, after an hour of ingestion around 80–90% of the available aspirin is found to be irreversibly bound [199, 200]. At this time the concentration of free acetylsalicylic acid in blood is too low for detection. This is why, the toxicity and the intake dose of aspirin is evaluated not by direct detection of the pharmaceutical but from the concentration of salicylate (a salt or ester of salicylic acid) in blood [202]. To be more specific, the pharmaceutical properties of aspirin are known to be dependent on the acetylating action of these molecules [203]. Compared to the acetylsalicylic acid, its metabolite - salicylic acid (SA), has a considerably longer half-life which may vary between 3 hours and 30 hours depending on the intake dose.

SA is also observed to be capable of binding to other molecules like proteins in blood or serum. The percentage of the bound SA molecules also depends on the intake dose, which relates to the concentration of SA. At low concentrations, around 90% of SA molecules can be bound. However, when the concentration is increased, the binding sites are saturated and the percentage of bound SA can be as low as 30% [204, 205].

After the metabolism of acetylsalicylic acid, the metabolites, namely salicylic acid and the group of molecules related with SA by their chemical structure (salicylates) are disposed from the body via urination. The time for the disposal of SA depends on the intake dose of aspirin. For example, at customary doses which are considered being from 325 mg to 500 mg, the half-life of SA in blood is observed to be from 3 hours to 5 hours. At more excessive doses, the pharmacokinetic pathway rate of SA decreases. For example, at the intake dose of 3.6 g, the half-life of SA molecules is observed to increase to 12–16 h [206, 207]. To be clear, SA concentration in blood that is higher than 4 mM is considered to be dangerous, while concentrations below 3 mM are considered to be therapeutic. When the SA concentration in blood exceeds 5 mM it is considered lethal. The peak value of the SA concentration in blood is 0.3 mM at the aspirin intake dose of 640 mg and it is reached in 30-60 minutes after consumption [208]. While the intake of 1.2 g of acetylsalicylic acid results in a maximum concentration of SA value of 0.7 mM after 1 h [209]. It should be noted that salicylic acid or other salicylates are also present in other biological fluids. However, the average concentration in these fluids is a lot smaller than in blood. For example, the detectable concentration of SA in synovial fluid is as two times, and in cerebrospinal fluid and perilymph five times lower than the concentration in blood [210].

Various methods have been already implemented for the direct or indirect detection of aspirin in blood [211-213]. However, the proposed methods either involve laborious chemical treatment of the samples or require sophisticated and costly equipment. Furthermore, the samples that were measured during these studies are whole blood or blood serum which were spiked with acetylsalicylic or salicylic acid and no real-life samples were analysed. The SERS spectroscopy has also been applied for the detection of aspirin in blood employing microgels and agglomerates of silver nanocubes [214]. However, this study was performed using the blood of rats that was spiked with 30 mg/dl of aspirin and did not reflect the real clinical problem.

4.1.3. Acetaminophen (Paracetamol)

N-acetyl-para-aminophenol (APAP), also known as acetaminophen or paracetamol is an over-the-counter pain and fever reducer mostly ingested orally. Like acetylsalicylic acid it is a non-steroidal and anti-inflammatory drug considered as analgesic. Paracetamol is also one of the primary choices for a fast relief. In fact, it is the first choice of painkillers in USA and Europe. Acetaminophen is often included in other pharmaceutical products and is combined with active substances like opioids. Therefore, many people are unaware of its consumption. This can lead to severe outcomes, since overdosing on acetaminophen causes severe liver toxicity. What is more, the overdosing of paracetamol is one the leading causes of the liver transplantation in the world [215, 216]. It is noteworthy that paracetamol poisoning is common and dangerous for both the children and adults [217]. The blood concentration of paracetamol is dose dependent. For example, after oral ingestion of 1.5 g of paracetamol, the peak level of paracetamol reaches 17.5 mg/L after 40 minutes. Meanwhile, after consuming 4 g of paracetamol, the peak concentration 62.4 mg/L was reached after 60 minutes [218]. The safe dose of paracetamol is considered to be up to 4 g/day for adults and 60 mg/kg per day for children. Acute toxicity of paracetamol develops when the dose is above 140 mg/kg [219]. Upon consumption, acetaminophen is quickly absorbed by the gastrointestinal tract. Therefore, its concentration reaches therapeutic levels from 30 minutes to two hours. In blood paracetamol is mainly found not bound to plasma proteins. The half-life of paracetamol is 1.5-2.5 hours at normal doses [220]. However, in the case of overdosing the half-life is prolonged and is evaluated to be around 4-8 hours [217]. Paracetamol is metabolised in the liver via three main metabolic pathways [221]. Most of the acetaminophen molecules are metabolised into inactive compounds via glucuronidation (52-57%), and sulfation (30-44%). However, around 5-10% of the molecules are metabolised by cytochrome P450 enzymes to a reactive metabolite N-acetyl-p-benzoquinone imine (NAPQI), which is responsible for the paracetamol induced liver toxicity. Under high doses of ingestion, the first two metabolic pathways are saturated and more toxic metabolites are produced. It is known, that around 5% of acetaminophen is excreted nonmetabolized and the amount increases when higher doses of acetaminophen is consumed. Paracetamol is mostly disposed via renal excretion.

Detection of paracetamol was already performed with various methods like chromatography [222-224], immunoassays [225, 226]. These methods

perform well and have high sensitivity of detection. However, the cost of reagents and equipment, and the overall time of the analysis are too high. Therefore, novel detection methods are being developed. The SERS spectroscopy is not an exception. It has already been proposed for the detection of paracetamol [227, 228]. Nonetheless, the detection capabilities were tested only for model samples of the drug in water or synthetic urine.

4.1.4. Caffeine

Caffeine is one of the most popular psychoactive drugs that is easy to come by worldwide. Since it is a legal substance, it is in the composition of many beverages and foods. These products are widely consumed every day for the purpose of stimulating the central nervous system. Besides that, when consumed caffeine is also responsible for increasing the energy metabolism in the brain, activating the noradrenaline neurons, affecting the local release of dopamine and other bodily functions [229]. Because of the popularity of this molecule, the pathways of the metabolism of caffeine in the human body have been thoroughly studied for several decades and it is now quite well-understood. Foremost, it was determined that within an hour after ingestion caffeine is absorbed by the stomach (around 20%) and the small intestine and enters the blood [230]. In blood plasma the concentration of caffeine is determined to be the highest. There it can be present both bound to proteins and free. In fact, it was determined that the ratio of the concentrations of these two types of caffeine molecules (bound and free) in plasma is almost equal [231, 232]. However, caffeine is highly soluble in water what results in the ability of this molecule to easily enter the tissue water compartment. Because of this, when absorbed in blood caffeine is distributed through almost all bodily fluids. For example, it is detectable in high concentrations in saliva [233]. In fact, it was determined that in saliva the concentration of caffeine is proportional to the concentration of caffeine molecules that are found non-bound to proteins in plasma [231]. The estimated concentration of caffeine in human saliva is from 65% to 85% that of the concentration in plasma. Caffeine is mainly metabolised in the liver. The first step of the metabolism of caffeine is the demethylation of molecules by the isoenzyme CYP1A2. Then, the process of a successive demethylation which involves other isoforms of CPY is carried out [234]. The rate at which caffeine molecules are metabolised varies. As a result, the half-life of caffeine (time required for half of the molecules to be metabolised) can be different for an individual person. The half-life is also found to be dependent on the intake

dose of caffeine. For example, in healthy humans, the metabolism rate of caffeine can be described by the first-order kinetics if the intake dose is in the range from 2 mg/kg to 10 mg/kg. The dose of caffeine here is expressed in a mass of caffeine for a unit of body mass. Nonetheless, it is determined that on average for a 4 mg/kg dose of caffeine the half-life is round 5.5 hours. The final step of caffeine metabolism is disposal, which is typically done via renal excretion. However, the caffeine molecules which were not metabolised are reabsorbed back into the body, and the whole cycle begins again. This shows that the reabsorption of caffeine molecules also limits the rate of their metabolism [235].

The process of caffeine metabolism results in the three main products - paraxanthine, theobromine and theophylline, which are also active compounds, and thus undergo further metabolization. The yield of the production of these metabolites differs what results in the different concentrations of the products which are found in the human body after caffeine consumption. It was determined that paraxanthine is the most abundant metabolite of caffeine. In fact, the creation of these molecules is around 8 times and 23 times faster than that of theobromine or theophylline, respectively. Therefore, almost 80% of caffeine molecules during their metabolism in the end are converted to paraxanthine [236]. Keeping this in mind, it can be reasonably assumed that only the concentration paraxanthine can be investigated in order to evaluate the metabolism of caffeine. It has been shown that the concentration ratio of the paraxanthine and caffeine molecules in plasma and as well in saliva increases overtime. This is because the concentration of caffeine is found to be highest around 30 minutes after consumption and then gradually decreases while the paraxanthine concentration increases and reaches its maximum at around 5-6 h after ingestion. It is also estimated that the concentration of paraxanthine becomes higher than caffeine at around 8-10 h after ingestion of caffeine [237].

The pharmacokinetic studies of paraxanthine have shown that that the clearance rate of paraxanthine is very similar to that of caffeine [238]. Results of pharmacokinetics of caffeine and paraxanthine provide information that at least one hour after consumption both molecules should be present in saliva. In such case spectral bands of both of the molecules should be observable in the SERS spectra of human saliva. Detection of caffeine intake could be achieved by detecting one of these molecules.

In biological fluids caffeine is detected utilizing the standard techniques of metabolomics [239-241]. However, other methods are also being employed [242]. In case of vibrational spectroscopy methods, they have

already been implemented for investigation of caffeine and saliva [243-245]. Several biological fluids were also analysed using the EC-SERS spectroscopy [246-248]. Nonetheless, detection of caffeine or other similar types of drugs in biological fluids via the EC-SERS spectroscopy have never been investigated. Also, as already mentioned, only model samples have been used in the research. Even though the analysis of the real-life samples is more complicated, it is necessary to analyse such samples in order to adapt spectroscopic or other types of methods for clinical practice.

4.2. EXPERIMENTAL DETAILS OF THE SERS SPECTROSCOPY OF BLOOD

4.2.1. Preparation and characterisation of colloidal solutions of silver and gold nanoparticles

In this work various colloidal solutions of silver and gold nanoparticles were prepared since the main goal was to find the most suitable solution for the detection of aspirin traces in human blood. Silver and gold were chosen since they are routinely used to enhance the Raman scattering of molecules. It is known that in most cases silver produces higher enhancement factor than gold, however silver nanoparticles are less stable than nanoparticles prepared from gold.

The synthesis procedures differed in the surface chemistry approaches for the preparation of the nanoparticles. The key difference was the use of different capping agents, which were used during the synthesis. Capping agents have a great importance since they can influence the interaction between the analyte molecule and the nanoparticle. Also, different capping agents are used in order to shape the prepared nanoparticles. For example, the Lee-Meisel synthesis procedure which was described in the previous chapter uses tri-sodium citrate for stabilization. Such nanoparticle stabilization is based on the electrostatic forces (two nanoparticles cannot agglomerate because of the repellent force of the adsorbed citrate molecules). The analyte molecules can adsorb on such nanoparticles in two ways: 1) by substitution of citrate molecules on the surface of the nanoparticle; 2) or by the interacting with the citrate [249]. Nanoparticles can also be stabilised by steric stabilisation. This type of stabilization is based on mechanical repulsion of polymeric species. Steric stabilization of nanoparticles was achieved using polyvinylpyrrolidone K30 (PVP), which because of different adsorption properties on the crystal structures allows the preparation of various shapes of

nanoparticles [250]. The synthesis of non-spherical structures is beneficial since they can increase the enhancement of the Raman scattering. Polymer use also changes the adsorption of the analyte, since the interaction between the analyte molecule and polymer is also different.

For the preparation of silver nanoparticles, three different synthesis procedures were used. These were: 1) nanoparticles stabilised with citrate (Ag-cit), 2) nanoparticles prepared by polyol synthesis procedure and stabilised with PVP (Ag-PVP), 3) nanoparticles prepared by reduction with sodium borohydride and stabilised with PVP (Ag-BH₄). Two nanoparticle solutions were synthesised from gold via two different procedures which were as follows: 1) nanoparticles stabilised with citrate (Au-cit), and 2) nanoparticles stabilised with PVP (Au-PVP). The chemicals used for synthesis of the nanoparticles were as follows: extra pure silver nitrate (AgNO₃), tetrachloroauric (III) acid trihydrate 99.5% (HAuCl₄·3H₂O), anhydrous tri-sodium citrate (C₆H₅Na₃O₇) which were bought from *Merck Group* (Germany), polyvinylpyrrolidone K30 (C₆H₉NO)_n and sodium borohydride (NaBH₄) which were bought from *Carl Roth* (Germany). All glassware was cleaned using Aqua Regia solution (3:1 hydrochloric acid to nitric acid) and washed with deionized water. Deionized ultra-pure water (18.2 MΩcm⁻¹) was used in the preparation of all aqueous solutions.

The synthesis procedures are described in brief below. The citrate stabilised silver nanoparticle preparation was done in regard to the Lee-Meisel procedure [114]. This procedure was already described in the previous chapter (Chapter 2) so it will only be briefly overviewed here. A mixture of 9 mg of silver nitrate and 50 ml of deionized water was heated until a boiling. After that, 1 ml of an aqueous solution of 1% (m/v) of trisodium citrate was added. The whole mixture was kept at near boiling temperature for an additional hour and then cooled to room temperature.

Ag-PVP nanoparticles were synthesised by polyol process with PVP. This procedure yields spherically shaped nanoparticles [250]. To produce the nanoparticles, the mass of 1 g of PVP K30 was dissolved in 50 ml of deionized water. Next, the solution was heated to the temperature of 80°C. Finally, 1 mg of AgNO₃ was added to the solution. The final solution was kept at 80°C for an additional hour. Constant stirring was applied during the whole procedure.

Ag-BH₄ nanoparticles were prepared by two step procedure adapted from the procedure described by D. Aherne et al. [115]. This synthesis yields non-spherical nanoparticles, since PVP reduces nanoparticle growth in certain crystallographic axis. The first step of the synthesis procedure is the preparation of the seed solution. This was accomplished by heating 2 ml of a

0.12 M solution of PVP to boiling. Then 4 ml of a 1 mM solution of AgNO_3 and 2 ml of a 2.5 mM solution of tri-sodium citrate were added. Finally, 0.06 ml of a freshly prepared solution of 10 mM of sodium borohydride was added. The second step of the procedure is the growth of the nanoparticles. This was completed by first diluting the seed solution six times. Then, 75 μl of a solution of 10 mM of ascorbic was added to 3 ml of the diluted seed solution. The synthesis ended by the addition of 3 ml of a 0.5 mM solution of AgNO_3 to the mixture. Constant stirring was applied throughout the whole procedure.

Au-cit nanoparticles were prepared in accordance to the synthesis procedure described by Turkevich et al. [251]. At first, 100 ml of a 5 mM solution of HAuCl_4 was brought to boiling. Second, 5 ml of a 1% solution of tri-sodium citrate was added and the final mixture was kept at boiling temperature for an additional hour. Constant stirring was applied throughout the whole procedure.

Au-PVP nanoparticles were prepared by polyol synthesis method [252]. Firstly, 25 ml of a 0.12 mM solution of PVP was heated to boiling. Secondly, 25 ml of a 1 mM solution of tetrachloroauric acid was preheated to 60°C and added into the heated mixture. The mixture was kept at boiling point for an additional hour. When the synthesis was finished, the excess amount of PVP was removed by diluting the prepared solution with deionized water, centrifuging and discarding the supernatant. This was repeated three times. Constant stirring was applied throughout the whole procedure.

The prepared colloidal solutions were centrifuged for 10 minutes with a speed of 6500 rpm in order to increase the nanoparticle concentration in the solution. After centrifuging, one-third of the initial volume was taken as a supernatant and discarded.

All colloidal solutions were characterized by measuring their UV-Vis absorption spectra. The spectra were collected in the wavelength region from 250 nm to 800 nm with a spectral resolution of 5 nm. Spectra were recorded using spectrophotometer Lambda 1050 (Perkin-Elmer, USA) equipped with two sources: halogen and deuterium lamps. Three detector system (photomultiplier tube, InGaAs and PbS) was used for the signal detection.

4.2.2. Preparation of blood samples

Two types of samples (model and real-life) were prepared. Model samples were prepared from the fresh blood which was collected from the finger of volunteers using a standard finger-stick sampling technique. Volunteers went

on an overnight fasting before the collection of blood. Next, deionized water was used to dilute the blood or its serum samples. Finally, salicylic acid or acetaminophen was mixed in acquiring the needed concentrations of the drug. Real-life samples were prepared by collecting blood from the volunteers before and after ingesting a dose of 3.2 g of soluble aspirin (Aspirin-C) or a 4 g dose of paracetamol. Pre-processing of all blood samples was performed by first mixing 400 μL of the collected blood with 50 μL of dicynone. Then, the mixture was centrifuged for 10 minutes with a force of 5000 xg. This was done in order to separate blood serum from the whole blood. Chemicals used for sample preparation were as follows: pure salicylic acid ($\text{C}_7\text{H}_6\text{O}_3$) and acetaminophen ($\text{C}_8\text{H}_9\text{NO}_2$) which were purchased from *Sigma-Aldrich* (USA), o-acetylsalicylic acid ($\text{C}_9\text{H}_8\text{O}_4$) 99% purity which was purchased from *Alfa Aesar* (Germany), uric acid ($\text{C}_5\text{H}_4\text{N}_4\text{O}_3$) 99% - *Sigma-Aldrich* (USA). The pH of model samples was altered with sodium hydroxide (NaOH) 2 M solution bought from *Carl Roth* (Germany) in order to achieve the pH value as observed in the real-life samples. Coagulation agent – dicynone (etamsylate), was used (*Lek Pharmaceutical and Chemical Company*) for serum separation from the whole blood. Human blood serum was bought from *Thermo Fisher Scientific* (USA).

For the SERS measurements samples were prepared on an aluminium surface which was pre-cleaned using methanol and deionized water. The SERS active layers of nanoparticles were prepared by drying 25 μL of concentrated colloidal solution on the cleaned aluminium surface. Upon measurement, 25 μL of sample solution was placed on the nanoparticle layer.

4.2.3. SERS spectroscopy of blood

All spectra were acquired with *Bruker* MultiRAM FT-Raman spectrometer equipped with 1064 nm Nd:YAG laser. Liquid nitrogen cooled Ge diode detector was used for detection of the SERS signal. Sample excitation and collection of scattered light was performed using microscopy stage of the spectrometer equipped with reflecting objective - a 90-degree angle gold-plated parabolic mirror. All spectra were collected using a laser power of 300 mW, which was found to give the best intensity of the spectra without overheating the sample. Excitation beam was focused to a 100 μm diameter spot what gives the intensity of $4.8 \cdot 10^8 \text{ W/m}^2$. The spectra were measured with the 4 cm^{-1} spectral resolution. The resulting spectrum was taken as an average of 300 interferograms, which were then Fourier transformed using Blackman-Harris 3 term apodization function and a zero-filling factor of two.

4.3. SERS STUDY OF BLOOD: RESULTS AND DISCUSSION

This research was done in order to apply the surface enhanced Raman spectroscopy method for the detection of trace amounts of pharmaceuticals in human blood. The SERS method was selected since it allows extremely sensitive and at the same time fast detection of various compounds. This is especially important since nowadays a lot of health-related information can be found online. Thus, self-evaluation of health – matching the symptoms to the specific illness, is becoming more popular [253]. This, however, should be strictly done only by the medical experts. In fact, the lack of proper knowledge results in such bizarre recommendations as injecting oneself with disinfectants to cure infections and so on. Furthermore, much of the information which is published online does not go through any regulations or censorship, and thus it can be highly misleading for a common person. Therefore, the unguided self-medication often leads to serious health risks and can even result in organ failure or death [254]. Even though all pharmaceuticals pose a health risk, over the counter (OTC) drugs because of their availability can be the most dangerous. Keeping this in mind, acetylsalicylic acid and paracetamol, which are the primary choices for a fast relief, were chosen in this work. During the treatment of the patients, it is very important to be able to quickly assess and determine the overdosing agent. Detection of pharmaceuticals or other compounds is done by drug screening via blood and urine. As already mentioned, the most popular techniques for this task are liquid chromatography tandem mass spectrometry (LC-MS) and gas chromatography tandem mass spectrometry (GC-MS) [255-257].

Here, the SERS is implemented as a method for a faster and still sensitive detection of salicylic acid and paracetamol in blood. The label-free SERS approach employing colloidal nanoparticles was used. It must be noted that even though the SERS spectroscopy has already been applied for the detection of aspirin and paracetamol in blood, the viability of the method has never been tested on the real-life human blood samples.

4.3.1. Characterisation and selection of the colloidal solutions of nanoparticles

Biological fluids are complex samples containing various molecules such as proteins, carbohydrates, salts, and other, which can adsorb on the nanoparticles. These molecules can interfere or weaken the SERS signal of the drugs or their metabolites, which are sought to be detected. Hence, the goal of detecting a certain molecule in the blood or its serum is not a trivial task.

Also, detection of certain molecules in blood or blood serum samples differ from the analysis of the extracellular fluid or bacteria samples which has been presented in the previous sections. Therefore, various colloidal solutions of nanoparticles were synthesised in this work and their efficiency to enhance the Raman scattering of the molecules under investigation was evaluated. A solution which would allow to achieve the highest enhancement of the Raman scattering of salicylic acid was determined and used in further research. It is distinguished that the SERS intensity strongly depends on the distance between the nanoparticle and adsorbate. Even higher enhancement values are observed when chemical adsorption is also present [258]. It was previously determined that SA molecules adsorb on the citrate capped nanoparticles through the carboxylic group what may lead to the chemical adsorption as well [259].

The basic characterization of the colloidal solutions was done by measuring and comparing the UV-Vis absorption spectra of these solutions. The measured spectra are presented in the Fig. 25.

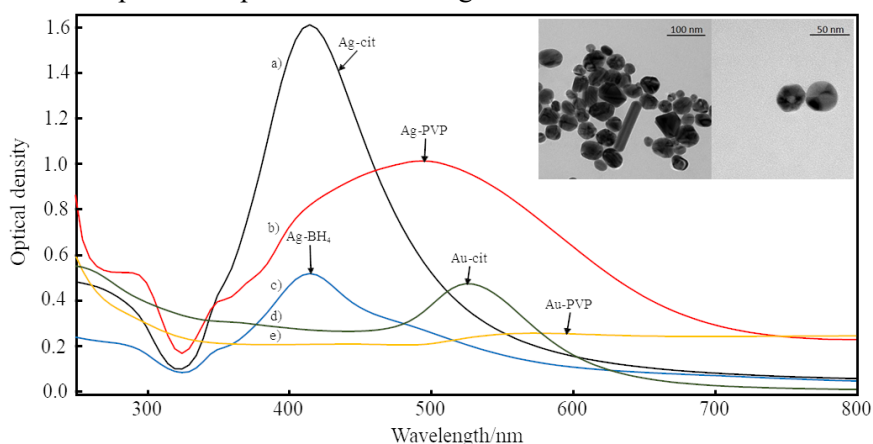


Fig. 25. The UV-Vis absorption spectra of all synthesised colloidal solutions (a) Ag-cit, (b) Ag-PVP, (c) Ag-BH₄ PVP, (d) Au-cit, (e) Au-PVP.

The spectra presented in the Fig. 25 already show that Ag-cit NPs contain the highest concentration of nanoparticles since it has the most intense absorption maximum. The absorption band is located at 412 nm, what in accordance to the Mie scattering theory results in the average nanoparticle size of 57 nm. The absorption peak of the Ag-BH₄ is also located at 412 nm however, the absorption peak is less intense what suggests that this colloidal solution would give the lower enhancement value. The absorption band of the colloidal solution of the polymer capped silver nanoparticles Ag-PVP is

observed at around 500 nm. This would mean that the particles should be much larger. The absorption spectra of the colloidal solutions of gold nanoparticles did not produce satisfactory results. The absorption band of Au-cit is relatively weak and broad, and the absorption of Au-PVP colloidal solution was observed to be almost monotonous over the whole measured wavelength range. This suggests that even larger distribution of nanoparticle size was present in these solutions. Since the solution of Au-PVP nanoparticles exhibited the unusual absorption spectrum, the TEM image of these nanoparticles was taken. It was determined that the colloidal solution of Au-PVP nanoparticles were triangular or irregularly shaped (see Appendix II, Fig. 1). In addition, these particles are a lot bigger with the average size of around 120 nm and the range of particle diameter was evaluated to be from 30 nm to 200 nm.

The analysis of the UV-Vis absorption spectra and the TEM images showed that none of the synthesised colloidal solutions were completely uniform in respect to the particle size. However, it is not a drawback since the size of NPs does not affect the positions of the vibrational bands observed in the SERS spectra. The size can only be a factor for the overall intensity of the spectrum. For the detection of SA in blood, the use of such colloidal solutions was not problematic since the detection of the molecule was supposed to be achieved by evaluating the relative intensity of the spectral bands. Furthermore, the collected SERS spectra were normalized. For this reason, the absolute intensity of the spectrum was not relevant.

It should also be briefly noted that none of the synthesised colloidal solutions had the wavelength which corresponds to the plasmon resonance comparable to the wavelength of the excitation laser. In theory, matching of the laser wavelength and the wavelength, corresponding to the plasmon resonance, is favourable. However, since it has already been described in the previous chapter, the applicability of such solutions is viable via dark-modes [41] and will not be discussed in detail.

As mentioned earlier, the colloidal solution that produced the highest value of enhancement was chosen as the best. For this, the SERS spectra of an aqueous solution of 1 mM SA was collected using the SERS active layers prepared with different colloidal nanoparticles. The collected SERS spectra together with the calculated signal-to-noise ratios (S/N) and analytical enhancement factors (E) of each nanoparticle type are presented in the Fig. 26. These parameters were calculated considering the vibrational band of SA located at 1034 cm^{-1} as a reference point. Analytical enhancement factor was

calculated by the equation (6) keeping other factors like laser wavelength, power, area of measurement, measurement time and other constant.

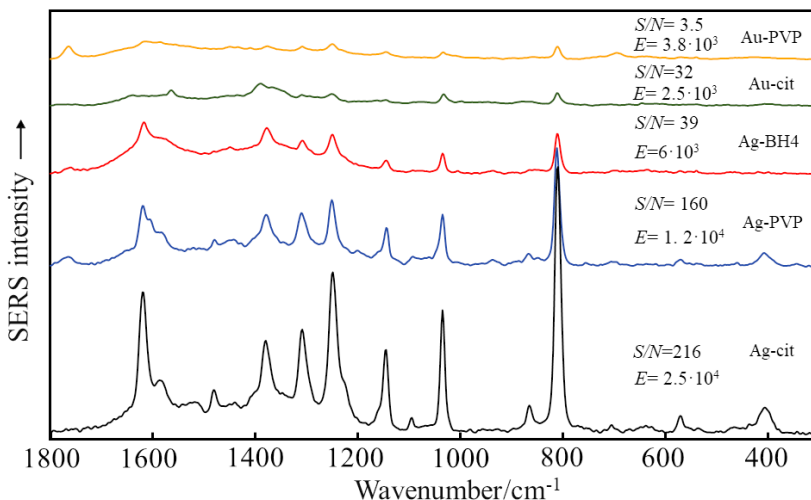


Fig. 26. The SERS spectra of the aqueous solution of salicylic acid (1 mM) collected using SERS active layers prepared from different silver and gold nanoparticles.

The SERS spectra presented in the Fig. 26 are self-explanatory. It can be clearly observed that the highest analytical enhancement factor E ($2.4 \cdot 10^4$) and resulting the highest S/N ratio (216) is reached when Ag-cit nanoparticles are used. The lowest parameter values were observed while using the SERS active layers prepared from gold nanoparticles. These layers displayed 40 times lower S/N ratio and 10 times lower enhancement of Raman spectral bands. In fact, during all performed SERS experiments when gold nanoparticles were used, the analytical enhancement factor was observed not to exceed the value of $3.8 \cdot 10^3$. Such value is not sufficient for the efficient and determined detection of SA in blood serum. Additionally, the SERS spectra of SA collected using the active layers prepared from the Au-cit and Au-PVP nanoparticles contain the spectral bands which arise from the molecules in the composition of these colloidal solutions. For example, several other vibrational bands from carboxylate group of sodium citrate namely symmetric vibration $\nu_{\text{sym}}(\text{COO}^-)$ located at 1390 cm^{-1} and 1368 cm^{-1} , asymmetric vibration $\nu_{\text{asym}}(\text{COO}^-)$ located at 1565 cm^{-1} , and deformation vibration $\delta(\text{COO}^-)$ located at 892 cm^{-1} are observed in the SERS spectra of salicylic acid collected using the layer prepared from Au-cit NPs [260, 261]. Similarly, when using the SERS active layers prepared from Au-PVP nanoparticles,

broad spectral bands located in the wavenumber range from 1615 cm^{-1} to 1585 cm^{-1} are seen. These spectral bands may be attributed to $\nu(\text{C-N})$ and $\nu(\text{C=O})$ vibrations of the lactam ring of the PVP molecule [262]. The appearance of these spectral bands indicates that PVP was adsorbed on the surface of nanoparticle through the oxygen of the carbonyl group [263, 264]. This could have resulted from the PVP not being firmly adsorbed on Au surface or that excessive amount of the PVP was present. Normally, these vibrational bands should not be observed when PVP is adsorbed on the surface of nanoparticles. Having these results in mind, colloidal solutions of gold nanoparticles were not considered for further use.

A relatively high intensity of the SERS spectra was observed when using Ag-PVP nanoparticles. However, the overall intensity was still lower than the one achieved when using Ag-cit NPs. What's more, unwanted additional spectral bands were observed in the SERS spectra. Under powerful laser radiation PVP may not be stable and could dissociate leaving products whose spectral band were observed at 1039 cm^{-1} . In accordance to the literature, this spectral band could be associated with the oxidation products forming between PVP and Ag [263, 264]. The preparation of nanoparticles where PVP is used requires extensive washing in order to remove the excess PVP. Therefore, the harder preparation procedure with the above-mentioned cons of this colloidal solution led to the decision not to use it for further experiments.

Finally, the use of Ag-BH₄ for further research was also dismissed since the value of analytical enhancement factor produced by the SERS active layers prepared from this colloidal solution was not high. In addition, the preparation of the Ag-BH₄ nanoparticles consists of two steps what is more laborious.

To conclude the selection process of the colloidal nanoparticles, solution of Ag-cit nanoparticles was chosen for further experiments since the SERS active layers prepared from it produced the highest analytical enhancement factor. Furthermore, in contrast to other types of colloidal solutions, the preparation of this colloidal solution is easier. The chosen colloidal solution was centrifuged at the speed of 6500 rpm, which was found to be optimal in the SERS analysis described in Chapter 2.

4.3.2. The SERS analysis of model blood and salicylic acid samples

The spectroscopic analysis of model samples of salicylic acid mixed with whole blood or its serum was performed in order to investigate the possibility of the detection of SA and to find the spectral markers indicating the presence

of this molecule. The SERS spectrum of SA (see Fig. 26) contains several vibrational bands. Of these the combination of a ring stretching and $\delta(\text{C-COO})$ scissoring vibration located at 809 cm^{-1} , combination of $\delta(\text{CH})$ bending and ring stretching vibrations - 1034 cm^{-1} , combination of $\delta(\text{C-H})$ bending and $\nu(\text{C-O})$ vibrations - 1248 cm^{-1} , combination of ring stretching and $\delta(\text{OH})$ bending vibrations - 1612 cm^{-1} are the most intense vibrations of salicylic acid which could be viewed as potential spectral markers. It is distinguished that the vibrations which have a vibrational transition moment perpendicular to the nanoparticle surface are enhanced the most [258, 265, 266]. This suggests that the SA molecule is adsorbed on the nanoparticle surface through its carboxylic group. In fact, in accordance to the literature, this is supposed to be the case [259, 267]. The most intense spectral bands are always the first option when spectral markers are chosen. However, in order to use them for identification, it should be inspected whether these bands do not overlap with the spectral bands of other constituents in the sample. In order to confirm if it is possible to use the chosen spectral marker bands for the detection of SA overdose in the whole blood, samples of fresh human blood and its serum spiked with high concentration of salicylic acid were prepared. The pH of the samples was measured and was adjusted to resemble the normal pH of blood which is observed with the same SA concentration [268]. The pH was varied by adding small amounts of strongly diluted hydrochloric acid or sodium hydroxide. The collected SERS spectra of the whole human blood, its serum, and their mixtures with SA (5 mM) are presented in Fig. 27.

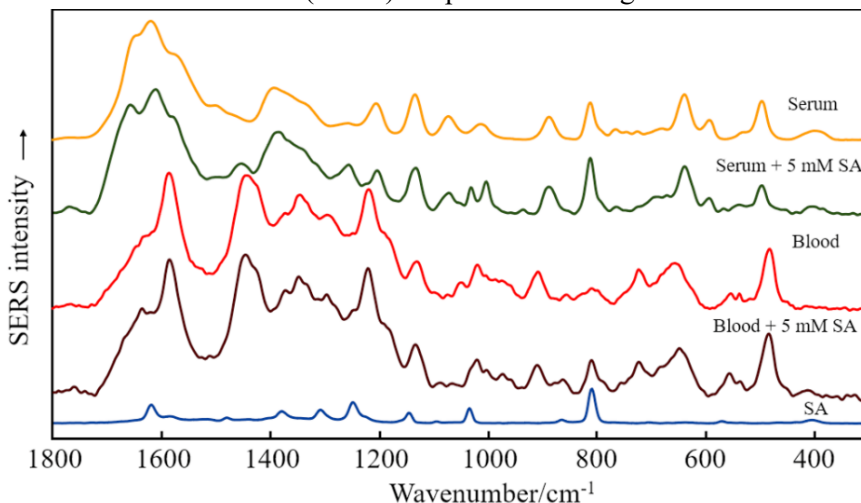


Fig. 27. The SERS spectra of: serum, SA in serum (5 mM), whole blood, SA in whole blood (5 mM), and aqueous solution of SA (1 mM).

As with other biological samples, the SERS spectra of the whole human blood contain various vibrational bands which are difficult to interpret. The spectra of blood from the same patient can equally vary with time because of the biochemical reactions taking place in it (see Appendix II, Fig. 2). The observed changes could be explained by the chemical decomposition of cells and cellular metabolites, proteins and other compounds that constitute blood. Despite this, in the SERS spectra presented in the Fig. 27 it can be observed that upon the addition of SA into the blood or its serum a band located at 809 cm^{-1} appears. This band is one of the marker bands of SA and it would seem that it could be used for the detection. However, it was observed that in the SERS spectrum of blood the intensity variation in the spectral region of this band is high. This was visualized and the relative standard deviation was calculated. The averaged spectrum of blood and the standard deviation of intensities are presented in the Appendix II, Fig. 3. The calculated value of the relative standard deviation was 54%. This shows that the intensity varies a lot, and thus the spectral region of the marker band located at 809 cm^{-1} could not be precisely used for detection of salicylic acid when its concentration is below 5 mM. Detection of lower concentrations could be possible with increased statistical importance for example longer scanning time what is not favourable in practical use. Therefore, blood serum was chosen for analysis.

Blood serum is considered to be an extracellular fluid. Even though it consists of more than 4000 chemical components, the most SERS active is uric acid (UA). Uric acid is a product of human metabolism. Hence, its concentration is dependent on the diet, overall health, physical activity of the person. The concentration of UA in blood serum that is between the range of $140\text{ }\mu\text{M}$ and $420\text{ }\mu\text{M}$ is considered normal. Compared to the concentration of SA which is observed after consumption of aspirin, the concentration of UA is low. However, UA shows an affinity to adsorb on the silver surface and therefore is extremely SERS active. Such behaviour leads to the ability to detect uric acid at extremely low concentrations [269, 270]. Furthermore, this means that the SERS spectrum of human serum will be mostly dominated by vibrational bands of uric acid. This is also beneficial and disadvantageous, since SERS activity of UA will influence the detection of SA in human serum but will also make the analysis of the SERS spectrum relatively simple. Similar to the SERS spectrum of blood, an intense SERS spectral band of SA is observed at 809 cm^{-1} . However, it cannot be used for precise detection of SA, since it is completely overlapped by the vibrational band located at 811 cm^{-1} in the SERS spectrum of the blood serum. This band is associated

with the $\nu(\text{C-N}) + \text{ring}$ vibration of the UA molecule. Nevertheless, it can be observed that besides the band located at 809 cm^{-1} more spectral markers of SA can be observed in the spectrum of blood serum and SA (5 mM). For example, a vibrational band of SA located at 1032 cm^{-1} is observed. The position of this band was observed shifted in blood since it was located at 1034 cm^{-1} when the SERS spectrum of aqueous solution of SA was analysed. The band located at 1248 cm^{-1} could be used for detection but only at high concentrations since it is not observed when concentration of salicylic acid is low. One more interesting observation is the decrease in the ratio of integral intensities of spectral bands located at 1073 cm^{-1} and 1012 cm^{-1} . The behaviour of these spectral markers and whether they are reliable was tested by measuring the SERS spectra of blood serum with different concentration of salicylic acid. These spectra are presented in the Fig. 28.

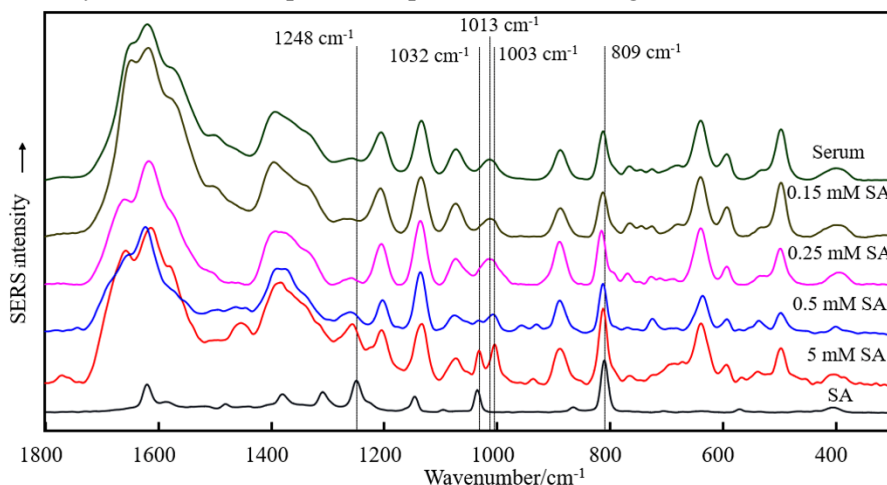


Fig. 28. The SERS spectra of: blood serum, blood serum mixtures with different concentration of salicylic acid, aqueous solution of SA (1 mM).

Analysis of the SERS spectra of blood serum with different concentration of salicylic acid presented in the Fig. 28 has shown that the spectral markers are reliable and can be used for the detection of aspirin use. Thus, it was determined that SERS analysis of the serum was a better option than the analysis of the SERS spectra of the whole blood.

Furthermore, it was observed that the relative intensities of the vibrational bands in the SERS spectrum of the blood serum change when concentration of SA is increasing. To be more precise, the intensity of the vibrational bands of UA decreases, and the intensity of vibrational bands located at 1003 cm^{-1} , 1447 cm^{-1} and 1694 cm^{-1} increases. This intensity change can be reasoned by

changes in serum pH due to the elevated concentration of salicylic acid. The acidic environment leads to weaker adsorption of uric acid molecules and allows the adsorption of other constituents of the blood serum.

It can be also observed that the intensity of the band at 1012 cm^{-1} increases with the increasing concentration of SA. However, it is most likely that is resulted by the increase in intensity of the spectral band located at 1003 cm^{-1} . This spectral band could be attributed to the asymmetric ring vibrations of phenylalanine. Phenylalanine is an amino acid which is abundant serum protein (constitutes up to 5% of human serum albumin protein [271]). In addition, in serum it can be detected as a free amino acid with a normal concentration of $120\text{ }\mu\text{M}$. It should be noted that the band located at 1003 cm^{-1} can indicate both the Raman and the SERS spectra of phenylalanine since this band is the most intense in the both spectra. Therefore, it seems that the ability of uric acid to adsorb on the nanoparticle surface is reduced by the acidic environment, what results in the spectral band of phenylalanine to become more intense. Hence, it can be noted that competitive adsorption between uric acid and other constituents in the blood serum including salicylic acid is taking place.

The surface enhanced Raman scattering is known to be a surface-sensitive spectroscopy. This means that the enhancement of the Raman scattering signal will be highest for the molecules which are adsorbed or in a proximity to the surface of the nanoparticles. The nanoparticle surface can be viewed as stable with the surface area that does not change, so molecules compete for adsorption. Theoretical studies of salicylic acid showed that adsorption of SA on the surface of nanoparticles is most likely to be realized through the ionized carboxyl group [259, 267]. It is also in a good agreement with the experimental spectrum, where stretching vibration $\nu(\text{Ag-O})$ is observed [272]. The theoretical investigation of the adsorption of UA showed that uric acid molecule adsorbs on the surface of nanoparticles through ionized amide group [269, 270]. Because of the different molecular structure, the adsorption affinity of the molecules is affected differently when conditions in the sample change. In this manner, chemical properties of the solution, such as pH or physical properties like the electrostatic field on the NPs surface may reason the better adsorption of one molecular species over the other.

Since it was determined that salicylic acid and uric acid molecules compete for adsorption on the surface of the nanoparticle, it should not be unexpected that the intensity of spectral bands of UA would indicate a nonlinear dependence on the concentration of SA. This was examined by measuring the SERS spectrum of the aqueous solutions of uric acid and salicylic acid. The

concentration of uric acid was kept constant in all mixtures (200 μM) while the concentration of salicylic acid was increased from 0.25 mM to 10 mM. The dependence of the relative intensity of spectral bands of uric acid (1620 cm^{-1} , 637 cm^{-1} , 891 cm^{-1}) on the intensity of the spectral band of salicylic acid (1031 cm^{-1}) was calculated and is presented in the Fig. 29.

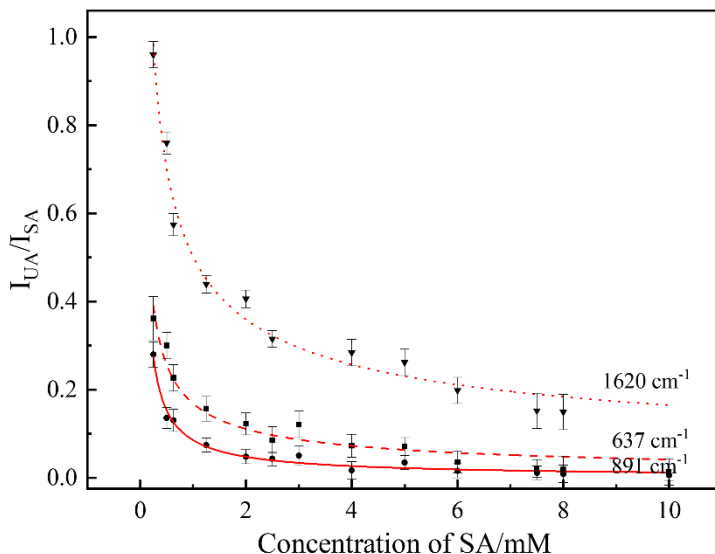


Fig. 29. The dependence of relative intensity ($I_{\text{UA}}/I_{\text{SA}}$) between the SERS spectral bands of UA (1620 cm^{-1} , 637 cm^{-1} , 891 cm^{-1}) and SA (1031 cm^{-1}).

Having proved the competitive adsorption of the molecules, we can go back to the spectral behaviour of the two vibrational bands located at 1073 cm^{-1} and 1012 cm^{-1} . This doublet can be now observed and analysed more clearly. It was observed that when the SA is present in blood serum with elevated concentrations, the spectral band 1032 cm^{-1} is prominent. When the concentration of salicylic acid is low, the intensity of this band decreases until it can only be detected as a shoulder of the spectral band of serum at 1012 cm^{-1} . Therefore, the decrease in the pH value of the solution results in the changes of the intensity of the doublet. For example, the ratio of the spectral doublet decreases from 1.8 in the SERS spectra of pure serum to 0.7 in the SERS spectra of serum with SA concentration of 5 mM. The lowest detected concentration of SA in serum was 3 mM. At this concentration, the intensity ratio of the spectral doublet was 1.67. This concentration in clinical practice is considered as mild toxicity. At this concentration, salicylic acid could be detected only as a shoulder of the spectral band located at 1012 cm^{-1} . Hence, it may be possible and beneficial to be able to detect salicylic acid in blood

serum through an indirect spectral marker – the intensity ratio of the spectral doublet.

The SERS spectra of serum at different pH values were measured in order to confirm the hypothesis that the change of the intensity ratio of the spectral doublet located at 1073 cm^{-1} and 1012 cm^{-1} is caused by changes in the acidity of the serum. The pH value was adjusted by adding different volume of highly diluted H_2SO_4 solution to 5 ml of blood serum. The collected SERS spectra of human blood serum at different pH values are presented in the Fig. 30.

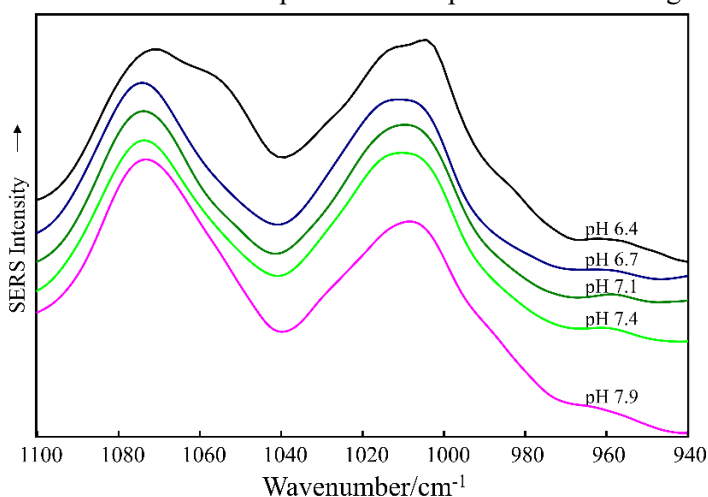


Fig. 30. The spectral doublet of the SERS spectra of human blood serum at different pH values.

As observed in the SERS spectra presented in the Fig. 30, the changes in the relative intensity of the spectral doublet located at 1073 cm^{-1} and 1012 cm^{-1} are indeed observed when the pH value of serum decreases. At the pH value of 6.4 the spectral band of phenylalanine located at 1003 cm^{-1} can be distinguished. Such behaviour can be explained by the decreased adsorption of the uric acid molecule on the surface of the nanoparticle because of the acidic environment. In such case, other molecules are able to adsorb better. As observed in the SERS spectra, this results in a lower intensity of the SERS spectral bands of UA and more intense spectral band of phenylalanine. This proves that the changes in the pH of the solution are reasoning the changes in relative intensity of this doublet. Furthermore, the increase in the intensity was observed not only of the vibrational band of phenylalanine but also of the spectral bands of uric acid located at 1013 cm^{-1} and 983 cm^{-1} . Also, the serum spectral band at 1073 cm^{-1} was observed to be comprised of two spectral bands which are located at 1069 cm^{-1} and 1059 cm^{-1} . These spectral changes can be

linked to the tautomeric changes of uric acid, which are influenced by the changing of pH of the solution.

It is established that uric acid displays extensive tautomerism [273-276]. In fact, it was theoretically evaluated that uric acid might form 35 tautomers [277]. These tautomeric forms differ by the proton binding site which can be either an oxygen atom what results in the forming of the OH group (enol tautomer) or a nitrogen atom, what results in the forming of the NH group (keto tautomer). Results of theoretical calculations have shown that of the possible tautomeric forms the most stable is the triketo form of uric acid [276]. However, three other tautomeric forms have a similar potential energy (it is slightly higher $\Delta H = 2 - 6$ kcal/mol). These are diketo or monoketo tautomers. When uric acid is in these forms, the hydrogen is bonded to the oxygen atoms of imidazole or pyrimidine rings. The most stable monoanion of uric acid is UAN-3 (what shows that the N-3 atom in the pyrimidine ring is deprotonated) which forms from the most stable triketo tautomer (see Appendix II, Fig. 4). The monoanion UAN-9 (formed by deprotonation of the imidazole ring) can also be present since it has a slightly higher potential energy ($\Delta H = 1 - 3$ kcal/mol). As a result, at normal pH of the aqueous solution, uric acid should exist as a mixture of two tautomeric forms of UAN-3 and UAN-9. Other monoanions have much less stability and can be considered not present [274, 275]. It is well-determined that the pKa value of uric acid is 5.4 which is higher than that of the salicylic acid (2.97). This means that at such pH value half of UA molecules are protonated. The further increase of the pH value results in the deprotonation of more molecules. On the contrary, more monoanions of uric acid are getting transformed to protonated neutral form when the pH value of solution decreases upon the increase in the concentration of SA and the acidification of blood. In our previous research *ab initio* calculations of the complexes between the most stable tautomers of uric acid and a nanoparticle simulated by the five-atom silver cluster were performed [270]. The results of these calculations have shown that the changes in the relative intensity of the spectral doublet could be explained by the uric acid molecule transformation from one tautomeric form to the other. In the triketo form, the ratio of the spectral doublet bands - C-N/N-C-C ring vibration at 1012 cm^{-1} , C-N/N-C-C stretching/OH bending at 1073 cm^{-1} is 1.4. Meanwhile, the intensity ratio of these bands in the monoanionic forms was evaluated to be about 0.2 (see Appendix II, Fig. 5).

4.3.3. The SERS analysis of real-life blood samples containing aspirin

The SERS spectra of blood serum after consumption of 3.2 g of aspirin were collected in order to test the viability of the proposed method for the detection of aspirin. The blood was collected, and the SERS spectra were registered at increasing periods of time after consumption. The spectra were collected as soon as the serum was separated from the whole blood. The collected SERS spectra are presented in the Fig. 31.

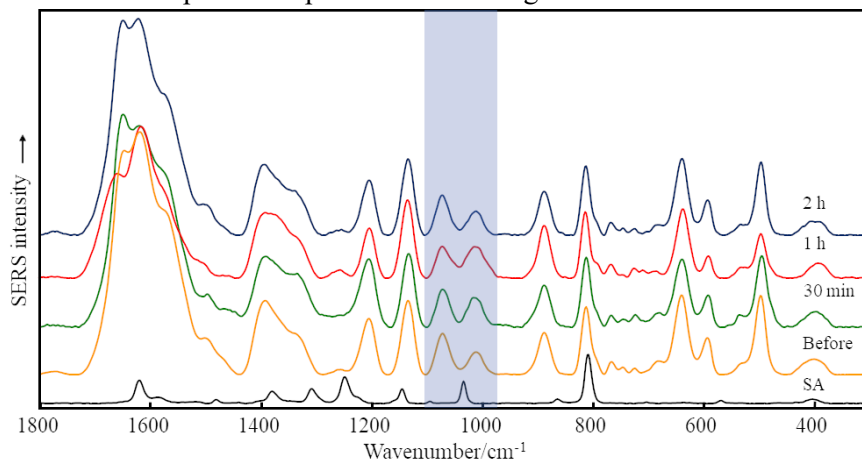


Fig. 31. The SERS spectra of: the blood serum collected at different periods of the consumption of aspirin, and aqueous solution of SA (1mM).

The spectral analysis of the real-life samples showed that the intensity ratio of the spectral doublet located at 1073 cm⁻¹ and at 1012 cm⁻¹ (highlighted in the Fig. 31) decreased with increasing time and reached a minimum value of 1.23 after 1 h. The intensity ratio was observed to increase to a value of 1.53 after 2 hours. The direct spectral marker of salicylic acid – a spectral band located at 1032 cm⁻¹, can be also observed in the SERS spectra, even though it can be distinguished only as a shoulder of another spectral band. In order to verify that this vibrational band can in fact be distinguished from the spectral bands of uric acid, a contour separation method was applied. The contour separation was performed in the spectral region from 1200 cm⁻¹ to 950 cm⁻¹ using the graphing and data analysis software “OriginPro 2018” [278]. Because of the broadening of the spectral bands, which is reasoned by the different effects, the starting contour for the spectral fitting was chosen to be Voigt. Nevertheless, during the software assisted fitting procedure the contributions of either the Gaussian or Lorenz contours to the overall fitting envelope is changed. The end result of the fitting thus can be dominated by

only the Gaussian or by Lorentz contour for some vibrational bands. The parameters of the fitting procedure are presented in the Appendix II, Fig. 6. The results of the fitting procedure are presented in the Fig. 32. The fitted spectral bands were assigned to the spectral band of uric acid (1085 cm^{-1} , 1072 cm^{-1} , 1050 cm^{-1}). These bands can be also observed overlapped in the SERS spectrum of uric acid. The second envelope of the spectral bands of uric acid it was determined to be combined of two bands located at 1013 cm^{-1} and 983 cm^{-1} . The vibrational band of salicylic acid was fitted by a contour with a peak value at 1031 cm^{-1} and the spectral band of phenylalanine – at 1003 cm^{-1} .

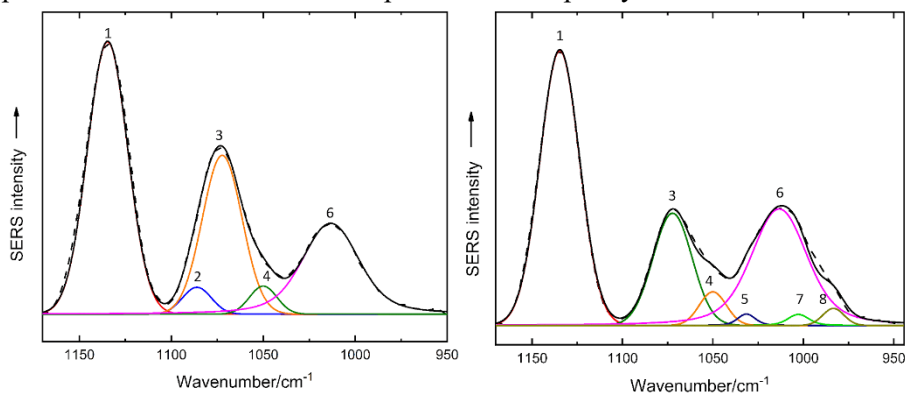


Fig. 32. The experimental and fitted SERS spectra of blood serum before and after 1 h of aspirin intake. The approximated spectra are denoted by a solid line; experimental spectra – dotted line. Band numbering is as follows: 1 – 1135 cm^{-1} (UA); 2 – 1085 cm^{-1} (UA); 3 – 1072 cm^{-1} (UA); 4 – 1050 cm^{-1} (UA); 5 – 1031 cm^{-1} (SA); 6 – 1013 cm^{-1} (UA); 7 – 1003 cm^{-1} (Phe); 8 – 983 cm^{-1} (UA).

The label-free SERS analysis of the whole blood and blood serum has shown that application of this method for the detection of aspirin is a viable procedure. The detection of aspirin was achieved by determining the presence of the main metabolite of aspirin - salicylic acid. Analysis of model samples has proven that in comparison with the whole blood serum is a more appropriate choice for the identification of the presence of salicylic acid. This is because there are fewer chemical constituents that interfere with the SERS spectrum in the composition of serum. Out of five different silver and gold colloidal solutions, the best one – providing the most efficient enhancement was found. This was the colloidal solution of nanoparticles containing the citrate capped spherically shaped silver nanoparticles. The average diameter of these nanoparticles was evaluated to be around 57 nm. The limit of detection (LOD) for salicylic acid in blood serum was 3 mM. This, in

accordance to the clinical standards, corresponds to mild toxicity levels. A few spectral markers, both direct and indirect, for the detection of salicylic acid were determined. Calibration curve – dependence of the intensity ratio of the band of uric acid and salicylic acid on the concentration of SA was made. The calibration curve is nonlinear what is explained by the competing adsorption between salicylic acid and uric acid molecules. It was determined that the increase of salicylic acid concentration in blood results in the disturbance of the adsorption process of uric acid what in turn results a better adsorption of salicylic acid and other molecules, for example phenylalanine. Analysis of the change in the relative intensities of the SERS spectral bands showed that intensity of the spectral band of phenylalanine located at 1003 cm^{-1} can be used as an indirect spectral marker related to concentration of salicylic acid in blood. Label-free method proved to be advantageous. However, in order to employ this technique clinically, achieving higher sensitivity would be beneficial. The sensitivity of the standard clinically used drug detection methods is still higher. Nonetheless, the SERS spectroscopy could be applied faster and cheaper what makes this method promising for the fast determination of the presence of drugs in the human body. Hence, this method could be used for the cases where fast information to decide further treatment is needed. It could also be adapted for a point-of-care analysis of aspirin use.

4.3.4. The SERS analysis of blood samples with paracetamol

As before, first the SERS spectra of blood and blood serum spiked with large concentration of acetaminophen (large enough for the spectral bands of paracetamol to be observed) were collected. This was done to test which of the two biofluids are better suited for the detection – to identify the possible spectral markers of the paracetamol. The collected SERS spectra of APAP in serum, blood and water are presented in Fig. 33. The presented spectra are shifted along the y-axis for clarity. It can be observed that the SERS spectra of paracetamol contain several intense vibrational bands that could be potentially used as spectral markers. Out of these, the band at 1597 cm^{-1} , which in accordance to the literature assigned to $\nu(\text{C}=\text{C})$ vibrations, is the most intense. However, the SERS spectra of both the blood and serum contain a broad and intense spectral band that overlaps this spectral marker band. In respect to that the second most intense vibrational band located at 1168 cm^{-1} was chosen as a spectral marker. This vibrational band is associated with $\delta(\text{phenyl-N})$ vibration and is not overlapped by vibrational bands of serum and blood. However, blood contains a lot more constituents, and as observed

before this makes the detection more difficult. Having this in mind, further spectroscopic analysis was conducted on the blood serum.

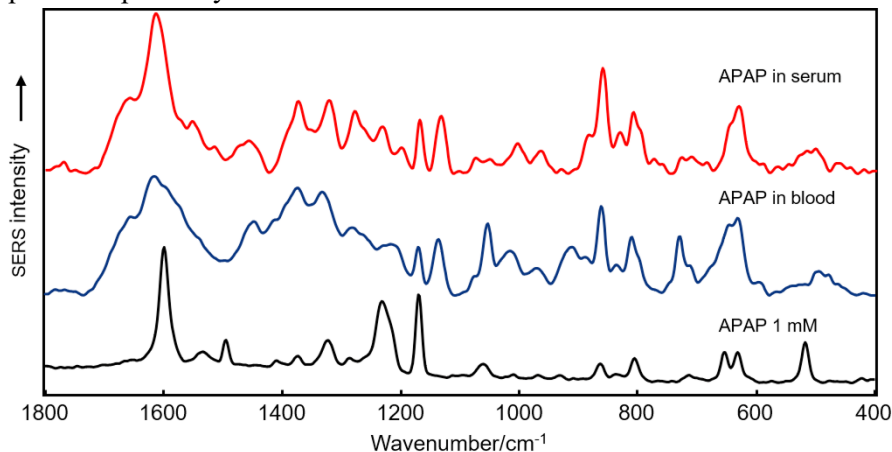


Fig. 33. The SERS spectra paracetamol in blood serum, whole blood and water.

The model blood serum samples with various concentrations of paracetamol were prepared and their SERS spectra were collected to test the lowest possible concentration of paracetamol which could be detected. The SERS spectra of blood serum, APAP and two mixtures of blood serum and APAP (10 mM and 1 mM) are presented in the Fig. 34. It can be noticed that detection of paracetamol via the spectral marker band at 1168 cm^{-1} is in fact possible as this spectral band can be observed in both selected mixtures. However, in the mixture with 1 mM concentration of acetaminophen the intensity of this band is very low. Nonetheless, upon a thorough analysis of the spectra it was determined that another spectral marker band could be used for the detection of paracetamol. This spectral band is located at 863 cm^{-1} and is associated with $\delta(\text{C-C})$ skeletal vibration. It must be noted that this band is only observed when the concentration of paracetamol is high enough. In the conducted experiments the value of such concentration was 1 mM.

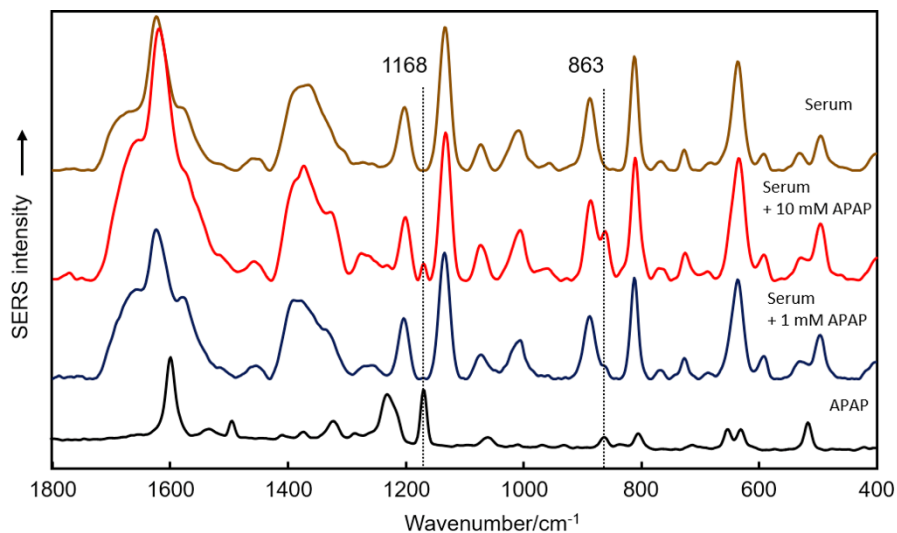


Fig. 34. The SERS spectra of blood serum, APAP, and mixture of serum with different concentrations of APAP: 10 mM, 1 mM.

Real pharmacokinetics experiments were carried out by collecting the spectrum of blood serum at different times after the consumption of 4 g dose of paracetamol. This concentration is relatively high and reaches the upper limit of the recommended daily intake. The SERS spectra of blood serum collected before, after 40 minutes and after 2 h of ingestion of 4 g of paracetamol are presented in the Fig. 35.

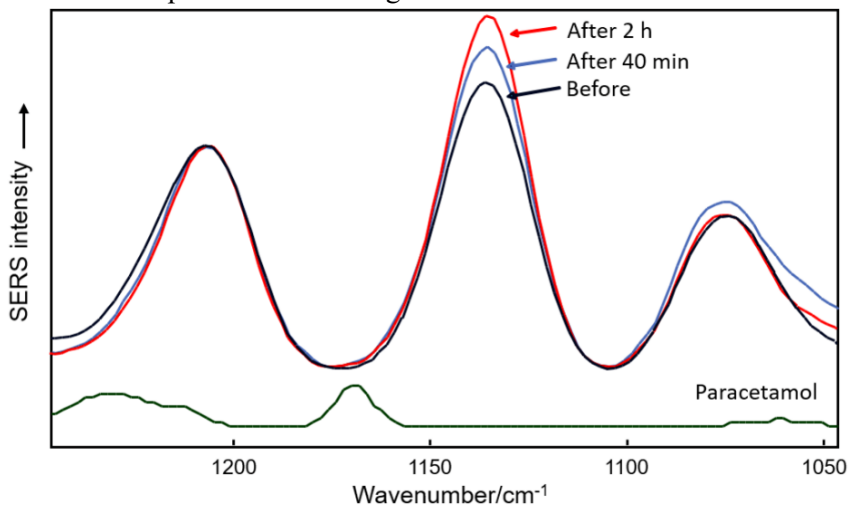


Fig. 35. The SERS spectra of blood serum before consumption of 4 g of paracetamol, after 40 min, and after 2 h.

Unfortunately, no spectral marker bands of paracetamol were observed in the presented SERS spectra. This result is reasoned by the strong adsorption of uric acid molecules whose vibrational bands dominate the SERS spectrum. Hence, it was determined that this approach is not suitable for the detection of paracetamol in real-life samples directly through the spectral marker bands of this molecule. However, some changes in the spectra were observed. It was determined that the intensity of the spectral band of uric acid at 1130 cm^{-1} increases with time. Also, the relative intensity of the neighbouring bands in regard to this spectral band changes. The increase the spectral bands may be reasoned by the presence of paracetamol or the changed adsorption of uric acid but this was not further investigated, since the direct spectral markers could not be observed. Therefore, with more research the colloidal label-free SERS approach for detection of paracetamol in blood could still be developed. Moreover, it may still be possible to detect paracetamol directly if one could eliminate or at least diminish the adsorption of uric acid on the surface of nanoparticles.

4.4. EXPERIMENTAL DETAILS OF THE EC-SERS SPECTROSCOPY OF SALIVA

4.4.1. Preparation of the SERS active electrode surface

The SERS active layers on the surface of the electrode were prepared in a simple fashion. A drop of the concentrated colloidal solution of citrated capped silver nanoparticles, which during the analysis of blood was evaluated to produce the highest enhancement, was dried on the surface of the working electrode. Beforehand, the process of cleaning and polishing the surface of the working electrode was carried out in the following manner. First, freshly prepared piranha solution was used in order to remove any excess molecules from the surface of the electrode. Second, the electrode was sonicated for five minutes in a solution of deionized water and methanol with a ratio of 1:1. Third, using sandpaper of ultra-fine roughness (P2500) and later using aluminium oxide polishing powder and polishing cloth the cleaned surface was polished. After each succeeding step the surface of the electrode was washed with deionized water. Finally, the electrode was again placed in the deionized water and methanol solution and sonicated for five minutes. Then a drop of the synthesised colloidal solution of AgNPs was dried on the cleaned and polished electrode surface to create the active SERS layer.

The synthesis procedure of the colloidal solution of citrate reduced and stabilised silver nanoparticles has already been mentioned in the previous sections. Thus, the detailed preparation procedure will not be discussed herein. Concentration of the silver nanoparticles in the solution was increased via centrifuging the colloidal solution for 10 minutes at the speed of 6500 rpm. Once again, after centrifuging half of the initial volume was considered a supernatant and was discarded. The prepared solution was characterized by collecting the UV-Vis absorption spectra of the solution and taking TEM images of the nanoparticles. However, since the results were almost identical to the ones described in the Chapter 2, in order not to repeat the same information the characterization of the nanoparticles will not be discussed. Aluminium oxide polishing powder (0.3 μm grain size) and the potassium chloride (3 M) solution used for the reference electrode were bought from *Methrohm Autolab* (Netherlands).

4.4.2. Sample preparation for the EC-SERS analysis

The control saliva samples (samples which would not contain caffeine or its metabolites) were taken from volunteers which have not ingested any caffeine containing products for at least 24 hours. Two types of real-life samples differing by the caffeine intake dose were taken as well. The 2 mg/kg and 3.5 mg/kg of caffeine were taken orally. Such doses were selected since they represent the clinical therapeutic and the low toxicity doses, respectively. Saliva samples for each dosage were collected at different time periods from 1 h to 10 h in respect to the time of caffeine ingestion. All samples (both control and real-life) were pre-processed in order to remove unwanted constituents of saliva, who could compromise the spectral analysis, like epithelium cells, bacteria, etcetera. The pre-processing of the saliva samples was done by centrifuging them at the speed of 13000 rpm for 10 minutes. In order to avoid sample degradation, the EC-SERS spectra of saliva were taken within an hour of the collection of the saliva. Control samples were also used to prepare the model samples of caffeine in saliva. These were prepared by dissolving the appropriate amounts of caffeine powder (*Sigma Aldrich*) in the saliva. The solutions of pure caffeine and paraxanthine (*Sigma Aldrich*) were prepared for the EC-SERS measurements by diluting required amounts of these substances in a solution of 0.1 M of H_2SO_4 (*Sigma Aldrich*) which was used as a supporting electrolyte. During the spectroscopic analysis of saliva, no electrolyte was used since various electrolytes are already found in its composition [279]. Oxygen dissolved in the solutions was removed by

purging the solutions with nitrogen before the collection of the EC-SERS spectra.

4.4.3. The EC-SERS spectroscopy of saliva

The EC-SERS spectra were collected using already described FT-Raman spectrometer MultiRAM from *Bruker* (Germany). Liquid cooled nitrogen cooled Ge diode detector and Nd:YAG laser source with a wavelength of 1064 nm from *Cobolt* (Sweden) were used. All spectra were also collected in a backscattering geometry using a gold plated 90-degree angle parabolic mirror objective. The spectra were collected in the wavenumber region from 4000 cm^{-1} to 150 cm^{-1} with a spectral resolution of 4 cm^{-1} . A total of 300 interferograms were averaged and Fourier transformed for the resulting spectrum of a sample. Blackman-Harris 3 term apodization function and a zero-filling factor of two were used in the Fourier transform algorithm.

A three-electrode setup was used to perform all electrochemical measurements. A silver working electrode (WE) with a diameter of 5 mm and a platinum counter electrode (CE) were chosen. As a reference electrode the double junction Ag/AgCl electrode filled with 3 M KCl solution was used. These electrodes were purchased from *Metrohm Autolab* (Netherlands). The potential applied to the electrodes during electrochemical measurements was controlled with a potentiostat/galvanostat PGSTAT302N purchased from *Metrohm Autolab* (Netherlands). A custom made three-electrode cell was used to perform measurements in a liquid state. A Raman grade calcium fluoride (CaF_2) optical window was attached to the cell in order to be able to measure the Raman scattering signal and to reduce the unwanted spectral bands arising from the experimental setup. In the case of CaF_2 glass it has one vibrational band, located at 325 cm^{-1} . The spectral region of this band is included in the spectra but was not investigated during spectral analysis. All glassware and the electrochemical cell were cleaned before every measurement using a piranha solution and deionized water. The potential of the working electrode was changed from the open circuit potential to -1.0 V with a step of -0.1 V. At each step the EC-SERS spectra were collected.

4.4.4. Theoretical calculations

Gaussian 09 software [118] was employed for the density functional theory calculations. Avogadro software [119] was used to create and visualize the geometries of molecules and complexes. Geometry optimization of the most

stable tautomeric forms of caffeine and paraxanthine [280] was carried out at B3LYP/6-311G* level of theory. For the simulation of the silver nanoparticle a geometry optimization of a 15-atom silver cluster was carried out at B3LYP/LANL2DZ level of theory. Complexes between the silver atom cluster and different orientations of the analyte molecules were calculated. The most probable adsorption geometry of caffeine and paraxanthine was then found by comparing the energies of the complexes. During DFT calculations the optimized structure of the silver cluster was “frozen” since it is not supposed to change during experiments. The calculated Raman spectra were used for assignment of the normal vibrations to the experimental spectrum. Computations were performed on resources at the High-Performance Computing Center “HPC Sauletekis” in Vilnius University Faculty of Physics.

4.5. EC-SERS STUDY OF SALIVA: RESULTS AND DISCUSSION

This work was dedicated to application of the EC-SERS spectroscopy for the detection of psychoactive drugs in human saliva in order to estimate their intake. The sensitive and fast identification of drug molecules can be lifesaving in the cases of accidental overdose. The problem of the increase in overdose cases is seen throughout the world and the number of such cases is seen to increase yearly [281]. In this work caffeine was chosen as a most simple psychoactive drug belonging to the alkaloid group – a vast group of naturally occurring molecules that contain nitrogen atom or atoms. Many of the abused drugs like cocaine, nicotine, morphine, methamphetamine also belong to the alkaloid group. Caffeine is considered a mild drug and its use is fairly regulated. Therefore, overdosing on caffeine is a common risk. The symptoms of caffeine overdosing depend on the dosage. At smaller doses of caffeine in plasma (around 15 mg/L) the symptoms may resemble that of anxiety with the main symptoms being nervousness, agitation, tremors and similar [282]. High toxicity doses (from 80 mg/L to 100 mg/L) can result in heart palpitations, seizures and death [283]. Overdosing on caffeine by consuming beverages is not common and is more likely to happen while consuming caffeine containing medication [284]. The sale of products with high concentration of caffeine is fairly regulated what resulted in the increase of overdose on caffeine and deaths related in the last years [285]. The clinical detection of caffeine as with other types of drugs are mostly done with the various high-performance liquid chromatography methods [286-288].

In this work the EC-SERS method is applied for the sensitive non-invasive detection of caffeine use from human saliva. Saliva as other biological fluids

is a complicated sample which contains various chemical species from proteins to nucleotides and electrolytes. As was seen previously this makes the chemical analysis and detection of a certain chemical molecule in biological fluids a complicated task. The EC-SERS approach was chosen, since the possibility to control the potential can facilitate the increased adsorption of the analyte molecules. This allows more precise and specific analysis of the complex samples like biological fluids.

As already mentioned, both caffeine and saliva were already analysed using vibrational spectroscopy methods. As well as, the EC-SERS spectroscopy was already proposed as a possible tool for the detection of molecules in biological fluids. Nonetheless, the method has not been tested for the detection of caffeine or other similar types of drugs. Furthermore, only model samples have been studied so far. Such approach does not constitute as a true application of the method. For this, the analysis of real-life samples which is far more complicated needs to be performed. Exactly this – the detection of caffeine used in real-life samples of human saliva via the label free EC-SERS spectroscopy, is achieved.

4.5.1. Spectral analysis of pure and model saliva samples

Pure saliva samples and model saliva spiked with caffeine samples were first analysed in order to collect more information about the arising problems and to find the best spectral markers for the detection of caffeine. Saliva samples as already mentioned were collected after caffeine fasting – not consuming caffeine containing products for at least 24 hours. This way control samples which would not contain caffeine or its metabolites were collected. While preparing the pure samples of caffeine and paraxanthine it was taken into account that the SERS spectra of these molecules change at different pH values [289]. Thus, the pH value of the prepared solutions was measured and if needed changed to resemble the pH value of the human saliva which on average is around 7.1. It is known that when caffeine is consumed the pH value of the saliva drops. However, it has been found that the pH value is restored in approximately 30 minutes [290]. Spectra analysis of the pure caffeine and paraxanthine samples has shown that when the electric potential value, which is applied to the WE, equals -0.5 V, the highest SERS signal of these molecules is observed. Because of this, all future EC-SERS measurements conducted in this work were performed at this value of the potential. The EC-SERS spectra of pure caffeine and paraxanthine solutions taken at different WE potential values are shown in Appendix II, Fig. 7. The

comparison of the collected spectra of pure saliva, 1 mM caffeine solution, and 1 mM paraxanthine solution are presented in the Fig. 36. To be clear, all spectra were collected at the potential value of -0.5 V. The EC-SERS spectra were shifted along the y-axis and the spectra of caffeine and paraxanthine were scaled down. The most prominent vibrational band positions are listed above each spectrum.

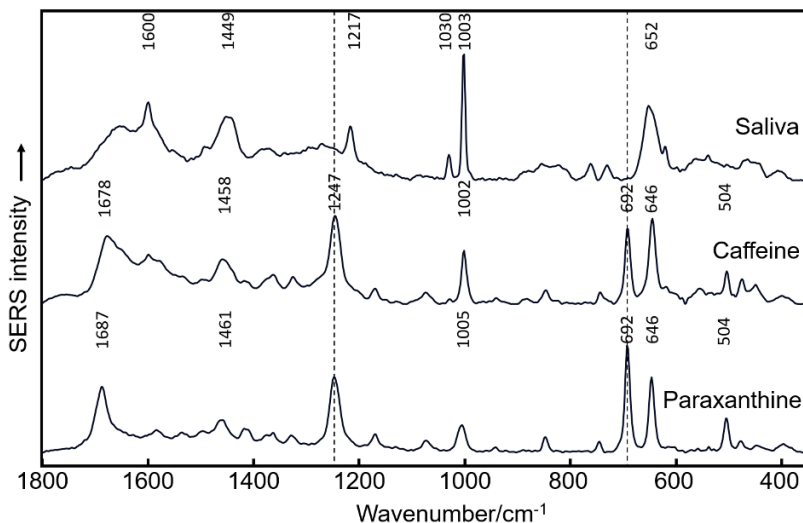


Fig. 36. The EC-SERS spectra of 1 mM solution of caffeine, 1 mM solution of paraxanthine, and pure saliva taken at the WE potential value of -0.5 V.

What can be noticed straightforward in the EC-SERS spectra presented in the Fig. 36 is that the spectrum of saliva is primarily dominated by the vibrational bands located at 1600 cm^{-1} , 1030 cm^{-1} , 1003 cm^{-1} , 652 cm^{-1} . These bands can be assigned to the vibrations of phenylalanine. This result is not surprising since phenylalanine is found in saliva in relatively high concentrations [291]. Furthermore, the vibrational bands of phenylalanine are often present in the both Raman and SERS spectra of various biological samples [292]. Besides the vibrational bands of phenylalanine, spectral bands most likely arising because of the vibrations of other structural molecules like amino acids, nucleic acids, collagen or lipids can be also observed in the spectrum of saliva [293]. In case of the EC-SERS spectra of caffeine and paraxanthine it was noticed that the most prominent vibrational bands of these molecules are located at the same wavenumbers. Only a slight shift of the bands related to the C-H vibrations were noticed. This is also not an

unexpected result since the structure of these two molecules differ only by one methyl group.

Theoretical DFT calculations of complexes between caffeine or paraxanthine molecules and the silver nanoparticle were performed in order to better understand the EC-SERS spectra of these molecules. The silver nanoparticle was simulated by a 15-atom silver cluster. First, geometries of the molecules were optimized and are presented in the Fig. 37. Then six complexes of caffeine and paraxanthine with different orientation in relation to the silver atom cluster were analysed (three for each molecule). The calculated energy differences of the complexes for each molecule and the geometries of the complexes are shown in the Appendix II, Fig. 8.

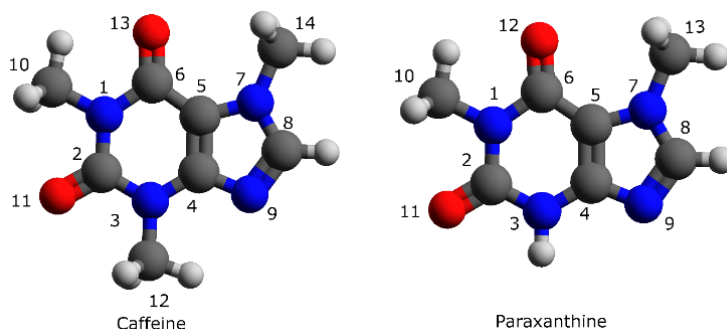


Fig. 37. The optimized geometries of the caffeine and paraxanthine molecules.

The DFT calculations have shown that most likely the caffeine and paraxanthine molecules adsorb on the silver surface through one of the oxygen atoms (atom No 11 see Fig. 37). This is because the energy of the complex with this geometry has the lowest energy value – is the most stable. The Raman spectra of the most stable complexes were then calculated. The calculated spectra were used for the assignment of the normal vibrations to the spectral bands observed in the experimental EC-SERS spectra. The full assignment of spectral bands of caffeine and paraxanthine are presented in Appendix II, Table 1. However, the positions of the main vibrational bands of the caffeine and paraxanthine molecules observed in their EC-SERS spectra and their assignment to the normal vibrations are as follows: $\nu(\text{C}=\text{O}) + \delta(\text{NH}) - 1687 \text{ cm}^{-1}$, $\delta(\text{CH}_3) + \delta(\text{NH}) + \delta(\text{CH}) - 1458 \text{ cm}^{-1}$ (caf), 1461 cm^{-1} (par), $\delta(\text{C-H}) + \nu(\text{N-C}) + \delta(\text{CH}_3) - 1247 \text{ cm}^{-1}$, $\nu(\text{N-C}) + \delta(\text{CH}_3) - 1002 \text{ cm}^{-1}$ (caf), 1005 cm^{-1} (par), $\nu(\text{N-CH}_3) + \delta(\text{N-C-N}) - 692 \text{ cm}^{-1}$, in plane pyrimidine ring breathing + $\delta(\text{C-N-C}) - 646 \text{ cm}^{-1}$, and in plane pyrimidine ring deformation + $\delta(\text{C-N-CH}_3) - 504 \text{ cm}^{-1}$. However, while

analysing the EC-SERS spectra of caffeine, paraxanthine, and saliva it was noticed that most of these vibrational bands overlap with the spectral bands observed in the EC-SERS spectrum of saliva. The use of the overlapped bands for the detection of caffeine is limited since the reason for the change in the band intensity cannot be correctly interpreted. Because of this, only two spectral bands which are least likely to overlap with the spectrum of saliva were chosen as potential spectral markers of caffeine and paraxanthine. These bands are located at 1247 cm^{-1} and 692 cm^{-1} and are assigned to the $\nu(\text{N-C}) + \delta(\text{CH}_3)$ and $\nu(\text{N-CH}_3) + \delta(\text{N-C-N})$ vibrations respectively. The positions of bands chosen as spectral markers are denoted in the EC-SERS spectra shown in the Fig. 36 with a dashed line.

As with the samples of pure compounds the EC-SERS spectra of the saliva sample were also collected at different WE potential values. This was done in order to check whether any new vibrational bands appear in the region of the chosen spectral markers (692 cm^{-1} and 1247 cm^{-1}). The EC-SERS spectra of pure saliva, collected at different potential values, and the EC-SERS spectra of 1 mM solution paraxanthine and 1 mM solution of caffeine, collected at -0.5 V , are presented in Fig. 38. For clarity all collected spectra were shifted along the y-axis. The spectra of caffeine and paraxanthine were scaled down.

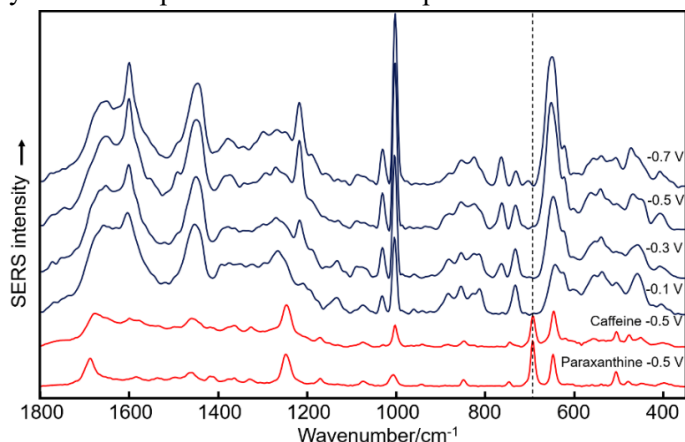


Fig. 38. The EC-SERS spectra of: human saliva taken at different potential values of the WE (blue), 1 mM solution of caffeine, and 1 mM solution of paraxanthine at WE potential value of -0.5 V (red).

Analysis of the EC-SERS spectra of saliva presented in the Fig. 38 have shown that with increasing of the negative potential the spectral band intensity changes. For example, intensity of the vibrational bands of phenylalanine is observed to increase when the negative potential applied to the WE is

increased. Thus, the spectrum of saliva is still dominated by the phenylalanine bands. At even higher potential values the intensity of some spectral bands starts to decrease. This could be explained by the phenylalanine molecule pushing out other molecules and adsorbing on the surface of the electrode. Also, the appearance of new spectral bands is observed. One of the such spectral bands is located 1247 cm^{-1} and is in the vicinity of one of the spectral marker bands that were chosen earlier. This is why, the spectral marker band, located at 1247 cm^{-1} was not considered for the identification of caffeine in further research. No new bands were observed to appear in the region of the chosen other spectral marker band located at 692 cm^{-1} . Thus, this spectral band can be used for detection of caffeine or paraxanthine in saliva.

When in saliva the adsorption of caffeine can be burdened. This is because other molecules in the composition of saliva are also able to adsorb on the surface. Thus, this competitive adsorption lowers the possibility of caffeine molecules to adsorb on the WE. Furthermore, as already described, in plasma some of the caffeine molecules are bound to saliva proteins what limits their ability to adsorb as well. In order to check whether caffeine molecule can be still detected in the presence of the saliva constituents model saliva and caffeine (2 mM) sample was made. The EC-SERS spectra of the model saliva and caffeine (2 mM) sample was collected at different potential values and is presented in the Fig. 39. The EC-SERS spectra of 1 mM solution of caffeine and 1 mM solution of paraxanthine (1 mM) collected at -0.5 V is also shown. For clarity, all presented spectra were shifted along the y-axis. The caffeine and paraxanthine spectra were also scaled down.

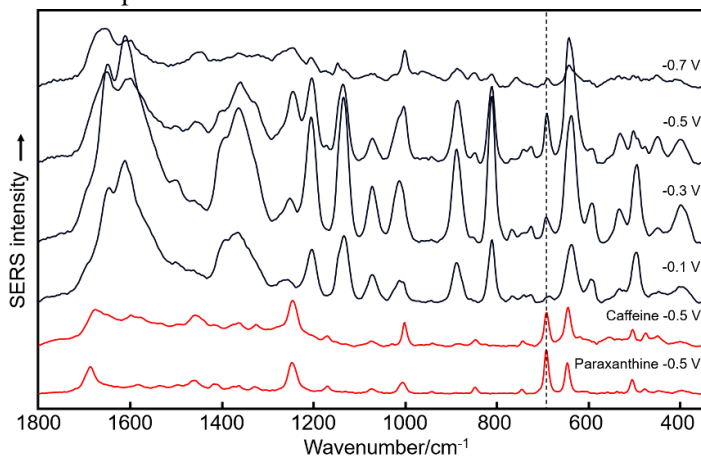


Fig. 39. The EC-SERS spectra of: model saliva and caffeine (2 mM) sample (blue) collected at different WE potentials (blue), 1 mM solution of caffeine, and 1 mM solution of at -0.5 V potential (red).

The analysis of the spectra presented in the Fig. 39 has shown that the spectral features of caffeine cannot be distinguished at low potential values. At these values only the spectral bands of the constituents of saliva are observed. It should also be noted that the addition of caffeine altered the adsorption of phenylalanine since the spectral bands of phenylalanine are observed with lower intensity. Because of this the spectral bands which in the EC-SERS spectra of saliva were observed with low intensity can now be clearly observed in the spectra of saliva and caffeine. The spectral marker bands of the caffeine appear with increasing of the negative potential value. The intensity of these bands was observed to reach the maximum value when the potential applied to the WE was -0.5 V. At the same time, the intensity of some spectral bands of saliva constituents decreases. This also indicates the altered adsorption of the saliva constituents what could result from the inhibited adsorption on the surface of the electrode by the caffeine molecules. The analysis of the model samples has shown that the detection of caffeine molecule in the presence of various constituents of saliva is possible. The applied potential value of -0.5 V was again proven as the best for the detection of caffeine since. At this potential value intensity of the marker bands was observed to be highest.

The region of the CH₃ stretch was also investigated in this work since it was thought to contain some additional information on the adsorption of caffeine. The CH₃ stretching region of the EC-SERS spectra collected at potential value of -0.5 V of pure saliva, saliva and caffeine model solution, caffeine, and paraxanthine are presented in Appendix II, Fig. 9. It was noticed that spectrum of caffeine, the band assigned to the $\nu(\text{CH}_3)$ vibrations is more intense than that of saliva or paraxanthine. Thus, the increase in intensity of this band could also be potentially used for the detection of caffeine.

4.5.2. Spectral analysis of real-life saliva samples containing caffeine

The real-life samples, as already mentioned, were taken from volunteers after they ingested 2 mg/kg or 3.5 mg/kg dose of caffeine. The spectra were registered within an hour of sample collection in order to avoid the degradation of the samples. Since -0.5 V was found to be the potential value best suited for the measurements, the EC-SERS spectra of all real-life samples were measured at this value. The EC-SERS spectra of the saliva taken after different time periods of the consumption of 3.5 mg/kg dose of caffeine, are presented in the Fig. 40. The scaled down EC-SERS spectra of 1 mM solutions

of caffeine and paraxanthine taken at -0.5 V are presented here as well. For clarity all spectra were shifted along the y-axis.

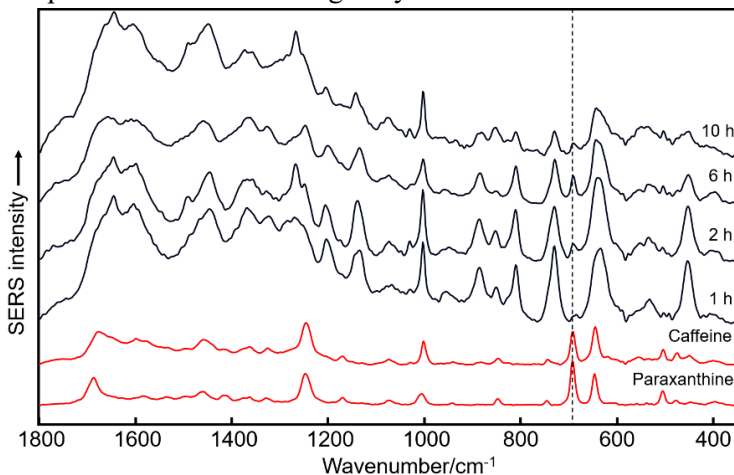


Fig. 40. The EC-SERS spectra taken at -0.5 V potential of: saliva collected at different time periods after consumption of 3.5 mg/kg dose of caffeine (blue), 1 mM solutions of caffeine, and paraxanthine (red).

While analysing the EC-SERS spectra presented in the Fig. 40 it was noticed that the spectral marker band of caffeine can already be observed in the sample which was taken after one hour of the consumption. However, the marker band is not very distinct. The intensity of the marker band is higher in the following samples which were taken after 2 h and 6 h after consumption and then decreases again in the sample taken after 10 h. This result is quite interesting since in accordance to the pharmacokinetic studies of caffeine the highest concentration of caffeine is found after 1 h of consumption. The low intensity of the spectral marker band of caffeine can be easily explained by the fact that the caffeine concentration resulting from the consumption dose of 3.5 mg/kg is only in the range of 30 μM [237]. This concentration is incomparably small with the one used for the model samples. This is why the intensity of the spectral marker band is low in the EC-SERS spectra of saliva taken after 1 hour of consumption. The increased intensity of this spectral band can be also explained. During the theoretical analysis of the caffeine and paraxanthine complexes it was noticed that the complexes of paraxanthine have a lower bonding energy than the complexes of caffeine. This suggests that paraxanthine is more likely to adsorb on the surface of the nanoparticles. In such case this would also result in the higher overall intensity of the EC-SERS spectrum of paraxanthine since the enhancement is dependent on

the distance between the nanoparticle and the analyte molecule. In fact, this result was observed when the EC-SERS spectra of 1 mM solutions of caffeine and paraxanthine were collected. Thus, these factors could explain the increasing intensity of the spectral marker band. The concentration of paraxanthine increases with time since more caffeine molecules are metabolised. Thus, after longer periods of time the paraxanthine is available to adsorb on the nanoparticles what, if we take into account the better adsorption and higher intensity of the spectra of paraxanthine, results in the increase of the intensity of the marker band. This finding can be backed by other researches which have shown that the concentration of paraxanthine increases after the consumption of caffeine and reaches its maximum at around 6 hours after consumption [234, 237]. The highest intensity of the marker band was also observed in the saliva samples collected 6 hours after caffeine consumption.

The analysis of the CH₃ stretching region of the EC-SERS spectra has also shown promising results. This region of the spectra is presented in the Fig. 41. The effect of caffeine consumption can be already observed after 1 h of consumption – intensity of the vibrational band related to the $\nu(\text{CH}_3)$ is increased. Then, it decreases in the spectra of saliva samples collected after longer periods after consumption. This would indicate that the concentration of caffeine decreases since it is being metabolized. Furthermore, the intensity decrease is not linear what also is with agreement to the caffeine concentration in human saliva profile.

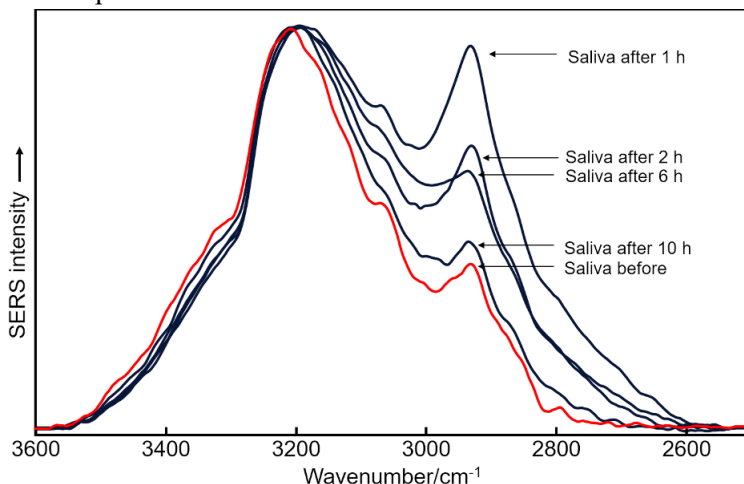


Fig. 41. The EC-SERS spectra collected at -0.5 V potential of: saliva taken at different times after the consumption of 3.5 mg/kg of caffeine, and pure saliva sample (red) presented in the CH₃ stretching region.

The EC-SERS spectra of saliva taken after consumption of a lower dose (2 mg/kg) were collected to ensure that the observed behaviour of the spectral markers is not a random coincidence. This dose of caffeine results in a concentration around 15 μM in saliva. The EC-SERS spectra were again collected at the WE potential value of -0.5 V. The collected spectra are presented in the Fig. 42. All spectra were shifted along the y-axis for clarity. Also, the scaled down spectra of 1 mM solutions of caffeine and paraxanthine are presented for comparison. In fact, similar results were observed. The spectral marker band, located at 692 cm^{-1} is observed to be low in intensity after 1 hour of consumption of caffeine. Then its intensity grows and it is observed to be highest in the EC-SERS spectra of saliva collected after 5 hours. It should be noted that the true maximum value may be seen later, however the approximate time of the maximum value is around 5-6 hours. Finally, the intensity of the marker band decreases. Also, it was observed that the intensity of the spectral marker band is lower in the EC-SERS spectra of the saliva after taking a lower dose of caffeine than in the spectra of saliva after taking a higher dose of caffeine. This shows a direct relation of the spectral marker band to the caffeine concentration in saliva.

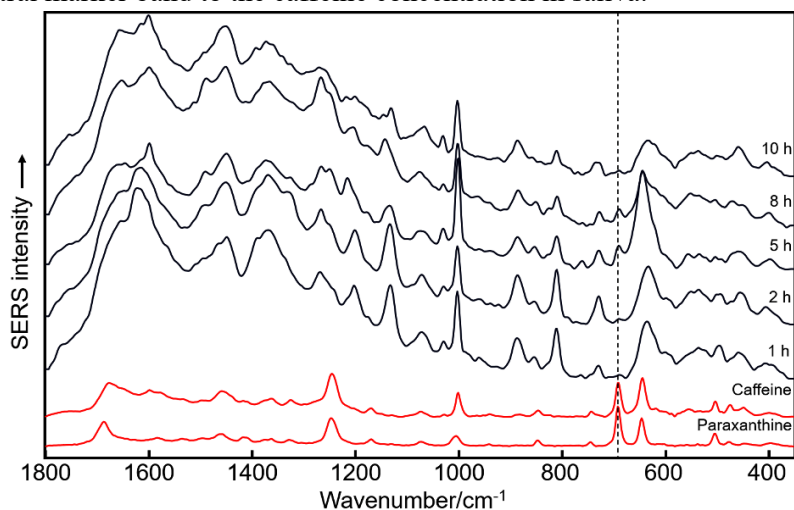


Fig. 42. The EC-SERS spectra collected at -0.5 V potential of: saliva taken at different time periods after the consumption of a 2 mg/kg dose of caffeine (blue), 1 mM solutions of caffeine, and paraxanthine.

As before, the region of the CH_3 vibrations was investigated. The EC-SERS spectra of saliva collected at different time periods after the consumption of 2 mg/kg dose of caffeine is presented in the Fig. 43. The same

tendency of the $\nu(\text{CH}_3)$ vibration band was observed. The intensity of the band was highest in the spectra of saliva taken after one hour of consumption and then gradually decreases with time what again indicates the metabolism of caffeine molecules. Once again, the overall intensity of the band was observed smaller than seen in the EC-SERS spectra of saliva after taking a bigger dose of caffeine. Since the behaviour of the spectral marker band was reproducible in the two experiments it can be stated that the presence of caffeine in saliva can be indicated from the spectral marker band located at 692 cm^{-1} , which arise directly from the adsorption of caffeine molecules and from the adsorption of its metabolite – paraxanthine.

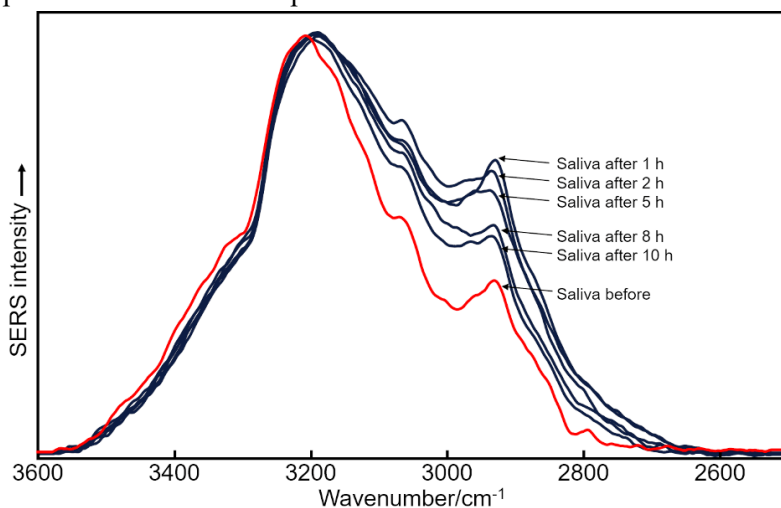


Fig. 43. The EC-SERS spectra collected at -0.5 V potential of: saliva taken at different times after the consumption of caffeine (2 mg/kg), and pure saliva sample (red) presented in the CH_3 stretching region.

The change of intensity over time of the observed vibrational marker bands which are located at 2930 cm^{-1} and 692 cm^{-1} was plotted and is shown in the Fig. 44. Both bands – the $\nu(\text{CH}_3)$ vibration band and the $\nu(\text{N-CH}_3) + \delta(\text{N-C-N})$, show similar intensity profiles at the two tested doses (2 mg/kg and 3.5 mg/kg). This proves the reliability of the EC-SERS method for the identification of caffeine use from human saliva. Furthermore, the observed intensity dependence on the caffeine dose shows that not only qualitative but also quantitative analysis can be performed. However, it should be mentioned that even though the $\nu(\text{CH}_3)$ spectral band showed promising results and is in good correlation with the pharmacokinetic profile of the caffeine in saliva [237] it should be used with caution. The intensity of the

said band is not only dependent on the vibrations of caffeine molecules but also on the other constituents and on the experimental setup. Thus, its intensity could be dramatically altered and does not depict the true information. The spectral marker band located at 692 cm^{-1} however can be used reliably since it is resulted only from the vibrations of caffeine or its metabolites (mainly paraxanthine). The intensity profile of this band is also in good correlation with the pharmacokinetics profile of paraxanthine in saliva as observed in the literature [237].

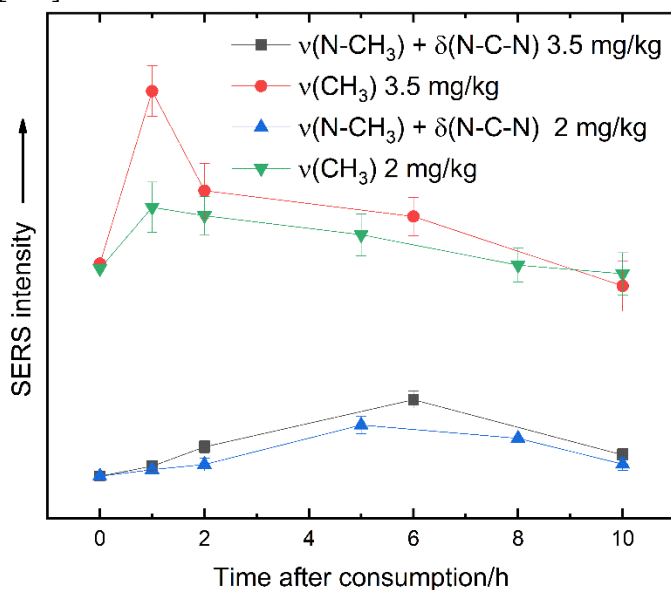


Fig. 44. The intensity changes over time of the two spectral marker bands of caffeine at 2930 cm^{-1} and 692 cm^{-1} in the EC-SERS spectra of saliva.

The spectral analysis of the real-life samples of two doses of caffeine (2 mg/kg and 3.5 mg/kg) in saliva has shown that the label-free EC-SERS spectroscopy can be potentially used for identification of caffeine use from human saliva. The results of the theoretical calculations have shown that caffeine and paraxanthine most likely adsorb on the nanoparticle surface through the one of the oxygen atoms and gave more insight into the nature of the vibrational bands seen in the EC-SERS spectra. Out of all spectral bands of caffeine the vibrational band located at 692 cm^{-1} was shown to be the most reliable for the identification of caffeine consumption. The intensity of the band is dependent on both the caffeine and paraxanthine presence and the change of the intensity over time is correlated with the concentration of the paraxanthine. These findings show that the detection of other potentially lethal

drugs in biological fluids should be also possible via the EC-SERS spectroscopy. The ability to control the potential applied to the WE increase the sensitivity of the detection by facilitating the adsorption of the analyte molecules. The detection limit of the EC-SERS method may not yet compare to the standard methods used in metabolomics such as the LC/MS or the GC/MS. However, the possibility of the fast analysis of the EC-SERS could be advantageous in certain clinical situations. Furthermore, the ability to use small and affordable screen-printed electrodes and portable systems could make this method highly valuable in case of life-threatening emergencies or for a point-of-care analysis.

CONCLUSIONS

1. The surface enhanced Raman scattering spectroscopy of extracellular matrix was shown to be a viable method for discrimination of normal and cancerous tissues. The sensitivity and specificity of the method reaches 93% in the case of kidney cancer. The spectral markers linked to the metabolic changes of cancerous cells – increased intensity of the spectral bands of glycogen and cysteine/lactic acid, were determined and used for identification of the cancerous tissues of kidney and bladder cancers, respectively.
2. It was shown that the SERS spectroscopy is sensitive enough to track chemical damages happening on the surface of bacteria cells. Analysis of the spectral data showed that rupturing of the outer membrane of the bacteria cell was the main effect of the inactivation of *E. coli* bacteria via chlorophyllin-based photosensitization and provided more insight into the overall inactivation mechanism.
3. The SERS spectroscopy was applied for the analysis of real-life blood and blood serum samples containing therapeutical concentrations of pharmaceutical drugs (acetylsalicylic acid and acetaminophen). It was determined that the label-free SERS spectroscopy of blood serum allows the detection of acetyl salicylic acid through its metabolite salicylic acid at the concentration level regarded as of low toxicity (3 mM) and detection of 1 mM of acetaminophen is possible in model samples but is burdened by the presence of uric acid in real-life conditions.
4. The label-free EC-SERS spectroscopy was applied for the detection of the consumption of psychoactive substance caffeine in real-life saliva samples. Detection of caffeine ingestion by analysing the intensity of the spectral markers related to caffeine or its metabolite paraxanthine via the EC-SERS spectroscopy was found to be possible even after 1 hour of consumption and at the concentration of caffeine as low as 15 μM .

FUTURE PROSPECTS

The research presented here shows the versatility of the SERS method in the biomedical field to analyse different types of biological samples. Furthermore, it was shown that SERS spectroscopy can be applied for the analysis of the clinical-type (real-life) samples, thus bringing the method closer to clinical applications. However, in order to truly employ the SERS spectroscopy for clinical diagnosis more research and development should be made. This section is dedicated to highlight the necessary steps for future projects.

In all SERS experiments it is of much importance to ensure the correct sample preparation procedure. This involves both the sample collection and preparation for the SERS measurements. In case of tissue analysis, it is advised to create a protocol for the collection of the tissue so that as much of sampling errors as possible would be avoided. This could involve additional steps of ensuring that the resected tissue is assigned to the correct category (normal or cancerous). Moreover, comparison between the results of histological and spectroscopical analysis is not only beneficial but should be continued until SERS spectroscopy would be validated as a stand-alone procedure. It is also worth considering of combining several spectroscopic techniques like SERS and ATR-FTIR to analyse the same sample. This could be done via combination of optical fiber and would improve the overall quality of the analysis possibly resulting in even higher specificity and sensitivity.

Sampling of biological fluids is straight-forward, since the standard sampling procedures are already described and used. Therefore, they should be implemented in the SERS analysis as well. An important point to consider in these measurements is the adsorption of other molecules in the composition of the analysed biofluid. What was shown in the presented research is that the uric acid and phenylalanine molecules are especially prone to adsorption on the nanoparticle surface. This influences the limit of the detection of the analyte under investigation. Therefore, it could be worthwhile to reduce the adsorption of such molecules. For example, as was shown in the presented research, the uric acid adsorption could be reduced by changing the pH of the sample. Such improvements could lead to increased sensitivity of detection and rival the one achieved in the standard clinical diagnosis.

Of course, SERS analysis could be improved by choosing other nanoparticles for the enhancement or Raman scattering. In this research label-free nanoparticles were used since they are by far more cost-efficient and faster to produce. If in some cases the cost reduction is not of concern

functionalized nanoparticles could be employed. Such particles could be tailored to adsorb only to the certain type of chemical groups thus increasing the sensitivity of the method. Different particles could be prepared for tissue, bacteria or biofluid analysis. However, what should be kept in mind is that besides the increase of the cost, in such case the preparation for the SERS analysis would become more difficult, since the versatility of the SERS method would be reduced.

Finally, implementation of the already available substrates or accessories is also possible. For example, the EC-SERS analysis of biofluids would be much more convenient if instead of electrochemical cells screen-printed electrodes would be used. This would allow faster analysis and easier preparation of the samples, since the amount of the sample required for the analysis would be reduced. Optical fiber covered with SERS active layers could be used for on-site analysis and could also reduce the time required for spectroscopic analysis. However, such accessories are not cost-efficient therefore a completely different set of research could be made to improve and develop low-cost substrates of this type.

SANTRAUKA LIETUVIŲ KALBA

ĮVADAS

Visose mokslo srityse pažangą nulemia galimybė surinkti kuo daugiau specifinės informacijos apie tiriamus objektus. Nuolatinis siekis tobulėti skatina vystyti ir diegti pažangias metodikas ar kurti naujus standartinių metodikų pritaikymo būdus. Biologijoje, o ypač moderniosios medicinos srityje tyrimų metu surenkamų duomenų specifiškumas yra nenuginčijamai svarbus. Tikslėsių duomenų surinkimas leidžia daug tiksliau suprasti sudėtingus ligų mechanizmus, padidina jų aptikimo jautrumą. Dėl to gali būti užtikrinta aukštesnė pacientų gydymo kokybė.

Tiriant biologinės kilmės mėginius yra reikalingi metodai, kuriais būtų galima analizuoti jų cheminę sandarą. Šiuo metu praktikoje yra taikomos kelios skirtingos analizės metodikos, kurios suteikia informacijos apie bandinio cheminę sandarą nuo atominio iki molekulinio lygmens. Viena tokių įvairiose srityse taikomų cheminės analizės metodikas apjungianti sritis yra virpesinė spektroskopija. Virpesinės spektroskopijos metodai suteikia informacijos apie bandinį sudarančių molekulių cheminius ryšius ir dėl to yra itin jautrūs cheminiams analitės pokyčiams. Dėl šios priežasties virpesinės spektroskopijos metodai – infraraudonųjų spindulių sugerties ir Ramano sklaidos spektroskopijos yra vis dažniau pritaikomos nustatant cheminę analitės sandarą, analizuojant molekulių struktūrą ar tiriant tarpmolekulines sąveikas biologinės kilmės bandiniuose [1-5]. Šie metodai turi privalumų pritaikant juos praktiškai, kadangi palyginus su kitomis cheminės analizės metodikomis bandinių paruošimo procedūros dažniausiai yra nesudėtingos ir greitos. Taip pat šių metodų suderinamumas su mikroskopijos metodikomis bei tai, kad tyrimams yra reikalingas nedidelis mėginio kiekis įgalina itin mažų bandinių spektrinę analizę. Dėl šių priežasčių virpesinės spektroskopijos metodai jau yra taikomi biologinių molekulių ar darinių struktūros ar sudėtingos sandaros bandinių, kaip ląstelės, biologiniai skysčiai ar audiniai, analizei [6-10].

Virpesinės spektroskopijos metodikos yra naudingos ne tik dėl to, jog suteikia informacijos apie cheminę bandinio sudėtį, bet ir dėl to, kad ši informacija yra itin vertinga. Žinoma, kad visos ligos yra nulemtos bei gali būti susietos su tam tikrais cheminiais ląstelės, genomo, metabolizmo ar kitais pokyčiais. Būtent šių pokyčių nustatymas yra vienas pagrindinių klinikinės diagnostikos uždavinių. Dėl to virpesinės spektroskopijos metodų jautrumas nedideliems cheminiams pokyčiams įgalina ankstyvą

įvairių ligų diagnozę. Analizuojant ir lyginant tam tikrų audinių, ląstelių, kūno skysčių cheminę sandarą, dar prieš pasirodant pirmiesiems ligos simptomams, būtų galima nustatyti netgi itin nedidelius pokyčius, kurių atsiradimas nurodo egzistuojančią ligą. Toks proveržis ankstyvoje klinikinėje diagnostikoje yra itin naudingas bei siekiamas. Dėl to šis virpesinės spektroskopijos metodų taikymo būdas šiuo metu yra sparčiai plėtojamas ir siekiant kuo greičiau pritaikyti metodus klinikinėje praktikoje yra atliekama daug mokslinių tyrimų [11-13]. Nepaisant galimybės diagnozuoti ligas ankstyvoje stadijoje, trumpas spektrinės informacijos rinkimo laikas yra dar vienas virpesinės spektroskopijos metodų pranašumas. Todėl nešiojamus spektrometrus suderinus su šviesolaidiniais zondais atsiranda galimybė surinkti nepriklausomą informaciją *in vivo*, kuri padėtų chirurgams greitai priimti tikslius ir teisingus sprendimus [14, 15].

Vis dėlto, didelio virpesinės spektroskopijos metodų potencialo neužtenka pritaikyti juos klinikinėje medicinoje. Šių metodų taikymas klinikinėje diagnostikoje dar nėra įprasta praktika dėl kelių priežasčių. Viena jų – sudėtinga kompleksinių bandinių, sudarytų iš daugelio molekulių, spektrų interpretacija. Tokių bandinių spektrai yra sudaryti iš daugelio persiklojusių virpesinių juostų. Dėl šios priežasties daugelyje mokslinių tyrimų tokių spektrų interpretacija yra tik preliminari. Norint patikslinti virpesinių juostų priskyrimus molekulių virpesiams yra reikalinga papildoma cheminių komponentų analizė bei teoriniai *ab initio* skaičiavimai [16-18]. Kita problema, kurią reikia išspręsti norint efektyviai pritaikyti virpesinės spektroskopijos metodus, yra optimalios bandinio paruošimo metodikos nustatymas. Pats paprasčiausias būdas – viso bandinio, pavyzdžiui audinio, analizė. Tačiau, toks būdas ne visuomet yra optimaliausias. Kaip jau minėta, spektriniai skirtumai, kuriuos lemia dėl ligos atsiradę cheminiai pokyčiai, yra labai nedideli. Todėl jie gali būti nepastebėti ar būti užgožti spektrinės perteklinės informacijos, susijusios su audinius sudarančiomis struktūrinėmis molekulėmis. Taigi, paruošiant bandinius, kuriuose nebūtų šių molekulių, galima supaprastinti spektrinę analizę. Kalbant apie audinius, tai gali būti atlikta nagrinėjant ne juos, o jų tarpląstelinį skystį [19-21]. Tokiais atvejais atlikus spektrinių duomenų apdorojimą yra pritaikomi daugialypiai chemometrijos metodai [22-24].

Dažnai molekulių koncentracija tiriamuose bandiniuose gali būti per maža, kad juos būtų galima tirti standartiniais spektriniais metodais. Su šia problema ypač susiduriama taikant Ramano sklaidos spektroskopiją. Vis dėlto, taikant nestandartinius spektrinius metodus, kaip paviršiaus

sustiprinta Ramano sklaido spektroskopija (angl. *surface enhanced Raman scattering* – SERS), yra galima ir tokio tipo bandinių cheminė analizė. Panaudojus metalines nanodaleles galima ženkliai sustiprinti Ramano sklaidos signalą ir tokiu atveju aptikti net itin mažos koncentracijos medžiagas. Šis metodas gali būti efektyviai taikomas aptikti narkotines medžiagas [25-27]. Taip pat paviršiaus sustiprinta Ramano sklaida gali būti suderinta su elektrocheminiais metodais. Tai įgalina valdyti analitės molekulių adsorbciją ir padeda selektyviai sustiprinti tam tikrų molekulių Ramano sklaidos signalą [28, 29]. Nepaisant to, daugelyje mokslinių tyrimų, kuriuose yra taikoma paviršiaus sustiprinta Ramano sklaidos spektroskopija, naudojami tik modeliniai bandiniai, užaugintos ląstelių kultūros ir t.t. Nors tokių tyrimų rezultatai ir yra tenkinantys, šie tyrimai neatspindi tikros klinikinės problemos. Norint paviršiaus sustiprintos Ramano sklaidos metodą pritaikyti klinikinėje diagnostikoje yra būtina jį pritaikyti realių bandinių analizei.

Galiausiai, siekiant bet kokią analizės metodiką pritaikyti klinikiniam tyrimams, ji pirmiausia turi būti patvirtinta atliekant klinikinius tyrimus, įvertinant siūlomo metodo tikslumą, jautrumą, specifiskumą. Taip pat siūlomi metodai negali prieštarauti bioetikos taisyklėms.

TIKSLAS IR UŽDAVINIAI

Atsižvelgiant į virpesinės spektrometrijos metodų praktinio pritaikymo problemas, pagrindinis disertacijos tikslas – sukurti naują virpesinės spektroskopijos pritaikymo metodiką biologinių bandinių (šlapimo sistemos vėžio, biologinių skysčių, bakterijų) analizei. Darbe dėmesys skiriamas virpesinės spektroskopijos metodo pritaikymui biologinių ir medicininių bandinių tyrimuose. Tikslui pasiekti buvo suformuluoti šie uždaviniai:

1. Pritaikyti SERS spektroskopiją įvairių žmogaus audinių vėžio analizei ir įvertinti metodo pritaikymo galimybę klinikuose tyrimuose.
2. Pritaikyti SERS spektroskopiją patogeninių bakterijų tyrimams.
3. Pritaikyti koloidinio SERS ir elektrocheminio SERS metodus vaistinių preparatų ir narkotinių medžiagų ar jų metabolitų aptikimui biologiniuose skysčiuose bei įvertinti metodų pritaikomumą klinikuose tyrimuose.

GINAMIEJI TEIGINIAI

1. Tarpląstelinio skysčio SERS spektroskopija gali būti efektyviai naudojama identifikuoti vėžinių audinių sritis pasiekiant didesnę nei 93% jautrumą ir specifiškumą. Tačiau, priklausomai nuo audinio tipo, identifikavimui turi būti naudojami skirtingi spektriniai žymenys – glikogeno, cisteino/pieno rūgšties spektrinės juostos.
2. SERS spektroskopija yra pakankamai jautrus metodas, leidžiantis identifikuoti *E. coli* bakterijų ląstelių membranos pažeidimus, atsiradusius po fotosensibilizavimo chlorofilinu.
3. SERS spektroskopija gali būti panaudota kliniškai reikšmingos koncentracijos (milimolių litre eilės) vaistinių medžiagų ar jų metabolitų aptikimui žmogaus kraujyje.
4. EC-SERS spektroskopija gali būti panaudota identifikuoti psichoaktyvių medžiagų vartojimą analizuojant žmogaus seiles. Kofeino atveju aptikimo riba siekia 15 mikromolių litre.

Publikacijų doktorantūros tema sąrašas

Publikacijos recenzuojamuose žurnaluose

1. M. Velička, M. Pučetaitė, V. Urbonienė, J. Čeponkus, F. Jankevičius, V. Šablinskas, Detection of cancerous kidney tissue by means of SERS spectroscopy of extracellular fluid, *Journal of Raman spectroscopy*, 2017, **48**, 1744.
2. M. Pučetaitė, M. Velička, V. Urbonienė, J. Čeponkus, R. Bandzevičiūtė, F. Jankevičius, A. Želvys, V. Šablinskas, G. Steiner, Rapid intra-operative diagnosis of kidney cancer by attenuated total reflection infrared spectroscopy of tissue smears, *Journal of Biophotonics*, 2018, **11**, 1.
3. S. Adomavičiūtė, M. Velička, V. Šablinskas, Detection of aspirin traces in blood by means of surface-enhanced Raman scattering spectroscopy, *Journal of Raman Spectroscopy*, 2020, **51**, 919.
4. B. Žudytė, M. Velička, V. Šablinskas, Ž. Lukšienė, Understanding *Escherichia coli* damages after chlorophyllin-based photosensitization, *Journal of Biophotonics*, 2020, **13**, 1.
5. M. Velička, E. Zacharovas, S. Adomavičiūtė, V. Šablinskas, Detection of caffeine intake by means of EC-SERS spectroscopy of human saliva, *Spectrochimica Acta Part A: Molecular and Biomolecular Spectroscopy*, 2021, **246**, 118956.

6. E. Zacharovas, M. Velička, G. Platkevičius, A. Čekauskas, A. Želvys, G. Niaura, V. Šablinskas, Discrimination between cancerous and normal bladder cancer tissues via SERS spectroscopy, *Pateiktas*.

Konferencijų darbai

1. M. Velička, M. Radžvilaitė, J. Čeponkus, V. Urbonienė, M. Pučetaitė, F. Jankevičius, G. Steiner, V. Šablinskas, Assignment of vibrational spectral bands of kidney tissue by means of low temperature SERS spectroscopy, *Proc. of SPIE*, 10068, 2017.

2. V. Šablinskas, M. Velička, M. Pučetaitė, V. Urbonienė, J. Čeponkus, R. Bandzevičiūtė, F. Jankevičius, T. Sakharova, O. Bibikova, G. Steiner, *In situ* detection of cancerous kidney tissue by means of fiber ATR-FTIR spectroscopy, *Proc. of SPIE*, 10497, 2018.

3. S. Adomavičiūtė, M. Velička, V. Šablinskas, Screening of usage of OTC drugs by means of SERS spectroscopy, *Proc. of SPIE*, 10894, 2019.

4. M. Velička, S. Adomavičiūtė, E. Zacharovas, V. Šablinskas, Application of label-free SERS and EC-SERS for detection of traces of drugs in biological fluids, *Proc. of SPIE*, 11257, 2020.

Publikacijų ne disertacijos tema sąrašas

1. M. Pučetaitė, M. Velička, J. Pilipavičius, A. Beganskienė, J. Čeponkus, V. Šablinskas, Uric acid detection by means of SERS spectroscopy on dried Ag colloidal drops, *Journal of Raman Spectroscopy*, 2016, **47**, 681.

2. J. Pilipavičius, R. Kaleinikaitė, M. Pučetaitė, M. Velička, A. Kareiva, A. Beganskienė, Controllable formation of high-density SERS-active silver nanoprisms layers on hybrid silica-APTES coatings, *Applied Surface Science*, 2016, **377**, 134.

3. E. Gaubas, T. Čeponis, L. Deveikis, D. Meškauskaitė, S. Miasojedovas, J. Mickevičius, J. Pavlov, K. Pūkas, J. Vaitkus, M. Velička, M. Zajac, R. Kucharski, Study of neutron irradiated structures of ammonothermal GaN, *Journal of Physics D: Applied Physics*, 2017, **50**, 1.

4. E. Gaubas, T. Čeponis, J. Mickevičius, J. Pavlov, V. Rumbauskas, M. Velička, E. Simoen, M. Zhao, Pulsed photo-ionization spectroscopy in carbon doped MOCVD GaN epi-layers on Si, *Semiconductor Science and Technology*, 2018, **33**, 1.

5. M. Valldeperas, M. Talaikis, S. K. Dhayal, M. Velička, J. Barauskas, G. Niaura, T. Nylander, Encapsulation of aspartic protease in nonlamellar lipid liquid crystalline phases, *Biophysical Journal*, 2019, **117**, 829.

6. V. Šablinskas, R. Bandzevičiūtė, M. Velička, J. Čeponkus, V. Urbonienė, F. Jankevičius, A. Laurinavičius, D. Dasevičius, G. Steiner, Fiber attenuated total reflection infrared spectroscopy of kidney tissue during live surgery, *Journal of Biophotonics*, 2020, **13**, 1.
7. S. Adomavičiūtė, M. Velička, V. Šablinskas, Fiber based SERS studies of cancerous tissues: toward clinical trials, *Proc. of SPIE* 11257, 2020.
8. R. Bandzevičiūtė, J. Čeponkus, M. Velička, V. Urbonienė, F. Jankevičius, A. Želvys, G. Steiner, V. Šablinskas, Fiber based infrared spectroscopy of cancer tissues, *Journal of Molecular Structure*, 2020, **1220**, 1.
9. Š. Svirskas, S. Balčiūnas, M. Šimėnas, G. Usevičius, M. Kinka, M. Velička, D. Kubicki, M. E. Castillo, A. Karabanov, V. V. Shvartsman, M. de Rosário Soares, V. Šablinskas, A. N. Salak, D. C. Lupascu, J. Banys, Phase transitions, screening and dielectric response of CsPbBr₃, *Journal of Materials Chemistry A* 2020, **8**, 14015.

Pranešimai konferencijose

1. M. Velička, J. Čeponkus, V. Šablinskas, Low Temperature Vibrational spectroscopy of cancerous biological tissue, Chemistry and Physics at Low Temperatures, Biaricas, Prancūzija, 2016.
2. J. Pilipavičius, R. Kaleinikaitė, M. Pučetaitė, M. Velička, A. Kareiva, A. Beganskienė, Study of silver nanoprisms assembly on hybrid silica-APTES coatings prepared via sol-gel process, Hint Workshop: Nanostructured materials: Protective and Functional coatings, surface treatment, bioceramics, biocomposites and membranes, Vilnius, Lietuva, 2016.
3. V. Urbonienė, M. Velička, J. Čeponkus, M. Pučetaitė, F. Jankevičius, V. Šablinskas, G. Steiner, Intra-operative on-line discrimination of kidney cancer from normal tissue by IR ATR spectroscopy of extracellular fluid, SPIE Photonics West, San Franciskas, JAV, 2016.
4. M. Velička, V. Urbonienė, F. Jankevičius, V. Šablinskas, Inkstų vėžio diagnostika paviršiaus sutiprintos Ramano sklaidos spektriniu metodu, Jaunųjų mokslininkų konferencija, Vilnius, Lietuva, 2017.
5. M. Velička, M. Radžvilaitė, J. Čeponkus, V. Urbonienė, M. Pučetaitė, F. Jankevičius, G. Steiner, V. Šablinskas, Assignment of vibrational spectral bands of kidney tissue by means of low temperature SERS spectroscopy, SPIE Photonics West, San Franciskas, JAV, 2017.
6. M. Radžvilaitė, M. Velička, V. Šablinskas, Low temperature study of extracellular fluid of kidney tissue by means of surface-enhanced Raman scattering spectroscopy, Open Readings, Vilnius, Lietuva, 2017.

7. M. Velička, M. Pučetaitė, J. Čeponkus, V. Urbonienė, F. Jankevičius, V. Šablinskas, Towards the detection of cancerous kidney tissue areas using surface enhanced Raman scattering spectroscopy, International conference on enhanced spectroscopies, Miunchenas, Vokietija, 2017.
8. M. Velička, M. Pučetaitė, J. Čeponkus, S. Adomavičiūtė, V. Urbonienė, F. Jankevičius, V. Šablinskas, Vėžinių inksto sričių nustatymas paviršiaus sustiprintos Ramano sklaidos metodu, Lietuvos nacionalinė fizikos konferencija, Vilnius, Lietuva, 2017.
9. M. Velička, S. Adomavičiūtė, V. Šablinskas, Formation of metal nanoparticle films for trace analysis of OTC drugs in biological fluids by means of SERS spectroscopy, European congress on molecular spectroscopy, Koimbra, Portugalija, 2018.
10. M. Velička, M. Pučetaitė, V. Urbonienė, R. Bandzevičiūtė, J. Čeponkus, F. Jankevičius, V. Šablinskas, G. Steiner, ATR-FTIR spectroscopy: towards *in vivo* detection of cancerous tissue areas, European congress on molecular spectroscopy, Koimbra, Portugalija, 2018.
11. S. Adomavičiūtė, M. Velička, V. Šablinskas, Detection of aspirin traces in blood by surface enhanced Raman scattering, Open Readings, Vilnius, Lietuva, 2018.
12. V. Šablinskas, M. Velička, M. Pučetaitė, V. Urbonienė, J. Čeponkus, R. Bandzevičiūtė, F. Jankevičius, T. Sakharova, O. Bibikova, G. Steiner, *In situ* detection of cancerous kidney tissue by means of fiber ATR-FTIR spectroscopy, SPIE Photonics West, San Franciskas, JAV, 2018.
13. R. Bandzevičiūtė, M. Velička, J. Čeponkus, V. Urbonienė, F. Jankevičius, V. Šablinskas, G. Steiner, Fiber based infrared spectroscopy of various cancer tissues, International conference on molecular spectroscopy, Vroclavas, Lenkija, 2019.
14. E. Zacharovas, M. Velička, Elektrocheminio SERS metodo taikymas kofeino pėdaskų seilėse nustatymui, Lietuvos nacionalinė fizikos konferencija, Kaunas, Lietuva, 2019.
15. S. Adomavičiūtė, M. Velička, V. Šablinskas, Nereceptinių vaistų likučių kraujyje diagnostiniai tyrimai SERS spektriniu metodu, Lietuvos nacionalinė fizikos konferencija, Kaunas, Lietuva, 2019.
16. R. Bandzevičiūtė, J. Čeponkus, M. Velička, V. Urbonienė, G. Mickūnaitė, F. Jankevičius, V. Šablinskas, G. Steiner, Šviesolaidinė ATR infraraudonoji spektroskopija vėžinių audinių diagnostikai, Lietuvos nacionalinė fizikos konferencija, Kaunas, Lietuva, 2019.

17. E. Zacharovas, M. Velička, V. Šablinskas, Detection of caffeine traces in saliva using electrochemical SERS method, Open Readings, Vilnius, Lietuva, 2019.
18. S. Adomavičiūtė, M. Velička, V. Šablinskas, Traces of paracetamol in blood as studied by means of colloidal SERS, Open Readings, Vilnius, Lietuva, 2019.
19. B. Žudytė, M. Velička, Ž. Lukšienė, V. Šablinskas, Understanding *E. coli* damage after chlorophyllin-based photosensitization using SERS, Open Readings, Vilnius, Lietuva, 2019.
20. S. Adomavičiūtė, M. Velička, V. Šablinskas, Screening of usage of OTC drugs by means of SERS spectroscopy, SPIE Photonics West, San Franciskas, JAV, 2019.
21. M. Velička, S. Adomavičiūtė, E. Zacharovas, V. Šablinskas, Label-free SERS and EC-SERS spectroscopies for detection of medicine traces in biological fluids, Summer School Spectroelectrochemistry, Drezdenas, Vokietija, 2019.
22. M. Velička, S. Adomavičiūtė, E. Zacharovas, V. Šablinskas, Application of label-free SERS and EC-SERS for detection of traces of drugs in biological fluids, SPIE Photonics West, San Franciskas, JAV, 2020.
23. S. Adomavičiūtė, M. Velička, V. Šablinskas, Fiber based SERS studies of cancerous tissues: toward clinical trials, SPIE Photonics West, San Franciskas, JAV, 2020.
24. E. Zacharovas, M. Velička, G. Platkevičius, A. Želvys, V. Šablinskas, Study of urinary bladder cancer by means of surface enhanced Raman scattering spectroscopy, Open Readings, Vilnius, Lietuva, 2020.

Darbo naujumas ir aktualumas

- SERS spektroskopija pirmą kartą pritaikyta inkstų ir pūslės audinių tarpląstelinio skysčio tyrimams. Nustatyti spektriniai žymenys, susiję su pakitusiu vėžinių ląstelių metabolizmu, leidžiantys klinikinių metodų reikalavimus atitinkančiu jautrumu ir specifiskumu (93%) identifikuoti šių audinių vėžį.
- Pritaikius žemos temperatūros SERS spektroskopiją ir teorinius *ab initio* skaičiavimus buvo patikslintas iki šiol naudotas preliminarus spektruose stebimų juostų priskyrimas normaliesiems molekulių virpesiams.
- SERS spektroskopija pritaikyta patogeninių bakterijų (*E. coli*) pažaidų po fotosensibilizavimo chlorofilinu identifikavimui. Nustatyta, kad pažaidos mechanizmas – bakterijų ląstelių išorinės membranos suardymas.

- SERS spektroskopija pritaikyta klinikinio tipo žmogaus kraujo bandinių tyrimuose. Nustatyta, kad SERS spektriniu metodu žmogaus kraujo serume galima aptikti klinikinio požiūriu reikšmingą (atitinkančią lengvą toksiškumą) aspirino koncentraciją (3 milimoliai litre). Paracetamolio aptikimas kraujo plazmoje nėra tikslus dėl kito plazmos komponento – šlapimo rūgšties įtakos.
- EC-SERS spektroskopija pritaikyta žmogaus seilių bandinių klinikinio tipo tyrimuose. Nustatyta, kad EC-SERS metodu analizuojant žmogaus seiles galima identifikuoti kofeino vartojimą. Aptikimo riba siekia 15 mikromolių litre.

DISERTACIJOS SANDARA

Disertaciją sudaro keturi skyriai, literatūros sąrašas ir du priedai. Įvade aptariama problematika, pristatoma disertacijos tematika ir aktualumas. Taip pat iškeliamas darbo tikslas ir suformuluojami pagrindiniai uždaviniai. Pateikiami ginamieji teiginiai, publikacijų ir pranešimų konferencijose sąrašas.

Pirmajame skyriuje glaustai aprašomi pagrindiniai paviršiaus sustiprintos Ramano sklaidos (angl. *surface enhanced Raman scattering* – SERS), elektrocheminio paviršiaus sustiprintos Ramano sklaidos (angl. *electrochemical surface enhanced Raman scattering* – EC-SERS) bei visiško vidaus atspindžio infraraudonosios sugerties (angl. *attenuated total internal reflection infrared absorption* – ATR-FTIR) metodai. Taip pat apžvelgiamas spektrinių duomenų apdorojimas ir dažniausiai naudojami daugialypiai chemometrinės analizės metodai.

Antrajame skyriuje aprašomas SERS spektroskopijos taikymas vėžinių audinių indentifikavimui. Glaustai aprašomi pagrindiniai vėžio, kaip ligos, principai, vėžinių susirgimų vystymasis ir pagrindinės savybės. Taip pat aprašoma klinikinė vėžinių darinių klasifikacija ir gradavimas. Specifiškai apibūdinami inkstų ir šlapimo pūslės vėžiniai susirgimai ir aptariamas pirmame skyriuje pristatytų metodikų taikymas šiuose moksliniuose vėžinių susirgimų tyrimuose. Skyriuje aprašomi eksperimentiniai spektrinės inkstų ir pūslės vėžio audinių tarpląstelinio skysčio analizės rezultatai, pateikiama statistinė užregistruotų spektrų analizė. Skyriuje pateikiami rezultatai yra paskelbti keturiose disertanto ir bendraautorių publikacijose.

Trečiajame skyriuje pristatomas SERS spektroskopijos taikymas ląstelių pažaidos analizei. Skyriuje nagrinėjama patogeninių bakterijų ir jų keliamos žalos problematika. Aprašoma dažniausiai žalą kelianti patogeninė bakterija – *Esherichia coli*, bei pristatoma chlorofilinu paremta

fotosensitizavimo procedūra ir jos principai. Šiame skyriuje aprašomi pagrindiniai minėtų patogeninių bakterijų ląstelių pažaidos analizės SERS spektroskopijos metodu rezultatai. Skyriuje pateikiami rezultatai yra paskelbti vienoje disertanto ir bendraautorių publikacijoje.

Ketvirtajame skyriuje aprašomas SERS ir EC-SERS spektroskopijos metodų taikymas vaistų ir psichoaktyvių preparatų aptikimui biologiniuose skysčiuose. Glaustai aprašomi dažniausiai taikomi analizės metodai, jų trūkumai. Skyriuje aprašomi tyrimo metu nagrinėti vaistiniai (acetilsalicilo rūgštis, paracetamolis) bei psichoaktyvūs (kofeinas) preparatai, jų metabolitai. Aptiriamos pagrindinės šių cheminių junginių savybės, poveikis žmogaus organizmui, metabolizmas ir farmakokinetika. Skyriuje aprašomi paminėtų vaistinių preparatų aptikimo žmogaus kraujyje SERS spektroskopijos metodu ir kofeino aptikimo žmogaus seilėse EC-SERS metodu tyrimo rezultatai. Skyriuje pateikiami rezultatai paskelbti keturiose autoriaus ir bendraautorių publikacijose.

TYRIMŲ METODIKA

Tyrimo objektai

Disertacijoje aprašomuose tyrimuose buvo tiriami trijų kategorijų objektai: audiniai ir jų tarpląstelinis skystis, bakterijų ląstelės, biologiniai skysčiai (žmogaus kraujas ir seilės).

Inkštų ir pūslės sveikų ir vėžinių audinių bandiniai buvo gauti iš Vilniaus universiteto ligoninės Santaros klinikų urologijos centro. Spektriniai inkštų audinių tyrimai yra patvirtinti Vilniaus regiono bioetikos komiteto (dokumento. Nr. 158200-15-803-312). Šlapimo pūslės audinių spektriniai tyrimai taip pat patvirtinti Vilniaus regiono bioetikos komiteto (dokumento. Nr. 2019/12-1178-665).

Escherichia coli bakterijų bandiniai prieš ir po fotosensitizacijos chlorofilinu procedūros buvo gauti iš Vilniaus universiteto, Fotonikos ir nanotechnologijų instituto, Antibakterinių fototechnologijų grupės.

Žmogaus kraujo ir seilių bandiniai buvo surinkti iš savanorių. Kraujo mėginiai buvo imami naudojant standartinę kraujo paėmimo iš piršto procedūrą.

SERS spektroskopija

Tiriamų bandinių SERS spektrai buvo registruojami sklaidos signalų stiprinimui naudojant sidabro ir aukso koloidinius tirpalus. Tirpalai buvo ruošiami pritaikius literatūroje aprašytas metodikas [114, 115, 250-252].

Koloidiniai nanodalelių tirpalai buvo koncentruojami juos centrifuguojant Heraus Megafuge 16 (*Thermo Fisher*, Lietuva) centrifuga.

Paviršiaus sustiprintos Ramano sklaidos spektrai buvo registruojami Furje transformaciją atliekančiu Ramano sklaidos spektrometru „MultiRAM“ (*Bruker*, Vokietija) su skystu azotu šaldomu puslaidininkiniu germanio detektoriumi. Žadinimui naudotas 1064 nm bangos ilgio lazeris (*Cobolt*, Švedija). Lazerio galia buvo parenkama pagal bandinio tipą, kad būtų gaunamas kuo intensyvesnis sklaidos signalas bei išvengiamas terminis bandinio pažeidimas. Bandinių žadinimui ir išsklaidytos spinduliuotės surinkimui buvo naudojamas 90 laipsnių kampo objektyvas su auksu dengtu hiperboliniu veidrodžiu. Objektyvo židinio nuotolis 33 cm, o jo sufokusuoto lazerio spinduliuotės diametras – 100 μm. Spektrai buvo registruojami taikant atgalinio sklaidymo geometriją. Spektrai registruoti 150-4000 cm⁻¹ spektrinėje srityje su 4 cm⁻¹ spektrine skyra.

Žemos temperatūros SERS tyrimams buvo naudojama šaldymo sistema Linkam LNP95 bei bandinio temperatūros valdymui pritaikytas bandinio laikiklis FTIR600 (Linkam Scientific, Jungtinė Karalystė). Temperatūriniai matavimai buvo atliekami temperatūrų srityje nuo 300 K iki 100 K keičiant temperatūrą kas 20 laipsnių.

EC-SERS spektroskopija

Registruojant tiriamų bandinių EC-SERS spektrus buvo naudojama trijų elektrodų sistema. Sidabro elektrodas, kurio skersmuo 5 mm, platinos elektrodas ir sidabro-sidabro chlorido (Ag/AgCl 3 M KCl) elektrodai buvo atitinkamai naudojami kaip darbinis, atraminis ir palyginamasis elektrodai. Tyrimų metu potenciostatu-galvanostatu PGSTAT302N (*Metrohm Autolab*, Olandija) buvo valdomas elektrodų potencialas. Paviršiaus sustiprintos Ramano sklaidos spektrai buvo registruojami keičiant darbinio elektrodo potencialą nuo atviros grandinės potencialo iki -1,0 V kas -0,1 V žingsnį. Prieš kiekvieno bandinio tyrimą darbinio elektrodo paviršius buvo nuvalomas mechaniškai ir elektrochemiškai bei nupoliruojamas naudojant aliuminio oksido pudrą ir poliravimo servetėlę. Elektrodo paviršius matavimams buvo ruošiamas ant jo užlašinant ir išdžiovinant koloidinio sidabro nanodalelių tirpalo lašą. Spektrai registruoti ta pačia įranga bei naudojant tuos pačius parametrus kaip ir registruojant SERS spektrus.

UV-Vis spektroskopija

Tyrimų metu paruošti koloidinių nanodalelių tirpalai buvo charakterizuojami registruojant jų sugerties spektrus. Spektrai buvo

registruojami spektrofotometru „Lambda 1050“ (Perkin Elmer, USA), turinčiu du spinduliuotės šaltinius (deuterio ir halogeninę lempas) bei trijų detektorių sistemą. Tirpalų sugertis registruota 1000-250 nm bangos ilgių srityje su 5 nm spektrine skyra.

ATR-FTIR spektroskopija

Siekiant patvirtinti SERS tyrimuose gautų rezultatų patikimumą, jie buvo palyginti su inkstų audinių tarpląstelinio skysčio tyrimų ATR-FTIR spektroskopijos metodu rezultatais. ATR-FTIR spektrai buvo registruojami „Alpha“ spektrometru (Bruker, Vokietija), turinčiu vieno atspindžio deimantinę prizmę, globalo šaltinį ir deuteruoto trigilicino sulfato (DTGS) detektorių. Spektrai registruoti 800-4000 cm^{-1} spektriniame diapazone su 4 cm^{-1} spektrine skyra.

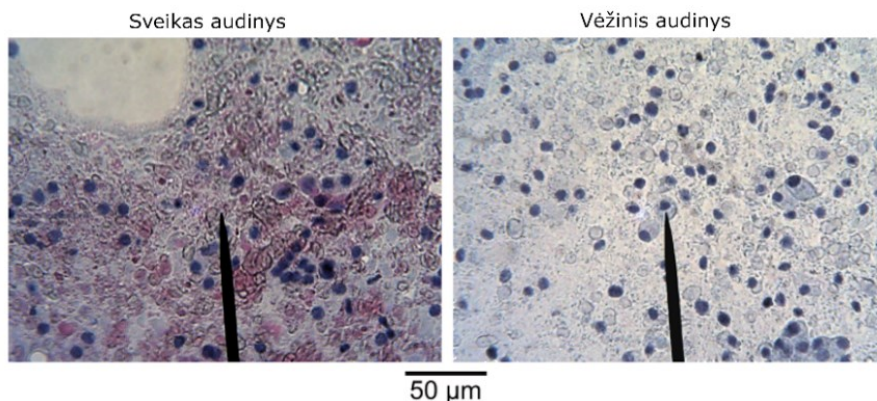
Teoriniai skaičiavimai

Siekiant patikslinti užregistruotų spektrų interpretaciją, stebimų virpesinių juostų priskyrimui normaliesiems molekulių virpesiams buvo atliekami teoriniai molekulių, adsorbuotų ant sidabro nanodalelės paviršiaus, skaičiavimai. Sidabro nanodalelės paviršius buvo simuliuojamas 15 sidabro atomų struktūra. Skaičiavimai atlikti Gaussian 09 [118] programiniu paketu. Molekulių, adsorbuotų ant sidabro nanodalelės sistemos, buvo skaičiuojamos B3LYP/6-311G*, o sidabro atomų struktūra B3LYP/LANL2DZ artiniais.

PAGRINDINIAI REZULTATAI

Inkstų ir šlapimo pūslės vėžio SERS tyrimai

Šiame poskyryje aprašomi inkstų ir šlapimo pūslės audinių tarpląstelinio skysčio SERS tyrimai, atlikti naudojant sidabro nanodalelių koloidinį tirpalą. Tarpląstelinio skysčio bandiniai buvo suformuojami braukiant tiriamu audiniu per kalcio fluorido ar aliuminio substrato pagrindą. Tokiu būdu suformuojamas tarpląstelinio skysčio sluoksnis, kuriame yra ir pavienių audinio ląstelių. Audinio ląstelės buvo aptiktos paruoštą bandinį nudažius standartiniu *Papanicolaou's* (PAP) ląstelių dažymo metodu ir bandinį stebint mikroskopu. Vėžinio ir sveiko inkstų audinių tarpląstelinio skysčio bandinių nuotraukos, stebint šiuos bandinius mikroskopu, yra pateiktos 1 pav. Registruojant šių bandinių SERS spektrus pirmiausia ant tarpląstelinio skysčio sluoksnių buvo užlašinamas paruoštas koloidinis tirpalas ir jis išdžiovinamas.

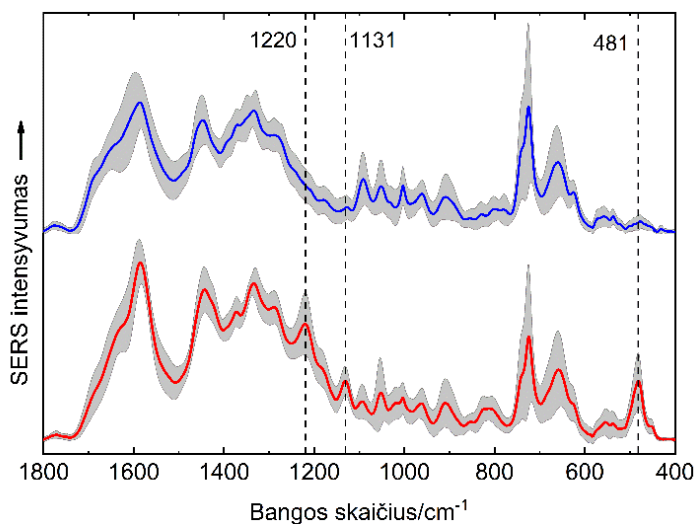


1 pav. Tarpląstelinio skysčio su pavienėmis ląstelėmis vaizdas, stebimas optiniu mikroskopu.

Tyrimo metu buvo įsitikinta, kad spektriniai audinių tyrimai nesuteikia detalios informacijos, leidžiančios identifikuoti vėžinius audinius, kadangi cheminiai, o kartu ir spektriniai skirtumai tarp sveikų ir vėžinių audinių yra nedideli. Registruojant audinių spektrus šie skirtumai yra užgožiami spektrinės informacijos, kuri yra būdinga abiem audinio tipams. Registruojant tarpląstelinį skystį yra išvengiama šios problemos.

Iš viso tyrimo metu buvo užregistruoti 85 pacientų vėžinių ir sveikų inkstų audinių tarpląstelinio skysčio SERS spektrai. Šių spektrų vidurkiai yra pavaizduoti 2 pav. Prieš skaičiuojant spektrų vidurkį visiems spektrams buvo

atlikta bazinės linijos korekcija bei pritaikytas vektorinis normalizavimas. Pilkos sritys pateiktuose spektruose vaizduoja standartinį virpesinių juostų intensyvumo nuokrypį. Aiškumo dėlei spektrai buvo paslinkti y-ašies atžvilgiu.

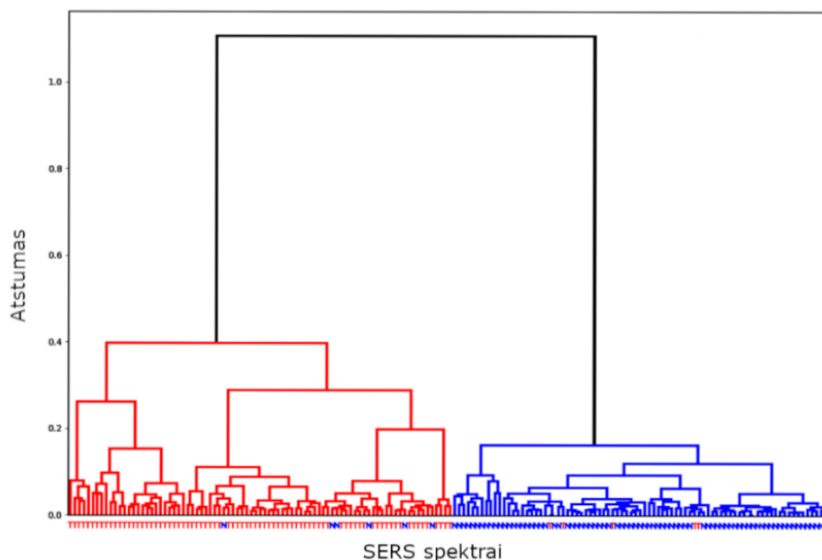


2 pav. Vėžinių ir sveikų inkstų audinių tarpląstelinio skysčio SERS spektrų vidurkiai.

Atlikus lyginamąją spektrų, pateiktų 2 pav., analizę buvo identifikuotos trys spektrinės juostos, kurios potencialiai gali būti laikomos spektriniais vėžinių audinių žymenimis. Šių juostų padėtys (1220 cm^{-1} , 1131 cm^{-1} , 481 cm^{-1}) spektruose pažymėtos punktyrinėmis linijomis. Siekiant nustatyti spektruose stebimų virpesinių juostų prigimtį, buvo atliekami papildomi eksperimentiniai tyrimai bei teoriniai molekulių, adsorbuotų ant sidabro nanodalelės paviršiaus, skaičiavimai. Užregistravus įvairių bandinio sudėtyje galimai esančių molekulių SERS spektrus, atlikus žemos temperatūros SERS tyrimus ir atlikus teorinius spektrų skaičiavimus, buvo sudaryta stebimų virpesinių juostų priskyrimo normaliesiems molekulių virpesiams lentelė. Nustatyta, kad spektrinės juostos, įvardintos kaip vėžio žymenys, yra susijusios su baltymų (amidais III virpesys ties 1220 cm^{-1}), baltymų ar lipidų ($\nu(\text{C-C})$, $\nu(\text{C-N})$ virpesys ties 1131 cm^{-1}) bei glikogeno (deformacinis virpesys ties 481 cm^{-1}) virpesiais. SERS tyrimų rezultatų patikimumui įvertinti inkstų audinių tarpląstelinio skysčio analizė buvo atlikta ir ATR-FTIR metodu. Nustatyta, kad identifikuoti spektriniai vėžinių audinių požymiai yra stebimi ir infraraudonosios sugerties spektruose, o tai patvirtina rezultatų, gautų taikant SERS metodą, patikimumą.

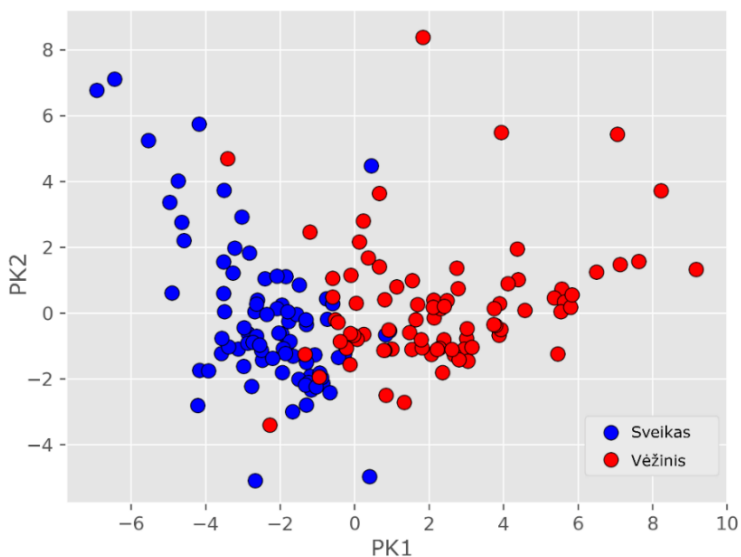
Stebimas didesnis spektrinių juostų, laikomų spektriniais vėžio žymenimis, intensyvumas vėžinių audinių tarpląstelinio skysčio SERS spektruose yra siejamas su pakitusiu vėžinių ląstelių metabolizmu. Vėžinėms ląstelėms yra būdinga pagreitėjusi proliferacija (augimas ir dauginimasis), taip pat naujų baltymų sintezė ir dar daugiau pakitimų [82, 86, 132-134]. Glikogeno kaupimas yra dar vienas pakitusio vėžinių ląstelių metabolizmo požymis. Sparčiai dalijantis vėžinėms ląstelėms pradeda trūkti deguonies – kraujotakos sistema nespėja vystyti aplink vėžinį audinį ir tiekti deguonies bei kitų maistinių medžiagų. Dėl šios priežasties hipoksinėje (deguonies stokojančioje) aplinkoje vėžinės ląstelės pradeda gaminti energiją ne įprastomis gliukozės oksidacijos reakcijoms, o anaerobine gliukozės fermentacija. Pastarosios reakcijos išeiga yra 18 kartų mažesnė, todėl vėžinių ląstelių aplinkoje, siekiant joms užsitikrinti pakankamą kiekį energijos, yra stebima padidėjusi gliukozės absorbcija ir jos kaupimas glikogeno pavidalu. Šis vėžinėms ląstelėms būdingas pakitimas dar yra vadinamas *Warburg* efektu [137].

Siekiant nustatyti ar SERS metodas yra tinkamas identifikuoti vėžinius inkstų audinius, buvo atlikta statistinė spektrų analizė. Spektrai buvo analizuoti dviem dažniausiai naudojamais statistinės analizės metodais - hierarchinės klasterinės analizės (HCA) ir principinių komponentų analizės (PCA) metodais. Analizė buvo atlikta naudojant „Python 3.7“ programavimo paketą. Taikant statistinės analizės metodus buvo nustatyta, kad tiksliausias vėžinių ir sveikų inkstų audinių SERS spektrų atskyrimas pasiekiamas tuomet, kai jie yra analizuojami spektrinės juostos, susijusios su glikogeno virpesiais, srityje. Hierarchinės klasterinės analizės rezultatai, gauti nagrinėjant spektrus spektrinės juostos, esančios ties 481 cm^{-1} , srityje, yra pateikti 3 pav. Statistinės analizės rezultatai parodė, kad inkstų audinių tarpląstelinio skysčio su pavienėmis audinio ląstelėmis tyrimas SERS metodu gali būti taikomas inkstų audinio vėžio identifikavimui dideliu tikslumu. Apskaičiuota, kad net ir su sąlyginai nedidele bandinių imtimi 93,5% spektrų buvo priskirti teisingoms kategorijoms.



3 pav. Dendrograma, sudaryta atlikus inkstų audinių tarpląstelinio skysčio SERS spektrų hierarchinę klasterinę analizę.

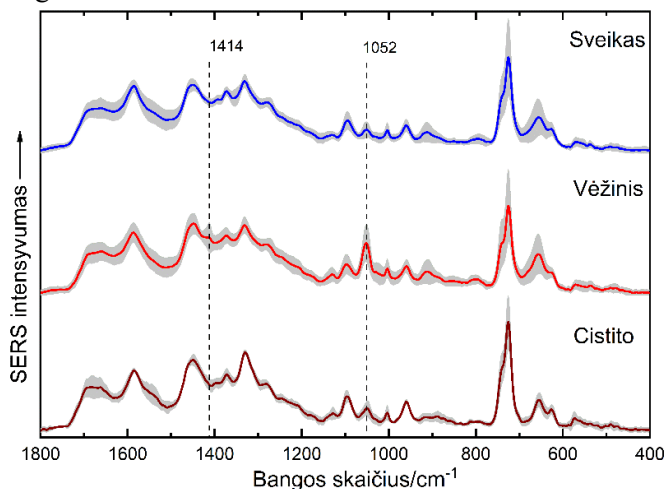
Panašūs rezultatai, siekiant atskirti vėžinių ir sveikų audinių tarpląstelinio skysčio SERS spektrus vienus nuo kitų, buvo gauti ir atlikus principinių komponentų analizę. Pirmųjų dviejų principinių komponentų projekcijų grafikas pateiktas 4 pav.



4 pav. Pirmųjų dviejų pagrindinių komponentų projekcijų grafikas, sudarytas atlikus inkstų audinių tarpląstelinio skysčio SERS spektrų PCA analizę.

Galima pastebėti, kad pagal PCA analizės rezultatus sudarytame projekcijų grafike galima atskirti vėžinių ir sveikų inkstų audinių tarpląstelinio skysčio SERS spektrų grupes. Tai patvirtina, kad taikant SERS metodą galima identifikuoti vėžinius inkstų audinius. Netikslumai gauti statistinės analizės metu gali būti siejami su neidealia bandinių paėmimo procedūra. Sveikų inkstų audinių mėginiai buvo imami iš artimos vėžiniams audiniams srities. Todėl tikėtina, kad kai kurie sveiko audinio bandiniai galėjo turėti ir nedidelį kiekį vėžinio audinio ar į sveiką audinį įsiskverbusių vėžinių ląstelių. Vėžinio audinio tarpląstelinio skysčio SERS spektrų priskyrimą sveikų audinių grupei galėjo lemti vėžinio audinio savybės, kurios skiriasi skirtingą stadiją ar piktybiškumo laipsnį turinčiuose vėžiniuose audiniuose. Vis dėlto, buvo įvertinta, kad SERS metodo specifiskumas ir jautrumas identifikuoti vėžinius audinius siekia 93% ir yra palyginami su klinikiniais tyrimu jautrumu ir patikimumu.

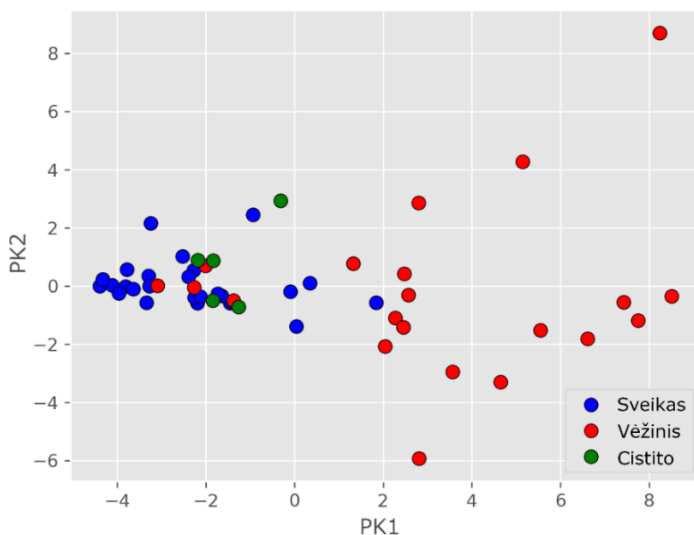
Šlapimo pūslės audinių tyrimo SERS metodu procedūra panaši į metodiką, taikytą tiriant inkstų audinius. Buvo suformuojamas audinio tarpląstelinio skysčio sluoksnis, ant jo užlašinamas ir išdžiovinamas koloidinis tirpalas ir registruojamas SERS spektras. Iš viso tyrimo metu buvo užregistruota 30 pacientų vėžinių, sveikų ir cistito (inkstų uždegimo) paveiktų audinių tarpląstelinio skysčio SERS spektrai. Šių spektrų vidurkiai pateikti 5 pav. Skaičiuojant spektrų vidurkius visiems spektrams buvo pritaikyta bazinės linijos korekcija ir vektorinis normalizavimas. Pilkos sritys atitinka spektrinių juostų intensyvumo standartinį nuokrypį. Pateikti spektrai buvo pastumti y-ašies atžvilgiu.



5 pav. Sveiko, vėžinio ir cistito paveiktų šlapimo pūslės audinių tarpląstelinio skysčio SERS spektrų vidurkiai.

Atlikus spektrų, pateiktų 5 pav., lyginamąją analizę buvo identifikuotos spektrinės juostos (ties 1414 cm^{-1} ir 1052 cm^{-1}), kurias galima laikyti spektriniais šlapimo pūslės vėžio požymiais. Spektrinės juostos, stebimos pūslės audinio tarpląstelinio skysčio SERS spektruose yra siejamos su tomis pačiomis molekulėmis, kurios buvo tiriamos inkstų audinių tyrimuose. Todėl pagal spektrinių juostų priskyrimą, atliktą analizuojant inkstų audinių tarpląstelinio skysčio SERS spektrus, identifikuotas juostas galima priskirti $\delta(\text{CH}_3)$ deformaciniams virpesiams baltymuose ar amino rūgštyse (juosta ties 1414 cm^{-1}) ar cisteino/pieno rūgšties molekulių $\nu(\text{C}-\text{O})$ ir $\nu(\text{C}-\text{N})$ virpesiams (juosta ties 1052 cm^{-1}). Vėžinių audinių tarpląstelinio skysčio SERS spektruose yra stebimas ir kitų virpesinių juostų, susijusių su cisteino virpesiais intensyvumo padidėjimas. Tačiau jis nėra toks žymus, o tai parodo, kad identifikuoto spektrinio žymens intensyvumui turi įtakos dar kitos molekulės, pavyzdžiui baltymai. Didesnė baltymų, kurie stabdo apoptozę (užprogramuotą ląstelės mirtį), skatina angiogenezę (kraujotakos sistemos augimą), lipidų pernešimą, koncentracija yra stebima vėžiniuose šlapimo pūslės audiniuose. Taip pat ši juosta gali būti priskirta ir pieno rūgšties virpesiams. Šios molekulės koncentracija vėžiniuose audiniuose padidėja dėl pakitusio gliukozės metabolizmo. Virpesinių juostų, priskiriamų cisteino virpesiams, intensyvumo padidėjimas gali būti siejamas su pakitusiu vėžinių ląstelių metabolizmu. Yra nustatyta, kad cisteino molekulės yra svarbios vėžio vystymuisi. Būtent tiriant šlapimo pūslės vėžį ir buvo aptikta vėžinių ląstelių priklausomybė nuo cisteino molekulių, kurios naudojamos kaip maistinės bei statybinės medžiagos. Kitų spektrinių požymių dėl mažos bandinių imties nebuvo galima identifikuoti. Todėl požymio, kuriuo galima būtų atpažinti cistito paveiktus audinius, nebuvo aptikta.

SERS metodo tinkamumas identifikuoti šlapimo pūslės vėžį taip pat buvo tikrinamas atliekant statistinę užregistruotų spektrų analizę. Kadangi tyrimo metu surinktas šlapimo pūslės bandinių kiekis nebuvo didelis, buvo atliekama tik principinių komponentų analizė. Analizė buvo atliekama keičiant spektrinės srities plotį bei sritį ir analizuojant gautus rezultatus. Nustatyta, kad geriausias vėžinių audinių tarpląstelinio skysčio SERS spektrų atskyrimas pasiekiamas užregistruotus SERS spektrus analizuojant su cisteino/pieno rūgšties molekulių virpesiais susijusios spektrinės juostos, esančios ties 1052 cm^{-1} , srityje. Spektrinės juostos, esančios ties 1414 cm^{-1} , intensyvumas yra pernelyg mažas, todėl statistinės analizės rezultatai nebuvo tenkinantys. Pagal šlapimo pūslės tarpląstelinio skysčio SERS spektrų statistinės analizės rezultatus sudarytas pirmųjų dviejų pagrindinių komponentų projekcijų grafikas yra pateiktas 6 pav.



6 pav. Pirmųjų dviejų pagrindinių komponentų projekcijų grafikas, sudarytas atlikus šlapimo pūslės audinių tarpląstelinio skysčio SERS spektrų PCA analizę.

Statistinės analizės rezultatai patvirtina, kad SERS metodas gali būti potencialiai pritaikytas ir šlapimo pūslės vėžio identifikavimui.

Inkstų ir šlapimo pūslės audinių SERS tyrimo rezultatai parodė, kad skirtingų audinių vėžio identifikavimui reikia rasti ir naudoti skirtingus spektrinius žymenis. Spektriniai žymenys, kaip ir tikėtasi, gali būti susieti su pakitusiu vėžinių ląstelių metabolizmu. Inkstu vėžio atveju patikimiausias žymuo yra su glikogeno virpesiais susijusi spektrinė juosta ties 481 cm^{-1} , o šlapimo pūslės atveju – su cisteino/pieno rūgšties virpesiais susijusi spektrinė juosta ties 1052 cm^{-1} . Statistinės užregistruotų SERS spektrų analizės rezultatai patvirtina, kad SERS metodas gali būti efektyviai pritaikytas audinių vėžio identifikavimui, o metodo patikimumas ir jautrumas siekia daugiau nei 93%, o tai tenkina klinikiniams tyrimams naudojamų metodų reikalavimus.

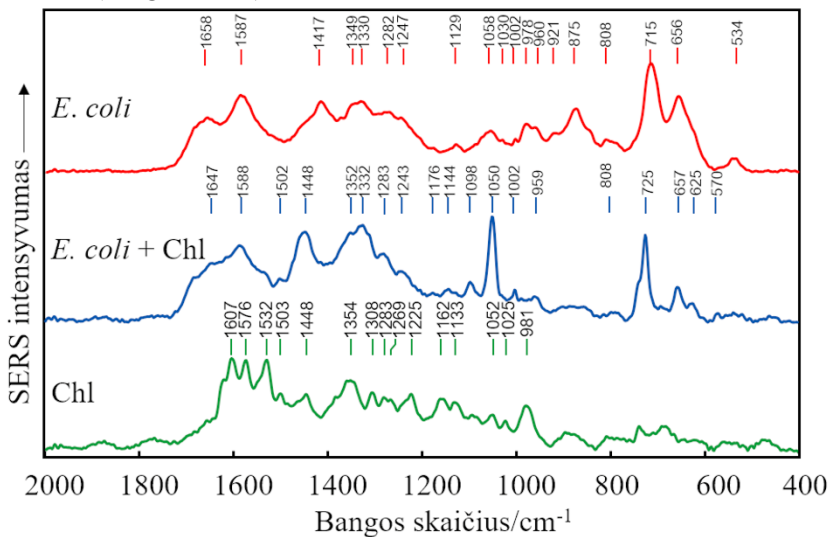
Patogeninių bakterijų pažaidos SERS tyrimas

Šiame poskyryje aprašomi patogeninių bakterijų pažaidos po fotosensibilizavimo chlorofilinu procedūros. Patogeninių bakterijų deaktyvavimas yra svarbus, kadangi maisto produktų užteršimas bakterijomis, kaip *Eschericia coli* (*E. coli*), kasmet lemia didelius ekonominius nuostolius, bei sukelia sunkias ligas, kurios gali baigtis mirtimi. Todėl šiam tyrimui ir

buvo pasirinktos *E. coli* bakterijos. Bakterijų deaktyvavimo fotosensibilizuojant chlorofilinu procedūra yra pranašesnė už standartinę procedūrą, kadangi chlorofilinas yra maisto papildas, nekenksmingas žmogaus organizmui ir jo panaudojimas nepakeičia maistinės produkto vertės [157, 161]. Jau yra žinoma, kad fotosensibilizavimo chlorofilinu metodas yra efektyvus [159, 160], tačiau norint sėkmingai pritaikyti jį praktikoje reikia gerai iširti šios procedūros mechanizmą, kad būtų galima jį patobulinti ir optimizuoti.

Bakterijų bandiniai buvo tiriami naudojant koloidinį sidabro nanodalelių tirpalą santykiu 1:1 jį sumaišius su paruošta bakterijų suspensija. Bakterijų suspensijos koncentracija – apie 10^7 CFU/ml (kolonijas formuojančių vienetų viename mililitre). Taip paruoštų bandinių spektrai buvo registruojami neišdžiūvę bei pakartotinai iškart jiems išdžiūvus.

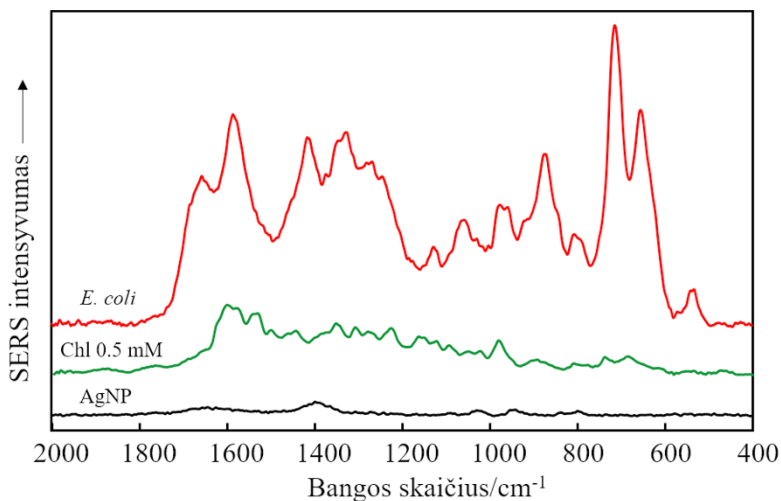
Užregistruoti kontrolinio (nepaveiktų) *E. coli* bakterijų, *E. coli* bakterijų po chlorofilinu paremtos fotosensibilizavimo procedūros ir vandeninio chlorofilino tirpalo SERS spektrai yra pateikti 7 pav. Aiškumo dėlei spektrai buvo paslinkti y-ašies atžvilgiu, o bendras chlorofilino spektro intensyvumas padidintas (daugiklis – 3).



7 pav. *E. coli* bakterijų prieš ir po chlorofilinu paremtos fotosensibilizacijos bei vandeninio chlorofilino tirpalo (0,5 mM) SERS spektrai.

SERS spektruose, pateiktuose 7 pav., galima pastebėti, kad bakterijų SERS spektrai, užregistruoti prieš fotosensibilizavimą ir po šios procedūros, turi esminių skirtumų. Pagrindiniai spektriniai skirtumai – spektrinių juostų,

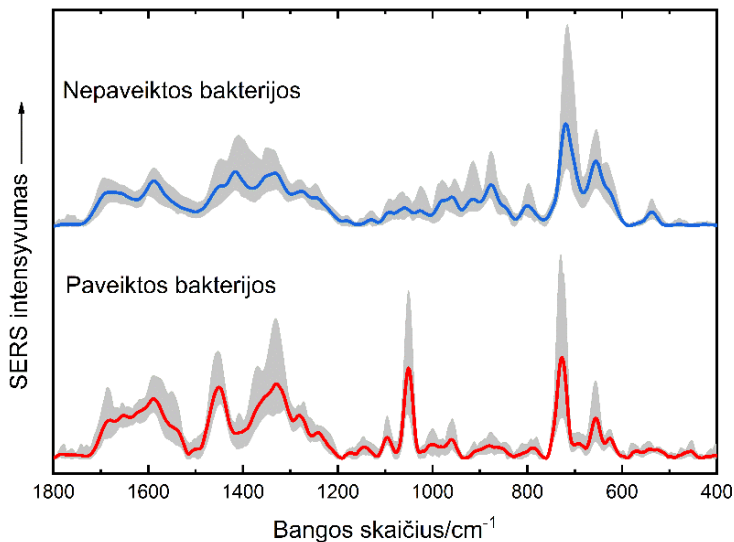
esančių ties 1448 cm^{-1} , 1098 cm^{-1} ir 1050 cm^{-1} , intensyvumo padidėjimas *E. coli* bakterijų spektre po fotosensibilizavimo. Šios spektrinės juostos atitinka deformacinius $\delta(\text{CH}_2)$ virpesius lipiduose (juosta ties 1448 cm^{-1}), $\nu(\text{C-C})$, $\nu(\text{C-O-C})$ ar $\nu(\text{O-P-O})$ virpesius lipiduose ir angliavandeniuose (juosta ties 1098 cm^{-1}) ir $\nu(\text{C-C})$, $\nu(\text{C-N})$ virpesius angliavandeniuose (juosta ties 1050 cm^{-1}) [166-169]. Kitas spektrinis bakterijų pažaidos požymis – spektrinių juostų ties 875 cm^{-1} bei 656 cm^{-1} intensyvumo sumažėjimas ar visiškai šių juostų išnykimas. Šios spektrinės juostos atitinka baltymų virpesines juostas. Stebimi skirtumai negali būti priskirti chlorofilino molekulei, kadangi pastarosios molekulės spektre nėra stebimos šios juostos. Taip pat chlorofilino spektro intensyvumas yra ženkliai mažesnis už bakterijų spektro intensyvumą, todėl šios molekulės spektras tik nežymiai prisideda prie bakterijų SERS spektre stebimų juostų intensyvumo. Bakterijų, vandeninio chlorofilino tirpalo ir sidabro nanodalelių tirpalų spektrų, juos užregistravus vienodomis sąlygomis, palyginimas yra pateiktas 8 pav. Spektrai pateikiami paslinkti y-ašies atžvilgiu. Pateiktuose spektruose matoma, kad bakterijų SERS spektras yra kelis kartus intensyvesnis nei chlorofilino spektras. Todėl šios molekulės spektras ir sidabro nanodalelių spektrai turi tik labai nedidelę įtaką užregistruotų bakterijų, kurios buvo fotosensibilizuojamos SERS spektrams.



8 pav. *E. coli* bakterijų, vandeninio chlorofilino tirpalo (0,5 mM) ir sidabro nanodalelių koloidinio tirpalo spektrų intensyvumų palyginimas.

Tyrimo metu SERS spektrai buvo registruojami keliuose skirtinguose bandinio taškuose, kad būtų įsitikinta, jog stebimi spektriniai pokyčiai nėra atsitiktiniai. Skirtinguose bandinio taškuose užregistruotų bakterijų SERS

spektrų vidurkiai yra pateikiami 9 pav. Pilkos sritys nurodo spektrų intensyvumo pokyčius. Tyrimo metu taip pat buvo įvertintas ir spektrinių duomenų atsikartojimas. Tai buvo įvertinta pakartotinai užauginus naujas *E. coli* bakterijų kolonijas, atlikus jų fotosensibilizavimą ir užregistravus jų SERS spektrus. Nustatyta, kad spektriniai požymiai yra atsikartojantys.



9 pav. Skirtinguose bandinio taškuose užregistruotų bakterijų SERS spektrų vidurkiai.

Aptikti spektriniai skirtumai tarp *E. coli* bakterijų SERS spektrų prieš ir po fotosensibilizavimo procedūros parodo, kad bakterijos deaktyvacija vyksta dėl cheminių jų pokyčių. Yra žinoma, kad deaktyvacijos proceso metu yra reikalingas artimas kontaktas tarp bakterijos ir fotosensityvios medžiagos [169]. Taip pat nustatyta, kad fotosensibilizavimo metu yra sukuriama laisvieji deguonies radikalai ar singletinis deguonis [155]. Nustatyta, kad ir fotosensibilizavimo chlorofilinu procedūros mechanizmas veikiausiai yra singletinio deguonies ar hidroksilo radikalų sukūrimas [171]. Tačiau nustatyta, kad šis mechanizmas nėra vienintelis, paaiškinantis bakterijų pažeidimus. Turint omenyje, kad fotosensibilizacijos procedūros metu yra sukuriama laisvieji deguonies radikalai bei atsižvelgus į stebimus spektrinius požymius prieita išvados, kad chlorofilinu paremtos fotosensibilizavimo procedūros metu yra pažeidžiamos bakterijų ląstelių membranos. Gram-neigiamų bakterijos turi ploną sluoksnį, sudarytą iš peptidoglikano. Šis yra apgaubtas dar vienu lipidų membranos sluoksniu, kuriame yra lipopolisacharidų ir lipoproteinų molekulių [172]. Pažeidus šiuos sluoksnius galima tikėtis, jog didesnis kiekis angliavandenių gali adsorbuotis

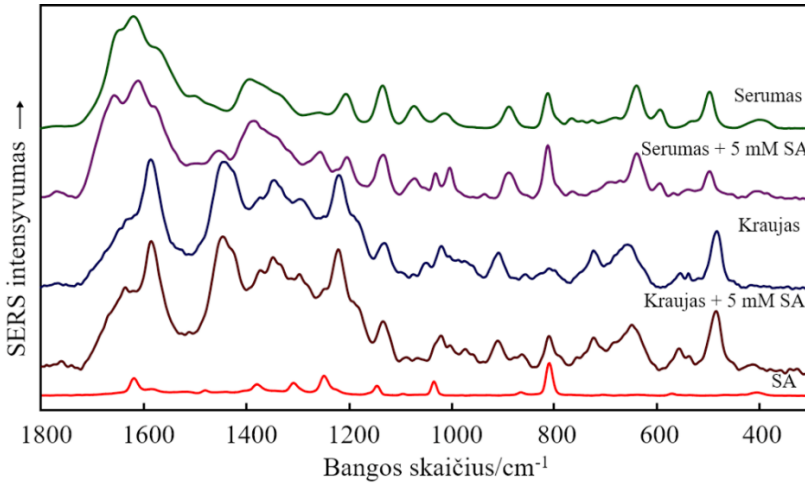
ant nanodalelių paviršiaus. Tai paaiškina stebimą spektrinių juostų, ties 1448 cm^{-1} , 1098 cm^{-1} ir 1050 cm^{-1} , intensyvumo padidėjimą. Spektrinių juostų, susijusių su baltymų virpesiais, sumažėjimas parodo, kad pažaidos mechanizmas veikiausiai susijęs ir su baltymų molekulių pokyčiais, kurie gali būti susieti su aktyvių deguonies radikalų poveikiu [174].

Šis tyrimas parodė, kad patogeninių *E. coli* bakterijų deaktyvacijos proceso – fotosensibilizavimo chlorofilinu, rezultatas yra šių bakterijų ląstelių išorinės membranos pažeidimas. Pažeidus bakterijų ląstelių membraną atsiranda daugiau laisvų angliavandenių bei lipidų molekulių ir jos lengviau gali adsorbuotis ant sidabro nanodalelių paviršiaus.

Vaistinių ir psichotropinių preparatų kraujyje ir seilėse SERS tyrimai

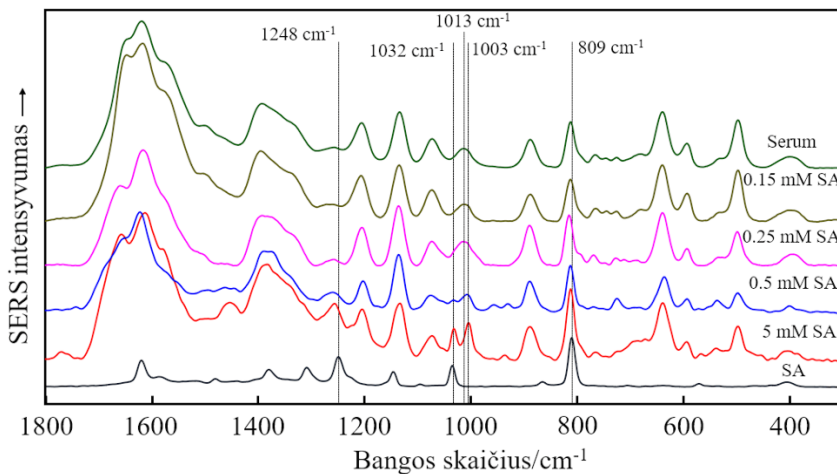
Šiame skyriuje aprašomi žmogaus biologinių skysčių (kraujo ir seilių) SERS tyrimai siekiant šiuose skysčiuose aptikti vaistinius ir narkotinius preparatus. Tokios metodikos, kuriomis būtų galima greitai ir tiksliai nustatyti kokias chemines medžiagas vartojo žmogus ir įgalinančios jų koncentracijos įvertinimą, yra naudingos klinikiniuose tyrimuose, kadangi suteikia informacijos, kuri leidžia parinkti specifinį gydymo metodą. Šiomis dienomis tai itin aktualu, kadangi žmonių perdozavimo vaistais ar narkotinėmis medžiagomis mastai vis didėja.

Acetilsalicilo rūgštis (aspirinas) ir acetaminofenas (paracetamolis) buvo pasirinkti šiuose tyrimuose. Šie vaistiniai preparatai SERS tyrimams buvo pasirinkti dėl to, kad jie yra nereceptiniai bei lengvai įsigijami. Abu šie vaistai yra priskiriami analgetikams ir prieš uždegiminiams vaistams, todėl jie yra vartojami įvairių uždegimų, skausmo ar kitų ligų malšinimui. Dėl to nėra keista, kad aspirinas ir paracetamolis yra vieni dažniausiai vartojamų vaistų pasaulyje. Dėl medicininių žinių trūkumo žmonės šiuos vaistus vartoja netinkamai – perdozuoja ar kombinauja su kitais reaguojančiais preparatais. Toks nereguliuojamas vartojimas dažnai lemia įvairių sveikatos komplikacijų atsiradimą ar netgi mirtį [254]. Aspirino ir paracetamolio aptikimo žmogaus kraujyje SERS tyrimai buvo atliekami naudojant savanorių kraują. Atsižvelgus į aspirino metabolizmą žmogaus kraujyje buvo nustatyta, kad tiesioginis šio vaisto aptikimas žmogaus kraujyje yra beveik neįmanomas. Todėl šį vaistą buvo bandoma aptikti nustatant jo metabolito – salicilo rūgšties buvimą kraujyje. Tyrimų metu pirmiausia buvo tiriami modeliniai bandiniai – žmogaus kraujas, kuriame ištirpintas atitinkamas kiekis vaisto ar jo metabolito. Žmogaus kraujo bei jo serumo ir šių biologinių skysčių mišinių su salicilo rūgštimi SERS spektrai yra pateikiami 10 pav.



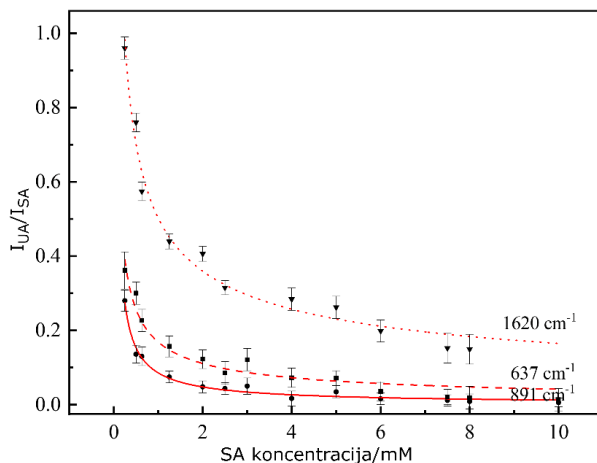
10 pav. Žmogaus kraujo, jo serumo ir šių biologinių skysčių mišinių su salicilo rūgštimi ir vandeninio salicilo rūgšties tirpalo (1 mM) SERS spektrai.

Palyginus SERS spektrus, pateiktus 10 pav., buvo nustatyta, kad salicilo rūgšties aptikimas tiesiogiai žmogaus kraujyje yra per daug sudėtingas, kadangi spektrinės salicilo rūgšties juostos persikloja su spektrinėmis juostomis, stebimomis žmogaus kraujo SERS spektre. Todėl kraujo serumas buvo įvertintas kaip geresnė terpė salicilo rūgščiai aptikti, nes kraujo serume yra mažiau komponentų ir tuo pačiu cheminių medžiagų, trukdančių aptikti salicilo rūgštį. Pastebėta, kad intensyviausia salicilo rūgšties spektrinė juosta persikloja su žmogaus kraujo serumo SERS spektre stebima šlapimo rūgšties spektrine juosta, tačiau salicilo rūgšties spektrinė juosta, esanti ties 1032 cm^{-1} , gali būti išskirta. Ši spektrinė juosta yra siejama su kombinuotais $\delta(\text{CH})$ deformacijos ir valentiniais žiedo virpesiais. Šlapimo rūgštis išskirta kaip labiausiai kraujo serumo SERS spektrą įtakojanti molekulė. Kad salicilo rūgštis tikrai gali būti identifikuota žmogaus kraujo serume pagal virpesinės juostos, esančios ties 1032 cm^{-1} , intensyvumą buvo įsitikinta užregistravus kraujo serumo ir skirtingos koncentracijos salicilo rūgšties mišinius. Šie spektrai yra pateikti 11 pav. Aiškumo dėlei spektrai paslinkti y-ašies atžvilgiu. Pateiktuose spektruose galima pastebėti, kad spektrinė juosta, išskirta kaip salicilo rūgšties spektrinis žymuo, esant mažesnėms šios molekulės koncentracijoms stebima tik kaip kraujo serumo SERS spektre stebimos juostos petys. Tačiau ši juosta gali būti išskirta naudojant analizės metodikas, kaip spektrinių kontūrų atskyrimą.



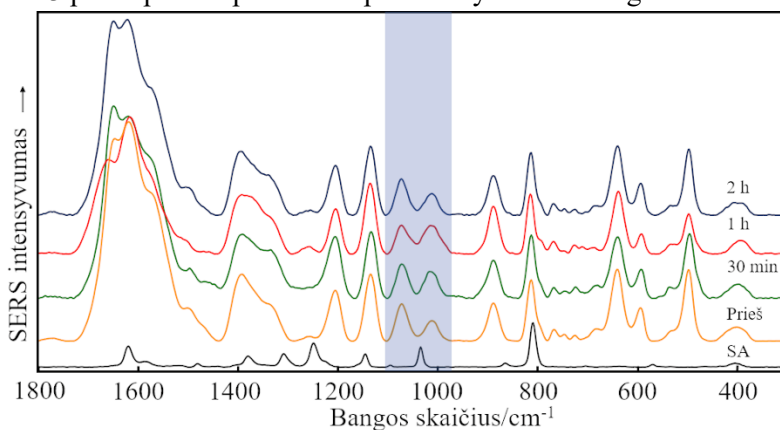
11 pav. Kraujo serumo mišinių, turinčių skirtingas salicilo rūgšties koncentracijas, salicilo rūgšties vandeninio tirpalo (1 mM) SERS spektrai.

Spektruose, pateiktuose 11 pav., pastebėtas ir netiesioginis salicilo rūgšties spektrinis žymuo - šlapimo rūgšties spektrinių juostų intensyvumo kitimas. Intensyvumo kitimas gali būti paaiškintas padidėjusiu terpės rūgštingumu dėl salicilo rūgšties atsiradimo. Šlapimo rūgščiai yra būdingos kelios tautomerinės formos, o kurioje tautomerinėje formoje bus molekulė priklauso nuo aplinkos pH vertės. Pagal gautus duomenis buvo nubrėžtos šlapimo rūgšties ir salicilo rūgšties spektrinių juostų intensyvumo santykio priklausomybė nuo salicilo rūgšties koncentracijos kreivės, kurias pateikiamos 12 pav.



12 pav. Šlapimo rūgšties ir salicilo rūgšties spektrinių juostų intensyvumo santykio priklausomybė nuo salicilo rūgšties koncentracijos.

Realūs žmogaus kraujo serumo bandiniai SERS tyrimams buvo ruošiami iš savanorių kraujo, kuris buvo surenkamas suvartojus 3,2 g aspirino. Surinktas kraujas buvo maišomas santykiu 8:1 su antihemoraginiu preparatu dicynone. Tuomet mišinys buvo centrifuguojamas 10 minučių 5000 xg išcentrine jėga ir taip atskiriamas kraujo serumas. Kraujo serumo bandiniai SERS tyrimams buvo ruošiami ant aliuminio substrato. Pirmiausia ant substrato buvo išdžiovinami sidabro nanodalelių koloidinio tirpalo lašai taip suformuojant SERS aktyvų sidabro nanodalelių sluoksnį. Tuomet ant suformuoto sluoksnio užlašinamas kraujo serumo lašas ir registruojamas SERS spektras. Realių žmogaus kraujo serumo bandinių SERS spektrai, užregistruoti prieš ir skirtingais laiko momentais po aspirino vartojimo pateikti 13 pav. Spektrai pateikiami paslinkti y-ašies atžvilgiu.

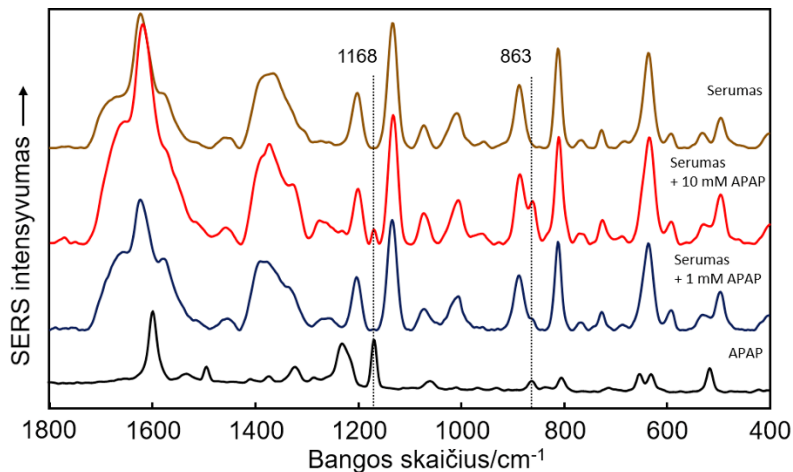


13 pav. Žmogaus kraujo serumo bandinių, surinktų prieš ir praėjus skirtingiems laiko momentams po 3,2 g aspirino dozės suvartojimo, ir vandeninio salicilo rūgšties tirpalo (1 mM) SERS spektrai.

Atlikus spektrų, pateiktų 13 pav., analizę buvo nustatyta, kad spektriniai salicilo rūgšties požymiai stebimi geriausiai praėjus vienai valandai po aspirino suvartojimo. Stebimi ir tiesioginiai (salicilo rūgšties spektrinės juostos) ir netiesioginiai (šlapimo rūgšties spektrinių juostų pokyčiai) požymiai. Nustatyta, kad aspiriną galima aptikti kai jo koncentracija yra 3 milimoliai litre, o tai atitinka lengvo toksiškumo koncentraciją.

Siekiant nustatyti galimybę SERS metodu aptikti paracetamolį (APAP) kraujyje taip pat pirmiausia buvo užregistruoti modelinių bandinių SERS spektrai. Kaip ir siekiant aptikti aspiriną, buvo nustatyta, kad kraujo serumo tyrimai yra efektyvesni dėl mažesnio biologinių komponentų kiekio šiame

biologiniame skystyje. Bandiniai buvo ruošiami pagal identišką procedūrą kaip ir tiriant aspirino aptikimą kraujyje. Žmogaus kraujo serumo, jo mišinių su dvejomis skirtingomis paracetamolio koncentracijomis ir vandeninio paracetamolio tirpalo (1 mM) SERS spektrai pateikti 14 pav. Aiškumo dėlei spektrai paslinkti y-ašies atžvilgiu.



14 pav. Žmogaus kraujo serumo, jo mišinių su paracetamoliu ir vandeninio paracetamolio tirpalo (1 mM) SERS spektrai.

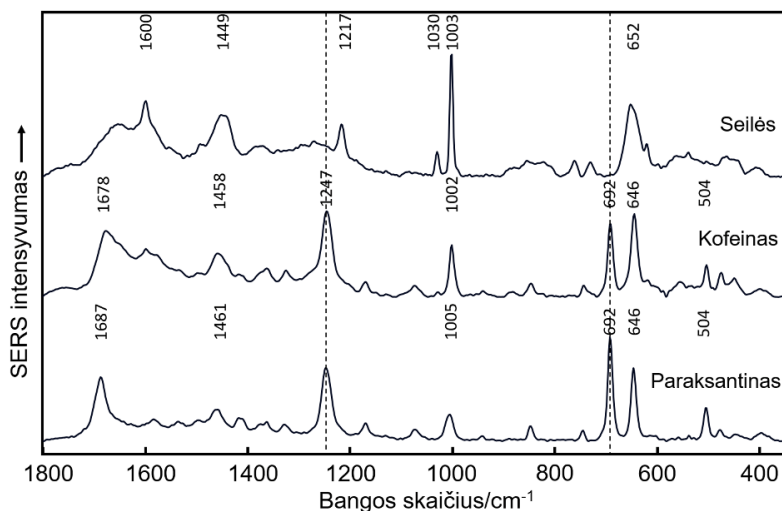
Atlikus lyginamąją spektrų analizę buvo identifikuoto spektrinės juostos, kurios gali būti naudojamos kaip spektriniai paracetamolio žymenys kraujo serume. Tai juostos, esančios ties 1168 cm⁻¹ (fenilo-N deformacinis virpesys) ir 863 cm⁻¹ (deformacinis skeletinis C-C virpesys). Nustatyta mažiausia galima aptikti paracetamolio koncentracija modeliniuose tirpaluose buvo 1 mM. Tačiau atlikus SERS tyrimą su realiais kraujo bandiniais, kurie buvo surinkti po 4 g paracetamolio dozės suvartojimo, buvo nustatyta, kad paracetamolio aptikti negalima. Paracetamolio aptikimą apsunkina serumo SERS spektre stebimos intensyvios šlapimo rūgšties spektrinės juostos. Todėl siekiant aptikti paracetamolį realiuose bandiniuose reiktų sumažinti šlapimo rūgšties molekulių adsorbciją ant sidabro nanodalelių paviršiaus.

Šio tyrimo metu buvo nustatyta, kad tiriant kraują SERS metodu galima identifikuoti aspirino vartojimą. Tai galima atlikti nustatčius šio vaisto metabolitą (salicilo rūgštį) kraujo serume. Tyrimo metu nustatyta, kad galima aptikti 3 mM salicilo rūgšties koncentracija, kuri klinikiniu požiūriu atitinka lengva apsinuodijimą. Taip pat nustatyta, kad modeliniuose tirpaluose paracetamolį galima aptikti kai jo koncentracija siekia 1 mM, tačiau realiuose

kraujo serumo bandiniuose paracetamolį aptikti yra sudėtinga, nes kraujo serumo SERS spektruose stebimos šlapimo rūgšties spektrinės juostos perkloja paracetamolio virpesines juostas.

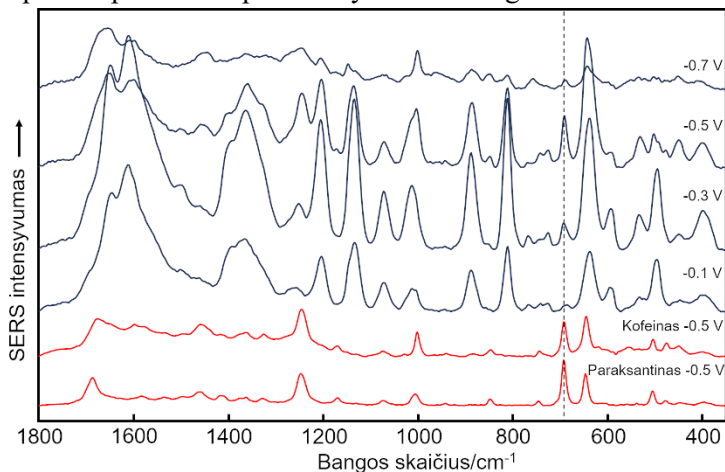
Siekiant įvertinti paviršiumi sustiprintos Ramano sklaidos tinkamumą identifikuoti psichoaktyvių medžiagų vartojimą buvo naudojamas elektrocheminis SERS (EC-SERS) metodas. EC-SERS metodas buvo pasirinktas dėl galimybės keisti molekulių adsorbciją keičiant darbinio elektrodo potencialą. Tokiu būdu galima iš dalies padidinti molekulių, kurias yra siekiama aptikti, adsorbciją, o tuo pačiu padidinti spektruose stebimų juostų intensyvumą. Kaip tiriamoji molekulė buvo pasirinktas kofeinas, kadangi jis yra priskiriamas psichoaktyvių medžiagų grupei ir yra lengvai prieinamas ir vartojamas dideliu mastu. Tyrimo metu buvo atsižvelgiama į kofeino metabolizmą. Kadangi kofeinas yra greitai absorbuojamas ir skaidomas organizme, jo buvimą galima aptikti tiesiogiai arba aptinkant jo metabolitus – paraksantiną, teobrominą bei teofiliną. Šiame tyrime buvo pasirinktas tik paraksantinas, kadangi į šią molekulę yra suskaidoma apie 80% visų kofeino molekulių.

Tyrimo metu pirmiausia buvo nustatyti spektriniai žymenys, kuriais galima identifikuoti tiriamas molekules seilėse. Buvo užregistruoti seilių, vandeninių kofeino (1 mM) ir paraksantino (1 mM) tirpalų SERS spektrai. Šie spektrai yra pateikiami 15 pav. Aiškumo dėlei šie spektrai paslinkti y-ašies atžvilgiu.



15 pav. Žmogaus seilių, vandeninių kofeino (1 mM) ir paraksantino (1 mM) tirpalų SERS spektrai.

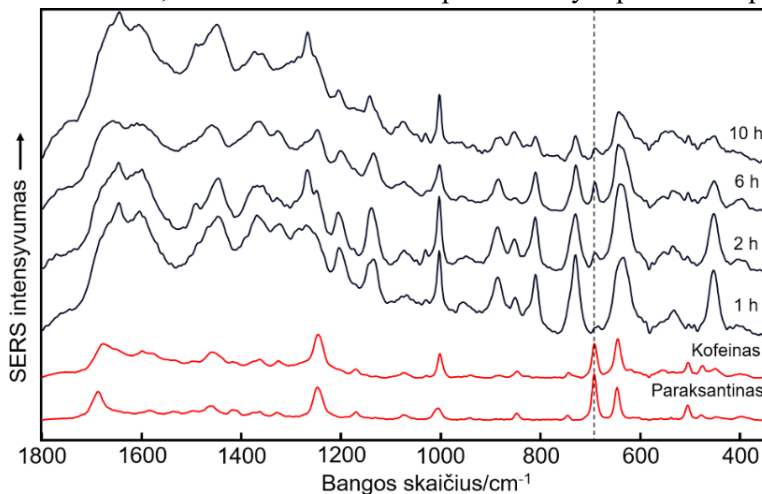
Palyginus užregistruotus spektrus buvo identifikuotos dvi spektrinės juostos, esančios ties 1247 cm^{-1} (kombinacinis $\delta(\text{C-H}) + \nu(\text{N-C}) + \delta(\text{CH}_3)$ virpesys) ir 692 cm^{-1} (kombinacinis $\nu(\text{N-CH}_3) + \delta(\text{N-C-N})$ virpesys), geriausiai tinkančios nustatyti kofeino ir paraksantino buvimą mišiniuose. Kadangi kofeino ir paraksantino cheminė sudėtis yra labai panaši, šių molekulių spektrai irgi yra panašūs ir juose stebimos abi spektrinės juostos. Tiriant modelinius seilių ir kofeino mišinius buvo įvertinta darbinio elektrodo potencialo įtaka stebimiems EC-SERS spektrams. Nustatyta, kad optimalus potencialas kofeino aptikimui (ties šia potencialo verte stebėtas didžiausias kofeino spektrinių juostų intensyvumas) yra $-0,5\text{ V}$. Žmogaus seilių ir kofeino mišinio EC-SERS spektrai, užregistruoti esant skirtingoms darbinio elektrodo potencialo vėrtėms, bei kofeino ir paraksantino tirpalų (1 mM) EC-SERS spektrai, užregistruoti ties $-0,5\text{ V}$ darbinio elektrodo potencialo verte, pateikti 16 pav. Spektrai pateikiami paslinkti y-ašies atžvilgiu.



16 pav. Žmogaus seilių ir kofeino mišinio, kofeino ir paraksantino tirpalų (1 mM) EC-SERS spektrai.

Atlikus modelinių tirpalų EC-SERS spektrų analizę buvo nustatyta, kad spektrinė juosta, stebima ties 1247 cm^{-1} , negali būti patikimai panaudota kofeino ir paraksantino aptikimui, nes ji persikloja su spektrinėmis juostomis, stebimomis žmogaus seilių EC-SERS spektre, kurios atsiranda keičiant darbinio elektrodo potencialą. Nustatyta, kad tik spektrinė juosta, esanti ties 692 cm^{-1} , gali būti patikimai panaudota kofeino ir paraksantino identifikavimui. Realūs žmogaus seilių bandiniai EC-SERS tyrimams buvo surinkti iš savanorių prieš ir praėjus įvairiems laiko periodams po to kai jie suvartojo 2 mg/kg ir $3,5\text{ mg/kg}$ kofeino dozes. Prieš šiuos tyrimus savanoriai

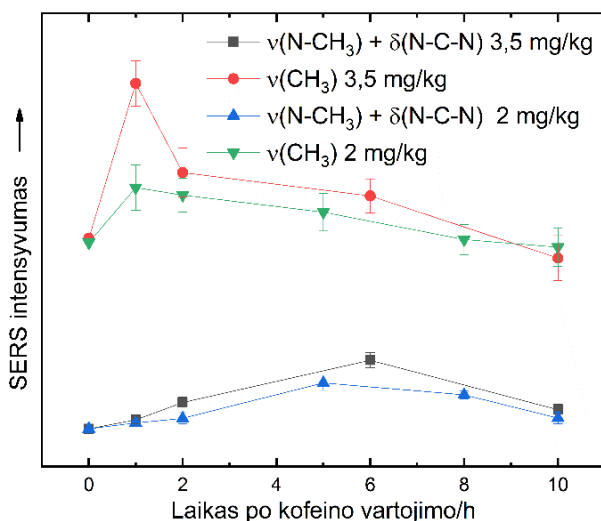
turėjo nevirtoti kofeino turinčių produktų bent 12 valandų. EC-SERS tyrimams surinktos seilės buvo centrifuguojamos 10 minučių 13000 apsisukimų per minutę greičiu siekiant pašalinti epitelio ląsteles, bakterijas ir kitus komponentus. Seilių, surinktų skirtingais laiko periodais po 3,5 mg/kg kofeino dozės suvartojimo, kofeino ir paraksantino EC-SERS spektrai, užregistruoti ties -0,5 V darbinio elektrodo potencialu yra pateikti 17 pav.



17 pav. Seilių, surinktų skirtingais laiko momentais po 3,5 mg/kg kofeino dozės suvartojimo, kofeino ir paraksantino EC-SERS spektrai, užregistruoti ties -0,5 V darbinio elektrodo potencialo verte.

Žmogaus seilių spektruose, pateiktuose 17 pav., galima pastebėti, kad spektrinė juosta, išskirta kaip kofeino ir paraksantino spektrinis žymuo, yra stebima praėjus 1 h po kofeino vartojimo. Taip pat stebimas šios spektrinės juostos intensyvumo padidėjimas, kuris pasiekia maksimalią vertę po 6 valandų nuo kofeino dozės suvartojimo. Vėliau spektrinės juostos intensyvumas vėl pradeda mažėti. Toks spektrinės juostos intensyvumo kitimas gerai sutampa su paraksantino žmogaus seilėse koncentracijos kitimu, kuris buvo įvertintas kituose tyrimuose [237]. Todėl padaryta išvada, kad stebima spektrinė juosta yra susijusi su paraksantino koncentracija seilėse. Taigi, kofeino aptikimas yra netiesioginis, o galimas aptinkant jo metabolitą. Taip pat buvo pastebėta dar viena spektrinė juosta, kurios intensyvumas seilių bandinių, surinktų skirtingais laiko momentais po kofeino vartojimo, EC-SERS spektruose kinta. Ši spektrinė juosta stebima ties 2930 cm^{-1} . Buvo pastebėta, kad šios spektrinės juostos intensyvumo kitimas atitinka kofeino koncentracijos kitimą seilėse po kofeino vartojimo [237]. Naudojantis šiuo spektriniu žymeniu galima būtų identifikuoti kofeino vartojimą tiesiogiai. Vis

dėlto, reikia pabrėžti, kad $\nu(\text{CH}_3)$ virpesių sritis nėra patikima, kadangi ir kitos molekulės, esančios seilių sudėtyje, šioje srityje gali lemti spektrinės juostos intensyvumą. Todėl norint pritaikyti šį spektrinį žymenį reiktų atlikti papildomus tyrimus ir įsitikinti jo patikimumu. Abiejų spektrinių žymenų intensyvumo kitimo priklausomybė nuo seilių surinkimo laiko po kofeino vartojimo pavaizduota 18 pav.



18 pav. Spektrinių kofeino ir paraksantino žymenų intensyvumo kitimo priklausomybė nuo laiko po 3,5 mg/kg ir 2 mg/kg kofeino dozių suvartojimo.

Intensyvumo kitimo profiliuose, pateiktuose 18 pav., matyti, kad spektrinių juostų intensyvumas tuo pačiu laiku po kofeino suvartojimo yra didesnis tuomet, kai buvo suvartota didesnė kofeino dozė. Tai parodo, kad tyrimo metodas tinka ne tik kokybinei, bet ir kiekybinei kofeino analizei. Tačiau šio tyrimo metu kiekybinės analizės galimybė nebuvo tirta ir norint šį metodą pritaikyti kiekybinėje analizėje reikia optimizuoti bandinių surinkimo, paruošimo ir spektrų registravimo metodikas.

Šis tyrimas parodė, kad EC-SERS metodas gali būti panaudotas psichoaktyvių medžiagų vartojimo nustatymui tiriant žmogaus seiles. Nustatyta, kad spektriniais žymenys yra susiję ne tik su kofeino, bet ir jo metabolito paraksantimo koncentracija žmogaus seilėse. Tyrimo rezultatai leidžia teigti, kad EC-SERS metodu kofeiną galima aptikti kai jo koncentraciją yra 15 mikromolių litre. Optimizavus metodiką galima būtų pasiekti žemesnį aptikimo lygį ir pritaikyti metodą kiekybinei analizei.

IŠVADOS

1. Inkstų ir šlapimo pūslės vėžys gali būti identifikuotas SERS metodu tiriant tarpląstelinį audinio skystį, tačiau skirtingų audinių vėžio identifikavimui reikia naudoti skirtingus spektrinius žymenis. Inkstu vėžio identifikavimui patikimiausias žymuo yra su glikogeno virpesiais susijusi spektrinė juosta ties 481 cm^{-1} , o šlapimo pūslės atveju – su cisteino/pieno rūgšties virpesiais susijusi spektrinė juosta ties 1052 cm^{-1} . SERS metodu pasiektas 93% vėžio identifikavimo jautrumas ir specifiskumas atitinka klinikiniam tyrimams naudojamų metodų reikalavimus.

2. SERS metodas yra pakankamai jautrus tirti bakterijų ląstelių pažeidimo tyrimus. *E. coli* bakterijų deaktyvacijos proceso – fotosensibilizavimo chlorofilinu, metu yra pažeidžiamos bakterijų ląstelių išorinės membranos. Pažeidus bakterijų ląstelių membraną ją sudarančios angliavandenių bei lipidų molekulės gali adsorbuotis ant sidabro nanodalelių paviršiaus.

3. SERS metodu galima identifikuoti aspirino vartojimą aptinkant jo metabolitą (salicilo rūgštį) kraujo serume. Salicilo rūgšties aptikimo riba – 3 milimoliai litre. Ši koncentracija klinikinio požiūriu atitinka lengvą apsinuodijimą. Modeliniuose tirpaluose paracetamolį galima aptikti kai jo koncentracija siekia 1 milimolį litre, tačiau norint paracetamolį aptikti realiuose kraujo serumo bandiniuose reikia sumažinti šlapimo rūgšties molekulių adsorbciją ant nanodalelių paviršiaus.

4. Seilių tyrimas EC-SERS metodu gali būti panaudotas psichoaktyvių medžiagų vartojimo nustatymui. Spektuose stebimi spektriniai žymenis, susiję ne tik su kofeino, bet ir jo metabolito paraksantimo koncentracija žmogaus seilėse. Panaudojus šiuos spektrinius žymenis EC-SERS metodu galima aptikti kofeiną, kai jo koncentraciją yra 15 mikromolių litre.

BIBLIOGRAPHY

- [1] E. Wiercigroch, E. Szafraniec, K. Czamara, M. Z. Pacia, K. Majzner, K. Kochan, A. Kaczor, M. Baranska, K. Malek, *Spectrochim. Acta, Part A* 2017, **185**, 317.
- [2] K. B. Bec, J. Grabska, C. W. Huck, *Anal. Chim. Acta*, 2020, **113**, 150.
- [3] H. Li, R. Lantz, D. Du, *Molecules*, 2019, **24**, 186.
- [4] C. Farber, J. Li, E. Hager, R. Chemelewski, J. Mullet, A. Yu. Rogachev, D. Kurouski, *ACS Omega*, 2019, **4**, 3700.
- [5] M. J Baker, J. Trevisan, P. Bassan, R. Bhargava, H. J. Butler, K. M. Dorling, P. R. Fielden, S. W. Fogarty, N. J. Fullwood, K. A. Heys, C. Hughes, P. Lasch, P. L. Martin-Hirsch, B. Obinaju, G. D. Sockalingum, J. Sulé-Suso, R. J. Strong, M. J. Walsh, B. R. Wood, P. Gardner, F. L. Martin, *Nat. Protoc.* 2014, **9**, 1771.
- [6] N. Gierlinger, *Appl. Spectrosc. Rev.* 2018, **7**, 517.
- [7] A. V. Vlasov, N. L. Maliar, S. V. Bazhenov, E. I. Nikelshparg, N. A. Brazhe, A. D. Vlasova, S. D. Osipov, V. V. Sudarev, Y. L. Ryzhykau, A. O. Bogorodskiy, E. V. Zinovev, A. V. Rogachev, I. V. Manukhov, V. I. Borshchevskiy, A. I. Kuklin, J. Pokorný, O. Sosnovtseva, G. V. Maksimov, V. I. Gordeliy, *Crystals*, 2020, **10**, 1.
- [8] A. Rohman, A. Windarsih, E. Lukitaningsih, M. Rafi, K. Betania, N. A. Fadzillah, *Biomed. Spectrosc. Imaging* 2019, **8**, 55.
- [9] Z. Movasaghi, S. Rehman, I. U. Rehman, *Appl. Spectrosc. Rev.* 2007, **42**, 493.
- [10] S. Sabbatini, C. Conti, G. Orilisi, E. Giorgini, *Biomed. Spectrosc. Imaging*, 2017, **6**, 85.
- [11] W. Petrich, *Appl. Spectrosc. Rev.* 2011, **36**, 181.
- [12] M. J. Baker, H. J. Byrne, J. Chalmers, P. Gardner, R. Goodacre, A. Henderson, S. G. Kazarian, F. L. Martin, J. Moger, N. Stone, J. Sulé-Suso, *Analyst*, 2018, **143**, 1735.
- [13] A. A. Bunaciu, H. Y. Aboul-Enein, S. Fleschin, *Appl. Spectrosc. Rev.* 2015, **50**, 176.
- [14] H. Ahn, H. Song, D.-M. Shin, K. Kim, J.-r. Choi, *Appl. Spectrosc. Rev.* 2018, **53**, 264.
- [15] D. DePaoli, É. Lemoine, K. Ember, M. Parent, M. Prud'homme, L. Cantin, K. Petrecca, F. Leblond, D. C. Côté, *J. Biomed. Opt.* 2020, **25**, 1.
- [16] S. F. Parker, *RSC Adv.* 2018, **8**, 23875.

- [17] S. A. Fischer, T. W. Ueltschi, P. Z. El-Khoury, A. L. Mifflin, W. P. Hess, H.-F. Wang, C. J. Cramer, N. Govind, *J. Phys. Chem. B*, 2016, **120**, 1429.
- [18] A. Taghzadeh, U. Leffers, T. G. Pedersen, K. S. Thygesen, *Nat. Commun.* 2020, **11**, 1.
- [19] L. Nannan, V. Untereiner, I. Proutt, C. Boulagnon-Rombi, C. Colin-Pierre, G. D. Sockalingum, S. Brézillon, *Front. Cell Dev. Biol.* 2020, **8**, 1.
- [20] R. M. Spiers, J. Marzice, E. M. Brauchle, S. E. Cross, R. H. Vaughan, P. A. Bateman, S. J. Hughes, K. Schenke-Layland, P. R. V. Johnson, *Acta Biomater.* 2019, **99**, 269.
- [21] Z. Xu, X. Ge, W. Huang, D. Lin, S. Wu, X. Lin, Q. Wu, L. Sun, *Spectrosc. Lett.* 2017, **50**, 17.
- [22] C. Kendall, M. Isabelle, F. Bazant-Hegemark, J. Hutchings, L. Orr, J. Babrah, R. Baker, N. Stone, *Analyst* 2009, **134**, 1029.
- [23] O. J. Old, L. M. Fullwood, R. Scott, G. R. Lloyd, L. M. Almond, N. A. Shepherd, N. Stone, H. Barrd, C. Kendall, *Anal. Methods* 2014, **6**, 3901.
- [24] C. L. M. Morais, K. M. G. Lima, M. Singh, F. L. Martin, *Nat. Protoc.* 2020, **15**, 2143.
- [25] A. Jaworska, S. Fornasaro, V. Sergo, A. Bonifacio, *Biosensors* 2016, **6**, 1.
- [26] C. Chen, W. Liu, S. Tian, T. Hong, *Sensors* 2019, **19**, 1.
- [27] B. Yu, M. Ge, P. Li, Q. Xie, L. Yang, *Talanta* 2019, **191**, 1.
- [28] S. D. Bindsri, D. S. Alhatab, C. L. Brosseau, *Analyst* 2018, **143**, 4128.
- [29] K. Dai, R. Huang, R. Jiang, H.-X. Ke, F. Li, S. Jin, D.-Y. Wu, Z.-Q. Tian, *J. Raman Spectrosc.* 2012, **43**, 1367.
- [30] R. Minnes, M. Nissinmann, Y. Maizels, G. Gerlitz, A. Katzir, Y. Raichlin, *Sci. Rep.* 2017, **7**, 4381.
- [31] H. Ghimire, M. Venkataramani, Z. Bian, Y. Liu, A. G. U. Perera, *Sci. Rep.* 2017, **7**, 16993.
- [32] H. J. Butler, P. M. Brennan, J. M. Cameron, D. Finlayson, M. G. Hegarty, M. D. Jenkinson, D. S. Palmer, B. R. Smith, M. J. Baker, *Nat. Commun.* 2019, **10**, 4501.
- [33] J. Lv, L. Zhang, J. Feng, Y. Liu, Z. Wang, M. Zhao, R. Shi, *Spectrosc. Lett.* 2011, **44**, 312.
- [34] K. Al-Jorani, A. Rüther, R. Haputhanthri, G. B. Deacon, H. L. Li, C. Cullinane, B. R. Wood, *Analyst*, 2018, **143**, 6087.
- [35] S. Kino, S. Omori, T. Katagiri, Y. Matsuura, *Biomed. Opt. Express* 2016, **7**, 701.
- [36] K. M.-C. Beyer-Hans, M. Werner, S. Angelika, S. Veli, O. Ozturk, G. Emingil, N. Bostanci, *Proteomics: Clin. Appl.* 2020, **14**, 1900092.

- [37] E. P. Mwangi, E. G. Minja, E. Mrimi, M. G. Jiménez, J. K. Swai, S. Abbasi, H. S. Ngowo, D. J. Siria, S. Mapua, C. Stica, M. F. Maja, A. Olotu, M. T. Sikulu-Lord, F. Baldini, H. M. Ferguson, K. Wynne, P. Selvaraj, S. A. Babayan, F.O. Okumu, *Malar. J.* 2019, **18**, 341.
- [38] S. Schlücker, *Surface Enhanced Raman Spectroscopy: Analytical Biophysical and Life Science Applications*, Wiley-VCH, Germany, 2011.
- [39] B. S. Renee, R. Frontiera, A.-I. Henry, E. Ringe, R. P. Van Duyne, *Mater. Today* 2012, **15**, 16.
- [40] Z. Starowicz, R. Wojnarowska-Nowak, P. Ozga, E. M. Sheregii, *Colloid Polym. Sci.* 2018, **296**, 1029.
- [41] S. J. Barrow, X. Wei, J. S. Baldauf, A. M. Funston, P. Mulvaney, *Nat. Commun.* 2012, **3**, 1275.
- [42] E. C. Le Ru, S. A. Meyer, C. Artur, P. G. Etchegoin, J. Grand, P. Lang, F. Maurel, *Chem. Commun.* 2011, **47**, 3903.
- [43] E. Le Ru, P. Etchegoin, *Principles of Surface-Enhanced Raman Spectroscopy: and Related Plasmonic Effects*, Elsevier, Netherlands, 2009.
- [44] E. C. Le Ru, E. Blackie, M. Meyer, P. G. Etchegoin, *J. Phys. Chem. C* 2007, **111**, 13794.
- [45] L. Xie, J. Lu, T. Liu, G. Chen, G. Liu, B. Ren, Z. Tian, *J. Phys. Chem. Lett.* 2020, **11**, 1022.
- [46] L. M. Almeahmadi, S. M. Curley, N. A. Tokranova, S. A. Tenenbaum, I. K. Lednev, *Sci. Rep.* 2019, **9**, 1.
- [47] H.-K. Choi, K. S. Lee, H.-H. Shin, J.-J. Koo, G. J. Yeon, Z. H Kim, *Acc. Chem. Res.* 2019, **52**, 3008.
- [48] Y. Yu, T.-H. Xiao, Y. Wu, W. Li, Q.-G. Zeng, L. Long, Z.-Y. Li, *Adv. Photonics* 2020, **2**, 1.
- [49] R. Pilot, *J. Raman Spectrosc.* 2018, **49**, 954.
- [50] A. P. Craig, A. S Franca, J. Irudayaraj, *Annu Rev Food Sci Technol.* 2013, **4**, 369.
- [51] H. Kearns, R. Goodacre, L. E. Jamieson, D. Graham, K. Faulds, *Anal. Chem.* 2017, **89**, 12666.
- [52] X. Zhao, M. Li, Z. Xu, *Front. Microbiol.* 2018, **9**, 1.
- [53] E. V. Shabunya-Klyachkovskaya, O. S. Kulakovich, S. V. Gaponenko, *Spectrochim. Acta, Part A* 2019, **222**, 1.
- [54] R. A. Alvarez-Puebla, L. M. Liz-Marzán, *Angew Chem Int Ed Engl.* 2012, **5**, 11214.
- [55] A. Bonifacio, S. Cervo, V. Sergo, *Anal Bioanal Chem* 2015, **407**, 8265.
- [56] V. Turzhitsky, L. Zhang, G. L. Horowitz, E. Vitkin, U. Khan, Y. Zakharov, L. Qiu, I. Itzkan, L. T. Perelman, *Small*, 2018, **14**, 1.

- [57] L. Guerrini, R. A. Alvarez-Puebla, *Cancers*, **11**, 748.
- [58] A. Chakraborty, A. Ghosh, A. Barui, *J. Raman. Spectrosc.* 2019, **51**, 7.
- [59] J. R. Anema, J.-F. Li, Z.-L. Yang, B. Ren, Z.-Q. Tian, *Annu. Rev. Anal. Chem.* 2008, **4**, 129.
- [60] H.-M. Kim, D.-M. Kim, C. Jeong, S. Y. Park, M. G. Cha, Y. Ha, D. Jang, S. Kyeong, X.-H. Pham, E. Hahm, S. H. Lee, D. H. Jeong, Y.-S. Lee, D.-E. Kim, B.-H. Jun, *Sci. Rep.* 2018, **8**, 1.
- [61] T. Yaseen, H. Pua, D.-W. Sun, *Trends Food Sci. Technol.* 2018, **72**, 162.
- [62] Y. Li, Q. Wei, F. Ma, X. Li, F. Liu, M. Zhou, *Acta Pharm. Sin. B* 2018, **8**, 349.
- [63] G. Weng, Y. Yang, J. Zhao, J. Li, J. Zhu, J. Zhao, *Mater. Chem. Phys.* 2020, **253**, 1.
- [64] H. Fisk, C. Westley, N. J. Turner, R. Goodacre, *J. Raman Spectrosc.* 2015, **47**, 59.
- [65] P. A. Mosier-Boss, *Nanomaterials* 2017, **7**, 142.
- [66] X. Sun, H. Li, *Curr. Nanosci.* 2016, **12**, 175.
- [67] S. Zaleski, K. A. Clark, M. M. Smith, J. Y. Eilert, M. J. Doty, R. P. Van Duyne, *Anal. Chem.* 2017, **89**, 2497.
- [68] B. L. Goodall, A. M. Robinson, C. L. Brosseau, *Phys. Chem. Chem. Phys.* 2013, **15**, 1382.
- [69] T. P. Lynk, C. S. Sit, C. L. Brosseau, *Anal. Chem.* 2018, **90**, 12639.
- [70] R. A. Karaballi, A. Nel, S. Krishnan, J. Blackburn, C. L. Brosseau, *Phys. Chem. Chem. Phys.* 2015, **17**, 21356.
- [71] R. A. Karaballi, S. Merchant, S. R. Power, C. L. Brosseau, *Phys. Chem. Chem. Phys.* 2018, **20**, 4513.
- [72] https://sdbs.db.aist.go.jp/sdbs/cgi-bin/direct_frame_top.cgi, viewed on 2020-07-01.
- [73] <https://webbook.nist.gov/chemistry/name-ser/>, viewed on 2020-07-01.
- [74] S. Pilleron, D. Sarfati, M. Janssen-Heijnen, J. Vignat, J. Ferlay, F. Bray, I. Soerjomataram, *Int. J. Cancer* 2018, **144**, 49.
- [75] Q.-l. Dong, X.-y. Xing, *Cancer Cell Int.* 2018, **18**, 205.
- [76] K. Vinasco, H. M. Mitchell, N. O. Kaakoush, N. Castaño-Rodríguez, *Biochim. Biophys. Acta, Rev. Cancer* 2019, **1872**, 1.
- [77] D. van Elsland, J. Neefjes, *EMBO Rep.* 2018, **19**, 1.
- [78] S. Sarkar, G. Horn, K. Moulton, A. Oza, S. Byler, S. Kokolus, M. Longacre, *Int J Mol Sci.* 2013, **14**, 21087.
- [79] G. M. Cooper, *The Cell: A Molecular Approach, 2nd edition*, Sinauer Associates, Sunderland, Massachusetts, 2000.

- [80] L. Sieverling, C. Hong, S. D. Koser, P. Ginsbach, K. Kleinheinz, B. Hutter, D. M. Braun, I. Cortés-Ciriano, R. Xi, R. Kabbe, P. J. Park, R. Eils, M. Schlesner, PCAWG-Structural Variation Working Group, B. Brors, K. Rippe, D. T. W. Jones, L. Feuerbach, PCAWG Consortium, *Nat. Commun.* 2020, **11**, 733.
- [81] S. Spranger, T. F. Gajewski, *Annu. Rev. Cancer Biol.* 2018, **2**, 213.
- [82] A. R. M. R. Amina, P. A. Karpowicz, T. E. Carey, J. Arbisera, R. Nahta, Z. G. Chen, J.-T. Dong, O. Kucuk, G. N. Khan, G. S. Huang, S. Mi, H.-Y. Lee, J. Reichrath, K. Honoki, A. G. Georgakilas, A. Amedei, A. Amin, B. Helferich, C. S. Boosani, M. R. Ciriolo, S. Chen, S. I. Mohammed, A. S. Azmi, W. N. Keith, D. Bhakta, D. Halicka, E. Niccolai, H. Fujii, K. Aquilano, S. S. Ashraf, S. Nowsheen, X. Yang, A. Bilslund, D. M. Shin, *Semin. Cancer Biol.* 2015, **35**, 55.
- [83] I. Zuazo-Gatzelu, O. Casanovas, *Front. Oncol.* 2018, **8**, 1.
- [84] A. Fadaka, B. Ajiboye, O. Ojo, O. Adewale, I. Olayide, R. Emuowhochere, *J Oncol Sci*, 2017, **3**, 45.
- [85] H. Sun, L. Chen, S. Cao, Y. Liang, Y. Xu, *Genomics, Proteomics Bioinf.* 2019, **17**, 273.
- [86] D. Hanahan, R. A. Weinberg, *Cell* 2011, **144**, 646.
- [87] J. D. Brierley, M. K. Gospodarowicz, C. Wittekind, *TNM Classification of Malignant Tumours, 8th Edition*, Willey Blackwell, 2017.
- [88] M. C. S. Wong, W. B. Goggins, B. H. K. Yip, F. D. H. Fung, C. Leung, Y. Fang, S. Y. S. Wong, C. F. Ng, *Sci. Rep.* 2017, **7**, 15698.
- [89] E. T. Lam, S. Nabi, E. R. Kessler, B. Bernard, T. W. Flaig, *F1000Research* 2018, **7**, 307.
- [90] V. F. Muglia, A. Prando, *Radiol Bras.* 2015, **48**, 166.
- [91] J. J. Hsieh, M. P. Purdue, S. Signoretti, C. Swanton, L. Albiges, M. Schmidinger, D. Y. Heng, J. Larkin, V. Ficarr, *Nat. Rev.* 2017, **3**, 1.
- [92] F. Bray, J. Ferlay, I. Soerjomataram, R. L. Siegel, L. A. Torre, A. Jemal, *Ca-Cancer J. Clin.* 2018, **68**, 394.
- [93] H. D. Yuk, C. W. Jeong, C. Kwak, H. H. Kim, K. C. Moon, J. H. Ku, *BMC Cancer*, 2019, **19**, 1.
- [94] X. Zhang, Y. Zhang, *Cell Biochem. Biophys.* 2015, **73**, 65.
- [95] S. Daneshmand, S. T. Bazargani, T. J. Bivalacqua, J. M. Holzbeierlein, B. Willard, J. M. Taylor, J. C. Liao, K. Pohar, J. Tierney, B. Konety, *Urol. Oncol.: Semin. Orig. Invest.* 2018, **36**, 361.
- [96] G. Mowatt, J. N'Dow, L. Vale, G. Nabi, C. Boachie, J. A. Cook, C. Fraser, T. R. L. Griffiths, *Int J Technol Assess Health Care*, 2011, **27**, 3.
- [97] M. S. Flezar, *Radiol. Oncol.* 2010, **44**, 207.

- [98] E. Oeyen, L. Hoekx, S. De Wachter, M. Baldewijns, F. Ameye, I. Mertens, *Int. J. Mol. Sci.* 2019, **20**, 821
- [99] P. C. Benias, R. G. Wells, B. Sackey-Aboagye, H. Klavan, J. Reidy, D. Buonocore, M. Miranda, S. Kornacki, M. Wayne, D. L. Carr-Locke, N. D. Theise, *Sci. Rep.* 2018, **8**, 1.
- [100] M. A. Mori, R. G. Ludwig, R. Garcia-Martin, B. B. Brandão, C. R. Kahn, *Cell Metab.* 2019, **30**, 656.
- [101] E.-J. Kim, M.-J. Choi, J.-H. Lee, J.-E. Oh, J.-W. Seo, Y.-K. Lee, J.-W. Yoon, H.-J. Kim, J.-W. Noh, J.-R. Koo, *Plos One* 2017, **12**, 1.
- [102] T. Lilo, C. L. M. Morais, K. M. Ashton, A. Pardilho, C. Davis, T. P. Dawson, N. Gurusinge, F. L. Martin, *Anal. Bioanal. Chem.* 2019, **412**, 1077.
- [103] H. Karabeber, R. Huang, P. Iacono, J. M. Samii, K. Pitter, E. C. Holland, M. F. Kircher, *ACS Nano* 2014, **8**, 9755.
- [104] S. Rehman, Z. Movasaghi, J. A. Darr, I. U. Rehman, *Appl. Spectrosc. Rev.* 2010, **45**, 355.
- [105] L. Shen, Y. Du, N. Wei, Q. Li, S. Li, T. Sun, S. Xu, H. Wang, X. Man, H. Bing, *Spectrochim. Acta, Part A* 2020, **237**, 118364.
- [106] E. Kaznowska, J. Depciuch, K. Łach, M. Kołodziej, A. Koziorowska, J. Vongsvivut, I. Zawlika, M. Cholewa, J. Cebulski, *Talanta*, 2018, **186**, 337.
- [107] K. Zhang, C. Hao, Y. Huo, B. Man, C. Zhang, C. Yang, M. Liu, C. Chen, *Lasers Med Sci.* 2019, **34**, 1849.
- [108] K.-Y. Su, W.-L. Lee, *Cancers* 2020, **12**, 115.
- [109] G. W. Auner, S. K. Koya, C. Huang, B. Broadbent, M. Trexler, Z. Auner, A. Elias, K. C. Mehne, M. A. Brusatori, *Cancer Metastasis Rev.* 2018, **37**, 691.
- [110] D. J. Anderson, R. G. Anderson, S. J. Moug, M. J. Baker, *BJS Open* 2020, **4**, 554.
- [111] R. M. Davis, B. Kiss, D. R. Trivedi, T. J. Metzner, J. C. Liao, S. S. Gambhir, *ACS Nano*, 2018, **12**, 9669.
- [112] J. Ollesch, M. Heinze, H. M. Heise, T. Behrens, T. Brüning, K. Gerwert, *J. Biophotonics* 2014, **7**, 210.
- [113] V. Urbonienė, M. Pučetaitė, F. Jankevičius, A. Želvys, V. Šablinskas, G. Steiner, *J Biomed Opt.* 2014, **19**, 1.
- [114] P. C. Lee, D. Meisel, *J. Phys. Chem.* 1982, **86**, 3391.
- [115] D. Aherne, D. M. Ledwith, M. Gara, J. M. Kelly, *Adv. Funct. Mater.* 2005, **18**, 2005.
- [116] S. Z. Malynych, *J. Nano- Electron. Phys.* 2010, **78**, 5.
- [117] D. Paramelle, A. Sadovoy, S. Gorelik, P. Free, J. Hogleya, D. G. Fernig, *Analyst* 2014, **139**, 4855.

- [118] Gaussian 09, Revision D.01, M. J. Frisch, G. W. Trucks, H. B. Schlegel, G. E. Scuseria, M. A. Robb, J. R. Cheeseman, G. Scalmani, V. Barone, B. Mennucci, G. A. Petersson, H. Nakatsuji, M. Caricato, X. Li, H. P. Hratchian, A. F. Izmaylov, J. Bloino, G. Zheng, J. L. Sonnenberg, M. Hada, M. Ehara, K. Toyota, R. Fukuda, J. Hasegawa, M. Ishida, T. Nakajima, Y. Honda, O. Kitao, H. Nakai, T. Vreven, J. A. Montgomery, Jr., J. E. Peralta, F. Ogliaro, M. Bearpark, J. J. Heyd, E. Brothers, K. N. Kudin, V. N. Staroverov, T. Keith, R. Kobayashi, J. Normand, K. Raghavachari, A. Rendell, J. C. Burant, S. S. Iyengar, J. Tomasi, M. Cossi, N. Rega, J. M. Millam, M. Klene, J. E. Knox, J. B. Cross, V. Bakken, C. Adamo, J. Jaramillo, R. Gomperts, R. E. Stratmann, O. Yazyev, A. J. Austin, R. Cammi, C. Pomelli, J. W. Ochterski, R. L. Martin, K. Morokuma, V. G. Zakrzewski, G. A. Voth, P. Salvador, J. J. Dannenberg, S. Dapprich, A. D. Daniels, O. Farkas, J. B. Foresman, J. V. Ortiz, J. Cioslowski, and D. J. Fox, Gaussian, Inc., Wallingford CT, 2013.
- [119] M. D. Hanwell, D. E. Curtis, D. C. Lonie, T. Vandermeersch, E. Zurek, G. R. Hutchison, *J. Chem.*, 2012, **4**, 17.
- [120] J. A. Combs, G. M. DeNicola, *Cancers* 2019, **11**, 678.
- [121] J. Serpa, *Front. Oncol.* 2020, **10**, 947.
- [122] S. Li, L. Li, Q. Zeng, Y. Zhang, Z. Guo, Z. Liu, M. Jin, C. Su, L. Lin, J. Xu. S. Liu, *Sci. Rep.* 2014, **5**, 1.
- [123] S. Mert, E. Ozbek, A. Otunctemur, M. Culha, *J. Biomed. Opt.* 2015, **20**, 1.
- [124] S. Mert, M. Culha, *Appl. Spectrosc.* 2014, **68**, 617.
- [125] Y. Hong, Y. Li, L. Huang, W. He, S. Wang, C. Wang, G. Zhou, Y. Chen, X. Zhou, Y. Huang, W. Huang, T. Gong, Z. Zhou, *J. Biophotonics* 2020, **13**, 1.
- [126] C. Jing, Y. Fang, *J. Chem. Phys.* 2007, **332**, 27.
- [127] B. Yan, B. Li, Z. Wen, X. Luo, L. Xu, L. Li, *BMC Cancer* 2015, **15**, 1.
- [128] D. Lin, S. Feng, J. Pan, Y. Chen, J. Lin, G. Chen, S. Xie, H. Zeng, R. Chen, *Opt. Express* 2011, **19**, 13565.
- [129] D. Lin, J. Pan, H. Huang, G. Chen, S. Qiu, H. Shi, W. Chen, Y. Yu, S. Feng, R. Chen, *Sci. Rep.* 2013, **4**, 1.
- [130] K. Zhanga, C. Haob, B. Mana, C. Zhanga, C. Yanga, M. Liua, Q. Penga, C. Chen, *Vib. Spectrosc.* 2018, **98**, 82.
- [131] C. E. Zois, A. L. Harris, *J. Mol. Med.* 2016, **94**, 137.
- [132] N. J. Kelly, J. F. A. Varga, E. J. Specker, C. M. Romeo, B. L. Coomber, J. Uniacke, *Oncogene*, 2018, **37**, 651.
- [133] A. Rybarczyk, J. Klacz, A. Wronska, M. Matuszewski, Z. Kmiec, P. M. Wierzbicki, *Oncol. Rep.* 21017, **38**, 427.

- [134] V. A. Valera, E. Li-Ning-T, B. A. Walter, D. D. Roberts, W. M. Linehan, M. J. Merino, *J. Cancer* 2010, **1**, 184.
- [135] J. Coates, *Interpretation of Infrared Spectra. A Practical Approach*, in: *Encyclopedia of Analytical Chemistry*, John Wiley & Sons, Ltd., Chichester 2006.
- [136] A. C. S. Talari, M. A. G. Martinez, Z. Movasaghi, S. Rehman, I. U. Rehman, *Appl. Spectrosc. Rev.* 2017, **52**, 456.
- [137] O. Warburg, *Science*, 1956, **123**, 309.
- [138] G. G. Amuran, I. P. Eyuboglu, I. Tinay, M. Akkiprik, *Medical Sciences* 2018, **6**, 1.
- [139] A. Teixeira, J. F. Hernandez-Rodriguez, L. Wu, K. Oliveira, K. Kant, P. Pairao, L. Dieguez, S. Abalde-Cela, *App. Sci.* 2019, **9**, 1.
- [140] N. Merino, H. S. Aronson, D. P. Bojanova, J. Feyhl-Buska, M. L. Wong, S. Zhang, D. Giovannelli, *Front. Microbiol.* 2019, **10**, 1.
- [141] P. Chellamuthu, F. Tran, K. Pavan, T. Silva, M. S. Chavez, M. Y. El-Naggar, J. Q. Boedicker, *Microb. Biotechnol.* 2018, **12**, 161.
- [142] J. J. Hug, D. Krug, R. Muller, *Nat. Rev. Chem.* 2020, **4**, 172.
- [143] I. Y. Sengun, S. Karabiyikli, *Food Control* 2011, **22**, 647.
- [144] S. Raveendran, B. Parameswaran, S. B. Ummalyma, A. Abraham, A. K. Mathew, A. Madhavan, S. Rebello, A. Pandey, *Food Technol. Biotechnol.* 2018, **56**, 16.
- [145] P. Chattopadhyay, G. Banerjee, S. Mukherjee, *3 Biotech* 2017, **7**, 1.
- [146] L. Ruiu, *Insects* 2015, **6**, 352.
- [147] Ian Rowland, Glenn Gibson, Almut Heinken, Karen Scott, Jonathan Swann, Ines Thiele, Kieran Tuohy, *Eur. J. Nutr.* 2018, **57**, 1.
- [148] K. Yoshii, K. Hosomi, K. Sawane, J. Kunisawa, *Front. Nutr.* 2019, **6**, 1.
- [149] M. Vouga, G. Greub, *Clin. Microbiol. Infect.* 2016, **22**, 12.
- [150] F. Chowdhury, I. A. Khan, S. Patel, A. U. Siddiq, N. C. Saha, A. I. Khan, A. Saha, A. Cravioto, J. Clemens, F. Qadri, M. Ali, *PLoS One* 2015, **10**, 1.
- [151] A. Wallin, Ž. Lukšienė, K. Zagminas, G. Surkiene, *Medicina* 2007, **43**, 278.
- [152] S. K. Pankaj, H. Shi, K. M. Keener, *Trends Food Sci. Technol.* 2018, **71**, 73.
- [153] A. Lianou, K. P. Koutsoumanis, J. N. Sofos, *Microbial Decontamination in the Food Industry: Novel Methods and Applications*, Woodhead Publishing Ltd., Cambridge, 2012.

- [154] J. Fanzo, N. Covic, A. Dobermann, S. Henson, M. Herrero, P. Pingali, S. Staalg, *Glob. Food Sec.* 2020, **26**, 1.
- [155] M. Wainwright, T. Maisch, S. Nonell, K. Plaetzer, A. Almeida, G. P. Tegos, M. R. Hamblin, *Lancet Infect. Dis.* 2017, **17**, 49.
- [156] M. Krüger, P. Richter, S. M. Strauch, A. Nasir, A. Burkovski, C. A. Antunes, T. Meißgeier, E. Schlücker, S. Schwab, M. Lebert, *Microorganisms* 2019, **7**, 59.
- [157] Ž. Lukšienė, *Novel Food Preservation and Microbial Assessment Techniques*, CRC Press, FL, États-Unis, 2014.
- [158] I. Buchovec, V. Lukseviciute, A. Marsalka, I. Reklaitis, Ž. Lukšienė, *Photochem. Photobiol. Sci.* 2016, **15**, 506.
- [159] Ž. Lukšienė, E. Paskeviciute, *J. Appl. Microbiol.* 2011, **110**, 1274.
- [160] K. Aponiene, Ž. Lukšienė, *J. Photochem. Photobiol. B* 2015, **142**, 257.
- [161] E. Paskeviciute, B. Zudyte, Ž. Lukšienė, *J. Photochem. Photobiol. B* 2018, **182**, 130.
- [162] Ž. Lukšienė, L. Brovko, *Food Eng. Rev.* 2013, **5**, 185.
- [163] I. Buchovec, V. Lukseviciūtė, R. Kokštaite, D. Labeikyte, L. Kaziukonyte, Ž. Lukšienė, *J. Photochem. Photobiol. B* 2017, **172**, 1.
- [164] L. L. Thomas, PhD thesis, Iowa State University, 1991.
- [165] Y. Liu, H. Zhou, Z. Hu, G. Yu, D. Yang, J. Zhao, *Biosens. Bioelectron.* 2017, **94**, 131.
- [166] A. Walter, A. März, W. Schumacher, P. Rösch, J. Popp, *Lab Chip* 2011, **11**, 1013.
- [167] A. Sengupta, M. L. Laucks, E. J. Davis, *Appl. Spectrosc.* 2005, **59**, 1016.
- [168] Z. Movasaghi, S. Rehman, I. U. Rehman, *Appl. Spectrosc. Rev.* 2007, **42**, 493.
- [169] I. O. Bacellar, M. C. Oliveira, L. S. Dantas, E. B. Costa, H. C. Junqueira, W. K. Martins, A. M. Durantini, G. Cosa, P. Di Mascio, M. Wainwright, R. Miotto, R. M. Cordeiro, S. Miyamoto, M. S. Baptista, *J. Am. Chem. Soc.* 2018, **140**, 9606.
- [170] E. Alves, M. A. Faustino, M. G. Neves, A. Cunha, J. Tome, A. Almeida, *Future Med. Chem.* 2014, **6**, 141.
- [171] T. Yu, J. Bai, K. Hu, Z. Wang, *Ultrason. Sonochem.* 2003, **10**, 33.
- [172] A. Colniță, N. Dina, N. Leopold, D. Vodnar, D. Bogdan, S. Porav, L. David, *Nanomaterials* 2017, **7**, 248.
- [173] L. Teng, X. Wang, X. Wang, H. Gou, L. Ren, T. Wang, Y. Wang, Y. Ji, W. E. Huang, J. Xu, *Sci. Rep.* 2016, **6**, 1.
- [174] Z. N. Kashmiri, S. A. Mankar, *Int. J. Curr. Microbiol. App. Sci.* 2014, **3**, 34.

- [175] H. A. Krebs, *Annu. Rev. Biochem.* 1950, **19**, 409.
- [176] L. C. P. M. Schenkels, E. C. I. Veerman, A. V. Nieuw Amerongen, *Crit Rev Oral Biol Med* 1995, **6**, 161.
- [177] D. P. Lima, D. G. Diniz, S. A. Saliba, M. D. Hissako, S. C. Okamoto, *Int. J. Infect. Dis.* 2010, **14**, 184.
- [178] D. Ilic, M. Djulbegovic, J. H. Jung, E. C. Hwang, Q. Zhou, A. Cleves, T. Agoritsas, P. Dahm, *BMJ* 2018, **362**, 3519.
- [179] W. V. Gonzales, A. T. Mobashsher, A. Abbosh, *Sensors* 2019, **19**, 800.
- [180] K. M. Koo, P. N. Mainwaring, S. A. Tomlins, M. Trau, *Nat. Rev. Urol.* 2019, **16**, 302.
- [181] S. Liu, B. Zhou, J. D. Valdes, J. Sun, H. Guo, *Hepatology* 2019, **69**, 1816.
- [182] A. Havelka, K. Sejersen, P. Venge, K. Pauksens, A. Larsson, *Sci. Rep.* 2020, **10**, 1.
- [183] L. M. Coutinho, M. C. Ferreira, A. Luiza L. Rocha, M. M. Carneiro, F. M. Reis, *Adv. Clin. Chem.* 2019, **89**, 59.
- [184] A. Zhang, H. Sun, P. Wang, Y. Han, X. Wang, *J. Proteomics* 2012, **75**, 1079.
- [185] J. H. Wang, J. Byun, S. Pennathur, *Semin Nephrol.* 2010, **30**, 500.
- [186] J. Li, H. Xie, A. Li, J. Cheng, K. Yang, J. Wang, W. Wang, F. Zhang, Z. Li, H. S. Dhillon, M. S. Openkova, X. Zhou, K. Li, Y. Hou, *Oncotarget* 2017, **18**, 46834.
- [187] P. S. Sharma, K. R. Nandimath, S. V. Hiremath, K. Burde, *J Oral Maxillofac Surg Med Pathol* 2020, **32**, 65.
- [188] J. R. Denery, A. A. K. Nunes, M. S. Hixon, T. J. Dickerson, K. D. Janda, *PLoS Neglected Trop. Dis.* 2010, **4**, 834.
- [189] Q. Wang, P. Gao, F. Cheng, X. Wang, Y. Duan, *Talanta* 2014, **119**, 299.
- [190] F. Cheng, Z. Wang, Y. Huang, Y. Duan, X. Wang, *Clin. Chim. Acta* 2015, **447**, 23.
- [191] E. M. Berendsen, E. Levin, R. Braakman, D. van der Riet-van Oeveren, N. J. Sedee, A. Paauw, *Future Microbiol.* 2017, **12**, 1135.
- [192] M. D. Ward, T. Kenny, E. Bruggeman, C. D. Kane, C. L. Morrell, M. M. Kane, S. Bixler, S. L. Grady, R. S. Quizon, M. Astatke, Lisa H. Cazares, *Clin. Proteomics* 2020, **17**, 1.
- [193] S. K. Arya, P. Estrela, *Sensors* 2018, **18**, 1.
- [194] C. Li, Y. Yang, D. Wu, T. Li, Y. Yin, G. Li, *Chem Sci.* 2016, **7**, 3011.
- [195] M. J. Baker, S. R. Hussain, L. Lovergne, V. Untereiner, C. Hughes, R. A. Lukaszewski, G. Thiéfin, G. D. Sockalingum, *Chem. Soc. Rev.* 2016, **45**, 1803.

- [196] H. K. Vlckova, V. Pilarova, P. Svobodova, J. Plisek, F. Svec, L. Novakova, *Analyst*, 2018, **143**, 1305.
- [197] J. Goswami, *J. Chromatogr. Sep. Tech.* 2015, **6**, 1.
- [198] Z. Chen, Y. Gao, D. Zhong, *Biomed. Chromatogr.* 2020, **34**, 1.
- [199] A. G. Gilman, T. W. Rall, A. S. Nies, P. Tylor, *The Pharmaceutical Basis of Therapeutics, 8th Edition*, Pergamon Press, USA, 1990.
- [200] J. Nagelschmitz, M. Blunck, J. Kraetzschmar, M. Ludwig, G. Wensing, T. Hohlfeld, *Clin Pharmacol.* 2014, **6**, 51.
- [201] V. Cotty, F. Zurzola, T. Beezley, A. Rodgers, *J. Pharm. Sci.* 1965; **54**, 868.
- [202] C. Dale, A. A. M. Aulaqi, J. Baker, R. C. Hobbs, M. E. L. Tan, C. Tovey, I. A. L. Walker, J. A. Henry, *QJM* 2005, **98**, 113.
- [203] L. Tóth, L. Muszbek, I. Komáromi, *J. Mol. Graphics Modell.* 2013, **40**, 99.
- [204] S. Lee, D. Johnson, J. Klein, J. Eppler, *Vet. Hum. Toxicol.* 1995, **37**, 224.
- [205] Y. M. Jean, Y. Yamamoto, R. B. Gaynor, *Nature* 1998, **396**, 77.
- [206] N. Muir, J. D. Nichols, J. M. Clifford, M. R. Stillings, R. C. Hoare, *Curr. Med. Res. Opin.* 1997, **13**, 547.
- [207] A. K. Done, *Pediatrics* 1960, **26**, 800.
- [208] W. D. Masonx, N. Winer, *J. Pharm. Sci.* 1981, **70**, 262.
- [209] L. Ross-Lee, M. Elms, B. E. Cham, F. Bochner, I. H. Bunce, M. J. Eadie, *Eur. J. Clin. Pharmacol.* 1982, **23**, 545.
- [210] K. Schrör, *Acetylsalicylic acid*, John Wiley & Sons, Germany, 2016.
- [211] G. P. McMahon, M. T. Kelly, *Anal. Chem.* 1998, **70**, 409.
- [212] Y. Kim, J.-Y. Jeon, S.-H. Han, N. Ha, K. Jang, M.-G. Kim, *Transl Clin Pharmacol*, 2018, **26**, 1.
- [213] M. M. D. C. Vila, M. Tubino, G. de Oliveira Neto, *J. AOAC Int.* 2001, **84**, 32.
- [214] D. J. Kim, T. Y. Jeon, S. G. Park, H. J. Han, S. H. Im, D. H. Kim, S. H. Kim, *Small* 2017, **13**, 1.
- [215] J. Tanne, *BMJ* 2006, **322**, 628.
- [216] S. E. Gulmez, D. Larrey, G.-P. Pageaux, J. Bernuau, F. Bissoli, Y. Horsmans, D. Thorburn, P. A. McCormick, B. Stricker, M. Toussi, S. Lignot-Maleyran, S. Micon, F. Hamoud, R. Lassalle, J. Jové, P. Blin, N. Moore1, *Br. J. Clin. Pharmacol.* 2015, **80**, 599.
- [217] M. J. Hodgam, A. R. Garrard, *Crit. Care Clin.* 2012, **28**, 499.

- [218] R. D. Fannin, M. Russo, T. M. O'Connell, K. Gerrish, J. H. Winnike, J. Macdonald, J. Newton, S. Malik, S. O. Sieber, J. Parker, R. Shah, T. Zhou, P. B. Watkins, R. S. Paules, *Hepathology* 2010, **5**, 227.
- [219] T. M. Caparrotta, D. J. Antoine, J. W. Dear, *Eur. J. Clin. Pharmacol.* 2018, **74**, 147.
- [220] M. R. McGill, H. Jaeschke, *Pharm. Res.* 2013, **30**, 2174.
- [221] L. L. Mazaleuskaya, K. Sangkuhl, C. F. Thorn, G. A. FitzGerald, R. B. Altman, T. E. Klein, *Pharmacogenet. Genomics* 2015, **25**, 416.
- [222] R. K.-T. Kam, M. H.-M. Chan, H.-T. Wong, A. Ghose, A. M. Dondorp, K. Plewes, J. Tarning, *Future Sci. OA* 2018, **4**, 1.
- [223] R. Whelpton, K. Fernandes, K. A. Wilkinson, D. R. Goldhill, *Biomed. Chromatogr.* 1993, **7**, 90.
- [224] B. Gorain, H. Choudhury, U. Nandi, A. Das, S. Dan, T. K. Pal, *J. AOAC Int.* 2019, **96**, 573.
- [225] D. W. Roberts, W. M. Lee, J. A. Hinson, S. Bai, C. J. Swearingen, R. T. Stravitz, A. Reuben, L. Letzig, P. M. Simpson, J. Rule, R. J. Fontana, D. Ganger, K. R. Reddy, I. Liou, O. Fix, L. P. James, *Clin. Gastroenterol. Hepatol.* 2017, **15**, 555.
- [226] B.-Y. Chan, H.-M. Tsang, C. W.-Y. Ng, W. H.-W. Ling, D. C.-W. Leung, H. H.-C. Lee, C. M. Mak, *J. Clin. Lab. Anal.* 2019, **32**, 1.
- [227] Z. Mukanova, K. Gudun, Z. Elemessova, L. Khamkhash, E. Ralchenko, R. Bukasov, *Anal. Sci.* 2018, **34**, 183.
- [228] E. de Barros Santos, E. C. N. L. Lima, C. S. de Oliveira, F. A. Sigolia I. O. Mazali, *Anal. Methods* 2014, **6**, 3564.
- [229] A. Nehlig, J. L. Daval, G. Debry, *Brain Res Brain Res Rev* 1992, **17**, 139.
- [230] M. J. Arnaud, *Caffeine, Coffee, and Health*, Raven Press, Ltd., New York, 1993.
- [231] Es. Zylber-Katz, L. Granit, M. Levy, *Clin Pharmacol Ther.* 1984, **36**, 133.
- [232] A. Lelo, D. J. Birkett, R. A. Robson, J. O. Miners, *Br. J. clin. Pharmac.* 1986, **22**, 177.
- [233] R. Newton, L. J. Broughton, M. J. Lind, P. J. Morrison, H. J. Rogers, I. D. Bradbrook, *Eur. J. Clin. Pharmacol.* 1981, **21**, 45.
- [234] M. Arnaud, *Methylxanthines, Handbook of Experimental Pharmacology 200*, Springer, New York, 2011.
- [235] A. Nehlig, *Pharmacol Rev*, 2018, **70**, 384.
- [236] Z. Jandova, S. C. Gill, N. M. Lim, D. L. Mobley, C. Oostenbrink, *Chem. Res. Toxicol.* 2019, **32**, 1374.

- [237] V. Perera, A. S. Gross, H. Xu, A. J. McLachlan, *J. Pharm. Pharmacol.* 2011, **63**, 1161.
- [238] A. Lelo, D. J. Birkett, R. A. Robson, J. O. Miners, *Br. J. clin. Pharmac.* 1986, **22**, 177.
- [239] Y. Suzuki, T. Uematsu, A. Mizuno, K. Fujii, M. Nakashima, *Ther Drug Monit.* 1989, **11**, 88.
- [240] J. J. Carvalho, M. G. Weller, U. Panne, R. J. Schneider, *Anal. Lett.* 2012, **45**, 2549.
- [241] M. Fenske, *Chromatographia* 2007, **65**, 233.
- [242] A. M.-Y. Liao, W. Pan, J. C. Benson, A. D. Wong, B. J. Rose, G. T. Caltagirone, *Biochemistry*, 2018, **57**, 5117.
- [243] O. Alharbi, Y. Xu, R. Goodacre, *Anal. Bioanal. Chem.* 2015, **407**, 8253.
- [244] X. Chen, H. Gu, G. Shen, X. Dong, J. Kang, *J. Mol. Struct.* 2010, **975**, 63.
- [245] A. Falamaş, H. Rotaru, M. Hedeşiu, *Lasers Med Sci.* 2020, **35**, 1393.
- [246] B. H. C. Greene, D. S. Alhatab, C. C. Pye, C. L. Brosseau, *J. Phys. Chem. C* 2017, **121**, 8084.
- [247] S. D. Bindsri, D. S. Alhatab, C. L. Brosseau, *Analyst* 2018, **147**, 4128.
- [248] L. Zhao, J. Blackburn, C. L. Brosseau, *Anal. Chem.* 2015, **87**, 441.
- [249] M. Rani, L. Moudgil, B. Singh, A. Kaushal, A. Mittal, G. S. S. Saini, S. K. Tripathi, G. Singh, A. Kaura, *RSC Adv.* 2016, **6**, 17373.
- [250] Y. Sun, X. Younan, *Science* 2002, **298**, 1.
- [251] J. Kimling, M. Maier, B. Okenve, V. Kotaidis, H. Ballot, A. Plech, *J. Phys. Chem. B* 2006, **110**, 15700.
- [252] M. Zhou, S. Chen, S. Zhao, *J. Phys. Chem. Lett.* 2006, **110**, 4510.
- [253] J. Mounteney, P. Griffiths, R. Sedefov, A. Noor, J. Vicente, R. Simon, *Addiction* 2015, **111**, 34.
- [254] C. J. Ruhm, *Health Affairs*, 2019, **38**, 1216.
- [255] L. B. Lea., S. Nogueira, R. A. Canevari, L. F. C. S. Carvalho, *Photodiagn. Photodyn. Ther.* 2018, **24**, 237.
- [256] A. L. Mitchell, K. B. Gajjar, G. Theophilou, F. L. Martin, P. L. Martin-Hirsch, *J. Biophotonics* 2014, **7**, 153.
- [257] A. A. Bunaciu, S. Fleschin, V. D. Hoang, H. Y. Aboul-Enein, *Crit. Rev. Anal. Chem.* 2016, **47**, 67.
- [258] P. L. Stiles, J. A. Dieringer, N. C. Shah, R. P. Van Duyne, *Annu. Rev. Anal. Chem.* 2008, **1**, 601.
- [259] P. J. G. Goulet, R. F. Aroca, *Can. J. Chem.* 2004, **82**, 987.
- [260] P. Wulandari, T. Nagahiro, N. Fukada, Y. Kimura, M. Niwano, K. Tamada, *J. Colloid Interface Sci.* 2015, **438**, 244.

- [261] F. D. C. Vega, P. G. M. Torres, J. P. Molina, N. M. G. Ortiz, V. G. Hadjiev, J. Z. Medina, F. C. R. Hernandez, *J. Mater. Chem. C* 2017, **5**, 4959.
- [262] M. Verma, A. Kedia, M. B. Newmai, P. S. Kumar, *RSC Adv.* 2016, **6**, 80342.
- [263] C. Wu, B. P. Mosher, K. Lyons, T. Zeng, *J. Nanosci. Nanotechnol.* 2010, **10**, 2342.
- [264] P. S. Mdluli, N. M. Sosibo, P. N. Mashazi, T. Nyokong, R. T. Tshikhudo, A. Skepu, E. van der Lingen, *J. Mol. Struct.* 2011, **1004**, 131.
- [265] E. C. Le Ru, M. Meyer, E. Blackie, P. G. Etchegoin, *J. Raman Spectrosc.* 2008, **39**, 1127.
- [266] M. Moskovits, *J. Chem. Phys.* 1982, **77**, 4408.
- [267] J. L. Castro, M. R. López-Ramírez, J. F. Arenas, J. Soto, J. C. Otero, *Langmuir*, 2012, **28**, 8926.
- [268] J. Y. Qu, B. C. Wilson, D. Suria, *Appl. Opt.* 1999, **38**, 5491.
- [269] Y. Lu, C. Wu, R. You, Y. Wu, H. Shen, L. Zhu, S. Feng, *Biomed. Opt. Express* 2018, **9**, 4988.
- [270] M. Pučetaitė, M. Velička, J. Pilipavičius, A. Beganskienė, J. Čeponkus, V. Šablinskas, *J. Raman Spectrosc.* 2016, **47**, 681.
- [271] P. F. Spahr, J. T. Edsall, *J. Biol. Chem.* 1964, **239**, 850.
- [272] J. L. Castro, J. F. Arenas, M. R. López-Ramírez, J. C. Otero, *Biopolymers* 2006, **82**, 379.
- [273] M. Altarsha, G. Monard, B. Castro, *J. Mol. Struct.: THEOCHEM* 2006, **761**, 203.
- [274] M.K. Shukla, P. C. Mishra, *J. Mol. Struct.* 1996, **377**, 247.
- [275] H. Ringertz, *Acta Crystallogr.* 1966, **20**, 397.
- [276] B. Nie, J. Stutzman, A. Xie, *Biophys. J.* 2005, **88**, 2833.
- [277] M. Altarsha, G. Monard, B. Castro, *Int. J. Quantum Chem.* 2007, **107**, 172.
- [278] OriginPro 2018, OriginLab Corporation, Northampton, MA, USA.
- [279] C. Labat, S. Thul, J. Pirault, M. Temmar, S. N. Thornton, A. Benetos, M. Bäck, *Disease Markers*, 2018.
- [280] S. Gomez, T. Giovannini, C. Cappelli, *Phys. Chem. Chem. Phys.*, 2020, **22**, 5929.
- [281] S. Zarei, Y. Salimi, E. Repo, N. Daglioglu, Z. Safaei, E. Güzel, A. Asadi, *Environ. Sci. Pollut. Res.* 2020, **27**, 36037.
- [282] S. Cappelletti, D. Piacentino, G. Sani, M. Aromatario, *Curr. Neuropharmacol.* 2015, **13**, 71.
- [283] J. V. Higdon, B. Frei, *Crit. Rev. Food Sci. Nutr.* 2006, **46**, 101.

- [284] P. Nawrot, S. Jordan, J. Eastwood, J. Rotstein, A. Hugenholtz, M. Feeley, *Food Addit Contam.* 2003, **20**, 1.
- [285] S. Cappelletti, D. Piacentino, V. Fineschi, P. Frati, L. Cipolloni, M. Aromatario, *Nutrients* 2018, **10**, 611.
- [286] F. Chen, Z.-Y. Hu, R. B. Parker, S. C. Laizure, *Biomed. Chromatogr.* 2017, **31**, 1.
- [287] R. del Carmen Lopez-Sanchez, V. J. Lara-Diaz, A. Aranda-Gutierrez, J. A. Martinez-Cardona, J. A. Hernandez, *J. Anal. Methods Chem.* 2018, **2018**, 1.
- [288] S. N. Alvi, M. M. Hammami, *J. Chromatogr. Sci.*, 2011, **49**, 292.
- [289] I. Pavel, A. Szeghalmi, D. Moigno, S. Cinta, W. Kiefer, *Byopolymers*, 2003, **72**, 25.
- [290] R. Hans, S. Thomas, B. Garla, R. J. Dagli, M. K. Hans, *Scientifica*, 2016.
- [291] H. M. Rad, M. Rabiei, A. Sobhani, M. S. Khanjani, M. R. Taramsar. E. K. Leili, *J. Oral Rehabil.* 2014, **41**, 759.
- [292] A. C. S. Talari, Z. Movasaghi, S. Rehman, I. ur Rehman, *Appl. Spectrosc. Rev.* 2015, **50**, 46.
- [293] I. M. Colceriu-Simon, M. Hedesiu, V. Toma, G. Armencea, A. Moldovan, G. Stiufiuc, B. Culic, V. Tarmure, C. Dinu, I. Berindan-Neagoe, R. I. Stiufiuc, M. Baciut, *Diagnostics*, 2019, **9**, 101.

APPENDIX I

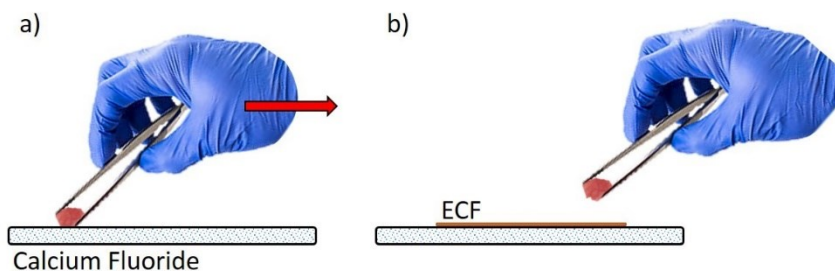


Fig. 1. The schematic of the preparation of the extracellular fluid layers: a) Pressing and sliding the cut tissue; b) releasing the tissue and letting the ECF to dry.

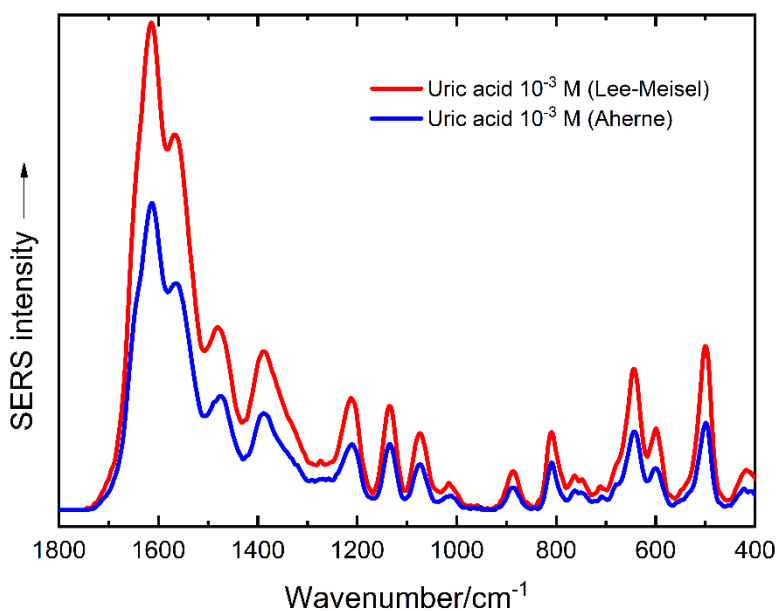


Fig. 2. Comparison of the enhancement of the uric acid spectrum using spherically shaped (Lee-Meisel) and prism shaped (Aherne) silver nanoparticles.

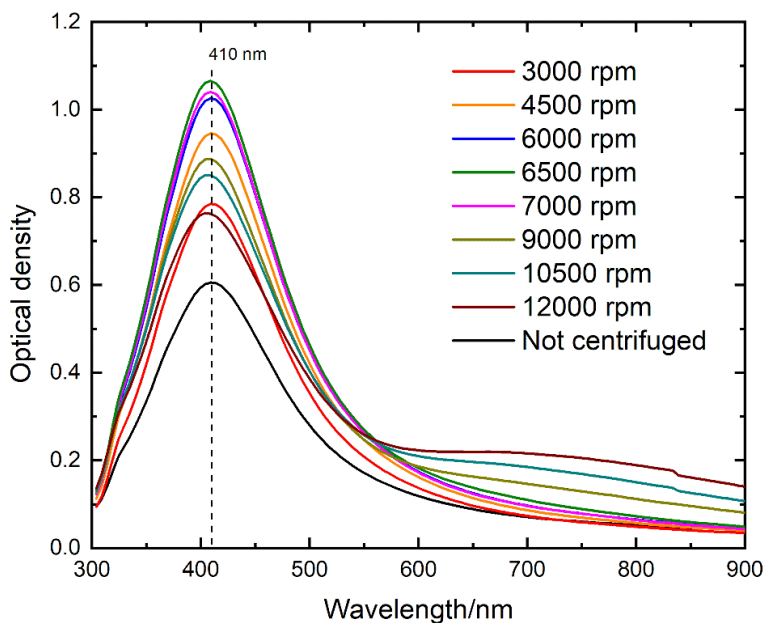


Fig. 3. The selected UV-Vis absorption spectra of the colloidal silver nanoparticle solutions before and after centrifuging at various speeds.

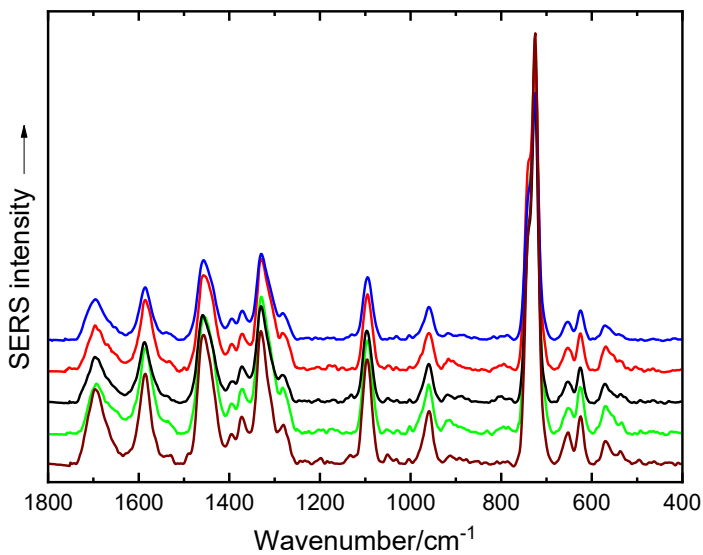


Fig. 4. The SERS spectra of the ECF of normal kidney tissue collected at five randomly chosen points of the sample.

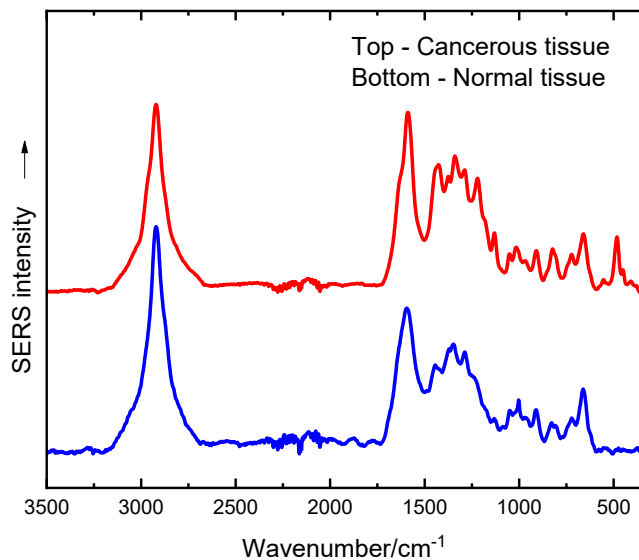


Fig. 5. The SERS spectra of the ECF of cancerous and normal kidney tissues presented in the wavenumber region of 3500-400 cm⁻¹.

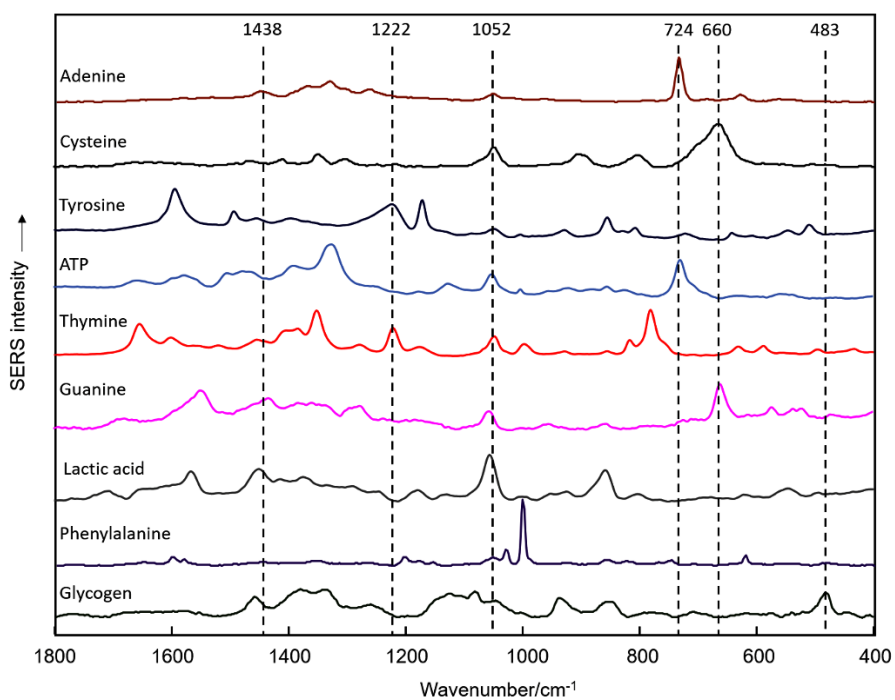


Fig. 6. The SERS spectra of the possible constituents of the extracellular fluid.

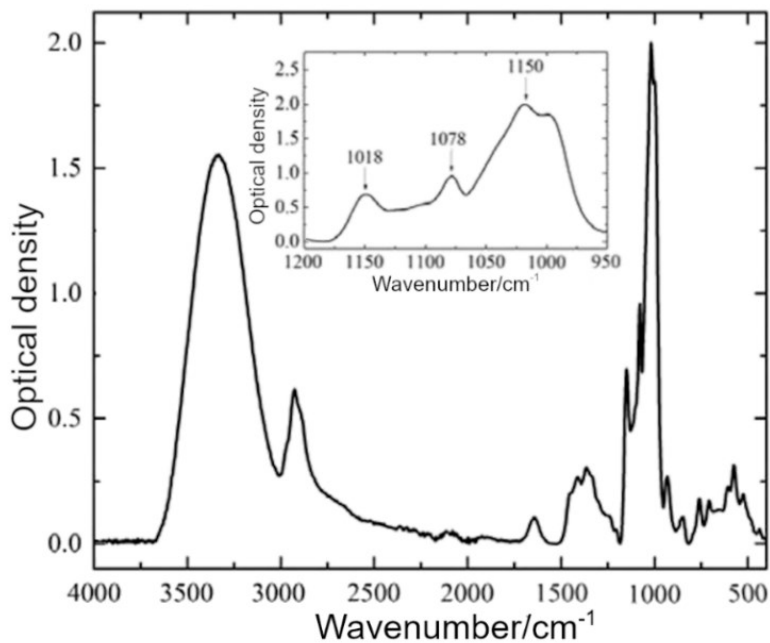


Fig. 7. The FTIR-ATR spectrum of glycogen. The inset shows the same spectrum in the wavenumber region 950-1200 cm⁻¹.

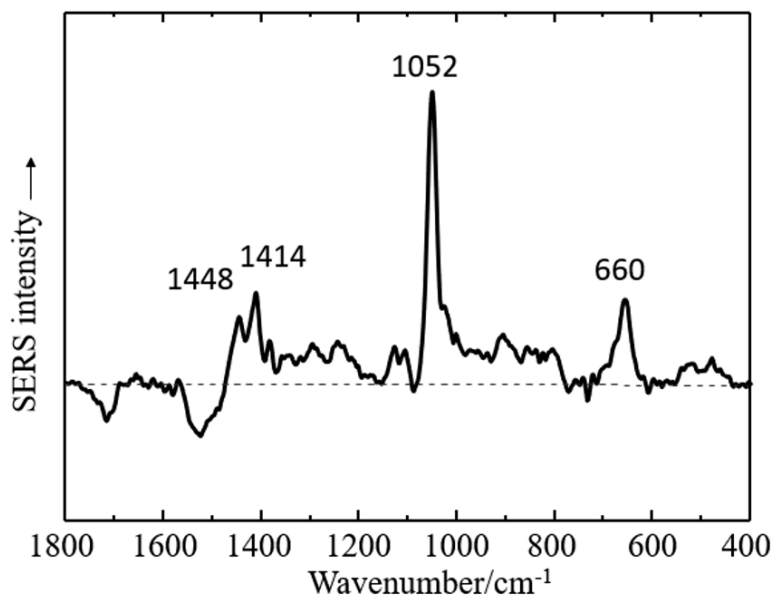


Fig. 8. The difference spectrum of the SERS spectra of the ECF of cancerous and normal bladder tissues.

APPENDIX II

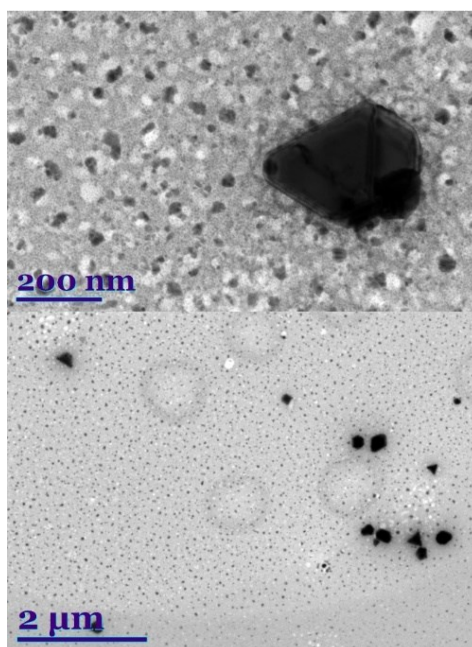


Fig. 1. The TEM images of the Au-PVP nanoparticles before and after the washing of the excess of PVP polymer.

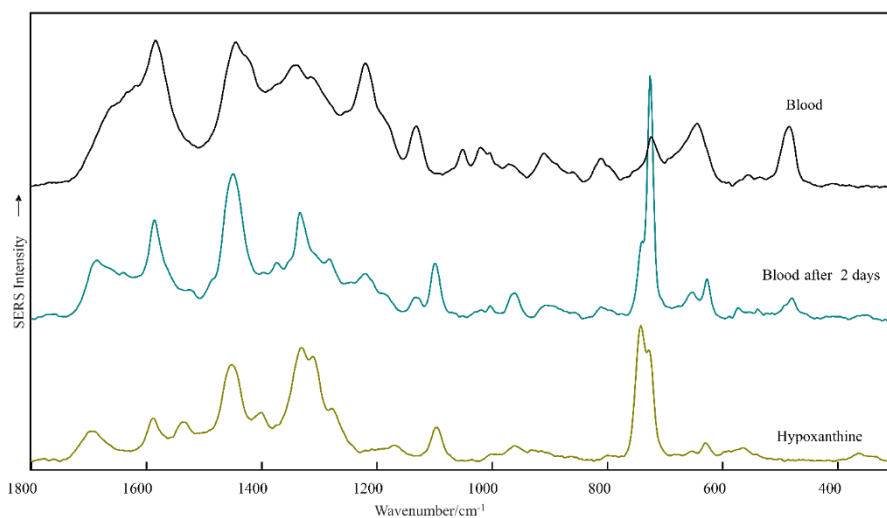


Fig. 2. The SERS spectra of human blood taken right after and after two days of the collection of blood sample, and the SERS spectrum of hypoxanthine.

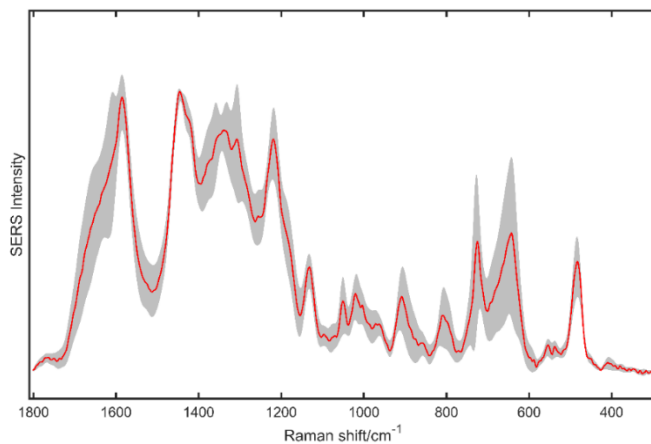


Fig. 3. The averaged SERS spectra of human blood (red). Standard deviation of the band intensities (grey).

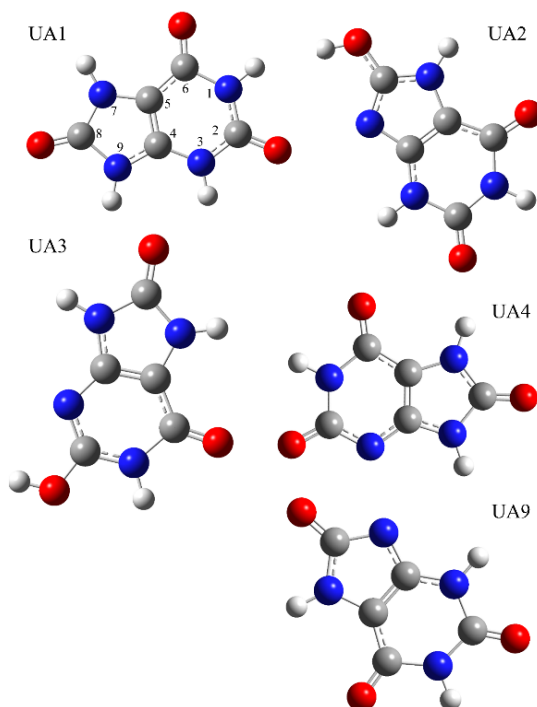


Fig. 4. The theoretically calculated (B3LYP/6-311G++) structures of the most stable tautomers and monoanions of uric acid: triketo tautomer (UA1); diketo (UA2); diketo (UA3); monoanion (UA4); monoanion (UA9).

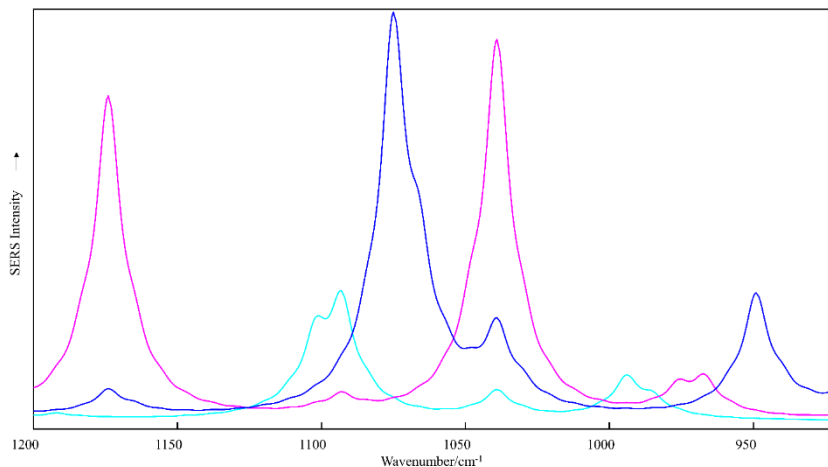


Fig. 5. The theoretically calculated (B3LYP/6-311G++) SERS spectra of the most stable tautomers of uric acid shown in the spectral range of 1060-922 cm^{-1} . Triketo tautomer (UA1) – light blue, diketo (UA3) – pink; monoanion (UA9) – dark blue.

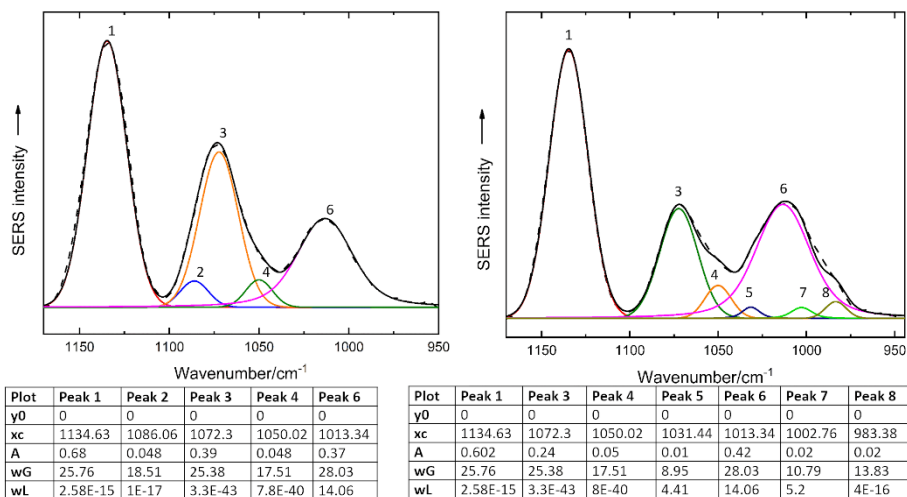


Fig. 6. The experimental and fitted SERS spectra of blood serum collected before and after the consumption of 3.2 g of aspirin. The spectra are shown in the spectral range of 1200-950 cm^{-1} .

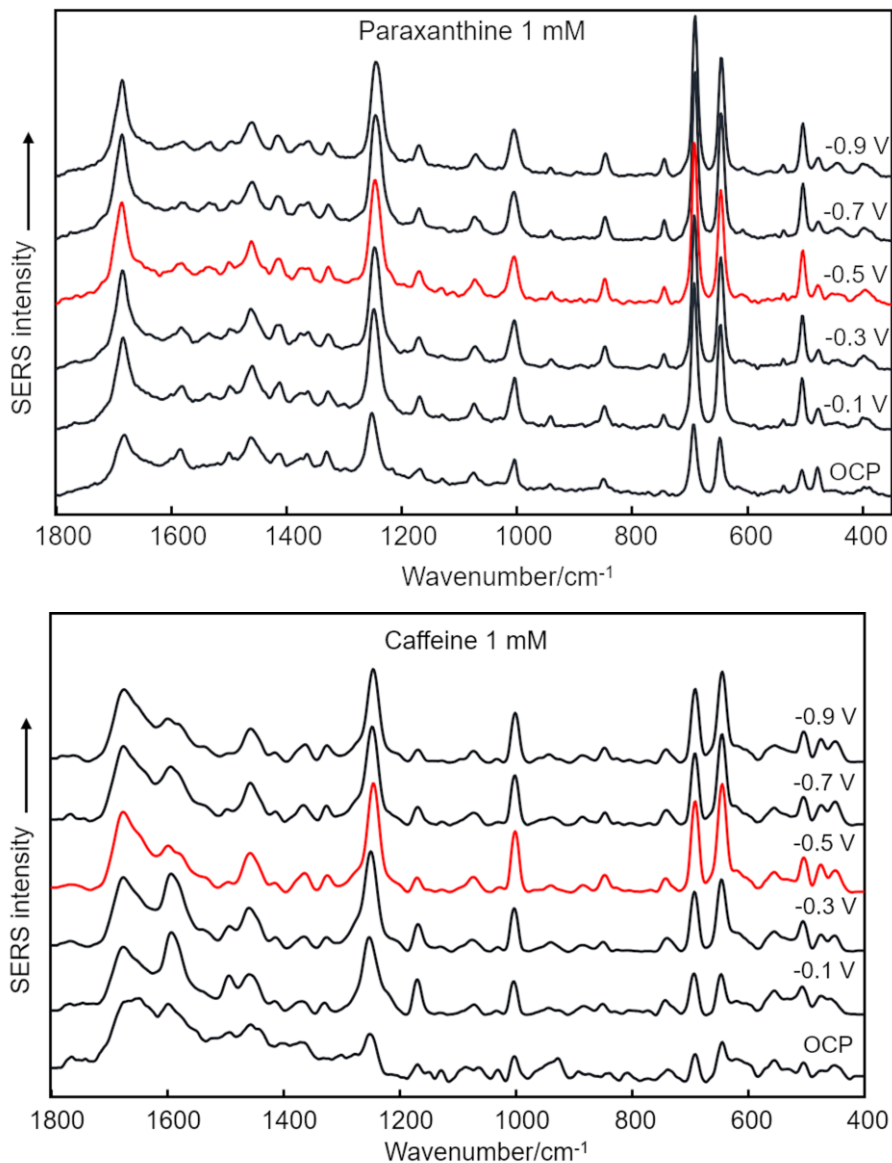


Fig. 7. The EC-SERS spectra of 1 mM of paraxanthine (top) and 1 mM of caffeine (bottom) taken at different WE potential values. A solution of 0.1 M H₂SO₄ was used as an electrolyte.

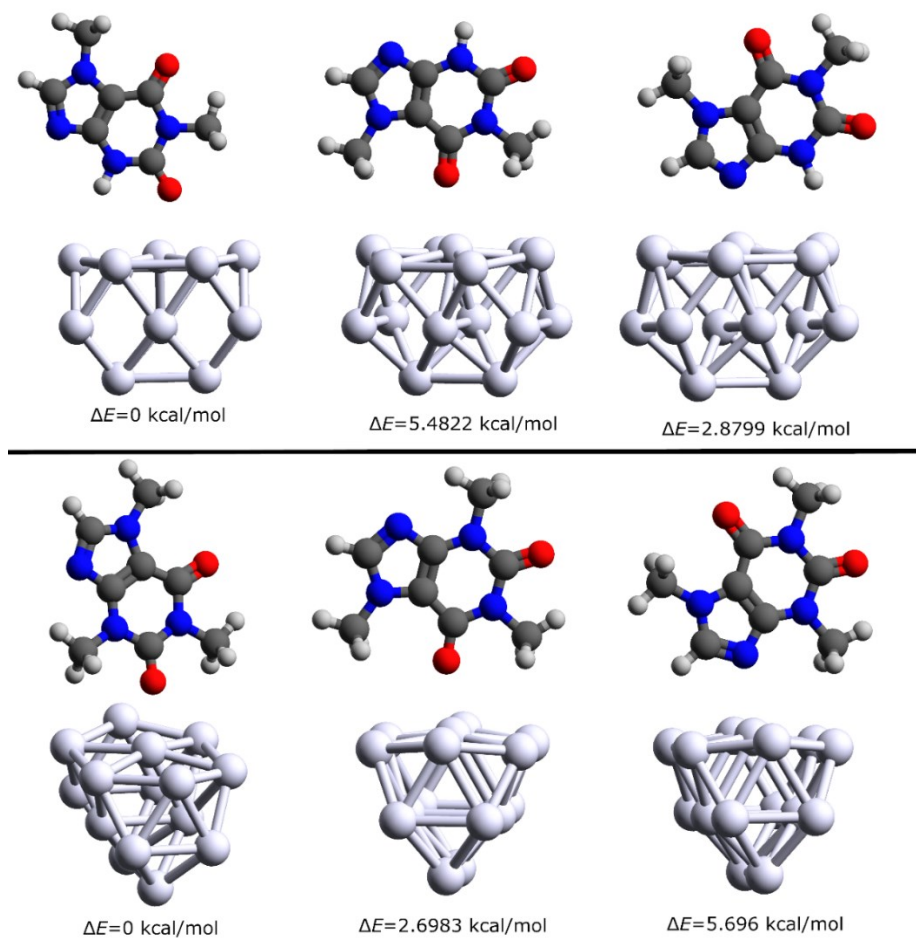


Fig. 8. The theoretically calculated caffeine and paraxanthine complexes with a silver nanoparticle simulated by 15 atom Ag atom cluster. The energy differences of the complexes are calculated in respect to the most stable complex of caffeine and paraxanthine respectively.

Table 1. Positions of the vibrational bands observed in the spectra of caffeine and paraxanthine and their assignment.

Wavenumber, cm ⁻¹		Assignment
Caffeine	Paraxanthine	
2930	2940	$\nu(\text{CH}_3)$
1680	1688	$\nu(\text{C}=\text{O}) + \delta(\text{NH})$
1595	1586	$\nu(\text{C}-\text{N}) + \delta(\text{CH}_3) + \delta(\text{NH})$
1537	1537	$\delta(\text{CH}_3)$
1496	1501	$\delta(\text{CH}_3)$
1458	1461	$\delta(\text{CH}_3) + \delta(\text{NH}) + \delta(\text{CH})$
1415	1415	$\delta(\text{CH}_3) + \nu(\text{N}-\text{C}=\text{N}) + \nu(\text{C}-\text{N})$
1362	1363	$\nu(\text{C}-\text{N}) + \delta(\text{CH}_3) + \delta(\text{NH})$
1328	1328	i. p. pyrimidine, imidazole ring deformation
1246	1247	$\delta(\text{C}-\text{H}) + \nu(\text{N}-\text{C}) + \delta(\text{CH}_3)$
1172	1172	$\nu(\text{N}-\text{CH}_3) + \nu(\text{C}-\text{NH})$
1130	1132	$\nu(\text{N}-\text{C}-\text{N}) + \delta(\text{CH}_3)$
1074	1074	$\nu(\text{N}-\text{C}) + \delta(\text{CH}_3)$
1002	1006	$\nu(\text{N}-\text{C}) + \delta(\text{CH}_3)$
941	941	$\delta(\text{C}-\text{C}-\text{N}) + \delta(\text{N}-\text{C}-\text{N})$
849	849	$\delta(\text{C}-\text{N}-\text{CH}_3) + \delta(\text{N}-\text{C}-\text{N})$
745	745	o. p. pyrimidine ring deformation
692	692	$\nu(\text{N}-\text{CH}_3) + \delta(\text{N}-\text{C}-\text{N})$
647	647	i. p. pyrimidine ring breathing + $\delta(\text{C}-\text{N}-\text{C})$
505	505	i. p. pyrimidine ring deformation + $\delta(\text{C}-\text{N}-\text{CH}_3)$
475	478	i. p. pyrimidine ring deformation
449	453	$\delta(\text{C}-\text{N}-\text{CH}_3) + \delta(\text{C}-\text{C}=\text{O})$
400	395	$\delta(\text{C}-\text{N}-\text{CH}_3)$

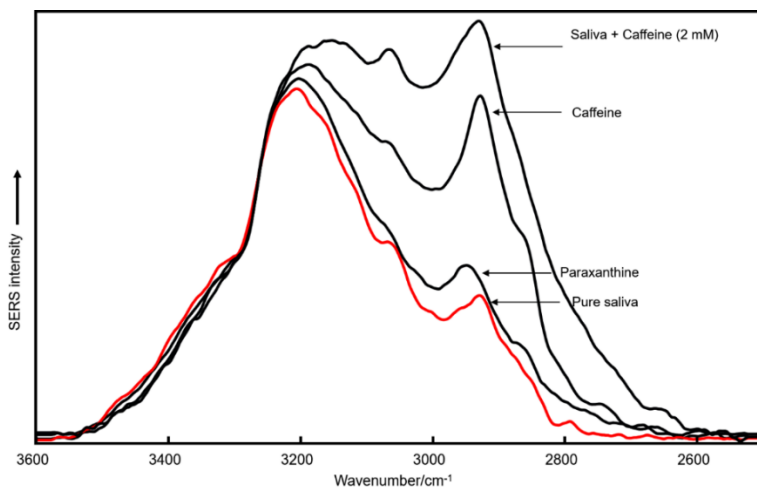


Fig. 9. The EC-SERS spectra of caffeine (1 mM), paraxanthine (1 mM), pure saliva, model saliva and caffeine (2 mM) samples in the $\nu(\text{CH}_3)$ region.

CURRICULUM VITAE

Name: Martynas
Surname: Velička
Date of birth: 1991-02-26
Place of birth: Šiauliai, Lithuania
E-mail: velicka.m@gmail.com

Education:

2016-2020 Vilnius University, Faculty of Physics
Ph.D. studies.

2014-2016 Vilnius University, Faculty of Physics
Master's degree, Magna Cum Laude.

2010-2014 Vilnius University, Faculty of Physics
Bachelor's degree, Cum Laude.

2006-2010 Šiaulai Didždvaris Gymnasium.

2006-2010 Young Physicists' School "Fotonas".

2007-2010 Lithuanian Young Mathematicians School.

1998-2006 Šiauliai Secondary School "Salduvė".

1999-2006 Šiauliai Singing School "Dagilėlis".

Work experience:

2020 – now Center for Physical Sciences and Technology,
Junior Researcher

2020 – now "ART21", *Researcher.*

2016 – now Vilnius University, Institute of Chemical
Physics, *Lecturer.*

2018-2020 "Spektrolabas", *Researcher.*

2018 Vilnius University, Institute of Chemical
Physics, *Junior Researcher.*

2015 – 2018 Vilnius University, Institute of Chemical
Physics, *Technician.*

2017 "Interlux", *Documentation specialist.*

2014 – 2016 Vilnius University, Institute of Chemical
Physics, *Laboratory Assistant.*

LIST OF PUBLICATIONS

1. M. Velička, M. Pučetaitė, V. Urbonienė, J. Čeponkus, F. Jankevičius, V. Šablinskas, Detection of cancerous kidney tissue by means of SERS spectroscopy of extracellular fluid, *Journal of Raman spectroscopy*, 2017, **48**, 1744.

<https://doi.org/10.1002/jrs.5232>

2. M. Pučetaitė, M. Velička, V. Urbonienė, J. Čeponkus, R. Bandzevičiūtė, F. Jankevičius, A. Želvys, V. Šablinskas, G. Steiner, Rapid intra-operative diagnosis of kidney cancer by attenuated total reflection infrared spectroscopy of tissue smears, *Journal of Biophotonics*, 2018, **11**, 1.

<https://doi.org/10.1002/jbio.201700260>

3. S. Adomavičiūtė, M. Velička, V. Šablinskas, Detection of aspirin traces in blood by means of surface-enhanced Raman scattering spectroscopy, *Journal of Raman Spectroscopy*, 2020, **51**, 919.

<https://doi.org/10.1002/jrs.5853>

4. B. Žudytė, M. Velička, V. Šablinskas, Ž. Lukšienė, Understanding *Escherichia coli* damages after chlorophyllin-based photosensitization, *Journal of Biophotonics*, 2020, **13**, 1.

<https://doi.org/10.1002/jbio.202000144>

5. M. Velička, E. Zacharovas, S. Adomavičiūtė, V. Šablinskas, Detection of caffeine intake by means of EC-SERS spectroscopy of human saliva, *Spectrochimica Acta Part A: Molecular and Biomolecular Spectroscopy*, 2021, **246**, 118956.

<https://doi.org/10.1016/j.saa.2020.118956>

6. E. Zacharovas, M. Velička, G. Platkevičius, A. Čekauskas, A. Želvys, G. Niaura, V. Šablinskas, Discrimination between cancerous and normal bladder cancer tissues via SERS spectroscopy, Submitted.

7. M. Velička, M. Radžvilaitė, J. Čeponkus, V. Urbonienė, M. Pučetaitė, F. Jankevičius, G. Steiner, V. Šablinskas, Assignment of vibrational spectral bands of kidney tissue by means of low temperature SERS spectroscopy, *Proc. of SPIE* 10068, 2017.

<https://doi.org/10.1117/12.2252907>

8. V. Šablinskas, M. Velička, M. Pučetaitė, V. Urbonienė, J. Čeponkus, R. Bandzevičiūtė, F. Jankevičius, T. Sakharova, O. Bibikova, G. Steiner, *In situ* detection of cancerous kidney tissue by means of fiber ATR-FTIR spectroscopy, *Proc. of SPIE* 10497, 2018.

<https://doi.org/10.1117/12.2289393>

9. S. Adomavičiūtė, M. Velička, V. Šablinskas, Screening of usage of OTC drugs by means of SERS spectroscopy, *Proc. of SPIE* 10894, 2019.

<https://doi.org/10.1117/12.2508276>

10. M. Velička, S. Adomavičiūtė, E. Zacharovas, V. Šablinskas, Application of label-free SERS and EC-SERS for detection of traces of drugs in biological fluids, *Proc of SPIE*, 11257, 2020.

<https://doi.org/10.1117/12.2542306>

NOTES

NOTES

Vilnius University Press
Saulėtekio al. 9, LT-10222 Vilnius
e-mail. info@leidykla.vu.lt,
www.leidykla.vu.lt
Print run copies 25